Illinois U. Library

ЖУРНАЛ
ЭКСПЕРИМЕНТАЛЬНОЙ И ТЕОРЕТИЧЕСКОЙ
ФИЗИКИ
АКАДЕМИЯ НАУК СССР

SOVIET PHYSICS

JETP

VOLUME 3 NUMBER 4

A Translation
of the
Journal of Experimental and Theoretical Physics
of the
Academy of Sciences of the USSR

NOVEMBER, 1956

Published by the
AMERICAN INSTITUTE OF PHYSICS
INCORPORATED

SOVIET PHYSICS
JETP

A translation of the Journal of Experimental and Theoretical Physics of the USSR.

A publication of the

AMERICAN INSTITUTE OF PHYSICS

Governing Board

Frederick Seitz, *Chairman*
Allen V. Astin
Robert F. Bacher
W. S. Baird
H. A. Bethe
R. T. Birge
Frank D. Dexter
I. C. Gardner
S. A. Goudsmit
Charles Kittel
Hugh S. Knowles
R. B. Lindsay
William F. Meggers
Harry F. Olson
R. R. Palmer
R. F. Paton
Eric Rodgers
Ralph A. Sawyer
H. D. Smyth
Mark W. Zemansky

Administrative Staff

Henry A. Barton, *Director*
Mark W. Zemansky, *Treasurer*
Wallace Waterfall, *Executive Secretary*
Theodore Vorburger, *Advertising Manager*
Ruth F. Bryans, *Publication Manager*
Alice Mastropietro *Circulation Manager*
Kathryn Setze, *Assistant Treasurer*
Eugene H. Kone, *Director of Public Relations*

American Institute of Physics Advisory Board on Russian Translatio

Elmer Hutchisson, *Chairman*
Dwight Gray, Morton Hamermesh, Vladimir Rojansky, Victor Weisskopf

Editor of Soviet Physics
Robert T. Beyer, Department of Physics, Brown University, Providence, R.I.

Soviet Physics is a monthly journal published by the American Institute of Physics for the purpose of making available in English reports of current Soviet research in physics as contained in the Journal of Experimental and Theoretical Physics of the Academy of Sciences of the USSR. The page size of Soviet Physics will be 7⅞" x 10½", the same as other Institute journals.

Transliteration of the names of Russian authors follows the system employed by the Library of Congress.

This translating and publishing project was undertaken by the Institute in the conviction that dissemination of the results of researches everywhere in the world is invaluable to the advancement of science. The National Science Foundation of the United States encouraged the project initially and is supporting it in large part by a grant.

The American Institute of Physics and its translators propose to translate faithfully all the material in the Journal of EXPERIMENTAL AND THEORETICAL PHYSICS OF THE USSR appearing after January 1, 1955. The views expressed in the translated material, therefore, are intended to be those expressed by the original authors, and not those of the translators nor of the American Institute of Physics.

Two volumes are published annually, each of six issues. Each volume contains the translation of one volume of the Journal of EXPERIMENTAL AND THEORETICAL PHYSICS OF THE USSR. New volumes begin in February and August.

Subscription Prices:

Per year (12 issues)	
United States and Canada	$60.00
Elsewhere	64.00
Back Numbers	
Single copies	$ 6.00

Subscriptions should be addressed to the American Institute of Physics, 57 East 55 Street, New York 22, New York.

Copyright by American Institute of Physics 1956

SOVIET PHYSICS

JETP

SOVIET PHYSICS JETP VOLUME 3, NUMBER 4 NOVEMBER, 1956

Nikolai Nikolaevich Semenov

(On the sixtieth anniversary of his birth)

J. Exptl. Theoret. Phys. (U.S.S.R.) 30, 625-627 (April, 1956)

NIKOLAI Nikolaevich Semenov is one of the greatest Soviet physicists, noted for his works in many fields of physics, and chiefly in the new branch of science, created by him, on the borderline between physics and chemistry.

N. N. Semenov was born in Saratov, April 15, 1896. In 1913 he completed the course at the higher school in Samara and enrolled in the physical-mathematical faculty of the University of St. Petersburg. While still a university student, Nikolai Nikolaevich began to engage in scientific investigation. He took an active part in the work of the student physics circle founded by A. F. Ioffe, many of whose members have now become great scholars. In 1916, at the age of twenty, he published his first work on the collisions of electrons with molecules.

On graduating from the university in 1917, N. N. Semenov worked at the University of Tomsk as an assistant in the physics department. In 1920, at the invitation of A. F. Ioffe, he returned to Leningrad and began work in the State Physico-Technical Roentgenological Institute, where he was associate director and headed the laboratory of electron physics (since 1931 this has been the Institute of Chemical Physics of the U.S.S.R., with Nikolai Nikolaevich as permanent director down to the present time).

At the beginning of his scientific activity N. N Semenov studied mainly elementary processes (together with V. N. Kondrat'ev, A. I. Leipunskii and others). They investigated the ionization potentials of vapors of salts and of metallic vapors, and processes of dissociation and recombination. In these works there were discovered the phenomena of dissociation of diatomic molecules by electron impact and the direct recombination of a normal and an excited atom with the emission of a light quantum. The results of these works were published in the report "Chemistry and Electron Phenomena" (1924) and later, together with V. N. Kondrat'ev and Iu. B. Khariton, in the book "Electron Chemistry" (1927).

During this same time Nikolai Nikolaevich gave much attention to electrical phenomena in gases and solids. Together with A. F. Val' ter he carried out many investigations on electric fields, the passage of electric current through gases, breakdown of vacuum, and breakdown of solid dielectrics. As a result of his work on the breakdown of solid dielectrics he and V. A. Fock developed a theory of thermal breakdown.

A considerable number of N. N. Semenov's works at this time were devoted to molecular phenomena in the condensation of vapors on cold surfaces. Together with Iu. B. Khariton and A. I. Shal'nikov he investigated critical phenomena in the condensation of vapors and of molecular beams, and discovered the dependence of the critical condensation temperature on the vapor density. N. N. Semenov and Ia. I. Frenkel gave an exhaustive theory of these phenomena. Investigations were also made on the joint condensation from two molecular beams with formation of a molecularly dispersed mixture, which was of interest for the study of reactions in the solid phase.

The interest of N. N. Semenov in molecular beams was of long standing; as early as 1920 he and P. L. Kapitza projected the application of molecular beams in an inhomogeneous magnetic field to measure the magnetic moments of atoms and molecules. Later this work was successfully carried out by Stern and Gerlach.

The world-wide fame of N. N. Semenov is most of all connected with his works on chemical kinetics. He always displayed enormous interest in the investigation of chemical phenomena by physical methods, believing that physics is the key to the most interesting and at the same time the least studied problems of chemistry, and that a close union of physics and chemistry must lead to new achievements of science.

As is well known, the application of physics to chemistry led to the creation of a most important branch of chemistry --the theory of chemical equilibria. But the question of the speeds of chemical reactions remained almost completely undeveloped. A theory of the speeds of chemical reactions can be constructed only on the basis of a known mechanism of chemical changes. In the first attempts to construct a theory of the speeds of chemical reactions (van't Hoff) the transformation of individual molecules was represented as a single elementary act, expressed by the overall stoichiometric equation of the reaction, i.e., as a direct interaction between saturated molecules. It was also supposed that in the accomplishment of the reaction there must exist some sort of energetic barrier, connected with the breaking up and regrouping of the bonds. These ideas about the direct molecular interaction have been found to be applicable only in very rare cases.

It has been established that a chemical change takes place in several stages with the formation of a whole series of intermediate products. But this conception also failed to provide the key to an understanding of the mechanism of the progress of chemical reactions and to the calculation of their speeds. For the solution of this problem it was necessary to seek an essentially new mechanism of the progress of chemical reactions.

The fundamental accomplishment of N. N. Semenov and the school he founded lies in the fact that he was the first to construct a chain theory of chemical reactions. The basic role in the mechanism of a chain chemical reaction is played by free radicals. The initial formation of an individual free radical is regarded as an extremely rare and difficult event, but once having been formed, the radical enters into interaction with molecules of the system, is repeatedly regenerated, and thus produces a long chain of chemical changes up to the time when, through causes that are accidental from the point of view of the reaction (destruction at the wall of the vessel, interaction with some other sort of active center), it ends its existence.

Of particular importance was the discovery by Semenov of reactions with branched chains, in which the radicals in the course of their interactions with the molecules are not only regenerated, but also multiplied. If the multiplication predominates over the destruction of radicals, the reaction proceeds with an acceleration, which can lead to an explosion. The actual course of the reaction depends in an essential way on external conditions; for example, if the destruction of active radicals occurs at the walls of the vessel, then the acceleration of the reaction depends in a critical way on the dimensions of the vessel, the pressure, admixtures of inert gas, etc. For example, at a given temperature, pressure, composition of the mixture, and condition of the surface of the walls of the vessel, there exists a critical size of the vessel, beginning at which the multiplication of active centers predominates over their destruction. This size is also the critical one with regard to the chain reaction. This was first discovered in 1926 by Iu. B. Khariton and Z. Val'ta in experiments on the oxidation of phosphorous vapor. The correct interpretation of these experiments was also the initial link in the creation of the chain theory. A model example of a reaction with branching chain is the reaction of oxidation of hydrogen.

$$\begin{gathered} OH + H_2 = H_2O + H, \\ H + O_2 = OH + O, \\ O + H_2 = OH + H. \end{gathered}$$

The result of this chain is that from two molecules of hydrogen and one molecule of oxygen there are obtained, through the participation of an OH radical, one molecule of water and two new radicals OH and H. Thus in the course of the reaction the number of radicals increases sharply.

At the present time the nuclear chain reaction of uranium fission is well known to all. This reaction was predicted theoretically on the basis of the chain theory of chemical reactions. We note that in the case of the nuclear reaction the mechanism of the elementary act and the "active center", i.e., the neutron, were comparatively well known, whereas in the development of the theory of chemical chain reactions, on the other hand, it was necessary to draw the conclusion about the mechanism of the reaction and the nature of the active centers--the free radicals--from the behavior of the reaction itself.

The large amount of experimental and theoretical material accumulated at the Institute of Chemical Physics up to 1934 served as the foundation of N. N. Semenov' s classic monograph ''Chain Reactions'', constantly used as a reference by all workers in the field of chemical physics both in the U. S. S. R. and abroad. The general theory of chain reactions worked out in this book was developed further by Semenov and his collaborators for various classes of chemical reactions: oxidations, polymerizations, thermal cracking, and so on, and is still being elaborated in the Institute of Chemical Physics.

The characteristic feature of the investigations being conducted at the present time is the study of the detailed chemical mechanism of chain reactions, and the determination of the nature of concrete active centers--the atoms and radicals responsible for the development of the process by the chain mechanism.

One of the important branches of chemical kinetics is the theory of combustion and explosion. The introduction of chain concepts has shown itself very fruitful here. The possibility of the occurrence of a chain explosion is readily understood in the case of branching chains. Besides chain explosion, Nikolai Nikolaevich also studied thermal explosion. The theory of thermal explosion which he originated is closely related in method to the theory of thermal breakdown of dielectrics which was mentioned earlier. Under certain conditions the heat produced in the course of a reaction does not have time to be conducted away from the reaction zone and raises the temperature of the system, accelerating the reaction and thus simultaneously speeding up the evolution of heat. These concepts are also essential for an understanding of thermonuclear reactions.

To N. N. Semenov, together with Ia. B. Zel'dovich, there also belongs the credit for important works on the mechanism of combustion and the propagation of flames.

At the present time the theory of the mechanism of chemical processes is still being developed on the basis of the chain theory. Nikolai Nikolaevich is taking the most active part in the development of this theory, penetrating exceptionally deeply into all the questions connected with chemical kinetics, and is the intellectual leader and inspirer of the school he has founded.

The range of Nikolai Nikolaevich's interests is extraordinarily wide. Together with the continuation of the work on the kinetics of various chemical processes, he gives great attention to scientific and methodical questions of nuclear physics. On his initiative and with his direct participation, a series of investigations of nuclear reactions with fast particles was set up in the Institute of Nuclear Problems of the Academy of Sciences of the U.S.S.R. In his study of fast particles, Semenov became interested in the problem of constructing a linear accelerator for the production of large currents. His splendid physical intuition, clearness of thought, and inventiveness enable him to lead the work of a whole association of workers both in this field and in a number of other branches of physics and technology.

N. N. Semenov reaches his sixtieth birthday in the full flower of his creative powers. His colleagues in the Institute of Chemical Physics and many other physicists and chemists of the Soviet Union, having known Nikolai Nikolaevich throughout several decades, have always admired his unusual theoretical activity. All who have ever had personal dealings with Nikolai Nikolaevich or who have made use of his work, wish with all their hearts that he may continue this creative activity for many years.

Translated by W. H. Furry
1 32

The Compton Effect at High Energies

A. A. Abrikosov
Institute of Physical Problems, Academy of Sciences, USSR

(Submitted to JETP editor, April 15, 1955)
J. Exptl. Theoret. Phys. (U.S.S.R.) 30, 386-398 (February, 1956)

The Compton effect is investigated at high energies. Those terms are analyzed which arise from diagrams giving the maximum power of $\ln(\omega/m)$ with each power of e^2. Such terms are of order $[e^2\ln^2(\omega/m)]^n$. Formulas are given for single and multiple Compton effect, for the distribution of secondary photons in energy and angle, and for the energy distribution of secondary electrons. At small angles a peculiar change in the scattering is found, which leads to a change in the refractive index of energetic photons in matter.

In an earlier paper[1] the scattering of an electron by an external field was analyzed, and it was found that at high energies the leading terms in each order of perturbation theory were those containing with every power of e^2 the square of a large logarithm, for example $\ln^2(E/m)$. This was true so long as we were not concerned with the radiation of exceedingly soft photons for which $\ln(m/\omega) > \ln(E/m)$. Here we study in the same approximation the behavior of the Compton effect at high energies. We shall see that the behavior is no longer described, as it was for the scattering problem, by a decrease of the simple effect compensated by an increase of multiple processes.

1. THE COMPTON EFFECT AT NOT TOO SMALL ANGLES

We begin with the simple Compton scattering of a photon by an electron. We use the following notations: p_1 and p_2 are the 4-momenta of the initial and final electron, l_1 and l_2 of the initial and final photon. The momenta satisfy the relation

$$p_1 + l_1 = p_2 + l_2, \tag{1}$$

and we write

$$p = p_1 - p_2 = l_2 - l_1. \tag{2}$$

From Eq. (1) we deduce

$$\begin{aligned}(p_1l_1) &= (p_1p_2) + (p_1l_2) - m^2 \\ &= (p_1l_2) - {}^1/{}_2p^2.\end{aligned} \tag{3}$$

In the electron rest system the scalar products become

$$(p_1l_1) = m\omega_1,\ (p_1p_2) = mE_2,\ (p_1l_2) = m\omega_2,$$

where ω_1 and ω_2 are the energies of initial and final photon, and E_2 the final electron energy. Thus (p_1l_1) is in all cases larger than the other two scalar products. For the relative magnitude of the other two products, we have two extreme cases to consider.

$$\text{I)}\ (p_1p_2) \approx (p_1l_1) \gg (p_1l_2) \tag{4}$$

or

$$\text{II)}\ (p_1l_2) \approx (p_1l_1) \gg (p_1p_2). \tag{5}$$

In Case I the photon transfers almost all its energy to the electron, and in Case II the electron receives only a small part of the energy. If $\omega_1 \gg m$, then case II corresponds to very small angle scattering. Equation (1) implies

$$\omega_1\omega_2(1-\cos\theta) = m(\omega_1-\omega_2), \tag{6}$$

where θ is the photon scattering angle in the rest system of the electron. Case II requires $\omega_1 - \omega_2 \ll \omega_1$ or $\theta \ll \sqrt{m/\omega} \ll 1$. Since the total cross section is proportional to a logarithmic integral, the small-angle region cannot make a significant contribution to it.

We consider first Case I, which is all that is needed for the total cross section. The matrix element for the Compton effect in zero-order approximation is proportional to

$$\frac{\gamma_\sigma(\hat{p}_1+\hat{l}_1)\gamma_\tau}{2(p_1l_1)} - \frac{\gamma_\tau(\hat{p}_1-\hat{l}_2)\gamma_\sigma}{2(p_1l_2)}. \tag{7}$$

We always omit m in the numerator, because the terms in m are negligible at high energies. The first term arises from the diagram in which the photon l_1 is first absorbed and the photon l_2 is emitted afterwards, the second term for the diagram in which the order is inverted. Because we are considering Case I, the second term is much larger than the first. Thus the fundamental Feynman diagram for the Compton effect is the one shown in Fig. 1*a*. We shall not go further into the calculation of the single Compton effect. We mention only the fact that, if the total cross section is expressed as an integral over ω_2, the important range of integration is $m \ll \omega_2 \ll \omega_1$. In this range the integration over ω_2 behaves logarithmically.

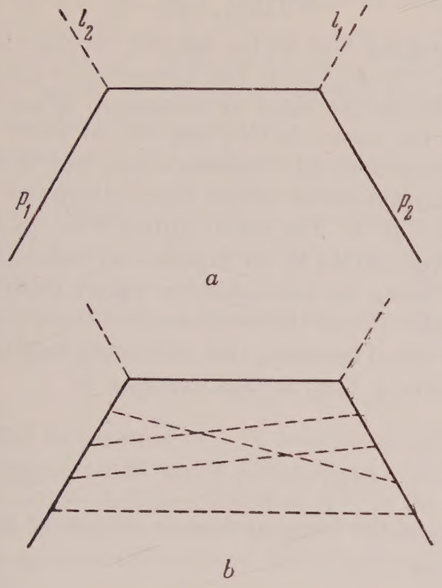

FIG. 1

We now introduce virtual lines. Since the radiative corrections to electron and photon propagators contain only a single large logarithm, these corrections need not be considered. The vertex parts in this diagram have one large electron momentum (in the sense that the square of the 4-momentum is large)and twosmall momenta corresponding to the free electron and photon. In the important range of integration, $(p_1 - l_2)^2 \approx -2(p_1 l_2) = 2m\omega_2 \gg m^2$. Sudakov[2] has proved that such vertex parts do not give doubly-logarithmic terms. Hence we need only consider diagrams of the kind shown in Fig. 1*b*.

We begin with the first-order radiative correction. This is described by an integral which we multiply on the left by $\hat{p}_1$ and on the right by $\hat{p}_2$ to obtain the result

$$j = \frac{e^2}{\pi i}\int \frac{\hat{p}_1\gamma_\mu(\hat{p}_1 - \hat{k})\gamma_\tau(\hat{p}_1 - \hat{l}_2 - \hat{k})\gamma_\sigma(\hat{p}_2 - \hat{k})\gamma_\nu \hat{p}_2 d_{\mu\nu}(k)\, d^4k}{[(p_1 - k)^2 - m^2]\,[(p_1 - l_2 - k)^2 - m^2]\,[(p_2 - k)^2 - m^2]\, k^2}\,. \tag{8}$$

It differs from the integral considered previously[1] by having an extra factor in the denominator. We decompose k into components along the small vectors p_1 and p_2 and in the plane perpendicular to p_1 and p_2, as in Reference 1,

$$k = p_1\left(\frac{a^2u - av}{a^2 - 1}\right) + p_2\left(\frac{a^2v - au}{a^2 - 1}\right) + k_\perp,\quad x = -k_\perp^2,$$

with $a = (p_1 p_2/m^2)$. Then

$$(p_1 - l_2 - k)^2 - m^2 \approx -2(p_1 l_2) - 2(k_\perp,\ (p_1 - l_2)_\perp) + k^2.$$

We used the fact that in the important range u and v are small. The extra factor in the denominator now depends on the angle in the plane of $k_\perp$. Averaging over this angle, we find

$$\overline{[(p_1 - l_2 - k)^2 - m^2]^{-1}} = \{[k^2 - 2(p_1 l_2)]^2 + 4x(p_1 - l_2)_\perp^2\}^{-1/2}. \tag{9}$$

Here $(p_1 - l_2)_\perp$ is the component of $(p_1 - l_2)$ in the plane of $k_\perp$. The square of it is $(p_1 - l_2)_\perp^2 = (p_1 - l_2)^2 - (p_1 - l_2)_\parallel^2$. Since $(p_1 - l_2)_\parallel^2 \ll (p_1 - l_2)^2$, we write $(p_1 - l_2)_\perp^2 \approx (p_1 - l_2)^2$. Therefore the square root in Eq. (9) is $-2(p_1 l_2)$ when $x \ll (p_1 l_2)$, and is k^2 when $x \gg (p_1 l_2)$.

In the first case we are reduced to the same integral. which was evaluated for the vertex parts,[2] though the range of the variables is different, and there is the extra constant denominator $-2(p_1 l_2)$. In the second case we have an extra k^2 in the denominator, and so the terms in the numerator containing $\hat{k} \ldots \hat{k}$ become important. But in this case we find $(p_1 p_2)$ instead of $(p_1 l_2)$ in the denominator. Since $(p_1 p_2) \gg (p_1 l_2)$, the contribution from the range $x \gg (p_1 l_2)$turns out to be negligible.

Thus we are dealing with an integral similar to the one considered earlier.[1] We may therefore neglect $\hat{k}$ in the numerator and change $d_{\mu\nu}(k)$ into $\delta_{\mu\nu}$. The doubly-logarithmic integral is obtained after taking the residue of the x-integration at the point $k^2 = 0$. To determine the ranges of integration of the variables u and v, we use the results of the earlier paper.[1] We shall not consider secondary photons with energy less than m in the laboratory system. This means that any number of such soft photons may be emitted during the primary process.

In general, to find the cross section, we ought to sum over processes involving any number of real photons, integrating over each photon momentum up to $(pk) \sim m^2$. But we showed before[1] that such a summation gives the same result as putting

$$(p_1^2 - m^2)/2m \sim m, \quad (p_2^2 - m^2)/2m \sim m/(p_1 p_2) \tag{10}$$

in our integrals. The limit of the x-integration is set, as we have seen, by the condition

$$x \ll (p_1 l_2). \tag{11}$$

Since we are taking the residue at the point $k^2 = 0$ or $x = (p_1 p_2)uv$, Eq. (11) reduces to

$$k^2 = 0 \quad \text{or} \quad x = (p_1 p_2)uv: \qquad |uv| \ll (p_1 l_2)/(p_1 p_2). \tag{12}$$

In terms of the variables $\lambda = -\ln v$, $\mu = -\ln u$, the region of integration has the form shown in Fig. 2. The integral is proportional to the shaded area and is equal to

$$J = -\frac{\hat{p}_1 \gamma_\tau (p_1 - p_2) \gamma_\sigma \hat{p}_2}{2(p_1 l_2)} \times \left[-\frac{e^2}{2\pi}\left(\frac{3}{2}\ln^2\frac{(p_1 p_2)}{m^2} - \frac{1}{2}\ln^2\frac{(p_1 p_2)}{(p_1 l_2)}\right)\right]. \tag{13}$$

This result differs from the zero-order approximation (7) only by the factor in square brackets.

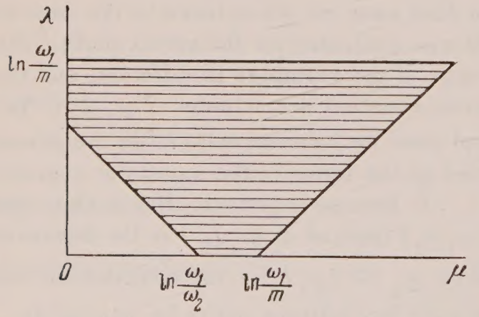

FIG. 2

Let there now be two virtual photons. In this case the extra denominator in the matrix element becomes

$$(p_1 - l_2 - k_1 - k_2)^2 - m^2 \approx -2(p_1 l_2) - 2(k_{1\perp}, (p_1 - l_2)_\perp) - 2(k_{2\perp}, (p_1 - l_2)_\perp) + k_1^2 + k_2^2.$$

After averaging over all the angles, we find that the condition (12) applies to the momentum of each photon. Hence the range of integration of each photon is the same. In this way we can carry out the summation over all diagrams of the type of Fig. 1*b* with any number of virtual lines, using the method of Ref. 1. The result differs from the zero-order approximation by an exponential factor, the exponent being the expression in square brackets in Eq. (13). Hence the cross section for the single Compton-effect (meaning that only one photon is emitted with $\omega > m$) at high energies is

$$d\sigma = d\sigma_0 \exp\left[-\frac{e^2}{\pi}\left(\frac{3}{2}\ln^2\frac{\omega_1}{m} - \frac{1}{2}\ln^2\frac{\omega_1}{\omega_2}\right)\right], \tag{14}$$

where $d\sigma_0$ is the cross section in zero-order approximation

$$d\sigma_0 = (\pi e^4/m\omega_1)\, d\omega_2/\omega_2. \tag{15}$$

We have used the conditions (10) to replace the procedure of introducing fictitious values for $(p_1^2 - m^2)$ and $(p_2^2 - m^2)$ and calculating consistently the radiation of real photons with energy less than m in the electron rest system. We now investigate the radiation of secondary photons of higher energy. First we look at the double Compton effect in zero-order approximation. We can insert into the generalized Feynman diagram[1] three kinds of lines representing real photons. Lines connecting equal electron momenta, as we saw earlier,[1] give singly-logarithmic contributions when $p^2 - m^2 \ll m^2$ and otherwise give no logarithmic contributions at all. If a real photon line connects an electron line with momentum p_1 to a line with momentum $(p_1 - l_2)$, then the integral is the same as it would be for a virtual photon line overlapping one vertex, and this does not give doubly-logarithmic contributions either. A doubly logarithmic integral arises only when a real photon line connects electron lines with momenta p_1 and p_2, just as in the case of a virtual photon. The momenta of real photons satisfy the conditions

$$(p_1 k) \ll (p_1 p_2), \quad (p_2 k) \ll (p_1 p_2), \tag{16}$$

$$a\,(p_1k) > (p_2k) > (p_1k)\,/\,a, \qquad (17)$$

with $a = (p_2\,p_2)/\,m^2$. In terms of the variables λ and μ this means $\lambda, \mu > 0$, $\lambda - \ln a < \mu < \lambda + \ln a$. The condition $\omega > m$ gives $\lambda < \ln a$. These conditions on the ranges of integration for real photons are the same as for virtual photons.

It remains to see whether a condition analogous to equation (12) will exist. This condition arose from the electron line with momentum $(p_1 - l_2)$. In the formula for the transition probability, these lines give a factor $[(p_1 l_2)(p_2 l_1)]^{-1}$. We now have $(p_2 l_2) \neq (p_1 l_2)$ because the conservation of momentum gives

$$p_1 + l_1 = p_2 + l_2 + k, \qquad (18)$$

instead of equation (1). A detailed analysis of the new denominator, which we shall not reproduce here, shows that the condition (12) is the same for real as it was for virtual photons. Hence the ranges of integration for real and virtual photons are identical.

It is now wasy to write down the cross section for the n-fold Compton effect. As in Ref. 1, it follows a Poisson distribution

$$d\sigma = d\sigma_0\, e^{-\bar{n}}\, (\bar{n})^n / \,n!, \qquad (19)$$

in which the average multiplicity $\bar{n}$ is given by

$$\bar{n} = \frac{e^2}{\pi}\left(\frac{3}{2}\ln^2\frac{\omega_1}{m} - \ln^2\frac{\omega_1}{\omega_2}\right). \qquad (20)$$

2. PROPERTIES OF THE SECONDARY PHOTONS

We now examine the physical meaning of the results we have obtained. The important range of integration for the momenta of both virtual and real photons is defined by the conditions (16), (17) and (12). We write condition (12) in the form

$$(p_1k)\,(p_2k) \ll (p_1p_2)\,(p_1l_2). \qquad (21)$$

Within the important range, the cross section for double Compton effect in the zero-order approximation has the form

$$d\sigma = d\sigma_0\,\frac{e^2}{\pi}\,\frac{du}{u}\,\frac{dv}{v}. \qquad (22)$$

We can express u and v in terms of the energy and angle of the photon in the laboratory system,

$$u = \omega/\omega_1, \quad v = (\omega/m)(1 - \beta\cos\theta), \qquad (23)$$

where $\beta = \sqrt{E_2^2 - m^2}/E_2 \approx 1$

$$- m^2/2E_2^2 \approx 1 - m^2/\,2\omega_1^2$$

is the velocity of the outgoing electron. Then Eq. (22) takes the form

$$d\sigma = d\sigma_0\,\frac{2e^2}{\pi}\,\frac{d\theta}{\theta}\,\frac{d\omega}{\omega}. \qquad (24)$$

Here we used the fact that $v \ll 1$, which implies that also $\theta \ll 1$.

Equation (24) coincides with the result of a purely classical treatment. This becomes understandable if we write conditions (16) and (17), which limit the important range of integration, in the center of mass system. Equation (16) then implies

$$\omega_{cm} \ll \omega_{1\,cm}, \qquad (16')$$

which means that the secondary photon has a much smaller energy than the primary particles. Equation (21) gives

$$\omega_{cm}\sin\theta_{cm} \ll \omega_{2\,cm}\theta_{2\,cm}. \qquad (21')$$

This means that the transverse momentum of the secondary photon is much smaller than the transverse momentum of the primary. This is not a consequence of (16′); in fact $(p_1 l_2) \ll (p_1 l_1)$ implies $\theta_{2CM} \ll 1$, and so the transverse momentum of photon l_2 is much smaller than the longitudinal momentum.

Equations (16′) and (21′) show that in the important range of values of the momentum of the secondary photon, the radiation of that photon has a negligible reaction on the momenta of the primary particles, and so the secondary radiation can be treated classically. The same circumstance explains the fact which we discovered earlier, that the radiation of successive secondary photons is statistically independent. The probability that a certain number of successive independent events will occur follows a Poisson distribution, as we have found by actual calculation. Thus quantum electrodynamics here leads to the result that the important range of integration is the range where classical theory is valid. A correct treatment of the virtual processes leads to a Poisson distribution. Knowing this result, we can use the classical theory of radiation for practical calculations, the conditions for validity of classical methods being easily stated in the center of mass system.

We now collect some formulas which describe the secondary radiation. We have seen that the radiation of different secondary photons is independent. Therefore the coefficient of $d\sigma_0$ in Eq. (24) gives the distribution of secondary photons in energy and angle in the laboratory system. Conditions (16), (17) and (21) give the following limits to the distribution in the laboratory system,

$$\theta \gg m/\omega_1, \tag{25}$$

$$\theta \ll \sqrt{m/\omega} \quad \text{for} \quad \omega < \omega_2, \tag{26}$$

$$\theta \ll \sqrt{m\omega_2/\omega^2} \quad \text{for} \quad \omega > \omega_2, \tag{27}$$

$$m \ll \omega \ll \omega_1. \tag{28}$$

If we are interested only in the energy distribution, then Eq. (24) should be integrated over the range of angles defined by Eqs. (25)-(28). The result is

$$dn(\omega) = \frac{2e^2}{\pi}\frac{d\omega}{\omega}\ln\frac{\omega_1}{\sqrt{m\omega}} \quad \text{for} \quad \omega < \omega_2,$$

$$dn(\omega) = \frac{2e^2}{\pi}\frac{d\omega}{\omega}\ln\frac{\omega_1}{\omega}\sqrt{\frac{\omega_2}{m}} \quad \text{for} \quad \omega > \omega_2. \tag{29}$$

If we are only interested in the angular distribution of photons with energy greater than m, then Eq. (24) must be integrated with respect to ω. This gives

$$dn(\theta) = \frac{2e^2}{\pi}\frac{d\theta}{\theta}\ln\frac{\omega_1}{m} \quad \text{for} \quad \frac{m}{\omega_1} < \theta < \frac{\sqrt{m\omega_2}}{\omega_1},$$

$$dn(\theta) = \frac{2e^2}{\pi}\frac{d\theta}{\theta}\ln\frac{1}{\theta}\sqrt{\frac{\omega_2}{m}} \tag{30}$$

$$\text{for} \quad \frac{\sqrt{m\omega_2}}{\omega_1} < \theta < \sqrt{\frac{m}{\omega_2}},$$

$$dn(\theta) = \frac{2e^2}{\pi}\frac{d\theta}{\theta}\ln\frac{1}{\theta^2} \quad \text{for} \quad \theta > \sqrt{\frac{m}{\omega_2}}.$$

The average number of secondary photons for given ω_2 is obtained by integrating Eq. (29) or (30) with respect to ω or θ, respectively. The result agrees with Eq. (20).

We consider next the following question. From Eq. (29) we see that, although in the center-of-mass system the secondary photons are much softer than the primary outgoing photon; in the laboratory system the reverse may be true. We shall calculate the probability for a given energy loss of the outgoing electron, compared with the primary photon energy. We denote this energy loss of the electron by ϵ; it is equal to the sum of the energies of the outgoing photons. Since the integrals over the photon energies are always logarithmic, we may suppose that one of the outgoing photons carries a much larger energy than the others. So we have to deal with an integral over the energies and angles of outgoing photons, for a given value of the energy of the most energetic among them.

In the expression for the cross section there are two terms. One gives the probability that all the secondary photons have energy less than the primary outgoing photon. This is obtained by multiplying the zero-order cross section by the probability for the absence of secondary photons of energy greater than ω_2. From the Poisson law it follows that this probability is $e^{-\bar{n}}$, where $\bar{n}$ is the average number of secondary photons of energy greater than ω_2. To obtain $\bar{n}$ we integrate Eq. (29) with respect to ω from ω_2 to ω_1. This gives

$$d\sigma' = d\sigma_0 \exp\left(-\frac{e^2}{\pi}\ln\frac{\omega_1}{m}\ln\frac{\omega_1}{\omega_2}\right). \tag{31}$$

In the first term of the cross section, the energy removed by photons is the energy of the primary outgoing photon, so that we put $\omega_2 = \epsilon$ in Eq. (31).

The second term in the cross section gives the probability that one of the secondary photons has energy greater than ω_2. Hence ϵ is the energy of the hardest secondary photon. The probability that a secondary photon has energy in the interval $d\epsilon$ is

$$\frac{2e^2}{\pi}\frac{d\varepsilon}{\varepsilon}\ln\frac{\omega_1}{\varepsilon}\sqrt{\frac{\omega_2}{m}}.$$

For this to be the hardest photon it is necessary that photons of higher energy be absent. The corresponding probability is $e^{-\bar{n}}$, where $\bar{n}$ is obtained by integrating Eq. (29) with respect to ω from ϵ to ω_1, thus

$$\left(\bar{n} = \frac{e^2}{\pi}\ln\frac{\omega_1\omega_2}{\varepsilon m}\ln\frac{\omega_1}{\varepsilon}\right).$$

Since the primary outgoing photon has energy small compared with ϵ, we are not interested in the distribution of its energy and we integrate the cross section at once with respect to ω_2 from m to ϵ. The final expression for the cross section is obtained by adding this integral to equation (31).

We calculate the probability $dw(\epsilon)$ that the energy loss of the electron will lie in the interval $d\epsilon$. This is obtained by dividing $d\sigma$ by the total cross section, which is in turn the integral of $d\sigma$ with respect to ϵ from m to ω_1. The total cross section is equal to the zero-order expression for the Compton scattering

$$\sigma = (\pi e^4/m\omega_1)\ln(\omega_1/m). \tag{32}$$

This must be so, because the Poisson distribution is normalized to unity. The probability for an energy loss in the interval $d\epsilon$ is then

$$dw(\varepsilon) = \frac{1}{\ln(\omega_1/m)} \frac{d\varepsilon/\varepsilon}{(e^2/\pi)\ln^2(\omega_1 \varepsilon)} \left[\left(\frac{2e^2}{\pi}\ln^2\frac{\omega_1}{\varepsilon}+1\right) \times \exp\left(-\frac{e^2}{\pi}\ln^2\frac{\omega_1}{\varepsilon}\right) + \left(\frac{e^2}{\pi}\ln\frac{\omega_1}{\varepsilon}\ln\frac{\omega_1}{m}+1\right) \exp\left(-\frac{e^2}{\pi}\ln\frac{\omega_1}{\varepsilon}\ln\frac{\omega_1}{m}\right)\right]. \tag{33}$$

Equations (19), (20), (29), (30) apply unchanged to the process of multiple-photon annihilation of an energetic positron with an electron (again we consider only photons with energy greater than m). The diagram for this process is identical with the Compton-effect diagram. The difference is only that the most energetic particle is the positron instead of the incident photon; hence, we should replace ω_1 by the position energy E in the final results. Also, for the annihilation process case II cannot occur, and so the calculations we have made for case I apply directly to the positron cross section.

Our calculations of multiple radiation, although immediately applicable only to the two specific processes considered, contain in fact many features which are common to all processes involving secondary radiation. The two most important features are the classical behavior of the radiation, and the doubly-logarithmic order of magnitude of the radiation probability.

It is of interest to discuss the various practical conditions under which one of these processes might be observed. For definiteness we shall consider the multiple-photon annihilation of a positron. This process was studied by Gupta,[3] who suggested it as an explanation of the famous photon shower of Schein.[4] Gupta's preliminary calculation led to a completely incorrect result

$$d\sigma^{(n+2)} = d\sigma^{(2)}\left(\frac{e^2}{\pi}\ln^2\frac{E}{m}\right)^n,$$

quite different from Eq. (19). Gupta concluded that multiple-photon annihilation becomes highly probable at energies of the order of 10^{14} ev, comparable with the total energy of the Schein event. In fact, however, Eq. (20) shows that in the most favorable case 10^{-13} ev are necessary for the production of a single secondary photon. To produce on the average 20 photons, the number observed in the Schein event, we should need at least 10^{38} ev, an energy far beyond the range of validity of contemporary electrodynamics. In any case the positron spectrum in cosmic rays falls rapidly with energy, and particles of such high energy are certainly not present. Such a star might arise more easily from a multiple-photon fluctuation in the annihilation of a positron of much lower energy. Suppose $E = 10^{14}$ ev. The average number of secondary photons for a positron of this energy is about 1. The probability for creating 20 photons is then 10^{-18} times the probability for creating one.

Our equations thus show that with positrons of practically attainable energy the number of observable secondary photons will be quite small. This number may become even smaller as a result of the material in which the process occurs. The material produces this effect in two ways; by its refractive index, and by multiple scattering.

We consider first the effect of refractive index. The importance of this effect was pointed out by Ter-Mikaelyan.[5] It works as follows. In Eq (20), strictly speaking, there stands $[d\cos\theta(-\beta\cos\theta)]$, which for angles in the range $1 >> \theta >> (1-\beta)^{1/2}$ can be approximated by $[2d\theta/\theta]$. Here we took β to be equal to its vacuum value $\beta_0 = (E^2 - m^2)^{1/2}/E$. If the material has a refractive index n, then the true value of β is $\beta_0 n$. For photons of high energy

$$n^2 = 1 - (4\pi e^2 N/m\omega^2),$$

where N is the number of electrons per cubic centimeter. So we obtain in addition to Eq. (25) a new lower bound for θ,

$$\theta \gg \omega^{-1}\sqrt{4\pi e^2 N/m}. \tag{34}$$

The second effect of the material was noticed by Landau and Pomeranchuk.[6] It takes place as follows. Multiple radiation is a process extended over a certain time τ. During this time the radiating particle is multiply scattered, and this changes the probability of radiation. The result is another condition of the form $\theta >> \theta_p$ limiting the range in which the cross section behaves logarithmically.

The mean scattering angle θ_p is given by[7]

$$\overline{\theta_p^2} = xE_s^2/E^2\beta^2,$$

where

$$E_s = m\sqrt{4\pi/e^2} = 21\text{ eV},$$

and x is the distance in radiation lengths. Since $\beta = 1$, and the time entering into the process is of the order of magnitude

$$\tau \sim (\omega - kv)^{-1} \approx 2/\omega\theta^2,$$

the lower bound for the angle becomes

$$\theta \gg (2E_s^2 / E^2 X_0 \omega)^{1/4}, \qquad (35)$$

where X_0 is the radiation length of the material. In Fig. 3 the area of integration is shown in terms of the variables $\ln(\omega/m)$ and $\ln(l/\theta)$. In the lower right corner are lines representing the conditions (34) and (35). They are given by the equations

$$\ln\frac{1}{\theta_1} = \ln\frac{\omega}{m} + a, \quad \ln\frac{1}{\theta_2} = \frac{1}{4}\ln\frac{\omega}{m} + b,$$

$$a = \frac{1}{2}\ln\frac{m^3}{4\pi e^2 N}, \quad b = \frac{1}{4}\ln\frac{mX_0E^2}{2E_s^2}.$$

These lines cut a certain part out of the shaded area. The quantity $\overline{n}$ is proportional to the remaining area.

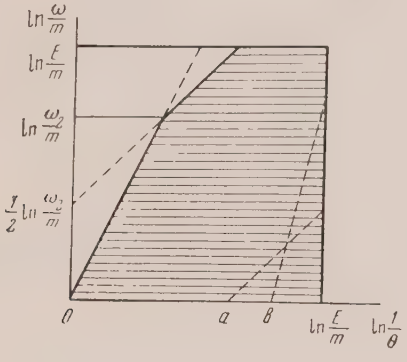

FIG. 3

The numerical value of the reduction in the area depends on the energy of the process and on the material. Thus, for the annihilation of a positron of energy $E=10^{14}$ ev in air, the most favorable case is $\omega_2=\omega_1$. In this case condition (34) removes 0.057 of the area, and condition (35) removes 0.066. The two conditions together reduce $\overline{n}$ by 0.083 of its original value. The effect of conditions (34) and (35) can be seen more clearly by looking at the energy which corresponds to a given $\overline{n}$. If these conditions are ignored, then $E= 10^{14}$ ev corresponds to $\overline{n}=1.27$. When the conditions are taken into account, the same value of $\overline{n}$ corresponds to $E= 2.2 \times 10^{14}$ ev.

3. THE COMPTON EFFECT AT SMALL ANGLES

Although the region of small angles [case II or equation (5)] is unimportant for calculating the total cross section, we shall study it in detail because an interesting effect occurs in it. We now deal with momenta satisfying the inequality $(p_1 l_2) \sim (p_1 l_2) >> (p_1 p_2)$. In this case both the Compton effect diagrams are of the same order of magnitude. We consider again an integral of the form of equation (8). In it there is a doubly-logarithmic region of the same kind as we found in Section 1, but without any limit on $|uv|$. The situation in this case looks at first glance identical with the situation in the scattering problem.[1]

However, this is not the only way to obtain a doubly-logarithmic integral. We make the substitution $k \to p_1 - k$. Then the integral takes the form

$$J = \frac{e^2}{\pi i}$$

$$\times \int \frac{\hat{p}_1 \gamma_\mu \hat{k} \gamma_\tau (\hat{k} - \hat{l}_2) \gamma_\sigma (-\hat{p} + \hat{k}) \hat{\gamma}_\nu \hat{p}_2 d_{\mu\nu} (p_1 - k)\, d^4k}{(k^2 - m^2)[(k - l_2)^3 - m^2][(k - p)^2 - m^2](k - p_1)^2}.$$

This integral can give a doubly-logarithmic contribution only when a factor k^2 appears in the denominator to cancel the small quantity $\hat{k}$ in the numerator. We resolve $k_{\parallel}$ into components along the small vectors l_2 and p_1; thus $k = p_1 u + l_2 v + k_\perp$. An extra power of k can come only from the factor ($[(k-p)^2 - m^2]$

We now examine this term in detail. If $u, v << 1$, it becomes

$$(k - p)^2 - m^2$$

$$= k^2 - m^2 + p^2 - 2k_\perp p_\perp \cos\varphi, \qquad (36)$$

and averaging over φ gives

$$\overline{[(k - p)^2 - m^2]^{-1}}$$

$$= [(p^2 + k^2 - m^2)^2 - 4x'\, p^2|]^{-1/2}.$$

To obtain a factor k^2 out of this, we must have

$$|uv| \gg |p^2| / (p_1 l_2). \qquad (37)$$

The situation here is just the opposite of what happened in the preceding paragraphs. In the x-integration the important contribution is the residue of the pole at $k^2 = m^2$. In order that $x > 0$ at the pole, we must have $(p_1 l_2)\, uv > m^2$. Together with Eq. (37), this condition may be written in the form

$$|uv| \gg (p_1 p_2) / (p_1 l_2). \qquad (38)$$

We now return to Eq. (36). If the ϕ-integration is carried out in the complex plane, the main contribution comes from the residue of the pole at which $[(p-k)^2 - m^2]$ vanishes. In the subsequent integration we set $k^2 = m^2$ and $|p^2| << x$, so that the pole occurs at a real value of ϕ. Thus we come to the conclusion that the values of k which are important in the integral are those at which both electron propagators have poles.

Since the small-angle scattering is almost coherent, we may assume the vectors p_1 and p_2 in the laboratory system to be small compared with l_1 and l_2. Consequently, the second factor k in the numerator can only come from the term $(-\hat{p} + \hat{k})$. The factors $\hat{k} \ . \ . \ . \ \hat{k}$ can then be replaced by $\hat{k}_\perp \ . \ . \ . \ \hat{k}_\perp$, since the remainder is an expression with uncompensated small factors in the numerator. For the same reason, when we average over the direction of k, it is sufficient to keep only the term $- 1/2 \ (\gamma_\mu \ . \ . \ . \ \gamma_\mu) \ x$. After this we carry out the calculation in exactly the same way as before, and obtain

$$J = \frac{e^2}{4\pi} \frac{\hat{p}_1 \gamma_\tau (-\hat{\iota}_2) \gamma_\sigma \hat{p}_2}{-2(p_1 l_2)} \ln^2 \frac{(p_1 l_2)}{(p_1 p_2)} . \quad (39)$$

Next we look at the matrix element corresponding to a diagram with two virtual photon lines. Suppose the two lines do not cross. Then the denominator is

$$\begin{aligned} &[(p_1 - k_1)^2 - m^2] \, [(p_1 - k_1 - k_2)^2 - m^2] \\ &\quad \times \ [(p_1 - l_2 - k_1 - k_2)^2 - m^2] \\ &\quad \times [(p_2 - k_1 - k_2)^2 - m^2] \\ &\quad \times \ [(p_2 - k_1)^2 - m^2] \, k_2^2 \, k_1^2 . \end{aligned}$$

We make the substitution $p_1 - k_1 - k_2 \rightarrow k_2, \quad p_1 - k_1 \rightarrow k_1$. This gives

$$\begin{aligned} &(k_1^2 - m^2) \ (k_2^2 - m^2) \\ &\quad \times \ [(k_2 - l_2)^2 - m^2] \, [(k_2 - p)^2 - m^2] \\ &\quad \times [(k_1 - p)^2 - m^2] \, (k_1 - k_2)^2 \, (k_1 - p_1)^2 . \end{aligned}$$

The integral over k_2 is now of exactly the same kind as the one considered previously. We first resolve $k_{2\parallel}$ into components along k_1 and l_2, and then find the k_1-integration has also the same form as before. But when the two photon lines cross, this does not happen.

We now examine various other arrangements of virtual lines which might give doubly-logarithmic terms. First we remark that the kind of doubly-logarithmic term obtained above is unique and does not arise from other types of diagram. However, the possibilities for obtaining infra-red integrals (with $k^2 = 0$) are greatly increased by inserting electron lines with $p^2 = m$. Suppose there is a diagram with one virtual photon line, giving an integral of the kind considered earlier (in Fig. 4 the heavy lines form such a diagram.) If we now add virtual lines with $k^2 = 0$, as shown in Fig. 4*a* by the lines labelled *1* and *2*, the leading terms will contain factors of the form $\ln [m^2/(k^2 - m^2)]$. But in the subsequent integration these lines do not give any contribution of the required order. Thus, if we begin with the diagram formed by the heavy lines, the addition of lines with $k^2 = 0$, either lying between the heavy lines or closer to the original vertices, does not give any new doubly-logarithmic terms.

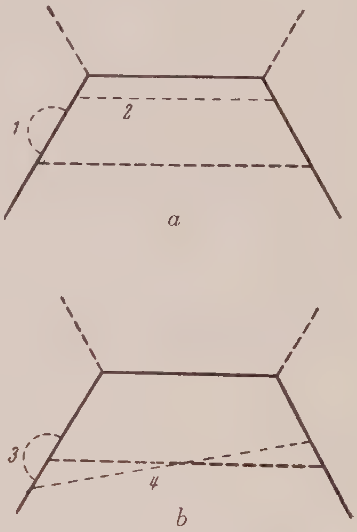

FIG. 4

Next we consider the addition of lines overlapping the ends of the heavy lines (line *3* in Fig. 4*b*). The original vertices have electrons incident with $p^2 = m^2$, and photons incident with momenta whose squares are much greater than m^2. In these circumstances infra-red terms appear. But if we add a line with $k^2 = 0$ intersecting the heavy line (line *4* in Fig. 4*b*), then it almost exactly cancels the infra-red term from the line *3* enclosing the vertex. In fact it is easy to verify that line *4* has no effect on the heavy line. The integral arising from line *4* is very similar to the integral arising from line *3*, only it has the opposite sign. In Ref. 1 we proved that integrals from infra-red virtual lines are proportional to the area of the shaded strip in Fig. 1 of Ref. 1. When we add the contributions from lines *3* and *4*, the result is proportional to the difference between the areas of two strips with width $\ln(kp_1/m^2)$ and $\ln[p_1(k-p)/m^2]$. So the sum is proportional to

$$\ln\frac{(kp_1)}{(p_1(k-p))} = -\ln\left[1-\frac{p^2}{2(p_1k)}\right]^{-1} \approx \frac{p^2}{2(p_1k)} \ll 1.$$

This is small by virtue of Eq. (38) and the fact that $v \ll 1$.

We are therefore left only with infra-red virtual lines which follow after the heavy lines. Also, if we consider generalized diagrams and put in real photon lines, we must study the effects of real lines corresponding to virtual lines of the types *3* and *4* (lines *1* and *2* in Fig. 5). But these real lines give small terms, just like the virtual lines. Therefore there remain only the real and virtual lines of the kind shown in Fig. 5*b* (lines *3* and *3′*). These lines represent the radiation of photons with $(p_1k) \ll (p_1p_2)$, which means that the photon energies are small compared with the electron recoil energy, which is itself very small in this case. Such soft photons are not of interest, and we do not wish to set any limit to the number of them which may be radiated. This implies that we take into account only the integrals arising from heavy lines.

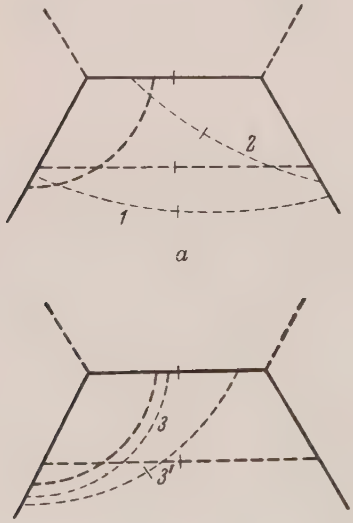

a

b

FIG. 5

Since the heavy lines do not cross, we can sum them by means of an integral equation. The equation

$$\hat{p}_1 M_{\tau\sigma}(p_1, p_2; p_1 - l_2)\hat{p}_2 = \frac{\hat{p}_1\gamma_\tau(\hat{p}_1-\hat{l}_2)\gamma_\sigma\hat{p}_2}{-2(p_1l_2)} + \frac{e^2}{\pi i}\hat{p}_1\int\gamma_\mu\frac{1}{\hat{k}-m}M_{\tau\sigma}(k, k-p; k-l_2) \times \frac{1}{\hat{k}-\hat{p}-m}\gamma_\mu\frac{d^4k}{(k-p_1)^2}\hat{p}_2 \qquad (40)$$

is satisfied by the sum of all matrix elements of the form (10). Neglecting some small terms, we look for a solution $M_{\tau\sigma}$ of the form

$$M_{\tau\sigma}(p_1, p_2; p_1 - l_2) = \frac{\gamma_\tau\hat{l}_2\gamma_\sigma}{2(p_1l_2)} f\left(\frac{(p_1l_2)}{(p_1p_2)}\right). \qquad (41)$$

We chose the argument of the function f so as to agree with equation (39). We can greatly simplify the equation for f, using the same method which we used to calculate the first approximation to $M_{\tau\sigma}$. We also introduce the logarithmic variables $(-\ln u) = \lambda$ and $(-\ln v) = \mu$. The range of integration is then a triangle bounded by the coordinate axes and by the line $\lambda + \mu = \alpha = \ln[(p_1l_1)/(p_1p_2)]$. The equation for f reduces to

$$f(\alpha) = 1 + \frac{e^2}{2\pi}\int^{\alpha} d\lambda \int_0^{\alpha-\lambda} d\mu\, f(\alpha-\lambda), \qquad (42)$$

or

$$f(\alpha^2) = 1 + \frac{e^2}{4\pi}\int_0^{\alpha^2} f(x)\,dx.$$

The solution is $f = \exp\left\{\frac{e^2}{4\pi}\alpha^2\right\}$.

When we sum the matrix elements of the other class, in which the photon l_1 is absorbed first and the photon l_2 emitted afterwards, the result differs from that obtained above only in the spinor factor. Since $(p_1l_2) \sim (p_1l_2)$, the function f is the same. Hence the cross section is given by multiplying the usual expression by the square of the f-factor.

The result is of interest because, unlike the cases considered earlier, it shows a doubly-logarithmic factor which is not simply a normalization of the cross section to compensate for multiple processes. The deviation of the cross section with emission of any number of secondary photons from the zero-approximation cross section occurs only at small angles, so that the effect resembles a diffraction phenomenon. The small-angle angular distribution in the laboratory system is

$$d\sigma = \frac{2\pi e^4}{m^2}\,\theta\, d\theta \exp\left(\frac{e^2}{2\pi}\ln^2\frac{m}{\omega_1\theta^2}\right) \qquad (43)$$

$$\text{при } \sqrt{m/\omega_1} \gg \theta \gg m/\omega_1,$$

$$d\sigma = \frac{2\pi e^4}{m^2}\,\theta\, d\theta \exp\left(\frac{e^2}{2\pi}\ln^2\frac{\omega_1}{m}\right) \qquad (44)$$

$$\text{при } \theta \ll m/\omega_1.$$

The most important effect here is the change in the coherent scattering, for which the amplitude is multiplied by $\exp\left(\frac{e^2}{4\pi}\ln^2\frac{\omega_1}{m}\right)$. This gives the following formula for the refractive index at high frequencies:

$$1 - n^2 = \frac{4\pi N e^2}{m\omega^2}\exp\left(\frac{e^2}{4\pi}\ln^2\frac{\omega}{m}\right). \qquad (45)$$

In conclusion I take the opportunity to thank Academician L. D. Landau for his valuable advice.

---

[1] A. A. Abrikosov, J. Exptl. Theoret. Phys. (U.S.S.R.) 30, 96 (1956); Soviet Phys. JETP 3, 71 (1956).

[2] V. V. Sudakov, J. Exptl. Theoret. Phys. (U.S.S.R.) 30, 87 (1956); Soviet Phys. JETP 3, 65 (1956).

[3] S. N. Gupta, Phys. Rev. 96, 1453 (1954).

[4] M. Schein, D. M. Haskin and R. G. Glasser, Phys. Rev. 95, 855 (1954).

[5] M. Ter-Mikaelian, Dokl. Akad. Nauk SSSR 94, 1033 (1954).

[6] L. D. Landau and I. Ia. Pomeranchuk, Dokl. Akad. Nauk SSSR 92, 535, 735 (1953).

[7] B. Rossi and K. Greisen, Revs. Mod. Phys. 13, 240 (1941).

Translated by F. J. Dyson
66

SOVIET PHYSICS JETP VOLUME 3, NUMBER 4 NOVEMBER, 1956

Concerning the Interaction Cross Sections of Neutrons with Nuclei

P. E. NEMIROVSKII

(Submitted to JETP editor December 1, 1954)
J. Exptl. Theoret. Phys. (U.S.S.R.) 30, 551-559 (March, 1956)

There is proposed a new quasi-classical solution of the Schrödinger equation for $E > |V|$. This approximation is applied to the solution of the problem of the motion of a neutron in a potential with a complex component. An explanation is obtained for the behavior of total cross sections in the energy region 20-100 mev. For energies of 2-10 mev the Schrödinger equation is solved for a complex potential which goes to zero exponentially at infinity. It is shown that the absorption cross section for a well with fuzzy edges does not have sharp maxima as a function of R and E. This is in contrast to the results for the absorption cross sections for a rectangular potential well. The agreement of the calculated absorption cross sections at 2.5 and 4.3 mev with experimental values is satisfactory.

FOR a long time it had been assumed that if the wavelength λ of a neutron is less than the nuclear radius R, then the cross section for all inelastic processes of neutrons with a nucleus is equal to πR^2. However, experiments determining the total cross sections for neutrons of energy of the order of 100 mev[1] showed that not every neutron impinging on a nucleus leads to an inelastic event. In order to explain these high-energy interactions it was proposed[2] that fast neutrons have a finite mean free path in nuclear matter. At the same time it was considered that nuclei were black for low energy neutrons. The rough theory of cross sections based on the idea of black nuclei with a sharp boundary[3] led to monotonically decreasing cross sections as a function of energy. This turned out to be in disagreement with measurements. It was shown experimentally[4] that total nuclear interaction cross sections have maxima and minima as the energy of the neutron is varied.

In order to explain these experimental facts there was proposed[5] the model of the semi-transparent nucleus. According to this model, 1-3 mev neutrons have a large mean free path in nuclear matter. This arises because at low energies the collisions of the incoming neutrons with the nucleons in the nucleus are hindered by the Pauli principle which restricts the possible momentum transfers between the colliding particles.

In this way there have arisen two models. They both utilize the assumption of a finite absorption coefficient in a nucleus but differ in a series of important characteristics. For low energies the model involves a nucleus with sharp boundaries but for high energies the model is an optical one. In a nuclear model involving sharp boundaries there are additional refraction effects which do not exist in the optical model. Actually, a model with sharp boundaries is applicable only when $\lambda \gg R$, i.e., in the region where there is no inelastic scattering. The conclusions from this model were set forth in a previous communication by this author[6]. In this paper we examine a nuclear model with a finite coefficient of absorption and a fuzzy boundary which goes over into the optical model at high energies. At low energies it gives results significantly different from those given by a model with a rectangular potential.

1. STATEMENT OF THE PROBLEM

It is assumed that the interaction of a neutron with a nucleus can be represented by a complex potential $V + iW$, dependent only upon the coordinate r (neglecting spin orbit interactions). For simplicity it is assumed that the real and imaginary potentials depend on r in the same way. For sufficiently small values of $r\,(r < r_0)$ the function $V + iW$ goes over into a constant. The main variation of this function takes place in a thickness $1.5\text{-}2 \times 10^{-13}$ cm. In this case the Schrödinger equation for the neutron has the form:

$$\Delta\psi + (2m/\hbar^2)\,[E + V(r)\,(1 + i\zeta)]\,\psi = 0, \qquad (1)$$

where $W(r) = \zeta V(r)$. We now make the substitution $k = (2mE)^{1/2}/\hbar$ and $K_0 = [2mV(0)]^{1/2}/\hbar$. Then, writing the function ψ in the form:

$$\psi = \sum_{l,\,m} \psi_l(r)\,\Phi_{l,\,m}(\vartheta, \varphi), \qquad (2)$$

we obtain for the radial function $\psi_l(r)$ the equation:

$$\frac{d^2(r\psi_l)}{dr^2} + [k^2 + K_0^2 f(r)\,(1 + i\zeta)]\,(r\psi_l) - \frac{l(l+1)}{r^2}(r\psi_l) = 0. \qquad (3)$$

When $r \le r_0$, $f(r) = f(r_0) = 1$; when $r \to \infty$, $f(r) \to 0$

(it is assumed that $f(r)$ approaches zero sufficiently rapidly--more rapidly than any power law).

In order to solve Eq. (3) it is convenient to make the substitution*:

$$\psi_l(r) = r^{-1/2}[u_l^{(2)}(r)\,H^{(2)}_{l+1/2}(kr) + \eta_l u_l^{(1)}(r)\,H^{(1)}_{l+1/2}(kr)]. \tag{4}$$

We then obtain the following equations for the functions $u_l^{(1)}$, $u_l^{(2)}$:

$$\frac{d^2u_l^{(1,2)}}{dr^2} + 2\frac{d\ln r^{1/2}H^{(1,2)}_{l+1/2}}{dr}\,\frac{du_l^{(1,2)}}{dr} + K_0^2 f(r)(1+i\zeta)\,u_l^{(1,2)} = 0. \tag{5}$$

When $r \to \infty$, Eq. (4) must approach the usual expression for the sum of incoming and outgoing waves, and thus:

$$\lim_{r\to\infty} u_l^{(1)}(r) = \lim_{r\to\infty} u_l^{(2)}(r) = 1.$$

It is more convenient to write Eq. (5) in terms of reduced coordinates $x = kr$:

$$\frac{d^2u_l^{(1,2)}}{dx^2} + 2\frac{d\ln x^{1/2}H^{(1,2)}_{l+1/2}(x)}{dx}\,\frac{du_l^{(1,2)}}{dx} + K_0^2 f(x)(1+i\zeta)\,u_l^{(1,2)} = 0. \tag{6}$$

The solution of Eq. (6) turns out to be simplest at high energies.

2. HIGH ENERGIES

If the energy is sufficiently high, then the functions u_l can be represented in the form:

$$u_l = \exp\left\{-\int_0^\infty S_l\,dx\right\}. \tag{7}$$

We then obtain for the function S_l the equation:

$$\frac{dS_l^{(1)}}{dx} + S_l^{(1)^2} + 2\,\frac{d\ln x^{1/2}H^{(1)}_{l+1/2}(x)}{dx}\,S_l^{(1)} + \frac{k_0^2}{k^2}f(x)(1+i\zeta) = 0. \tag{8}$$

Neglecting dS_l/dx by analogy with the similar quasi-classical problem we obtain:

$$u_l(x) = \exp\left\{\int_x^\infty \left(\frac{d\ln x'^{1/2}H^{(1)}_{l+1/2}(x')}{dx'} - \left[\left(\frac{d\ln x'^{1/2}H^{(1)}_{l+1/2}(x')}{dx'}\right)^2 - \frac{k_0^2}{a^2}f(x')(1+i\zeta)\right]^{1/2}\right)dx'\right\}. \tag{9}$$

In order that the function ψ_l be finite at zero it is necessary and sufficient that:

$$\eta_l = u_l^{(2)}(0)\,/\,u_l^{(1)}(0). \tag{10}$$

The function under the integral sign in Eq. (9) is finite everywhere on the real axis and therefore the evaluation of the integral presents no difficulty.

We now introduce the notation:

$$\operatorname{Re}\frac{d\ln x^{1/2}H^{(1)}_{l+1/2}(x)}{dx} = a_l, \qquad \operatorname{Im}\frac{d\ln x^{1/2}H^{(1)}_{l+1/2}(x)}{dx} = b_l. \tag{11}$$

If it is assumed that the real part of the potential is much larger than the imaginary (which is the case for a transparent nucleus), then the expression under the square root sign can be expanded:

$$[(a_l^2 + ib_l^2)^2 - c^2(1+i\zeta)]^{1/2} = i[(b_l - ia_l)^2 + c^2]^{1/2} - {}^1/_2 c^2\zeta[(b_l - ia_l)^2 + c^2]^{-1/2}.$$

Then η has the form:

$$\eta = \exp\left\{-2i\int_0^\infty [b_l(x) - \operatorname{Re}((b_l - ia_l)^2 + c^2)^{1/2}]\,dx - \zeta\int_0^\infty c^2(x)\frac{\operatorname{Re}\{[b_l(x) - ia_l(x)]^2 + c^2\}^{1/2}}{[(b_l^2 - a_l^2 + c^2)^2 + 4a_l^2b_l^2]^{1/2}}\,dx\right\}, \tag{12}$$

---

* $H^{(1,2)}_{l+1/2}$ are the Hankel functions of the first and second order with half integral indices.

where

$$\operatorname{Re}\{(b_l - ia_l)^2 + c^2\}^{1/2} = 2^{-1/2}\{(b_l^2 + c^2 - a_l^2) + [(b_l^2 + c^2 - a_l^2)^2 + 4a_l^2 b_l^2]^{1/2}\}^{1/2}.$$

It is now easy to get expressions for the total cross section and absorption cross section:

$$\sigma_{\mathrm{abs}} = \sum_{l=0}^{\infty}(2l+1)\pi\lambda^2(1-|\eta_l|^2) = \sum_{l=0}^{\infty}(2l+1)\pi\lambda^2\Big(1-\exp\Big\{-\frac{2k_0^2}{k^2}2^{-1/2}\zeta \times\int_0^{\infty} f(x)[b_l^2+c^2-a_l^2+\{(b_l^2+c^2-a_l^2)^2+4a_l^2b_l^2\}^{1/2}]^{1/2}[(b_l^2+c^2-a_l^2)+4a_l^2b_l^2]^{-1/2}dx\Big\}\Big), \tag{13}$$

$$\sigma_{\mathrm{tot}} = \sum_{l=0}^{\infty} 2(2l+1)\pi\lambda^2(1-|\eta_l|^2) = \sum_{l=0}^{\infty}2(2l+1)\pi\lambda^2\Big[1-\cos 2\int_0^{\infty}\Big\{b_l - 2^{-1/2}[b_l^2+c^2-a_l^2+\{(b_l^2+c^2-a_l^2)^2 + 4a_l^2b_l^2\}^{1/2}]^{1/2}\Big\}dx\,\exp\Big\{-\frac{k_0^2}{k^2}2^{-1/2}\zeta\int_0^{\infty}f(x)[b_l^2+c^2-a_l^2 + \{(b_l^2+c^2-a_l^2)^2+4a_l^2b_l^2\}^{1/2}]^{1/2}[(b_l^2+c^2-a_l^2)^2+4a_l^2b_l^2]^{-1/2}dx\Big\}\Big]. \tag{14}$$

Thus, the calculation of cross sections for any form of the potential can be carried out in this case by quadrature. However, the quadrature has to be carried out numerically and therefore it is convenient to expand the square root under the integral in a series, which is always possible if $k_0^2/k^2 \ll 1$.

The Eqs. (13) and (14) can then be put into the form, valid to order including k_0^4/k^4:

$$\sigma_{\mathrm{abs}} = \sum_{l=0}^{\infty}(2l+1)\pi\lambda^2\Big(1-\exp\Big\{-\frac{2k_0^2}{k^2}\zeta\int_0^{\infty}\frac{b_l}{b_l^2+a_l^2}f(x) \times\Big[1-\frac{k_0^2}{k^2}f(x)\frac{b_l^2-3a_l^2}{(b_l^2+a_l^2)^2}\Big]dx\Big\}\Big), \tag{15}$$

$$\sigma_{\mathrm{tot}} = \sum_{l=0}^{\infty}2(2l+1)\pi\lambda^2\Big(1-\cos\frac{k_0^2}{k^2}\int_0^{\infty}f(x)\frac{b_l}{b_l^2+a_l^2}\Big[1-\frac{k_0^2}{4k^2}\frac{b_l^2-3a_l^2}{(b_l^3+a_l^2)^2}\Big]dx \times\exp\Big\{-\frac{k_0^2}{k^2}\zeta\int_0^{\infty}\frac{b_l}{b_l^2+a_l^2}\Big[1-\frac{k_0^2}{2k^2}f(x)\frac{b_l^2-3a_l^2}{(b_l^2+a_l^2)^2}\Big]f(x)\,dx\Big\}\Big). \tag{16}$$

In the case when it is possible to neglect the term k_0^4/k^4 the expression under the integral sign for the harmonics with $l < kR$ is equal to the mean free path of a neutron with momentum l in a nucleus according to the optical model.

Let us assume that the potential at the nuclear boundary decreases exponentially according to $e^{-\alpha x}$. Then, using for the radius of the nucleus $R = r_0 + 1/\alpha$, we get from Eqs. (15) and (16) that the geometrical path of a neutron with momentum $l < kR$ is equal to $R - l(l+1)/2k^2R^2$ and does not depend on the magnitude of $1/\alpha$ for constant R. The boundary region is important only for $l \geq kR$.

When $1/\alpha \ll \lambda$, then at very high energies (in the approximation in which k_0^4/k^4 can be neglected) only waves with $l \ll kR$ penetrate into the nucleus. If $1/\alpha \geq \lambda$, then waves with $l > kR$ penetrate into the nucleus. In the first case the departure from geometrical optics consists only in the scattering of waves with $l = kR$; the contribution to the cross section of these tends to 0 like λ. If, however, the fuzzy region is larger than the wavelength, then the effect of the boundary on the magnitude of the cross section depends on the relative sizes of the wavelength and the nuclear radius.

For heavy nuclei having $R \sim 7-8\times10^{-13}$, the cross section increases by about 10% relative to that when $1/\alpha \ll \lambda$ and the same value of $r_0 + 1/\alpha$. For light nuclei the cross section increases very strongly. However, if it is assumed that $V(r)$ is proportional to the density of nuclear matter then, in this case, increasing the fuzziness (with an exponential form of the boundary) decreases the density of nuclear matter in the middle.

If the density of nuclear matter in the center is kept constant, then the absorption cross section depends very little on the form of the boundary (changing only by several percent). However, if it is assumed that $V(r)$ does not depend on nuclear density, there results a strong dependence of the cross section of light nuclei on the boundary behavior. At lower energies, when the second term in the exponent cannot be neglected, waves with $l > kR$ penetrate into the nucleus even for $1/\alpha \ll \alpha$*. This effect persists no matter how small the fuzziness. In this case the absorption cross section for sufficiently small path lengths of the neutron in the nucleus can be 15-20 percent greater than πR^2 even for heavy nuclei.

A more detailed study of the absorption coefficient cannot be carried out at present because of almost complete lack of experimental information on absorption cross section for energies with $E > V$.

An important conclusion follows from Eq. (16). The argument of the cosine decreases with increasing energy. At some energy it passes through the value 2π, and this corresponds to a minimum in the total cross section of a given l. At a still higher energy there appears a maximum corresponding to cosine $\varphi_l = 1$, that is, $\varphi_l = \pi$. After this, the cross section falls monotonically. The sum of the cross sections likewise has a maximum and minimum (although weaker). This maximum should be observed at higher energies for heavy nuclei than for light ones due to the longer path of the particle in the nucleus. This displacement of the maximum as a function of atomic weight is confirmed experimentally. From the position of the minimum in the cross section for Pb at $E = 55$ mev it is possible to evaluate the real part of the potential for $R = 1.2\times10^{-13}A^{1/3}$ (in the case of Pb the boundary shape has little influence on the cross section). This leads to $U(0) = 35\text{-}40$ mev.

It is worth mentioning that for $R = 1.2\times10^{-13}A^{1/3}$ the Fermi energy is equal to 31 mev and for this reason the potential U, taking into account the binding energy, should equal about 38 mev. Similar values are obtained also at lower energies.

At energies greater than 100 mev the simple model with a complex potential apparently is not applicable.

3. THE LIMITS OF APPLICABILITY OF THE QUASI-CLASSICAL METHOD

In order to make clear the limits of applicability of the quasi-classical solution, we return to Eq. (8). We write this equation in the form:

$$\frac{dS_l}{dx} + S_l^2 - S_l^{(0)2} + 2\,\frac{d\ln x^{1/2} H^{(1)}_{l+1/2}(x)}{dx}\,S_l - 2\,\frac{d\ln x^{1/2} H^{(1)}_{l+1/2}}{dx}\,S_l^{(0)} = 0. \qquad (17)$$

Then, assuming that the approximate solution $S_l^{(0)}$ is close to the exact solution S_l, the difference $S_l^2 - S_l^{(0)2}$ can be replaced by $2(S_l - S_l^{(0)})S_l^{(0)}$. In this we are neglecting the quantity $S_l - S_l^{(0)}$ as compared to $2S_l^{(0)}$. Equation (17) then takes the form:

$$\frac{dS_l}{dx} + 2\left[S_l - S_l^{(0)}\right]\left(\frac{d\ln x^{1/2} H^{(1)}_{l+1/2}}{dx} + 2S_l^{(0)}\right) = 0. \qquad (18)$$

This is a linear equation of the first order. After some transformations, the solution can be written in the form:

$$S_l = S_l^{(0)}(x) + \int_x^{\infty} dx'\,\frac{dS_l^{(0)}(x')}{dx'}\exp\left\{2\int_x^{x'}\left(\frac{d\ln x''^{1/2}H^{(1)}_{l+1/2}(x'')}{dx''} + S_l(x'')\right)dx''\right\}.$$

This solution is significantly more accurate than the second approximation of the usual quasi-classical method which can be obtained from it by using integration by parts:

---

* *Translator's note:* This looks like a typographical error. I think that it should be $1/\alpha \ll \lambda$.

$$S_l^{(1)} = S_l^{(0)} + \frac{1}{2}\frac{dS_l^{(0)}x}{dx}\left(\frac{a \ln x^{1/2} H^{(1)}_{l+1/2}}{dx} + S_l^{(0)}\right)^{-1} + I(x). \tag{19}$$

For *s*-waves the second term of (19) gives a factor which drops out when the amplitude of the scattered wave is calculated. For $V = E$ this term contributes ~ 20%. The magnitude of $I(X)$ is much smaller and for $E = V$ it is less than 1-2%. For $l \neq 0$ the second term of (18) does not drop out in the calculation of the scattered wave. However, when $l < kr_0$ the correction is small.

The correction is significant only when $l \sim kr_0$. When $U \sim E$ the contribution of the second approximation to the magnitude of η_l when $l = kR$ is smaller than $e^{-0.4i}$. The correction to the absorption cross section is not significant if the absorption is large. For this reason we can consider that Eqs. (13) and (14) are valid for $V < E$. However, it is not necessary to require the more stringent condition that $V \ll E$.

4. LOW ENERGIES

If $E < V(0)$, then the quasi-classical method of calculation is not satisfactory. In this case it is necessary to carry out calculations using an exact solution of Eq. (3) with a definite form for the boundary. The following calculations have been made on the assumption that $f(r) = e^{-\alpha(r-r_0)}$ when $r \geq r_0$. It is then necessary to satisfy the boundary condition when $r = r_0$:

$$\frac{1}{\psi_i}\frac{d\psi_i}{dr} = \frac{1}{\psi_a}\frac{d\psi_a}{dr}. \tag{20}$$

When $r \leq r_0$ the potential V is a constant, and therefore the solution is written in the form:

$$\psi = r^{-1/2} J_{l+1/2}(\varkappa r), \varkappa = [k^2 + k_0^2(1 + i\zeta)]^{1/2}. \tag{21}$$

In the region of changing potential $r \geq r_0$ a solution is sought, as earlier, in the form

$$\psi_a^{(1)(2)} = r^{-1/2} u_l^{(1)(2)} H^{(1)(2)}_{l+1/2}(kr).$$

Here we sought a solution of Eq. (6) in the form of a series involving an expansion in powers of k_0^2/α^2.

Let us make use of the condition $u_l = 1$ as $r \to \infty$. Then as a first approximation let us place $u_l = 1$ in Eq. (6), getting an equation of the first order for du_l/dr:

$$\frac{d^2u_l}{dy^2} + 2\frac{d \ln y^{1/2} H^{(1)}_{l+1/2}(ky/\alpha)}{dy}\frac{du_l}{dy} + \frac{k_0^2}{\alpha^2} f(y)(1 + i\zeta) = 0. \tag{22}$$

Finding du_l/dy from Eq. (22) and integrating a second time we get:

$$u_l^{(1)}(y) = 1 - \frac{k_0^2}{\alpha}(1 + i\zeta)\int\limits_y^\infty [y'^{1/2} H^{(1)}_{l+1/2}(ky'/\alpha)]^{-2} \times \int\limits_{y'}^\infty f(y'')[y''^{1/2} H^{(1)}_{l+1/2}(ky''/\alpha)]^2 \, dy' \, dy''. \tag{23}$$

Equation (23) can be transformed into a more convenient form:

$$u_l^{(1)}(y) = 1 - \frac{k_0^2}{\alpha^2}(1 + i\zeta)\int\limits_y^\infty y' [H^{(1)}_{l+1/2}(ky'/\alpha)]^2 f(y') \times \int\limits_y^{y'} [H^{(1)}_{l+1/2}(ky''/\alpha)]^{-2} \frac{dy' dy''}{y''}.$$

Evaluating the inside integral we then find finally:

$$u_l^{(1)}(y) = 1 - \frac{i}{2}\frac{k_0^2}{\alpha^2}(1 + i\zeta)\frac{\alpha}{k}\left\{\int\limits_y^\infty \frac{|P_l(ky'/\alpha)|^2}{(ky'/\alpha)^{2l}} f(y')\,dy' - \right. \tag{24}$$
$$\left. - \frac{P_l^x(ky/\alpha)}{P_l(ky/\alpha)}\int\limits_y^\infty \exp\left\{2i\frac{k}{\alpha}(y' - y)\right\}(ky'/\alpha)^{-2l}\{P_l(ky'/\alpha)\}^2 f(y')\,dy'\right\}.$$

In Eq. (24)

$$P_l(ky/\alpha) = \exp\left\{-i\frac{k}{\alpha}y\right\}(ky/\alpha)^{l+1/2}H_{l+1/2}^{(1)}(ky/\alpha).$$

If it is assumed that $1/\alpha = 1.5 - 2\times10^{-13}$, then the first approximation turns out to be insufficient and it is necessary to take 3-4 terms of the series for E = 3-10 mev. However, the integrals depend only on the single parameter k/α, and this significantly simplifies the calculations (the parameters k_0, ζ and r_0 can be varied at will).

The equation for the nth approximation can be obtained from Eq. (6) by introducing into it the (n-1)st approximation, and has the form:

$$u_l^{(1)[n]}(y) = 1 - \frac{i}{2}\frac{k_0^2}{\alpha k}(i + i\zeta)\left\{\int\limits_y^\infty (ky'/\alpha)^{-2l}\,|P_l(ky'/\alpha)|^2\,u_l^{(1)[n-1]}(y')f(y')dy'\right. \tag{25}$$
$$\left. - \frac{P_l^x(ky/\alpha)}{P_l(ky/\alpha)}\int\limits_y^\infty \exp\left\{2i\frac{k}{\alpha}(y' - y)\right\}[P_l(ky'/\alpha)]^2(ky'/\alpha)^{-2l}f(y')u_l^{(1)[n-1]}(y')dy'\right\}.$$

It should be pointed out that such complicated expressions are needed only for waves with small l (less than 5-6), for which quasi-resonances can exist.

The conditions for the existence of a quasi-resonance can be obtained quasi-classically starting from the condition that as $E \to \infty$ the argument of the cosine in Eq. (14) approaches $(2n+1)\pi$. Thus, for a potential with $1/\alpha \ll R$ we obtain:

$$(k_0^2R^2 - l^2)^{1/2} = (2n+1)\pi/2 \tag{26}$$
$$+ l\,\mathrm{arctg}[(k_0^2R^2 - l^2)^{1/2}/l]$$

This is in excellent agreement with the exact solution.

It should be pointed out that for a washed-out boundary having $1/\alpha \sim R$ the agreement is poorer. However, for calculations, especially when the nucleus is heavy (i.e., $1/\alpha < R$), the quasi-classical conditions can be used.

5. COMPARISON WITH EXPERIMENT

The data on inelastic scattering cross sections for energies of a few million volts are relatively meager. Moreover, at energies less than 2-3 mev the number of nuclear levels that can be excited is small, and therefore, especially in the case of magic nuclei, the decomposition of the intermediate nucleus can go by way of elastic scattering.

We have used the data of Pasechnik[7] on the inelastic scattering of 2.5 and 4.3 mev neutrons. In order to compare the theory with these experiments, the absorption cross section was calculated for neutrons of these energies as a function of nuclear radius. In this an exponential form of the boundary $e^{-\alpha r}$ was assumed with $1/\alpha = 1.45\times10^{-13}$ cm. The depth of the well was taken as 20 mev; however, the picture is little changed even if $V(0)$ = 40 mev. At E = 2.5 mev the absorption coefficient $V(0)\,\zeta$ was taken as 0.053 $V(0)$; at E = 4.3 mev the absorption coefficient was taken as 0.05 $V(0)$ and 0.11 $V(0)$.

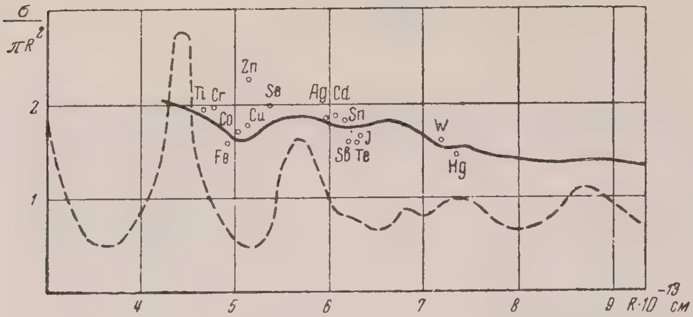

FIG. 1. Dependence of the inelastic scattering cross section on the nuclear radius for 2.6 mev; $\zeta = 0.05$. The continuous curve was computed for the model with diffuse boundaries, the broken curve for the model with sharp boundaries; the experimental points are marked by circles.

Figure 1 shows the results of the calculations of the absorption cross section $\sigma/\pi R^2$ as a function of $R = r_0 + 1/\alpha$ (solid curve). There are also presented the results of a calculation using a model with sharp boundaries and the same values of V and ζ (dashed curve). The circles denote the experimental points of Pasechnik, obtained using a threshold detector (Al). For these the nuclear radius was taken equal to $R = 1.25 \times 10^{-13} A^{1/3}$ As is seen the absorption cross sections from a model with a fuzzy boundary are about twice as large as those from a model with sharp boundaries. Also, the maxima are rather weak (the ratio of cross sections at maxima to that at minima is 1.3, whereas on the model with sharp edges this ratio exceeds 2). The experimental points scatter on both sides of the curve with fuzzy boundary. The magic nuclei have not been included in the data presented, since for these the inelastic scattering cross section is small because of the small number of levels available. The point for Zn is quite a bit off, its experimentally determined cross section being too high. In general, the data at 2.5 mev are less sensitive for comparison with theory than are the data at 4.3 mev.

Figure 2 shows the results of calculations for 4.3 mev neutrons. The solid curves give the cross sections for nuclei with fuzzy boundaries for the two absorption coefficients 0.05 $V(r)$ and 0.11 $V(r)$. The dashed curve corresponds to absorption cross sections for nuclei with a sharp boundary and $\zeta = 0.05$. For comparison there are given the experimental points of Pasechnik using $R = 1.25 \times 10^{-13} A^{1/3}$ cm. As is seen these points agree better with a curve for $\zeta = 0.11$ than with the curve for $\zeta = 0.05$.

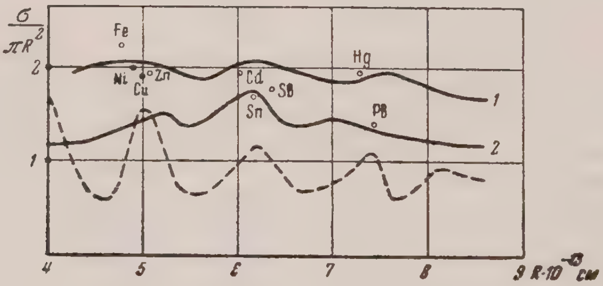

FIG. 2. Dependence of the inelastic scattering cross section on the nuclear radius for 4.3 mev. The continuous curves were computed for the model with diffuse boundaries, the broken curves for the model with sharp boundaries; the experimental points are marked by circles. For curve 1, $\zeta = 0.1$, for the other curves, $\zeta = 0.05$.

Thus, the experimental data indicate that the mean free path for neutrons of low energies is large (of the order of 2×10^{-12} cm), but that it rapidly decreases with increasing energy.

The nuclear model with a fuzzy boundary makes possible the reconciliation of nuclear radii obtained from other experiments (scattering of fast electrons) with those obtained from neutron cross sections. On the other hand, the model with sharp boundaries, even with a large absorption coefficient, gives cross sections equal to $1\text{-}1.2\pi R^2$, which by comparison with experimental data leads to very large radii: $R = 1.6 \times 10^{-13} A^{1/3}$. These are in sharp disagreement with results from all other experiments.

The maxima in absorption cross sections as a function of radius disappear in the model with washed-out boundaries at an energy of about 5 mev. At larger energies the absorption cross section is a monotonic function of the radius. The available data on inelastic scattering at $E = 14$ mev are not in contradiction with $R = 1.25 \times 10^{-13} A^{1/3}$, except for possibly the lightest nuclei. In this case the mean free path should be of the order of 3-4 $\times 10^{-13}$ cm, i.e., the nucleus should be black for waves with $l < kR$.

In contrast with absorption cross sections, the total cross sections will have maxima and minima for all values of l for which the nucleus is black because the phase of the scattered wave changes depending on R and E.

CONCLUSIONS

We have proposed a method of modulated spherical waves for studying the scattering of neutrons. This method, for $V(0) < E$ appears to be a generalization of the quasi-classical method.

In contrast to the usual quasi-classical approach, the proposed one satisfies exact boundary conditions. Higher approximations can easily be obtained, and thus a limiting transition to the exact phase analysis solution of the problem can be obtained.

The interaction cross sections of neutrons in all energy regions can be described using a model with fuzzy boundaries.

When $E > V(0)$ there is obtained a simple explanation of the maxima in total cross sections and likewise, of the deviations of total cross sections from $2\pi R^2$. At low energies the absence of sharp maxima in the absorption cross sections as a function of radius and energy, which are obtained from a model with sharp boundaries, is explained. Likewise the values of the cross sections are reconciled with the values of nuclear radii obtained from other experiments.

---

[1] L. J. Coak, I. Miller and J. Peterson Sewel, Phys. Rev. **75**, 7 (1949).

[2] H. Feshbach, R. Serber and J. Taylor, Phys. Rev. **75**, 1352 (1949).

[3] H. Feshbach and V. Weisskopf, Phys. Rev. **76**, 1550 (1949).

[4] D. Miller, R. Adair, C. Bockelman and S. Darden, Phys. Rev. **88**, 83 (1952).

[5] H. Feshbach, C. Porter and V. Weisskopf, Phys. Rev. **90**, 166 (1953).

[6] P. E. Nemirovskii, Dokl. Akad. Nauk SSSR **101**, 257 (1955).

[7] M. F. Pasechnik, Talk at the Geneva Conference, 1955.

Translated by A. Turkevich
99

SOVIET PHYSICS VOLUME 3, NUMBER 4 NOVEMBER, 1956

Dynamical Birefringence of Polymethylmethacrylate Solutions with Various Solvents and the Form of the Macromolecules

V. N. TSVETKOV, E. V. FRISMAN AND L. S. MUKHINA
Leningrad State University

(Submitted to JETP editor June 25, 1955)
J. Exptl. Theoret. Phys. (U.S.S.R.) 30, 649-660 (April, 1956)

An investigation was conducted of the dynamical birefringence of two fractions ($M = 3.5 \times 10^5$ and $M = 4.2 \times 10^6$) of polymethylmethacrylate in various solvents. The results obtained are compared with theories based on a molecular model of anisotropic ellipsoidal complexes, and on the model of elastic-viscous spheres. The experimental data are in better agreement with the model of anisotropic complexes.

---

1. INTRODUCTION

BIREFRINGENCE in the flow of a solution of a polymer is determined by the optical anisotropy of its molecules. As was shown earlier[1,2], the optical anisotropy of a macromolecule in solution may be due to asymmetry of its form (anisotropy of form) and to internal anisotropy (anisotropy of the substance of the molecular complex). Both anisotropy of form and internal anisotropy depend on the hydrodynamic forces acting on the molecular complex in a laminar flow. These forces deform the molecular complex, increasing the asymmetry of its form and evoking the photoelastic effect in the macromolecule, i.e., the appearance of optical anisotropy in its substance on account of the stresses arising there.

Experiments conducted over a broad range of flow velocity gradients[1] have shown that in the observed birefringence the role of the effect due to deformation of the macromolecules with an increase of velocity gradient. Thus, dynamical birefringence in a solution of a polymer observed in the region of large flow velocity gradients, is to a considerable extent a deformation effect, and in the case of equal indices of refraction of the polymer and the solvent, a photoelastic effect.

The nature of the effect observed in solutions of polymers at small flow velocity gradients g (under the conditions $g \to 0$) is an open question at the present time.

2. THEORY OF BIREFRINGENCE OF SOLUTIONS OF A POLYMER IN A WEAK FLOW

According to the statistical theory of Kuhn[3], the most probable form of a linear chain macromolecule in solution is the form of a coiled complex, the length of which is 2-3 times its transverse dimensions.

As an optical model of such a complex, we proposed[1] a particle of ellipsoidal form, thoroughly saturated with solvent, and having a mean index of refraction n_ω, differing from the index of refraction of the solvent n_s by the quantity $n_\omega - n_s$:

$$n_\omega^2 - n_s^2 = \omega^{-1}(n_k^2 - n_s^2). \qquad (1)$$

Here n_k is the index of refraction of the dry polymer, ω is its "volume" in solution determined by the relation

$$\omega = \rho V / m = V \rho N_A / M, \qquad (2)$$

where ρ is the density of the polymer, M its molecular weight, m the mass of the macromolecule, V the volume of the molecular ellipsoid (particle) in the solution, and N_A Avogadro's number.

According to the statistical theory[4], a molecular complex in the absence of external deforming forces has internal anisotropy; moreover, the difference between the indices of refraction of its substance under stresses parallel to the major and minor geometrical axes is

$$n_1^2 - n_2^2 = \left(\frac{n_s^2 + 2}{3}\right)^2 \frac{4\pi}{V} \frac{3}{5}(\alpha_1 - \alpha_2), \qquad (3)$$

where α_1 and α_2 are the principal polarizabilities of the segment in vacuum.

The anisotropy of form of an ellipsoidal molecular complex can be calculated by the application of the laws of colloidal optics[5-7], with the use of a molecular model[1] based on Eqs. (1) and (2). The total difference, obtained in this way, of the two principal polarizabilities of the molecular ellipsoid in solution, taking account of Eq. (3), is[2]

$$\gamma_1 - \gamma_2 = \frac{n_1^2 - n_2^2}{4\pi} V + \frac{(n_k^2 - n_s^2)^2}{16\pi^2 n_s^2 \omega^2} V (L_2 - L_1) \qquad (4)$$

$$= \left(\frac{n_s^2 + 2}{3}\right)^2 \frac{3}{5}(\alpha_1 - \alpha_2) + \left(\frac{n_k^2 - n_s^2}{4\pi n_s \rho N_A}\right)^2 \frac{M^2}{V}(L_2 - L_1),$$

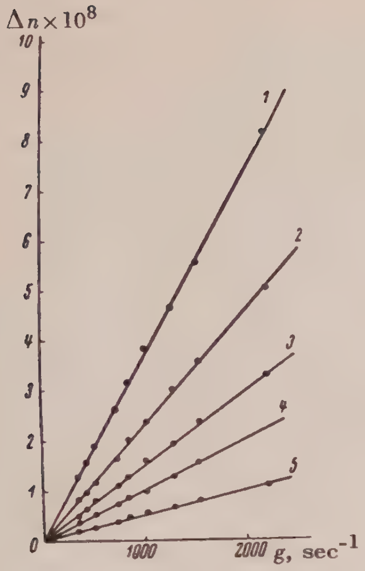

FIG. 1. Dependence of the magnitude of birefringence on the velocity gradient in solutions of polymethylmethacrylate in acetone. $M = 4.2 \times 10^6$: *1-c* = 0.5; *2-c* = 0.4; *3-c* = 0.3; *4-c* = 0.2; *5-c* = 0.1 (gm/100 cm^3).

where L_1 and L_2 are constants, depending on *p*, the ratio of the semiaxes of the ellipsoid.

Recently, Kopik[7] calculated the quantity $\gamma_1 - \gamma_2$, expressing it as a function of the distance *h* between the ends of the molecular chain. His result agrees precisely with ours, if we set $p = 2$ and $V = 0.3\,h^3$ in Eq. (4).

If birefringence in the flow of a solution of a polymer under the conditions $g \to 0$ is regarded as the result of the orientation of molecular complexes of asymmetric form, then the simple application of orientation theory for rigid ellipsoidal particles[8], with the use of Eq. (4), leads to the following expression for the dynamo-optical constant[2]:

$$[n] = \lim \left(\frac{\Delta n}{gc\eta_0}\right)_{\substack{g \to 0 \\ c \to 0}} = \frac{2\pi}{225}\frac{bN_A}{\eta_0 DM}\frac{(n_s^2+2)^2}{n_s}(\alpha_1 - \alpha_2) + \frac{bM}{120\pi\eta_0 DV\rho^2 N_A}\frac{(n_k^2 - n_s^2)^2}{n_s^3}(L_2 - L_1) = [n]_e + [n]_f. \tag{5}$$

Here η_0 is the viscosity of the solvent, Δn is the observed birefringence in the solution, *c* is the concentration in g/cm^3, *D* is the coefficient of rotational diffusion of the macromolecule, $b = (p^2 - 1)/(p^2 + 1)$; $[n]_e$ and $[n]_f$ are the parts of the dynamic-optical constant characterizing, respectively, the effect of internal anisotropy and the effect of the form of the macromolecule.

Another point of view concerning the nature of the Maxwell effect in a solution of a polymer under the conditions $g \to 0$ is developed by Cerf[9,10]. The model applied by us in the form of a colloidal particle whose mean index of refraction n_ω is determined by Eq. (1), is used in his theory for the characteristics of the optical properties of the molecule. However, in contrast to Kuhn, it is proposed in this theory that the statistically most probable form of a free macromolecule is a spherical complex of radius a_0, characterized by the internal

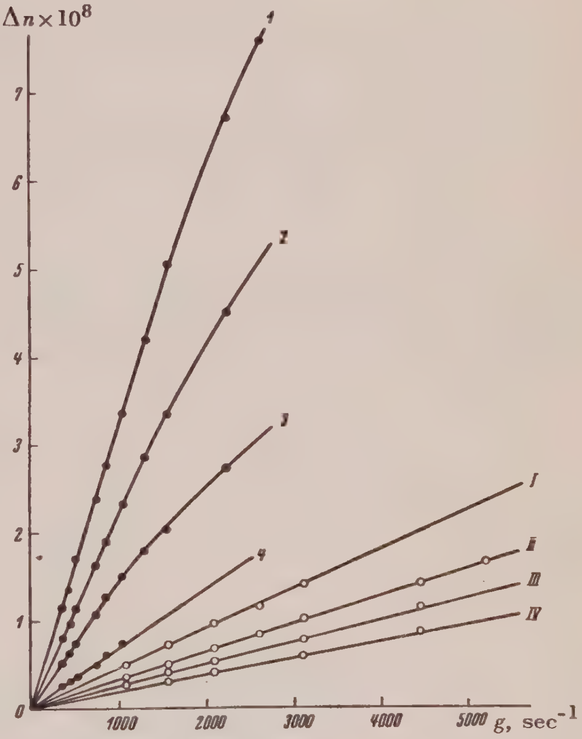

FIG. 2. Dependence of the magnitude of birefringence on the velocity gradient in solutions of polymethylmethacrylate in ethyl acetate. $M = 4.2 \times 10^6$: *1-c* = 0.4; *2-c* = 0.3; *3-c* = 0.2; *4-c* = 0.1 (gm/100 cm^3). $M = 3.5 \times 10^5$: *I-c* = 1.5; *II-c* = 1.2; *III-c* = 1.0; *IV-c* = 0.8 (gm/100 cm^3).

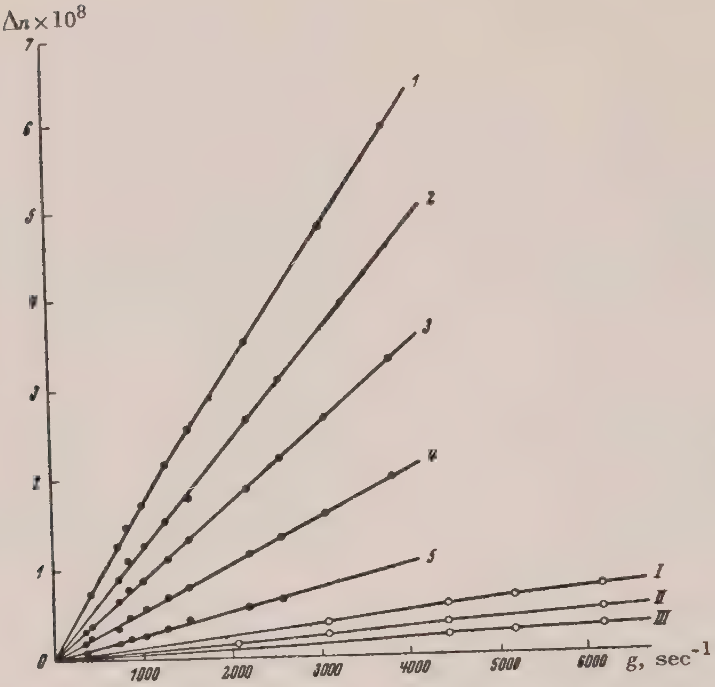

FIG. 3. Dependence of the magnitude of birefringence on the velocity gradient in solutions of polymethylmethacrylate in chloroform. $M = 4.2 \times 10^6$: 1-$c = 0.5$; 2-$c = 0.4$; 3-$c = 0.3$; 4-$c = 0.2$; 5-$c = 0.1$ (gm/100 cm^3). $M = 3.5 \times 10^5$: I-$c = 1.2$; II-$c = 1.0$; III-$c = 0.8$ (gm/100 cm^3).

viscosity η_i and the shear modulus of elasticity μ. Thermal motion may deform the molecular complex, transforming it into a spheroid, the major semiaxis of which is

$$a = a_0(1 + \delta). \tag{6}$$

Here δ denites the coefficient of deformation. The mean squared magnitude of Brownian deformation δ_0 is

$$\delta_0 = (kT/3V\mu)^{1/2}, \tag{7}$$

where T is the temperature and k is Boltzmann's constant.

In laminar flow, hydrodynamic forces also deform the macromolecule, transforming it into an ellipsoid with a ratio of semiaxes

$$p = 1 + (2{,}5/\mu)\eta_0 g. \tag{8}$$

Deformation of the elastic-viscous sphere evokes in it the appearance of optical anisotropy, leading to a form effect and to a photoelastic effect in the substance of the macromolecule.

Thus, the theory of the elastic-viscous sphere regards the Maxwell effect in a solution of a polymer, under the conditions $g \to 0$, as a composite phenomenon, evoked by the orientation of spheroids (coefficient of asymmetry of form δ_0) and their deformation in the flow. The relative role of these two effects depends on the relation between the viscosity of the solvent η_0 and the internal viscosity of the macromolecule η_i. For $\eta_i \gg \eta_0$ the effect is basically orientational; for $\eta_i \ll \eta_0$, it is deformational.

Cerf's theory leads to the following value of the dynamo-optical constant of the solution:

$$\Delta = \left(\frac{\Delta n}{g\eta_0 \Omega n_s}\right)_{\substack{g \to 0 \\ c \to 0}} \tag{9}$$

$$= 5\frac{\varepsilon}{\mu}\theta + \frac{2}{\mu}\left(\frac{n_\omega - n_s}{n_\omega}\right)^2 \theta = \Delta_e + \Delta_f;$$

$$\theta = [(\eta_0/\eta_i) + {}^4/_5\,\delta_0^2]/[(\eta_0/\eta_i) + {}^4/_3\,\delta_0^2], \tag{9'}$$

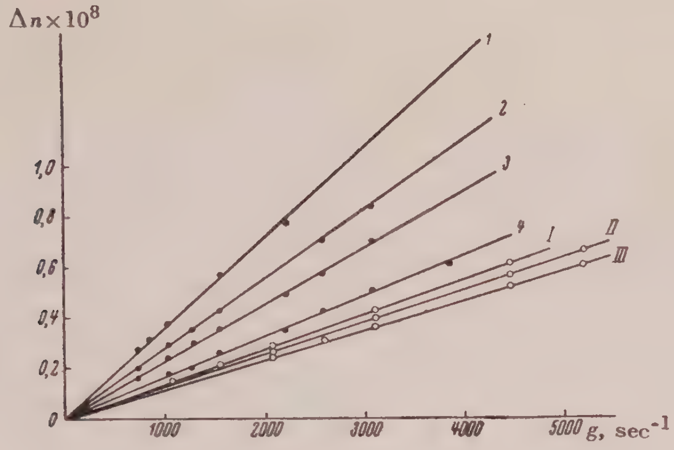

FIG. 4. Dependence of the magnitude of birefringence on the velocity gradient in solutions of polymethylmethacrylate in toluene. $M = 4.2 \times 10^6$: 1-c = 0.5; 2-c = 0.4; 3-c = 0.3; 4-c = 0.2 (gm/100 cm^3). $M = 3.5 \times 10^5$: I-c = 1.7; II-c = 1.5; III-c = 1.2 (gm/100 cm^3).

where Δ_e and Δ_f are the parts of the dynamo-optical constant due, respectively, to internal anisotropy and anisotropy of form of the macromolecule, Ω is the portion of the volume occupied by the particles in the solution, ϵ is the photoelastic coefficient of the substance of the macromolecule, determined from the relation

$$\frac{n_1 - n_2}{n_\omega} = \frac{5}{2} \epsilon \frac{\eta_0}{\mu} g, \tag{10}$$

where $n_1 - n_2$ is the difference between the principal indices of refraction of the substance of the

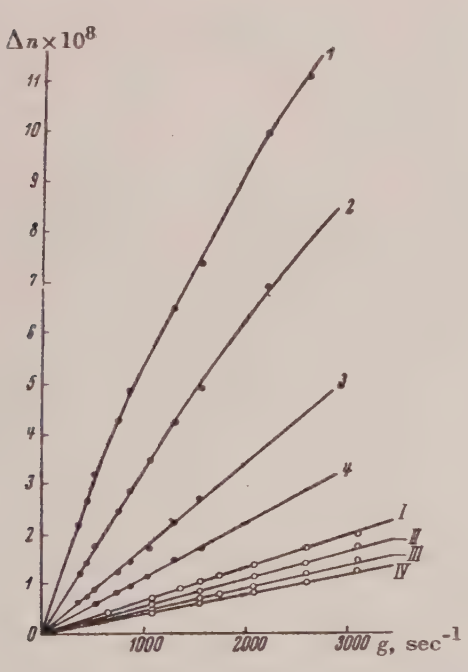

FIG. 5. Dependence of the magnitude of birefringence on the velocity gradient in solutions of polymethylmethacrylate in bromoform. $M = 4.2 \times 10^6$: 1-c = 0.4; 2-c = 0.288; 3-c = 0.147; 4-c = 0.1 (gm/100 cm^3). $M = 3.5 \times 10^5$: I-c = 1.2; II-c = 1.0; III-c = 0.8; IV-c = 0.6 (gm/100 cm^3).

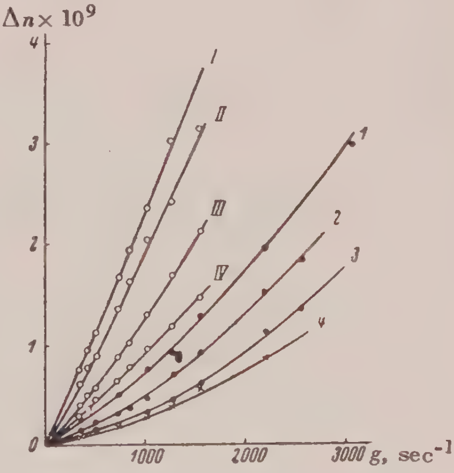

FIG. 6. Dependence of the magnitude of birefringence on the velocity gradient in solutions of polymethylmethacrylate ($M = 4.2 \times 10^6$) in two solvents. Bromobenzene: I-c = 0.5; II-c = 0.4; III-c = 0.3; IV-c = 0.2 (gm/100 cm^3). Chlorobenzene: 1-c = 0.5; 2-c = 0.4; 3-c = 0.3; 4-c = 0.2 (gm/100 cm^3).

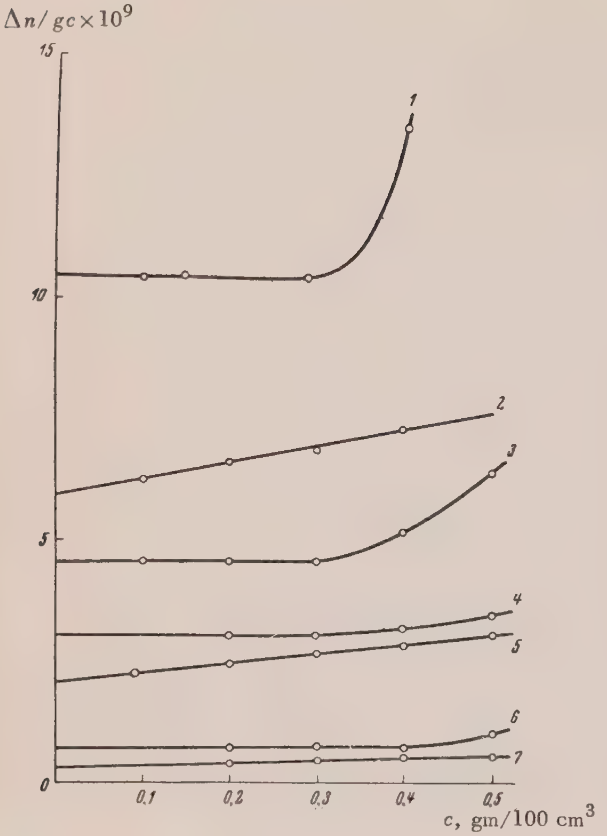

FIG. 7. Dependence of $\Delta n/gc$ on concentration for a fraction of polymethylmethacrylate ($M = 4.2 \times 10^6$) in various solvents: *1*-bromoform, *2*-ethyl acetate, *3*-acetone, *4*-bromobenzene, *5*-chloroform, *6*-chlorobenzene, *7*-toluene.

particle, arising in a mechanical field of gradient g.

As is shown by Eqs. (9) and (9′), the magnitude of the dynamo-optical constant Δ in the theory of the elastic-viscous sphere differs only by a factor of 3/5 for the two extreme conceivable cases of pure orientation ($\eta_0/\eta_i \ll \delta_0^2$) and pure deformation ($\eta_0/\eta_i \gg \delta_0^2$), and is determined by the quantities ϵ, μ, n_ω and n_s. Therefore, the measurement of Δ may not serve for a qualitative comparison of the roles of the orientational and deformational effects in the observed birefringence. The experimental determination of the quantities Δ_e and Δ_f separately leads to more instructive conclusions as will be shown below.

3. METHOD AND RESULTS OF THE INVESTIGATION

In conformance with previous results[1,11,12] in order to separate the effect of form from the effect of internal anisotropy, an investigation was conducted, in the present work, of birefringence in the flow of solutions of two fractions of polymethylmethacrylate in various solvents. The molecular weights of the fractions were determined by the magnitude of their characteristic viscosity $[\eta]$ in benzene, according to the formula[13]

$$[\eta] = 0.468 \times 10^{-4} M^{0.77}.$$

The optical setup used by us has been described earlier[14,15]. For the measurement of the magnitude of birefringence of solutions of the first fraction ($M = 4.2 \times 10^6$), a mica plate $0.04\,\lambda$ served as a compensator. For the investigation of the second fraction ($M = 3.5 \times 10^5$), where the magnitude of birefringence is very small, a mica plate ($0.019\,\lambda$) was used as a compensator ($\lambda = 5461$ Å). The phase difference arising in a solution with a given velocity gradient was calculated according to the formula

$$\delta = \sin \delta_0 \sin 2\,(\beta - \beta_0),$$

where β and β_0 are the extinction azimuths of the compensator in the presence and in the absence of a velocity gradient in the solution investigated, and δ_0 is the phase difference created by the compensator.

A universal dynamo-optimeter similar to those described in other works[14,15] was used for the measurements. The measurements were performed in a gap with an external rotor. The length of the layer of liquid worked was $l = 6$ cm. A rotor forming a gap $\Delta R = 0.86$ mm was used for the study of high-molecular fractions. The low-molecular fractions were investigated in a gap $\Delta R = 0.36$ mm. Laminar flow was maintained for all the solutions over the interval of velocity gradients investigated. All the measurements were made at the temperature $t = 21°$.

The dependence $\Delta n = f(g)$, obtained for the solutions studied, are presented graphically in Figs. 1-6. The figures show that for all the solutions of low-molecular fraction, the dependence $\Delta n = f(g)$ has the form of a straight line over the entire range of velocity gradients investigated. Similar behavior of solutions of high-molecular fraction depends on the solvent used.

In all cases, the experimental points permit a sufficiently trustworthy determination of the quantity $(\Delta n/g)_{g\to 0}$ of the solution. In the region of concentrations of interest to us, solutions of

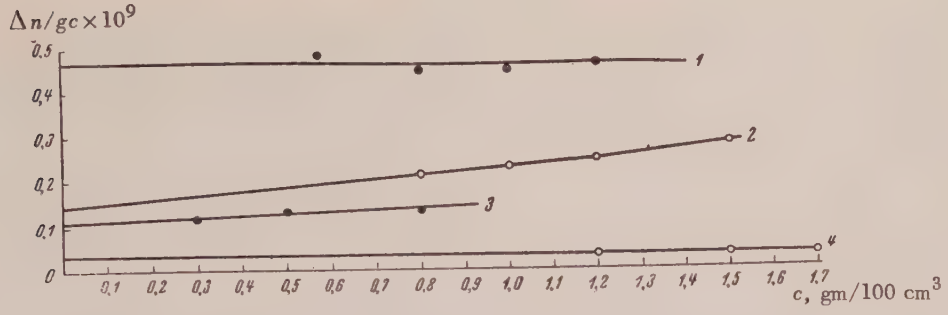

FIG. 8. Dependence of $\Delta n/gc_{g\to0}$ on concentration for a fraction of polymethylmethacrylate ($M = 3.5\times10^5$) in various solvents: *1*-bromoform, *2*-ethyl acetate, *3*-chloroform, *4*-toluene.

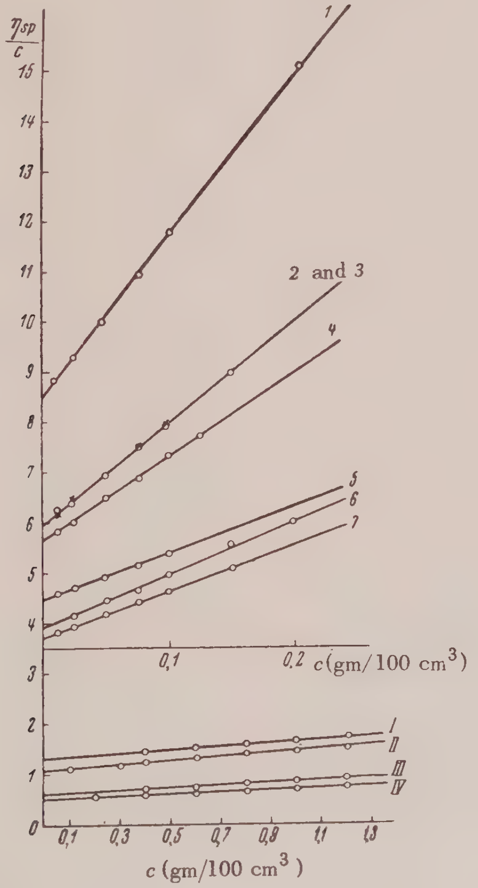

FIG. 9. Dependence of η_{sp}/c on concentration for fractions of polymethylmethacrylate in various solvents. $M = 4.2\times10^6$: *1*-chloroform, *2*-chlorobenzene, *3*-bromoform, *4*-bromobenzene, *5*-ethyl acetate, *6*-toluene, *7*-acetone. $M = 3.5\times10^5$: *I*-chloroform, *II*-bromoform, *III*-ethyl acetate, *IV*-toluene.

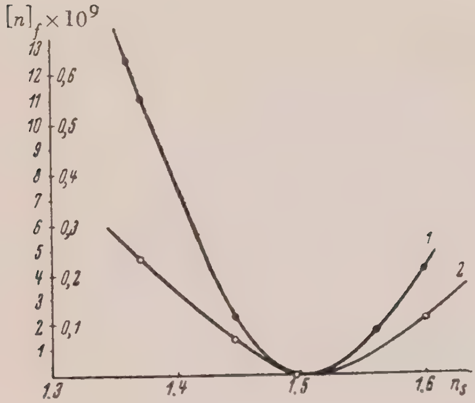

FIG. 10. Dependence of the part of the dynamo-optical constant $[n]_f$ due to the effect of form, on the index of refraction of the solvent n_s : 1-$M = 4.2 \times 10^6$, 2-$M = 3.5 \times 10^5$.

polymethylmethacrylate have a comparatively small magnitude of dynamical birefringence, which makes it necessary to take into account the role of its solvent. This was carried out by assuming additivity of the magnitude of birefringence of the solute and of the solvent. From the value of $(\Delta n/g)_{g\to 0}$ obtained for the solution, the value of $(\Delta n/g)_s$ corresponding to the solvent was calculated, which was measured in all cases when the role of the latter was clearly manifested. The value of $(\Delta n/g)_s$ for the solvents investigated are given in Table I.

The dynamic-optical constants $[n] = \lim\limits_{\substack{g\to 0\\ c\to 0}} \times (\Delta n/g\eta_0 c)$ of the fractions were found from curves of the concentration dependence of the quantity $c^{-1}(\Delta n/g)_{g\to 0} - c^{-1}(\Delta n/g)_s$ by the extrapolation of this quantity to zero concentration. These curves are shown in Figs. 7 and 8. The vlaues of $[n]$ obtained by this means for both fractions are given in columns 6 and 12 of Table I. Concentration measurements of relative viscosity (Fig. 9) permitted the determination of the characteristic viscosity of both fractions of polymethylmethacrylate in various solvents, the values of which are given in columns 5 and 11 of Table I.

4. DISCUSSION OF RESULTS

The experimental results obtained by us should be compared with the basic equations: with Eq. (5) of the theory of anisotropic complexes and with Eq. (9) of the theory of elasto-viscous spheres.

As is shown by Eq. (5), the value of $[n]_f$ may be determined, if the measured values of $[n]$, the dynamo-optical constant and $[n]_e$, the part of it determined by internal anisotropy of the complex, are known.

The hydrodynamical theories of solutions of macromolecules yield the general relation

$$D = RT / B\eta_0 [\eta] M, \qquad (11)$$

where B is a numerical coefficient depending on the particular hydrodynamic model of the molecule. Thus, for the statistics of a coiled complex, theory gives[16,17] $B = 4$, for an extended ellipsoid[18] $B = 6/F(p)$, where $F(p)$ is a form factor. With $p = 3$, $F(p) = 3/2$ and the result for the ellipsoid agrees with the formula for the complex.

Combining Eqs. (5) and (11), and setting $B = 4$, we get

$$[n]_e = 0.11\,[\eta]\,(b/kT)\,[(n_s^2 + 2)^2/n_s]\,(\alpha_1 - \alpha_2). \qquad (12)$$

It cannot be asserted *a priori* that the difference between the polarizabilities of the segment $\alpha_1 - \alpha_2$ in the solvent does not depend on the index of refraction of the latter. At the present time there are not sufficient data for a duscussion of this question. However, it seems probable to us that the effect of a change in $\alpha_1 - \alpha_2$ with a change in n_s will play a considerably smaller role than the effect of the form of the complex. Therefore, as a first approximation, we neglect these changes, and will consider the anisotropy of the segment to be the same in all of the solvents, and to coincide with the quantity $\alpha_1 - \alpha_2$ entering into Eq. (12).

With the use of a solvent whose index of refraction n_s coincides with the index of refraction n_k of the substance, the second term on the right hand side of Eq. (5) becomes zero, so that $[n] = [n]_e$. In our case, toluene satisfies the condition $n_k = n_s$. Thus, the dynamo-optical constant obtained for solutions in toluene, makes it possible to determine $(\alpha_1 - \alpha_2)$. Applying Eq. (12) to toluene, we get

$$\alpha_1 - \alpha_2 = \frac{[n]_t}{[\eta]_t}\,\frac{kT}{0{,}11b}\,\frac{n_t}{(n_t^2 + 2)^2}. \qquad (13)$$

The subscript t indicates that the solvent is toluene. Substituting Eq. (13) for $\alpha_1 - \alpha_2$ into Eq. (12), we obtain for the quantity $[n]_e$ in any solvent

TABLE I

Solvent				$M = 4.2 \times 10^6$			
Substance	$\left(\frac{\Delta n}{g}\right)_s \cdot 10^{12}$	$\eta_s \cdot 10^2$ poise	n_s	$[\eta]$, gm/100 cm^3	$[n] \cdot 10^7$	$[n]_e \cdot 10^7$	$[n]_f \cdot 10^7$
1	2	3	4	5	6	7	8
Chlorobenzene .	1.35	0.800	1,523	5.95	0.866	0.752	0.114
Toluene	0.79	0,589	1,498	3.87	0.480	0.480	0.000
Chloroform . .	0.13	0,592	1,446	8.45	3,340	1.015	2,325
Ethyl Acetate .	0.20	0,510	1.372	4.45	11,500	0.500	11.000
Bromoform . .	1.04	2.080	1.598	5.92	5.000	0.784	4,216
Bromobenzene .	2.20	1.167	1.560	5,65	2,545	0.737	1,808
Acetone	—	0.347	1.359	3,70	12,967	0.417	12.550

$$[n]_e = [n]_t \frac{[\eta]}{[\eta)_t} \frac{n_t}{n_s} \frac{(n_s^2+2)^2}{(n_t^2+2)^2} . \qquad (12')$$

The expression for $[n]_f$ entering into Eq. (5), may be transformed by the substitution in it of the coefficient of rotational diffusion from the relation

$$D = kT / \eta_0 V f_0, \qquad (11')$$

where f_0 is a form factor determined by Eq. (16). The use of (11′) and (12′) in Eq. (5) gives

$$[n]_f = \frac{M}{120 \pi \rho^2 RT} \{(L_2 - L_1) b f_0\} \frac{(n_k^2 - n_s^2)^2}{n_s^3} \qquad (14)$$

$$= [n] - [n]_t \frac{[\eta]}{[\eta]_t} \frac{n_t}{n_s} \frac{(n_s^2+2)^2}{(n_t^2+2)^2} .$$

All of the quantities entering into the right hand side of Eq. (14) are obtained from the experiments. The values of $[n]_e$, obtained from the experimental data through Eq. (12′), are presented in Table I for all the solvents investigated. Also tabulated is the quantity $[n]_f$, calculated as the difference between $[n]$ and $[n]_e$.

The dependence $[n]_f = f(n_s)$ is shown in Fig. 10 for the two fractions of polymethylmethacrylate. The ordinate has a scale corresponding to each molecular weight. It is evident from the graph that in both cases the points lie on parabolic curves, in agreement with Eq. (14).

Using the obtained values of $[n]_f$, the factor $(L_2 - L_1)bf_0$ of Eq. (14) may be calculated. The results for both fractions investigated are given in columns 9 and 15 of Table I. The factor $(L_2 - L_1)bf_0$ is a single-valued function of the ratio p of the axes of the macromolecule, and makes it possible to determine p through the use of the well-known relations[5-7]:

$$L_2 - L_1 \qquad (15)$$

$$= \frac{\pi}{p^2-1}\left(2p^2 + 4 - \frac{3p}{\sqrt{p^2-1}} \ln \frac{p+\sqrt{p^2-1}}{p-\sqrt{p^2-1}}\right);$$

$$\overline{f_0} \qquad (16)$$

$$= \frac{p^2}{4(p^4-1)}\left(-1 + \frac{2p^2-1}{2p\sqrt{p^2-1}} \ln \frac{p+\sqrt{p^2-1}}{p-\sqrt{p^2-1}}\right).$$

The values of p obtained in this way are given in columns 10 and 16 of Table I. Within the limits of experimental error, these quantities appear to be constants for a given fraction, independent of the solvent, and close to one-another for the two fractions investigated. The somewhat low value of p found for the low-molecular fraction is explained, possibly, by the large relative error in the determination of $[n]_e$ for this fraction. In any case, the experimental values of p, lying in a range from 2 to 3, may be considered to be in good agreement with the theoretical values predicted by the statistical theory of Kuhn[3].

The experimental data of Table I allow one comparison to be made with the results of orientation theory. Using Eqs. (12), (14), (11) and (11′), it is not difficult to obtain the relation

TABLE I

Substance	$M=4.2\times 10^6$		$M=3.5\times 10^5$					
	$(L_2-L_1)bf_0$ 9	$p=\frac{A}{B}$ 10	$[\eta]$,(gm/100 cm^3) 11	$[n]\cdot 10^7$ 12	$[n]_e\cdot 10^7$ 13	$[n]_f\cdot 10^7$ 14	$(L_2=L_1)bf_0$ 15	$p=\frac{A}{B}$ 16
Chlorobenzene .	24.4	2.32						
Toluene	—	—	0.58	0.058	0.058	0.000	—	—
Chloroform . . .	60.6	3.30	1.28	0,189	0.118	0.071	22.1	2.20
Ethyl Acetate . .	44.5	2.92	0.51	0.277	0.045	0.232	11.3	1.80
Bromoform . . .	40.8	2.82	1.06	0.224	0.111	0,113	13.2	1.85
Bromobenzene .	44.4	2.92						
Acetone	43.2	2.90						

$$\frac{[n]}{[\eta]}=\frac{[n]_e}{[\eta]}+\frac{[n]_f}{[\eta]}=0,11\ \frac{b}{kT}\frac{\left(n_s^2+2\right)^2}{n_s}(\alpha_1-\alpha_2) \tag{17}$$

$$+\frac{1}{30\pi\rho^2 N_A RT}\frac{\left(n_k^2-n_s^2\right)^2}{n_s^3}(L_2-L_1)\,b\,\frac{M^2}{V}$$

$$=\frac{[n]_t}{[\eta]_t}\frac{n_t}{n_s}\frac{\left(n_s^2+2\right)^2}{\left(n_t^2+2\right)^2}$$

$$+\frac{M}{[\eta]}\frac{\left(n_k^2-n_s^2\right)^2}{n_s^3}\{(L_2-L_1)\,bf_0\}\frac{1}{120\,\pi\rho^2 RT},$$

which indicates that in one and the same solvent, in the presence of the effect of form ($n_k\neq n_s$), the quantity $[n]/[\eta]$ must depend on the molecular weight of the fraction. Actually, experiments with fractions of polystyrene in butanone ($n_k-n_s = 0.21$) showed a sharp increase of $[n]/[\eta]$ with an increase in the molecular weight of the fractions[15]. On the contrary, for fractions of polybutadiene[19] and polystyrene[15] in solvents with indices of refraction close to the index of refraction of the polymer ($n_k-n_s\approx 0$), the experiments disclosed the constancy of $[n]/[\eta]$ with a change in M, which is in full agreement with Eq. (17).

A comparison of the magnitudes of $[n]/[\eta]$ for the two fractions of polymethylmethacrylate investigated in the present work, in four solvents, is made in Table II. In the last column of the Table, the ratio X is given, of the magnitudes of $[n]/[\eta]$ corresponding to the fractions $M = 4.2\times 10^6$ and $M = 3.5\times 10^5$ in one and the same solvent. The value of X increases with an increase in $n_k - n_s$, in accordance with Eq. (17). For toluene ($n_k = n_s$) one would expect $X = 1$. The too-high value $X = 1.24$, found in the experiment, is apparently associated with the fact that in the calculation of the quantity $[n]/[\eta]$, the extrapolation of $[\eta]$ to $g\to 0$ was not made, which for the high-molecular fraction may introduce a noticeable error in a direction to increase the values of $[n]/[\eta]$.

We compared the experimental results with Eq. (5) of the theory of anisotropic complexes. A similar comparison can be made with Eq. (9) of the theory of elasto-viscous spheres. For this,

TABLE II. Comparison of the magnitudes of $[n]/[\eta]$ for two fractions of polymethylmethacrylate in various solvents.

Solvent	n_k-n_s	$[n]/[\eta]\cdot 10^{10}$		$X=\left\{\left(\frac{[n]}{[\eta]}\right)_2\Big/\left(\frac{[n]}{[\eta]}\right)_3\right\}$
		$M=4.2\times 10^6$	$M=3.5\times 10^5$	
Toluene	0.002	1.24	1.00	1.24
Chloroform	0.054	3.95	1.48	2.66
Bromoform	0.098	8.44	2.11	4.00
Ethyl Acetate	0.128	25.80	5.45	4.75

TABLE III. Characteristic constants of macromolecules of poymethylmethacrylate according to the theory of elasto-viscous spheres.

Solvent	$M = 4.2\times10^6$			$M = 3.5\times10^5$		
	δ_0	p according to Eq. (22)	$\mu\cdot10^{-2}$	δ_0	p according to Eq. (22)	$\mu\cdot10^{-4}$
Bromoform	0.34	1.55	0,72	0.20	1.3	1,50
Chloroform	0.43	1,70	0,31	0.26	1.4	0.67
Ethyl Acetate	0.38	1.61	0,75	0.20	1.3	3.10
Chlorobenzene	0.27	1.41	1,17	—	—	—
Acetone	0.36	1.57	0,68	—	—	—
	0.38	1.61	0,93	—	—	—

the dynamo-optical constant Δ of Eq. (9) is transformed into the characteristic value $[n]$ of Eq. (5), by converting from the volume concentrations Ω to weight concentrations g/cm^3. Taking into account that in Eq. (9), $\Omega = VcN_A/M$, we obtain in place of (9),

$$[n] = \lim\left(\frac{\Delta n}{g\eta_0 c}\right)_{\substack{g\to0\\c\to0}} = \frac{5\varepsilon}{\mu}\theta\frac{n_s VN_A}{M} + \frac{2}{\mu}\left(\frac{n_\omega - n_s}{n_\omega}\right)^2\theta\frac{n_s VN_A}{M}, \tag{18}$$

and using Eqs. (1) and (2), we will have

$$[n]_e = 5n_s N_A\theta\frac{\varepsilon V}{\mu M}; \tag{19}$$

$$[n]_f = \frac{2}{\mu}\theta\frac{M}{V\rho^2 N_A}\frac{(n_k - n_s)^2}{n_s}.$$

It is convenient to modify expressions (19) somewhat, using in the formulas for $[n]_e$, the Einstein equation, appearing in the combination of (11) and (11′) for suspended spherical particles:

$$VN_A/M = [\eta]/2.5 \tag{20}$$

and introducing into the expression for $[n]_f$, the quantity δ_0 from Eq. (7) of the theory of elasto-viscous spheres. Then in place of Eq. (19) we obtain

$$[n]_e = 2n_s\theta[\eta]\varepsilon/\mu; \tag{21}$$

$$[n]_f = \frac{6M}{RT\rho^2}\frac{(n_k - n_s)^2}{n_s}\theta\delta_0^2.$$

Equations (21) apparently may be used for an approximate determination of the quantities ϵ/μ and δ_0 from the experimental data since variations of the unknown factor θ are insignificant ($1 \geq \theta \geq 3/5$). The quantity $[n]_e$ is obtained from measurements in toluene. According to the data in Table II, $[n]/[\eta]$ is close to 1×10^{-10} for both fractions in toluene. Therefore, assuming $n_s = 1.5$ and $\theta = 3/5$, we obtain $\epsilon/\mu = 5.5\times10^{-11}$ for both of the fractions investigated. Hence, taking Eq. (10) into account, it follows that $(n_1 - n_2)/n_\omega = 1.4\times10^{-10}\eta_0 g$. This means that the magnitude of the relative difference between the indices of refraction of the equivalent elasto-viscous sphere is determined by the magnitude of the shearing stress in the flow, and does not depend on the molecular weight (at least with a change of the latter from 3.5×10^5 to 4.2×10^6).

Expression (21) for $[n]_f$ is completely analogous in form to Eq. (14) and, therefore, conforms as well as Eq. (14), to the parabolic dependence $[n]_f = f(n_s)$ obtained experimentally. Values of δ_0 are given in Table III, calculated by Eq. (21) with the use of the experimental magnitudes of $[n]_f$ in Table I. Here, we have used $\theta = 3/5$, which corresponds to the case of pure orientation. In the case of pure deformation, $\theta = 1$, and the values of δ_0 become 1.3 times smaller than those given in Table III.

The ratios of the axes of the deformed sphere p may be calculated from the values of δ_0 according to the formula

$$p = (1 + \delta_0)^{3/2}. \tag{22}$$

The values thus obtained are represented in Table III. Combining Eq. (20) and the expression for $[n]_f$ in the form (19) yields

$$\mu = \frac{5\theta}{\rho^2[\eta][n]_f}\frac{(n_k - n_s)^2}{n_s}. \tag{23}$$

Relation (23) may be used for the determination of μ. The values of μ thus obtained are given in the last column of Table III. These values have the same order of magnitude in the various solvents and decrease with an increase of M, which is found fo be in agreement with the predictions of the theory of elasto-viscous spheres.

The coefficients of asymmetry δ_0 and p found by Eqs. (21) and (22) are practically the same for the various solvents and molecular weights. They are smaller in absolute value than the magnitudes of p calculated by Eq. (14), although of the same order of magnitude. However, the latter circumstance apparently is associated with peculiarities of the calculation of the optical effect of form in the theory of elasto-viscous spheres, because in principal, for the case of pure orientation ($\theta=3/5$), Eq. (21) could coincide exactly with Eq. (14) of the orientation theory. In any case, the values of p (or δ_0) from Eq. (14) as well as from Eq. (21) are sufficiently large. Therefore, even from the point of view of the theory of elastic spheres[10], it is not possible to neglect the effect of orientation in the region $g \to 0$ for the polymer $M = 4.2\times 10^6$. However, the most serious difficulty in the interpretation of our results from the point of view of the model of elasto-viscous spheres is the fact that, for this model, δ_0 should decrease with an increase of the molecular weight of the sample, while the experimental data lead to the conclusion that δ_0 practically does not change with a change of more than a factor of ten in M.

---

[1] V. N. Tsvetkov and E. V. Frisman, Acta Physiochim.USSR 20, 61, 363 (1945).

[2] V. N. Tsvetkov and E. V. Frisman, Dokl. Akad. Nauk SSSR **97**, 647 (1954).

[3] W. Kuhn, Kolloid Z. **68**, 2 (1934).

[4] W. Kuhn and H. Grun, Kolloid Z. **101**, 248 (1942).

[5] J. C. Maxwell, *Treatise on Electricity and Magnetism*, 1873.

[6] R. Gans, Ann. Physik **37**, 881 (1912).

[7] A. Peterlin, Makromolek. Chem. **13**, 102 (1954).

[8] A. Peterlin and H. A. Stuart, Z. Physik **112**, 1, 129 (1939).

[9] R. Cerf, J. Chim. Phys. **48**, 59, 85 (1951); **52**, 53 (1955).

[10] R. Cerf, J. Polymer. Sci. **12**, 15, 35 (1954).

[11] V. N. Tsvetkov and A. I. Petrova, Rubb. Chem. Tech. **19**, 360 (1946).

[12] V. N. Tsvetkov and A. I. Petrova, Zhurn. fiz. khim. **23**, 368 (1949).

[13] V. N. Tsvetkov, K. Z. Fattakhov and O. V. Kallistov, J. Exptl. Theoret. Phys. (U.S.S.R.) **26**, 351 (1954).

[14] E. V. Frisman and V. N. Tsvetkov, J. Exptl. Theoret. Phys. (U.S.S.R.) **23**, 690 (1952).

[15] E. V. Frisman and V. N. Tsvetkov, J. Tech. Phys. (U.S.S.R.) **25**, 448 (1955).

[16] W. Kuhn and H. Kuhn, Helv. Chim. Acta. **36**, 31 (1953).

[17] J. Riseman and J. C. Kirkwood, J. Chem. Phys. **17**, 442 (1949)

[18] W. Kuhn, H. Kuhn and P. Buchner, Ergebn. exakt. Naturwis. **25**, 100 (1951).

[19] V. N. Tsvetkov, A. I. Petrova and I. Ia. Poddubnyi, Zh. fiz. khim. **24**, 994 (1950).

Translated by D. Lieberman
135

SOVIET PHYSICS JETP VOLUME 3, NUMBER 4 NOVEMBER, 1956

Contribution to the Theory of Production and Annihilation of Antiprotons

L. M. Afrikian
P. N. Lebedev Physical Institute, Academy of Sciences, USSR
and
Physical Institute, Academy of Sciences, Armenian SSR

(Submitted to JETP editor January 18, 1955)
J. Exptl. Theoret. Phys. (U.S.S.R.) 30, 734-745 (April, 1956)

The processes leading to production of antiprotons by π-mesons on nucleons are considered in the framework of charge-independent pseudoscalar meson theory. The cross sections for these processes are calculated near the threshold. It is shown that the interaction between the particles in the final state may lead to a capture of the antiproton produced by a nucleon into a deuteron-like orbit. This last fact may make it difficult to detect antiprotons near the threshold because of the high capture probability, and the short life ($\tau \approx 10^{-21}$ sec) of the antiproton in the bound state with respect to annihilation.

Processes leading to antiproton production in nucleon-nucleon collisions are also considered. The cross sections for these processes are calculated near the threshold, taking into account the interaction between the created particles.

THE question of the existence and the properties of antiprotons (i.e., particles of proton mass and negative charge) has recently attracted a good deal of attention in connection with the possibility of obtaining such particles from new powerful accelerators.

It is well known that the hypothesis of the existence of an antiproton (and an antineutron) arose by analogy with the conception of the positron, which was the logical consequence of the relativistic quantum theory of the electron as a particle of spin ½. Indeed, from the description of the nucleon as an elementary particle of spin ½, which is therefore described by the corresponding Dirac equation

$$\{c(\vec{\alpha}\mathbf{P}) + \beta M\}\Psi_N = E\Psi_N,$$

the requirement that there should exist a complete set of linearly independent solutions of this equation leads one in a similar way to assume the existence of antiparticles, i.e., antinucleons, which have antiprotons and antineutrons as different charge states.

It should be stressed, however, that, in spite of its origin, the antiproton hypothesis is not an exclusive feature of the Dirac theory, but is based directly on the idea of charge conjugation symmetry, which is fundamental to the whole modern theory of elementary particles. Although one cannot rule out the possibility that the nucleon has to be described by an equation of a type other than Dirac's, the only rational approach to the antiproton problem at this time is from the point of view of the Dirac theory; however, we must then allow for the strong interaction of the nucleons with the meson field. A theoretical analysis of all experimental facts from the point of view indicated above gives us indirect evidence in favor of the existence of antiprotons.

We are thinking here, in the first place, of the well-known decay of the neutral π-meson into two γ-quanta which, apparently, can proceed only through the formation and annihilation of a virtual proton-antiproton pair: $\pi^0 \to p + \tilde{p} \to 2\gamma$; second, of the appearance of an appreciable S-wave contribution in the scattering and photoproduction of charged mesons on nucleons, in conditions when the nucleon may be taken as nonrelativistic. The last fact is also due to the contribution from virtual antiproton pairs (under the assumptions of the pseudoscalar coupling theory). Third, we have the fact that the masses of the charged π-mesons are equal in good approximation, and exceed that of the π^0 by about 9 electron masses.

This difference can be deduced in order of magnitude from the Coulomb mass defect in the virtual proton-antiproton system*, a state in which the π^0-meson spends part of its time.

But what are the possibilities of finding real antiprotons under laboratory conditions? The purpose of the present work is to obtain a theoretical estimate of the cross sections for the following effects: (1) the production of antiprotons by π-mesons on nucleons, (2) the production of antiprotons in nucleon-nucleon collisions.

The theoretical study of such problems meets at present with insuperable difficulties because of the lack of a consistent theory of nuclear forces, and of adequate methods for solving the quantum mechanical problems. For this reason we were forced to obtain preliminary estimates by means of perturbation theory, and consequently, our results cannot claim to have more than qualitative value, even within the limits of our assumptions.

---

* For this one has to use the known data on the electromagnetic dimensions of the proton.

Nevertheless, a comparison of the results of such calculations with experimental data may turn out to be of some use for constructing a more complete theory of these phenomena.

In the future we hope to treat the same problems more rigorously, on the basis of a semi-phenomenological method, and using the theory of the spin 3/2 state[1], i.e., allowing for excited ("isobaric") states of the nucleons.

I. PRODUCTION OF ANTIPROTONS IN π-MESON-NUCLEON COLLISIONS

Consider the following antiproton production processes:

a) $\pi^- + p \rightarrow n + p + \tilde{p}$;

b) $\pi^+ + n \rightarrow p + p + \tilde{p}$;

c) $\pi^- + n \rightarrow n + n + \tilde{p}$.

The threshold value of the kinetic energy of a π-meson for the production of a nucleon-antinucleon pair on a nucleon at rest is

$$T_\pi^{\min} = 4M - \mu (1 + \mu / 2M) = 3.45 \text{ bev.}$$

π-mesons of this energy begin to be emitted in a nucleon-nucleon collision when the energy of the incident nucleon (in the system in which the other nucleon is at rest) reaches the value

$$T_{N1}^{\min} = 4.15 \text{ bev.}$$

The matrix elements for the processes a), b) and c) were calculated in the first nonvanishing approximation, i.e., in the third order of perturbation theory. In this approximation the reaction of the self-field of the nucleon is neglected, and therefore such an approximation can have some kind of validity only near the threshold of the reaction, where the energy of the final nucleons (and of the antiproton) is much less than the excitation energy, $\Delta \approx 250$ mev, of the first isobaric state, i.e., as long as*

$$E - E_0 \ll 2\Delta. \qquad \text{(I.1)}$$

Near the threshold the modulus of the matrix element is a slowly varying function of the momenta of the particles in their final states, and may be represented by a series in powers of v/c. Thus, the energy dependence of the cross section is, in the indicated region, essentially determined by the statistical factor, together with general symmetry requirements. On the other hand it is easy to see that in the region limited above by (I.1) the kinetic energies of the particles in the final state do not exceed appreciably the depth of the potential well of the nuclear forces; hence, it is in general not legitimate to neglect the interactions in the final state. Therefore, the expressions for the antiproton production cross section which neglect the interactions in the final state can be right at best in a narrow energy interval, near the upper end of the threshold region. In therest of the region, closer to the threshold, the strong interactions between the particles must substantially affect the magnitude and the energy dependence of the cross sections.

One of the above processes, namely $\pi^- + p \rightarrow n + p + \tilde{p}$, was considered in a number of papers by various authors. This process was first studied by McConnell[2] using a generalized Weizsäcker – Williams method in the theory of radiation damping, but without allowing for exchange, or for the nucleon recoil, which are very important near the threshold. Later the same process was studied[3] by the same method as in Ref. 2, but with a phenomenological treatment of the damping. In addition, these authors[3] started from incorrect values for the threshold energy for pair creation*. In a short communication[5] calculations of cross section of the process under discussion were reported, using third-order perturbation theory, for the special case of pseudoscalar coupling. It must be pointed out that all these papers neglect the interaction of the particles in the final state since these authors[2,3,5] did not concentrate their attention on the threshold region, the only region which is in any sense accessible to the perturbation theory they were using.

1. *General statement of the problem and calculation of the cross sections without allowing for interactions in the final state.*

The basic equation of our problem is the Schwinger-Tomonaga equation

$$i\delta F[\zeta(r)] / \delta\zeta(r) = \hat{H}'(r) F[\zeta(r)], \qquad \text{(I.2)}$$

where $\hat{H}'$ is the Hamiltonian density of the interaction between the nucleon field and a pseudoscalar meson field.

$$\hat{H}' = ig\overline{\Psi}\tau_\alpha \gamma_5 \Psi \tilde{\varphi}_\alpha + \frac{f}{\mu} \overline{\Psi}\tau_\alpha \gamma_5 \gamma_\nu \Psi \frac{\partial \tilde{\varphi}_\alpha}{\partial x_\nu}; \qquad \text{(I.3)}$$

$$(\nu = 1, 2, 3, 4).$$

Here

---

* E_0 is the threshold energy in the laboratory system.

* The authors[3] quote a paper[4] which, however, gives the threshold energy only for pair production in an inelastic collision between particles, without any of them disappearing.

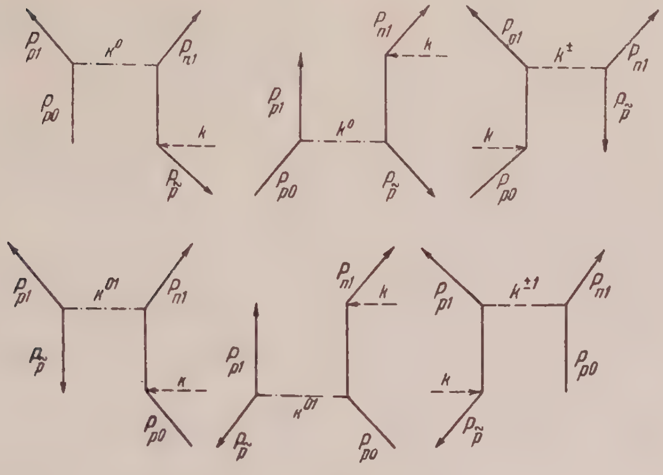

FIG. 1

$\gamma_k = \beta\alpha_k \quad (k = 1, 2, 3);$

$$\gamma_4 = \beta; \quad \gamma_5 = i\gamma_1\gamma_2\gamma_3\gamma_4;$$

τ_α are the isotopic spin matrices; g and f the coupling constants.

The operators of the free nucleon and meson ields are obtained from the equations

$$i\gamma_\nu \partial\Psi / \partial x_\nu - M\Psi = 0; \qquad \text{(I.4)}$$

$$i\partial\overline{\Psi} / \partial x_\nu \gamma_\nu + M\overline{\Psi} = 0;$$

$$\partial^2\tilde{\varphi}_\alpha / \partial x_\nu^2 - \mu^2 \tilde{\varphi}_\alpha = 0.$$

The solution of Eq. (I.2) amounts to the determination of the operator $\hat{S}$ which generates the final state function F_f of the whole system from the initial state function F_i: $F_f = \hat{S}F_i$. The probability of the transitions in the nucleon-meson field in which we are interested is then expressed in terms of the S matrix as

$$W_{if} = |S_{if}^{(n)}|^2, \qquad \text{(I.5)}$$

and we may write

$$S_{if}^{(n)} = R_{if}^{(n)} \delta(\Delta\overline{P}), \qquad \text{(I.6)}$$

where $R_{if}^{(n)}$ is the matrix element of the transition, $\delta(\Delta\overline{P})$ the four-dimensional delta-function, and $\overline{P}$ the four-momentum.

The differential cross section for nucleon-ntiproton production processes in a π-meson ucleon collision neglecting the interactions in he final state becomes

$$d\sigma = \frac{1}{2J_0}\sum_i^s\sum_f^s |R_{if}|^2 \rho_f \frac{1}{(2\pi)^4}\delta(\Delta E)\,\delta(\Delta\mathbf{P}); \qquad \text{(I.7)}$$

$$\rho_f = \frac{1}{(2\pi)^9}\prod_{k=1}^{3} d\mathbf{P}_k; \quad \Delta E = E_i - E_f; \Delta\mathbf{P} = \mathbf{P}_i - \mathbf{P}_f;$$

Here J_0 is the incident particle flux. The square modulus of the matrix element is to be averaged over the spin in the initial state, and summed over the spins in the final state, with the aid of the projection operators:

$$\Lambda_+ \to (\hat{P} + M)/2E \text{ for a nucleon;}$$

$$\Lambda_- \to (\hat{P}_\sim - M)/2E_\sim \text{ for an antiproton*.}$$

It is seen from (I.6) and (I.7) that the determination of the differential cross sections requires the solution of Eq. (I.3). The only Lorentz-invariant method for solving this equation which is known at present is the approximate representation of the state function F as a series in increasing powers of the coupling constant. For constructing this series one can immediately obtain the required operator $\hat{S}$ from the given operator $\hat{H}'$ using the well-known Feynman-Dyson prescriptions[6,7]. Thus, in the case of the process $\pi^- + p \to n + p + \tilde{p}$ we have for the transition matrix element in the first nonvanishing approximation six Feynman graphs (Fig. 1). Three of these graphs correspondto the possibility of an exchange between the recoil proton and the vacuum proton; they are a consequence of the antisymmetry of the wave amplitude of the initial state in the nucleon variables ξ:

---

* We use throughout the notation of Feynman[6], using for an arbitrary four vector a the convention $\hat{a} = \gamma_\nu a_\nu$ $(\nu = 1, 2, 3, 4)$, with $(\overline{a}\,\overline{b}) \equiv a_4 b_4 - \mathbf{ab}$, so that $\hat{P} \equiv i\beta(\partial/\partial t) + i\beta(\vec{\alpha}\nabla)$.

$$\chi_i(\xi_1, \xi_2, \eta) = 2^{-1/2}\{\Psi_{p_-}(\xi_1)\Psi_{p0}(\xi_2) - \Psi_{p_-}(\xi_2)\Psi_{p0}(\xi_1)\}\varphi(\eta).$$

Each of these graphs is equivalent to two chains of the ordinary perturbation theory, and contains as elements both the interaction of the nucleons with the external field (charged mesons) and the interaction of the nucleons with each other, which is transmitted by charged as well as neutral mesons.

The complete matrix element for the transition is

$$R_{if} = \sum_{n=1}^{6} R_{if}^{(n)}, \tag{I.8}$$

where

$$R_{if}^{(1)} = iA\left(\bar{u}_{p1}\left\{ig\gamma_5 + \frac{f}{\mu}\gamma_5\hat{k}^0\right\}\tau_0 u_{p0}\right)[k^{02} - \mu^2]^{-1}$$
$$\times\left(\bar{u}_{n1}\tau_0\left\{\left(ig\gamma_5 - \frac{f}{\mu}\gamma_5\hat{k}^0\right)[-\hat{P}_{\sim} + \hat{k} - M]^{-1}\left(ig\gamma_5 + \frac{f}{\mu}\gamma_5\hat{k}\right)\right\}\tau_- u_{\tilde{p}}\right);$$

$$R_{if}^{(2)} = iA\left(\bar{u}_{p1}\left\{ig\gamma_5 + \frac{f}{\mu}\gamma_5\hat{k}^0\right\}\tau_0 u_{p0}\right)[k^{02} - \mu^2]^{-1}$$
$$\times\left(\bar{u}_{n1}\tau_-\left\{\left(ig\gamma_5 + \frac{f}{\mu}\gamma_5\hat{k}\right)[\hat{P}_{n1} - \hat{k} - M]^{-1}\left(ig\gamma_5 - \frac{f}{\mu}\gamma_5\hat{k}^0\right)\right\}\tau_0 u_{\tilde{p}};$$

$$R_{if}^{(3)} = iA\sum_{k';k=+,-}\left(\bar{u}_{p1}\tau_k\left\{ig\gamma_5 - \frac{f}{\mu}\gamma_5\hat{k}^{\pm}\right\}[\hat{P}_{p0} + \hat{k} - M]^{-1}\right.$$
$$\left.\times\left\{ig\gamma_5 + \frac{f}{\mu}\gamma_5\hat{k}\right\}\tau_- u_{p0}\right)[k^{\pm 2} - \mu^2]^{-1}\left(\bar{u}_{n1}\left\{ig\gamma_5 + \frac{f}{\mu}\hat{k}^{\pm}\right\}\tau_{k'} u_{\tilde{p}}\right);$$

$$R_{if}^{(4)} = -iA\left(\bar{u}_{p1}\left\{ig\gamma_5 + \frac{f}{\mu}\gamma_5\hat{k}^{01}\right\}\tau_0 u_{\tilde{p}}\right)[k^{02} - \mu^2]^{-1}$$
$$\times\left(\bar{u}_{n1}\tau_0\left\{\left(ig\gamma_5 - \frac{f}{\mu}\gamma_5\hat{k}^{01}\right)[\hat{P}_{p0} + \hat{k} - M]^{-1}\left(ig\gamma_5 + \frac{f}{\mu}\gamma_5\hat{k}\right)\right\}\tau_- u_{p0}\right);$$

$$R_{if}^{(5)} = -iA\left(\bar{u}_{p1}\left\{ig\gamma_5 + \frac{f}{\mu}\gamma_5\hat{k}^{01}\right\}\tau_0 u_{\tilde{p}}\right)[k^{012} - \mu^2]^{-1}$$
$$\times\left(\bar{u}_{n1}\tau_-\left\{\left(ig\gamma_5 + \frac{f}{\mu}\gamma_5\hat{k}\right)[\hat{P}_{n1} - \hat{k} - M]^{-1}\left(ig\gamma_5 - \frac{f}{\mu}\gamma_5\hat{k}^{01}\right)\right\}\tau_0 u_{p0}\right);$$

$$R_{if}^{(6)} = -iA\sum_{k:k=+,-}\left(\bar{u}_{p1}\tau_k\left\{ig\gamma_5 - \frac{f}{\mu}\gamma_5\hat{k}^{\pm 1}\right\}[-\hat{P}_{\sim} + \hat{k} - M]^{-1}\right.$$
$$\left.\times\left\{ig\gamma_5 + \frac{f}{\mu}\gamma_5\hat{k}\right\}\tau_- u_{\tilde{p}}\right)[k^{\pm 12} - \mu^2]^{-1}\left(\bar{u}_{n1}\left\{ig\gamma_5 + \frac{f}{\mu}\gamma_5\hat{k}^{\pm 1}\right\}\tau_{k'} u_{p0}\right).$$

Here $(2\pi)^{-6} A = (2/\pi E_\mu)^{1/2}$; u_{p1}, u_{p0}, u_{n1}, $u_{\tilde{p}}$ are bispinors corresponding to the final and initial states of the recoil proton and to the states of the neutron-antiproton pair; $\hat{P}_{p1}$, $\hat{P}_{p0}$, $\hat{P}_{n1}$, $\hat{P}_{\tilde{p}}$ are the operators of the energy-momentum vectors of the particles in the states indicated by the subscript; $\hat{k}_1$, $\hat{k}_1^0$; $\hat{k}_1^{01}$, $\hat{k}_1^{\pm}$, $\hat{k}^{\pm 1}$ are the energy-momentum vectors of the real and virtual mesons (both neutral and charged).

By using the Dirac equation for the nucleons in their initial and final states:

$$(\hat{P}_{p0} - M)u_{p0} = 0; (-\hat{P}_{\tilde{p}} - M)u_{\tilde{p}} = 0; \qquad \bar{u}_{n1}(\hat{P}_{n1} - M) = 0; \quad \bar{u}_{p1}(\hat{P}_{p1} - M) = 0, \tag{I.9}$$

and remembering the relations $\gamma_5\gamma_\nu = -\gamma_\nu\gamma_5$; $\gamma_5^2 = -1$; $\hat{a}\hat{b} + \hat{b}\hat{a} = 2(\overline{a}\,\overline{b})$, it is easy to simplify the expression (I.8). We then form the square modulus of the matrix element and note that

$$\hat{P}^2 = M^2; \quad \hat{k}^2 = \mu^2; \quad \bar{\gamma}_5 = \gamma_4\overset{+}{\gamma}_5\gamma_4 = -\gamma_5,$$

We then obtain for $1/2\sum_i^s\sum_f^s|R_{if}|^2$ a very complicated experssion, which is valid in any coordinate system.

In the region of interest to us, in which the final particle energies are small, this expression takes a particularly simple form in the center-of-mass system in which the energy-momentum conservation equation $\overline{k} + \overline{P}_{p0} = \overline{P}_{n1} + \overline{P}_{\tilde{p}}$ becomes, in three-dimensional notation

$$\sqrt{k^2+\mu^2}+\sqrt{k^2+M^2} \qquad (\text{I.10})$$

$$= E_{n1}+E_{p1}+E_{\tilde{p}};$$

$$0 = \mathbf{P}_{n1}+\mathbf{P}_{p1}+\mathbf{P}_{\tilde{p}}.$$

Then we have near the threshold, where

$$|\mathbf{P}_{n1}| \approx |\mathbf{P}_{p1}| \approx |\mathbf{P}_{\tilde{p}}| \ll M$$

for *PS-PS* theory

$$\frac{1}{2}\sum_i^s\sum_f^s |R_{if}|^2 \approx 6.12\, g^6 \frac{\pi^3}{M^7}(2\pi)^8$$

and for *PS-PV* theory

$$\frac{1}{2}\sum_i^s\sum_f^s |R_{if}|^2 \approx 19.2\, f^6 \frac{\pi^3}{M^7}\left(\frac{M}{\mu}\right)^6 (2\pi)^8.$$

Thus, to the approximation used here, the differential cross section of the process depends on the momenta and directions of the final particles only through the element of phase space of the system in its final state:

$$(2\pi)^{-9}\, d\mathbf{P}_{n1}\, d\mathbf{P}_{p1}\, d\mathbf{P}_{\tilde{p}}\, \delta(\Delta E)\, \delta(\Delta\mathbf{P}).$$

The cross section for the production of an antiproton in a π-meson-proton collision becomes, in terms of the laboratory energy:

$$\sigma_1 = K_1(E_\mu - 4M)^2 / M^2\, \text{см}^2, \qquad (\text{I.11})$$

where $K_1 = 6.2 \times 10^{-30} g^6$ for *PS-PS*, and $K_1 = 2 \times 10^{-24} f^6$ for *PS-PV* theory.

In a similar manner we find for the cross section for antiproton production in a π^+-neutron collision*

$$\sigma_2 = K_2(E_\mu - 4M)^2/M^2\ \text{см}^2, \qquad (\text{I.12})$$

where $K_2 = 1.5 \times 10^{-30} g^6$ for *PS-PS*, and $K_2 = 1.2 \times 10^{-24} f^6$ for *PS-PV* theory.

Turning now to the antiproton production by a negative π-meson on a neutron

$$\pi^- + n \rightarrow n + n + \tilde{p},$$

we have in the first nonvanishing approximation six Feynman graphs. Without writing down the corresponding matrix elements we note as the distinguishing feature of this process that the modulus of the matrix element vanishes if we neglect the momenta in the final state. We therefore go to the next approximation, including terms of the order $|\mathbf{P}|^2/M^2$, and find for the total cross section

$$\sigma_3 = K_3(E_\mu - 4M)^3 / M^3\, \text{см}^2, \qquad (\text{I.13})$$

where $K_3 = 2.5 \times 10^{-34} g^6$ for *PS-PS* theory.

2. *Calculation of the antiproton production cross section with allowance for the interactions between particles in their final states.*

As already mentioned, the upper limit of validity of the approximation used above comes from the requirement that the energies of the final particles be small compared to the excitation energy of the first isobaric state. For antiproton production processes in π-meson-nucleon collisions this gives the condition (in the center-of-mass system):

$$E - 3M \ll \Delta \approx 2\mu \approx 300 \text{ mev} \qquad (\text{I.14})$$

or, in other words, the share of the energy belonging to each of the final particles must satisfy $\epsilon \ll 100$ mev. For the energy of the incident π-meson we have (in the laboratory system)

$$E_\mu - 4M \ll 3\mu \approx 450 \text{ mev}.$$

Thus, the approximation used above is valid at best if the energies of the final particles do not exceed 20-30 mev (in the center-of-mass system) and this is of the same order of magnitude as the depth of the potential well of the nuclear forces. Therefore, the expressions (I.11) to (I.13) which we obtained by neglecting the interactions between the particles in the final state, can be valid only in a narrow interval near the upper limit, since in the rest of the threshold region it is essential to allow for the interactions.

It is well known that the transition matrix element including the interaction between the created particles can be expressed as

$$R'_{if} \approx R_{if}\Phi(0), \qquad (\text{I.15})$$

where $\Phi(r)$ is the solution of the Schrödinger equation in the potential field of the interaction between the two components of the pair.

As regards the interaction between the created particles, which interact via the pseudoscalar meson field, we note that the sign of the coupling constant with this field is the same for nucleons and antinucleons*[8]. Hence, one may assume that, at any rate at large distances of the order of the

---

* It is easy to see that in this case, to the approximation considered here, there are only two Feynman graphs.

* We are informed by Markov that the contrary statement in his paper[8] is the result of an error.

π-mesonic forces, the nucleon-antinucleon force is similar to the nucleon-nucleon force. One may, therefore, for a crude estimate of the effect of the final-state interactions, use the phenomenological potential

$$V(r) = V_0 e^{-kr} / (1 - e^{-kr})$$

$V_0^{\text{trip}} = 46.6$ mev; $V_0^{\text{sing}} = 27.2$ mev; $k = \mu_\pi$, which fits the low-energy nucleon scattering. If the pair creation occurs in the continuous spectrum we have

$$\Phi(r) = Ar^{-1} e^{-(b-1)kr/2} (1 - e^{-kr}), \qquad \text{(I.16)}$$

where

$$A = \frac{1}{k} \left[\frac{\pi b \sin h\, 2\pi\alpha}{\alpha (\cos h\, 2\pi\alpha - \cos 2\pi \sqrt{(b-\alpha^2)})} \right]^{1/2},$$

and where $b = MV_0/k^2$; $\alpha = q/k$; q is the relative momentum of the components of the pair.

At low energies,

$$\Phi_s^2(0) \approx (q dq / 2\pi)\, bk \qquad \text{(I.17)}$$

and we find for the cross section for the production of an antiproton by a π^--meson on a proton

$$\sigma_1 = K_1' \left(\frac{E_\mu - 4M}{M} \right)^{3/2} \text{см}^2, \qquad \text{(I.18)}$$

where $K_1' = 1.5 \times 10^{-29} g^6$ for *PS-PS*, and $K_1' = 4.8 \times 10^{-25} f^6$ for PS-PV theory.

Similarly, we find for the production cross section by a π^+-meson on a neutron

$$\sigma_2 = K_1' \left(\frac{E_\mu - 4M}{M} \right)^{3/2} \text{см}^2, \qquad \text{(I.19)}$$

where $K_2' = 3.5 \times 10^{-30} g^6$ for *PS-PS* and $K_2' = 2.4 \times 10^{-25} f^6$ for *PS-PV* theory.

In the limiting case of low relative momenta of the created particles there exists not only the possibility of a deuteron being formed, but also of the antiproton being captured in a deuteron-like "orbit" around a nucleon. The cross section for this process can be estimated by taking as the wave function for this deuteron-like state the wave function of the bound *S* state in the Hulthén potential,

$$\Phi(r) = \left[\frac{kb(b^2 - 1)}{8\pi} \right]^{1/2} r^{-1} e^{-(b-1)kr/2} (1 - e^{-kr}).$$

The cross section for the formation of a bound pair by a π-meson on a proton is

$$\sigma_1 = K_1'' \left(\frac{E_\mu - 4M)}{M} \right)^{1/2} \text{см}^2, \qquad \text{(I.20)}$$

where $K_1'' = 5.3 \times 10^{-30} g^6$ for *PS-PS*, and $K_1'' = 1.1 \times 10^{-24} f^6$ for *PS-PV* theory.

The cross section for the formation of a bound proton-antiproton pair by a π^+-meson on a neutron is

$$\sigma_2 = K_2'' \left(\frac{E_\mu - 4M}{M} \right)^{1/2} \text{см}, \qquad \text{(I.21)}$$

where $K_2'' = 1.8 \times 10^{-30} g^6$ for *PS-PS* and $K_2'' = 5.4 \times 10^{-25} f^6$ for *PS-PV* theory.

In general, the ratio of the cross sections for pair creation in the bound state and in the continuous spectrum is equal to

$$\sigma_{\text{bound}} / \sigma_{\text{cont}} \approx \mu / (E_\mu - 4M).$$

It follows from this that if $E_\mu - 4M < \mu \approx 150$ mev, when the final kinetic energy per particle in the center-of-mass system is considerably less than the depth of the potential well of the nuclear forces, the process of formation in the bound state becomes dominant. Here in the case of process a) the probability of the creation of an antiproton in the bound state and that for the creation of a free antiproton and a deuteron are in the ratio 2:1. For processes b) and c), on the other hand, capture into bound states can arise only in the nucleon-antiproton system, because of the instability of the di-neutron and di-proton. This possibility of capture of the antiproton by a nucleon must, near the threshold, lead to a reduction of the number of observable antiprotons, in view of the practically instantaneous annihilation of a bound antiproton into π-mesons. For example, the mean life of an antiproton and a deuteron-like system due to the annihilation into two charged π-mesons is about $\tau = 10^{-21}$ sec if one assumes pseudoscalar coupling with $g^2 = 1/5$ (see Ref. 9 and part II of this paper).

By comparing these results with experiment, one may, in case the antiproton is discovered, establish the actual energy and angular dependence of the square modulus of the matrix element. Moreover, as we have indicated, a study of the energy dependence of the creation cross sections near the threshold may, to some extent, clarify the nature of the interactions in the nucleon-antiproton system and, in particular, answer the question as to the existence of a bound state in this system. We have above considered only the contribution of π-mesons to the nuclear forces. It is easy to see, however, that the pair creation processes depend to a substantial extent on the interaction at distances of the order of $\hbar/Mc$, where the fields of heavier mesons may contribute substantially.

II. PRODUCTION OF ANTIPROTONS IN NUCLEON-NUCLEON COLLISIONS

1. In addition to the processes involving the creation of nucleon-antiproton pairs in the collision of π-mesons with nucleons, there must also exist processes involving the creation of antiprotons by the virtual π-mesons in the field of the nucleons, The threshold (minimum) value of the total energy for the creation of an antiproton in a nucleon-nucleon collision is $W_0 = 8M$, corresponding to a kinetic energy of the incident nucleon (in the laboratory system) of $T_1 = 6M = 5.6$ bev. Such creation processes are

a) $p + p \rightarrow p + p + p + \tilde{p}$;

b) $n + p \rightarrow n + p + p + \tilde{p}$;

c) $n + n \rightarrow n + n + p + \tilde{p}$.

Since calculations of the cross section for processes a) and b) have already been published[10,11], we shall limit ourselves to the presentation of similar calculations for process c). It must here be pointed out that in these pspers[10,11] calculations of the creation cross sections near the threshold were carried out without allowing for the interaction between the created particles, so that these authors overlooked the possibility of creation in a bound state, which, in this region, is very important.

The differential cross section for the creation of an antiproton in a nucleon-nucleon collision is

$$d\sigma = \frac{1}{4J_0} \sum_i^s \sum_f^s |R_{if}|^2 \rho_f (2\pi)^{-4} \delta(\Delta E)\,\delta(\Delta P), \quad \text{(II.1)}$$

where, if the created particles are free,

$$\rho_f = (2\pi)^{-12} d\mathbf{P}_{N1}\, d\mathbf{P}_{N2}\, d\mathbf{P}_{N3}\, d\mathbf{P}_{\tilde{p}}.$$

The square modulus of the transition matrix element R_{if} is averaged over the spin directions in the initial, and summed over the spin directions in the final state.

For the processes a), b) and c) the first non-vanishing term in the expansion of the matrix element R_{if} in a perturbation series is of the fourth order. The leading term for process a) contains 36 Feynman graphs, whereas for b) and c) there are 28 graphs each. To this order effect a) depends exclusively on the interaction of the nucleons with the neutral meson field, whereas processes b) and c) involve both the neutral and the charged field. Half of the quoted number of graphs arises in each case from the antisymmetrization of the initial and final state functions of the system with repsect to the neutron and proton variables. This antisymmetrization is equivalent to allowing for exchange, and reduces the cross sections for processes b) and c) in the threshold region by about 50%. For process a) the exchange effect gives an additional limitation on the final states of the system, since the Pauli principle rules out the possibility of finding three protons in the same final S state. Without writing out the transition matrix elements in full, we give the value of the square modulus of the matrix element for process c), estimated near threshold for pseudoscalar coupling:

$$\frac{1}{4} \sum_i^s \sum_{f}^s |R_{if}|^2 \approx 1.6 \times 10^{-2} (2\pi)^{12} \frac{g^8}{M^{10}} \quad \text{(II.2)}$$

Thus, the energy dependence of the cross section near the threshold is given by the volume of phase space accessible in the final state

$$\Omega = (2\pi)^{-12} \iiiint d\mathbf{P}_{N1} d\mathbf{P}_{N2} d\mathbf{P}_{N3} d\mathbf{P}_{\tilde{p}}\, \delta(\Delta E)\,\delta(\Delta P) = \frac{1}{420} \frac{M^8}{(2\pi)^8} \left(\frac{E - 7M}{M}\right)^{7/2}. \quad \text{(II.3)}$$

The total cross section for antiproton creation in a neutron-neutron collision is, in the laboratory system, without allowing for the interactions between the created particles:

$$\sigma_3 = L_3 \left(\frac{E - 7M}{M}\right)^{7/2} \text{см}^2, \quad \text{(II.4)}$$

where $L_3 = 4.2 \times 10^{-34} g^8$ for *PS-PS*, and $L_3 = 3.6 \times 10^{-28} f^8$ for *PS-PV* theory.

The upper limit of the threshold region follows from the condition (cf. part I)

$$E - 2M \ll {}^1/_2 \Delta = 150 \text{ mev} \quad \text{(II.5)}$$

in the center-of-mass system, or $E - 7M \ll 2\Delta = 600$ mev in the laboratory system. It follows from (II.5) that the average kinetic energy for each final particle is not large compared to the depth of the potential well of the nuclear forces, and hence over most of the threshold region the interactions in the final state must be essential. Consider first the creation of interacting pairs of particles in the continuous spectrum. Then, by a similar method to that used in part I, we estimate for the cross section of process c) including the effect of the interaction between the particles of the pair:

$$\sigma_3' = L_3' \left(\frac{E - 7M}{M}\right)^{5/2} \text{см}^2, \quad \text{(II.6)}$$

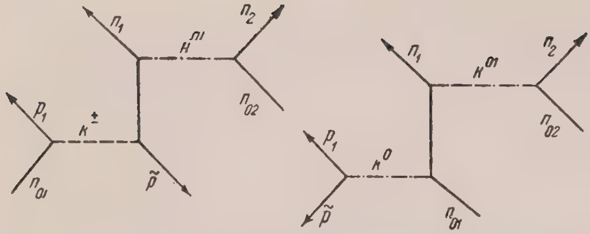

FIG. 2. Two types of Feynman graphs corresponding to process c) in the first nonvanishing order. Full lines represent nucleons, dot-dashed lines neutral π-mesons and broken lines charged π-mesons.

where $L_3' = 4.3 \times 10^{-32} g^8$ for *PS-PS*, and $L_3' = 2.8 \times 10^{-26} f^8$ for *PS-PV* theory.

In nucleon-nucleon collisions at energies close to the threshold we may find as one of the reaction products of process c) a deuteron, $n + n \rightarrow d^+ + \tilde{p} + n$. Equally, the possibility of a deuteron-like nucleon-antiproton system is not excluded, e.g., $n + n \rightarrow d^- + p + n$. The cross section for process c) with one bound pair of particles (of deuteron type) in the final state is

$$\sigma_3'' = L_3''\left(\frac{E-7M}{M}\right)^2 \text{см}^2, \qquad \text{(II. 7)}$$

where $L_3'' = 1.8 \times 10^{-33} g^8$ for *PS-PS*, and $L_3'' = 4 \times 10^{-29} f^8$ for *PS-PV* theory.

Turning finally to the possibility of having in the final state two bound pairs of particles, $n + n \rightarrow d^+ + d^-$, we find for the total cross section of this effect

$$\sigma_3''' = L_3'''\left(\frac{E-7M}{M}\right)^{1/2} \text{см}^2, \qquad \text{(II.8)}$$

where $L_3''' = 7 \times 10^{-34} g^8$ for *PS-PS*, and $L_3''' = 3.7 \times 10^{-27} f^8$ for *PS-PV* theory.

3. As was already mentioned, the production of antiprotons in bound deuteron-like states cannot be neglected in the energy region near the threshold. Such systems must, however, have an extremely short mean life with respect to the annihilation into π-mesons.

For example, the mean life of a bound deuteron-like nucleon-antiproton system, with respect to the decay into two π-mesons, is

$$\tau = 3V_0/4(\sigma_\pi v_{12})_{v_{12}\rightarrow 0}, \qquad \text{(II.9)}$$

where σ_π is the total cross section for the annihilation of a free nucleon-antiproton pair into two π-mesons, v_{12} is the relative velocity of the particles before annihilation; $V_0 \approx |\Psi(0)|^{-2}$ is the annihilation volume of the bound system. For the case $n + \tilde{p} \rightarrow \pi^- + \pi^0$ we have

$$(\sigma_\pi v_{12})_{v_{12}\rightarrow 0} = (\pi/2)(g^2/M)^2 \text{ for } PS\text{-}PS; \qquad \text{(II.10)}$$

$$(\sigma_\pi v_{12})_{v_{12}\rightarrow 0} = 2\pi(f^2/M)^2(M/\mu)^4 \text{ for } PS\text{-}PV.$$

For the case $p + \tilde{p} \rightarrow \pi^+ + \pi^-$

$$(\sigma_\pi v_{12})_{v_{12}\rightarrow 0} = (\pi/4)(g^2/M)^2 \text{ for } PS\text{-}PS \text{ and}$$

$$(\sigma_\pi v_{12})_{v_{12}\rightarrow 0} = \pi(f^2/M)^2(M/\mu)^4 \text{ for } PS\text{-}PV.$$

Inserting (II.10) and (II.11) in (II.9), we find:

1) The lifetime of a bound deuteron-like neutron-antiproton system with respect to the decay $d^- \rightarrow \pi^- + \pi^0$ is

$\tau = 3.2 \times 10^{-26} g^{-4}$ sec for *PS-PS*, and

$\tau = 6 \times 10^{-26} f^{-4}$ sec for *PS-PV* theory.

2) The lifetime of a bound deuteron-like proton-antiproton system with respect to the decay $d^0 \rightarrow \pi^- + \pi^+$ is

$\tau = 6.5 \times 10^{-22} g^{-4}$ sec for *PS-PS*, and

$\tau = 1.1 \times 10^{-26} f^{-4}$ sec for *PS-PV* theory.

Thus, antiproton creation processes at energies near the threshold may in many cases manifest themselves as the creation of pairs of correlated pairs of π-mesons*. It is then easy to see that the angle between the directions of emission of the two π-mesons in the center-of-mass system of the two original nucleons will tend to 180° at the threshold.

The author expresses sincere thanks to Professor V. L. Ginzburg and Professor M. A. Markov for their constant interest in this work and for their many discussions concerning the results.

---

* Multiple creation of mesons is also not excluded.

[1] V. L. Ginzburg, J. Phys. USSR 8, 33 (1944).

[2] J. McConnell, Proc. Irish Acad. 50, 189 (1945).

[3] M. Taketani and S. Machida, Prog. Theor. Phys. 6, 559 (1951).

[4] H. Feshbach and L. I. Schiff, Phys. Rev. 72, 254 (1947).

[5] C. W. Helstrom, Phys. Rev. 78, 88 (1950).

[6] R. P. Feynman, Phys. Rev. 76, 749, 769 (1949).

[7] F. J. Dyson, Phys. Rev. 75, 486 (1949).

[8] M. A. Markov, J. Exptl. Theoret. Phys. (U.S.S.R.) 21, 761 (1951).

[9] J. Ashkin, T. Auerbach and R. W. Marshak, Phys. Rev. 79, 266 (1950).

[10] D. Fox, Phys. Rev. **94**, 499 (1954).

[11] R. N. Thorn, Phys. Rev. 94, 501 (1954).

Translated by R. Peierls
148

SOVIET PHYSICS JETP VOLUME 3, NUMBER 4 NOVEMBER, 1956

The Conductivity of Silver Bromide in the Presence of Bromine

L. M. Shamovskii, A. A. Dunina and M. I. Gosteva
All-Union Scientific Research Institute for Mineral Resources

(Submitted to JETP editor May 9, 1955)
J. Exptl. Theoret. Phys. (U.S.S.R.) 30, 640-648 (April, 1956)

It was shown that silver bromide crystals, additively colored in bromine fumes, acquire hole conductivity, the magnitude of which is proportional to the square root of the partial pressure of halogen in the gas and rises with increase in temperature according to an exponential law. The magnitude of the hole conductivity in AgBr even for low pressures of bromine is comparable in value with the ionic conductivity of these crystals. In additive coloration, V_1 centers are formed. These are complex, consisting of a single vacant cation site with a hole localized on it. The thermal dissociation energy of V_1 centers in AgBr is estimated to be 0.3 ev. F-centers are not formed in silver bromide on account of lack of vacant anion sites in its structure. Neither atoms nor molecules of bromine dissolve and diffuse in the AgBr lattice.

1. INTRODUCTION

IN recent years, a large number of studies have been published concerned with clarification of the nature of the structural defects in the silver halides. On the basis of theoretical calculations[1] and experimental results[2-5] it has been established that in these crystals, Frenkel-type structural defects are formed. Seitz[6] and Mitchell[7], however, supposed that Schottky defects can exist as well in small concentrations. Such an interpretation was occasioned by the need to explain the mechanism of formation of the latent photographic image, and also the mode of development of silver dendrites in single crystals of AgBr in the process of electrolysis[8]. It was also assured that sensitizers, such as Ag_2S, aid in the formation of vacant anion sites in the crystal lattice. Hypotheses have also been expressed on the diffusion of anion vacancies pairwise with cation vacancies. Such groups do not have to reveal themselves in measurements of electrical conductivity and of transference numbers, despite the motion of anions. Such a hypothesis, however, is refuted by experimental data on self-diffusion, measured by means of radioactive tracers[9-11]. In particular, according to the data of Murina and his co-workers[10,11], the transference numbers for bromine ions in AgBr do not exceed 5.2×10^{-4} -- a value falling within the range of experimental errors*.

In subsequent works, Mitchell abandoned his initial point of view. Together with Hedges[11] he established that the internal latent image in silver bromide is formed on internal surfaces associated with the polyhedral structure of monocrystals, connected with the development of dislocations (where boundaries mesh) or mosaic blocks, owing to deformation under the influence of mechanical forces or temperature variations. Prolonged annealing of pure monocrystals near the melting point and slow cooling improved their structure, and in such specimens no latent image developed inside the crystal.

Meikliar and Putseiko[11] consider that it is unnecessary to hypothesize Schottky defects for the formation of F-centers in silver halides. As is known, on exposure of a crystal to ultraviolet light, electrons and holes arise. The latter are considered by the authors as neutral halogen atoms on lattice sites. It is assumed that in the process of photolysis, bromine atoms can pass into interstitial positrons, diffuse in the crystal lattice and leave it. Thus, vacant anion sites are formed, having deeper levels of electron localization than interstitial silver ions and, consequently, there emerge all conditions necessary for the existence of *F*-centers. These same color centers can, in the opinion of these authors, appear also as a result of thermal decomposition of the salt. In support of this point of view, the absorption spectra of AgBr and of AgCl crystals after transillumination or heating are cited. In both cases, new absorption bands were discovered with maxima* at 430-440 mμ in AgBr and at 370-380 mμ in AgCl. These bands are identified with the *F*-centers in the alkali halide salts on the basis that their position, to a first approximation, conforms to Mollwo's empirical formula $\nu d^2 = \text{const}$.

---

* Regrettably, these investigations were carried out on polycrystals. They should be repeated on monocrystals of a high degree of purity, annealed at high temperatures for elimination of their polyhedral structure.

Such a basis for the possibility of *F*-centers in silver halide salts seems inadequate to us. In fact, the photolysis of AgBr, not bromine atoms, but holes, are formed. The latter, in combination with vacant cation sites, can produce *V*-centers. A portion of the holes, migrating in the crystal, can reach the surface where they are localized (see below). Such motion is realized by an electronic mechanism without the transfer of the very atoms or ions of bromine in the crystal lattice. In the thermal decomposition of AgBr, bromine molecules likewise are formed only on the surfaces of the crystal.

The presence in the crystals of *V*-centers and of holes determines, according to the conditions of equilibrium, the occurrence of halogen atoms and molecules adsorbed on outer facets and along boundaries of contact of mosaic grains (if a specimen has a developed polyhedral substructure). Therefore, it is fully natural to expect the appearance of bands peculiar to halogen molecules in the absorption spectra of such crystals[15]. In fact, the additional bands observed by Meikliar and Putseiko in crystals of AgBr and AgCl fully correspond both in their shape and in the position of their maximum to the absorption spectrum characteristic of bromine or chlorine[16]. That band with maximum at 420 mμ was detected also by Mollwo[17] on the long wavelength edge of the *V* band in KBr, additively colored in an atmosphere of bromine.

In connection with the questions raised here, it seemed of interest to us to study the process of additive coloration of AgBr in bromine fumes as a function of temperature of the crystal and of partial pressure of halogen. Checking the change of conductivity of the crystal during its coloration, we had an opportunity to determine whether atoms or molecules of bromine can dissolve and diffuse in the silver bromide lattice, or whether this process is connected with the formation of *V*-centers and holes, the spatial migration of which is not related to the diffusion of halogen atoms. In the first case, the electrical conductivity of the crystals would remain unchanged, but in the second, it would vary in proportion to the concentration of holes. Studies of the equilibria in the process of additive coloration permit us to ascertain the structure of the *V*-centers which are formed and the energy of their thermal dissociation.

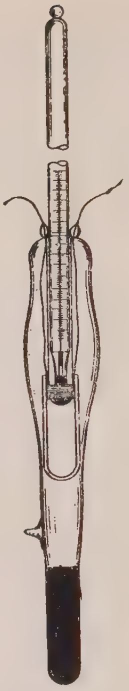

FIG. 1

II. EXPERIMENTAL METHODS

The additive coloration of monocrystals of silver bromide was carried out in a glass ampoule, which is shown schematically in Fig. 1. The monocrystal (in the form of a cylinder) was located in the upper half of the ampoule. Electrodes of sheet platinum were fastened on its end faces through a fine coating of graphite. Inside the ampoule, there was an extension to the level of the crystal for a thermometer, by means of which the temperature of the specimen was measured. Liquid bromine, previously purified by the method of Honigschmidt and Zintl[18], was situated in the

---

* That band with maximum at 430 mμ was found by Golub and Kirillov[14] in the absorption spectrum of a photochemically colored film of bromo-gelatin emulsion.

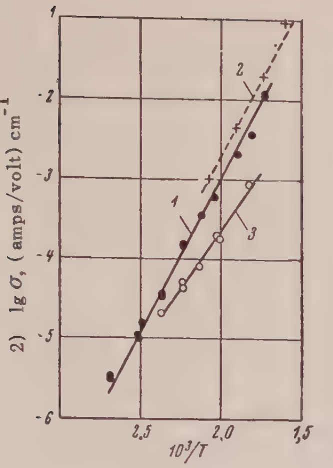

FIG. 2

lower portion of the ampoule. For removal of traces of moisture from the bromine, molten calcium bromide was used. After filling with bromine, the lower portion of the ampoule was cooled with dry ice, evacuated on a diffusion pump to 10^{-5} mm Hg and disconnected. Then the ampoule was placed in a two-stage furnace with two independent windings of nichrome wire. The upper and lower halves of the furnace were separated by a thermally insulated band. Such an apparatus design permitted the investigation of the conductivity of crystals at various temperatures and pressures of bromine. Thermostatting was done to an accuracy of ±0.5°. The lower portion of the ampoule with the liquid bromine was located in a hole in a massive aluminum block for the elimination of a temperature gradient along the height of the furnace. The partial pressure of bromine in the gaseous phase was determined according to the temperature of its saturated fumes. The measurements of the electrical conductivity of the crystals were carried out on alternating current from an audio-frequency generator at 1000 cycles with a bridge circuit using an alternating current amplifier for small voltages.

III. RESULTS OF THE EXPERIMENTS

At the begining of each series of measurements, the crystal was treated in bromine fumes at a pressure of 2 atms and temperature 300° C, in order to eliminate possible products of photolysis. After this, the bromine was frozen out during the simultaneous heating of the specimen. The electrical conductivity of silver bromide was determined in the interval from 100 to 300°. The results of these measurements are plotted in Fig. 2 (curve *1*). They can be presented in the form of

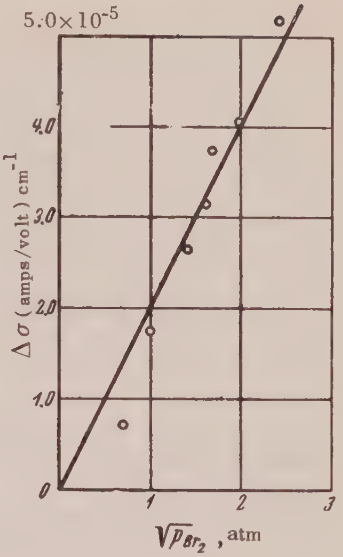

FIG. 3. Isotherm for 150° C

an equation

$$\sigma = 1.02\times10^5 \exp(-18\,200/RT)\ \Omega^{-1}cm^{-1}. \quad (1)$$

The electrical conductivity has the same temperature coefficient as in the work of Koch and Wagner[19] (curve *2* in Fig. 2), but a somewhat smaller factor before the exponential. Measurements of the resistivity of AgBr were then carried out at a fixed temperature with different pressures of bromine fumes. In contact with halogen fumes, the electrical conductivity of silver bromide increases both with rising temperature and with increasing partial pressure of halogen. Additional conductivity Δσ is related to the migration of holes which are formed in the crystal during additive coloration.

The quantity Δσ is calculated from the difference between the electrical conductivity of the crystal in the presence of bromine and without it (after freezing out). In the calculations it was assumed that in the overall electrical conductivity, the portion which comes from the ionic component remains unchanged in the presence of holes. Strictly speaking, this assumption is rather arbitrary, inasmuch as in the process of additive coloration, as will be shown below, a reduction in the equilibrium concentration of interstitial silver ions takes place. Besides that, a portion of the vacant sites are associated with holes in the form of electro-neutral complexes, motionless in an electric field. Thus, a certain number of structural defects does not participate in the transfer of electrical charge. At high temperatures and small partial pressures of halogen, however, the concentration of *V*-centers and holes is small,

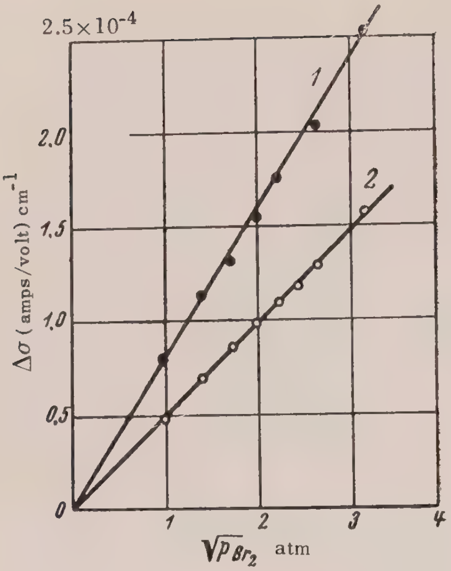

FIG. 4. *1*-Isotherm for 196° C, *2*-Isotherm for 175°.

and therefore they vary the equilibrium concentration of the structural defects in the crystal only insignificantly.

The process of additive coloration of AgBr in bromine fumes is completely reversible, as was established by us in specially arranged experiments.

At high temperatures, equilibrium is attained rapidly, approximately at the same speed with which bromine fumes enter or leave the atmosphere which surrounds the crystal. Therefore, quenching the crystal by rapid cooling fails to retain the *V*-centers.

In Figs. 3-5 the dependence of the change in hole-conductivity of silver bromide on the pressure of bromine is given, for four isotherms. In the coordinates chosen, the zero value of $\Delta\sigma$ corresponds to the conductivity of pure AgBr at the given temperature in the absence of bromine.

The results of the experiments are presented in Fig. 2 (curve *3*) and can be described in the form of an equation as a function of the pressure of the halogen fumes and of the temperature.

$$\Delta\sigma = 1.82\cdot 10^{2}\sqrt{p_{\mathrm{Br}_2}}\ \exp(-13\,520/RT)\ \Omega^{-1}\cdot cm^{-1}\ \mathrm{atm}^{1/2}. \tag{2}$$

The relative change of the hole-conductivity in comparison with the ionic is given by the relation

$$\frac{\Delta\sigma}{\sigma} = 1.78\cdot 10^{-3}\sqrt{p_{\mathrm{Br}_2}}\ \exp(4680/RT). \tag{3}$$

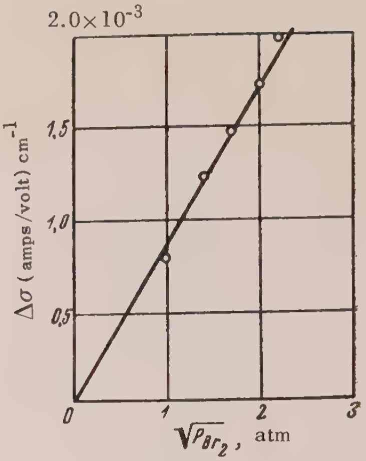

FIG. 5. Isotherm for 273° C

As is seen from Eq. (3), the relative conductivity is lowered with increase in temperature of the crystals. At room temperature (25°) the hole conductivity becomes equal to the ionic already at a bromine pressure of ~ 40 mm Hg.

IV. DISCUSSION OF THE RESULTS

Upon heating silver bromide in a bromine atmosphere, holes are formed in the crystals. Omitting the intermediate steps of the process (dissociation of bromine molecules into atoms and their adsorption on the faces of a crystal), one can write down this reaction in the form of an equation[15]

$$\mathrm{Br}_2(\mathrm{gas}) = 2\mathrm{Br}_G, \tag{4}$$

from which it follows that

$$C_{\mathrm{Br}_G} = \sqrt{K_1}\sqrt{p_{\mathrm{Br}_2}}, \tag{5}$$

where $C_{\mathrm{Br}G}$ is the equilibrium concentration of holes in the crystal, and K_1 is the equilibrium constant of the reaction (4).

The process of hole formation in a crystal during additive coloration (if we consider it in equilibrium with molecular bromine) is bimolecular. Therefore, the equilibrium concentration of holes under isothermal conditions varies in proportion to the square root of the partial pressure of bromine in the fumes [Eq. (5)]. The established relation (5) is confirmed by the experiments on the variation of the hole conductivity of AgBr ($\Delta\sigma$) as a function of bromine pressure (Figs. (3-5).

Positive holes and vacant cation sites inside the crystal interact with one another with the creation of V_1-centers*

$$Br_G + Ag^+_\square = [Ag^+_\square Br_G]. \tag{6}$$

Their equilibrium concentration is determined by the equation

$$C_{Ag^+_\square Br_G} = K_2 \cdot C_{Ag^+_\square} \cdot C_{Br_G}. \tag{7}$$

Here $Ag^+_\square Br_G$ denotes a V_1-center in the form of an associated complex of a vacant cation site ($Ag^+_\square$) and a hole (Br_G), and K_2 is the equilibrium constant of the reaction (6).

The process of the formation of V_1-centers (6) is likewise bimolecular, but opposite in direction to the process of hole formation (4). Taking into consideration the reversibility of both reactions and combining Eqs. (4) and (6), we find

$$Br_2 + Ag^+_\square = [Ag^+_\square Br_G] + Br_G, \tag{8}$$

whence we obtain

$$C_{[Ag^+_\square Br_G]} = K_3 p_{Br_2} C_{Ag^+_\square} / C_{Br_G}, \tag{9}$$

where $K_3 = K_1 K_2$.

Thus, in the final result, it turns out that the equilibrium concentration of V_1-centers varies proportionally to the pressure of bromine molecules. An analogous result as obtained by Mollwo[17] in the study of processes of additive coloration of KBr and KI in vapors of the corresponding halogens. Using the law of mass action, the author arrived at the incorrent conclusion that color centers are halogen molecules, dissolved in the crystal lattice. For this reason, Seitz supposed that in additive coloring V_2-centers are formed, which consist of a pair of holes associated with two vacant cation sites. These authors, however, did not take into account that structural defects of the crystal also take part in the process, and that along with V_1-centers free holes arise. The equilibrium concentration of holes unassociated, under given thermodynamic conditions, in the form of V_1-centers, likewise varies as a function of the partial pressure of bromine. Consequently, additive coloration cannot be compared with the ordinary process of solution.

Combining Eqs. (5) and (9), we find

$$C_{[Ag^+_\square Br_G]} = K_4 \sqrt{p_{Br_2}} C_{Ag^+_\square}. \tag{10}$$

In this equation $K_4 = K_3/\sqrt{K_1}$ or $K_4 \sqrt{p_{Br_2}} = K_2 \times C_{Br_G}$.

Consequently, the equilibrium concentration of V_1-centers varies proportionally to the product of the concentrations of the holes and of the vacant cation sites (for T = const) not connected under the given conditions with associated complexes.

Although the equilibrium concentration of V_1 centers rises with the pressure of bromine, nevertheless, the number of these centers cannot increase indefinitely. With an increase of holes, the concentration of cation vacancies decreases accordingly and so also does the possibility of formation of new V_1-centers. Furthermore, the engendering of holes in the lattice is attended with a loss from it of an equivalent number of mobile cations (interstitial silver ions), the concentration of which is determined by the characteristics of the crystal and depends only on its temperature. In the very process of additive coloration, new structural defects evidently do not arise, insofar as the energy of thermal dissociation of V_1-centers is considerably less than the work of transferring cations from lattice sites to interstitial positions.

The value of the activation energy [in Eq. (2)] for hole conductivity (0.586 ev) is not the heat effect of additive coloration, in the same way as also the corresponding values of energy computed by Mollwo from the variation of the equilibrium concentration of V_1-centers as a function of temperature. As follows from Eq. (8), for the calculation of the heat of formation of V_1-centers, one should also take into account the corresponding changes in the concentrations of cation vacancies and of holes, insofar as their activities are not equal to unity.

The hole conductivity of silver bromide $\Delta\sigma$ can be represented in the form of an equation

$$\Delta\sigma = e n_V \alpha \bar{v}, \tag{11}$$

where e is the elementary charge, n_v is the concentration of V_1-centers, α is the degree of their thermal dissociation and v the mobility of the holes. In this equation $n_V \alpha$ corresponds to the equilibrium concentration of holes. For an estimate of the value of the thermal dissociation energy of V_1-centers, one can assume that the mobility of the holes is independent of their concentration and does not vary with temperature (within narrow limits), and that the equilibrium concentration of V_1-centers, at a constant pressure sure of bromine, rises with temperature in proportion to the concentration of vacant cation sites ($n_{Ag^+_\square}$). According to Koch and Wagner

---

* Here, as also later on, a V_1-center is considered as an associated complex of a single cation vacancy in the lattice with a hole localized on it. According to their properties and the position of the band in the absorption spectrum of a crystal, V_1-centers correspond to the V_2-centers in Seitz's terminology[20].

$$n_{Ag^+_\square} = 29 \exp(-20\,000/2RT). \qquad (12)$$

Combining Eqs. (2), (11) and (12) and supposing that the process of dissociation of V_1-centers has a bimolecular mechanism, we find $\alpha \approx \exp \times (-7040/2RT)$. Consequently, to a first approximation, the energy of thermal dissociation of V_1-centers $\xi = 0.3$ ev*.

It is interesting to compare this value with the thermal dissociation energy of V_1-centers in alkali halide crystals. According to the observations of Mollwo[11], the mobility of color centers in KBr and KI decreases with an increase in their concentration. As the author himself also noted, however, these changes in mobility are merely apparent. They are determined by the degree of dissociation of the color centers. V_1-centers themselves are not accelerated in an electric field since they have no net charge. We have used the experimental data of Mollwo, who measured the apparent mobility of V_1-centers with their concentration fixed as a function of temperature and found their thermal dissociation energy equal to ~ 0.3 ev for KBr and ~ 0.34 ev for KI. As was to be expected, the energy of thermal dissociation of V_1-centers is considerably less than the energy of the optical transition in the maximum of the V_1 band (for KBr $\lambda_m = 267$ mμ or 4.64 ev). In the first case, a spatial separation of the holes from the cation vacancies occurs, while in the second, electrons make transitions from the fundamental band to levels of V_1-centers. The mechanisms of these processes are entirely different, but the final results are identical.

The formation and disappearance of holes during additive coloration always takes place only on boundary surfaces of the crystal. Holes can arise only during the presence of halogen atoms on the surface. While holes are being drawn out of the crystal, surface anions behave as traps for holes. Thereupon, they themselves are converted to atoms.

The conditions necessary for the additive coloration of crystals are determined to a considerable degree by the extent of dissociation of the halogen and also by the concentration and mobility of interstitial cations. Taking into account the reversibility of the process, we can examine the additive coloration as a function of the concentration of halogen atoms.

We worked out the equation for the free energy of the process of dissociation of bromine

$$^1/_2\,\mathrm{Br_2\,(gas)} = \mathrm{Br\,(gas)} \qquad (13)$$

according to the data of Lewis and Randall[21], and found

$$\Delta F^0_T = 21\,570 - 12.0\,T. \qquad (14)$$

Combining Eqs. (4) and (13), we find for the reaction* Br (gas) = Br_G, the equilibrium concentration of holes

$$C_{\mathrm{Br}_G} = \frac{\sqrt{K_1}}{\sqrt{K_5}}\, p_{\mathrm{Br}}\,, \qquad (15)$$

where K_5 is the equilibrium constant of the reaction (13). Taking into account Eq. (2), we find

$$\Delta\sigma = eC_{\mathrm{Br}_G}\bar{v} \qquad (16)$$

$$= 1{,}65 \times 10^{-4} \cdot p_{\mathrm{Br}} \exp(8050/RT).$$

If, as earlier, the mobility $\bar{v}$ is taken as a fixed quantity, then the energy of formation of holes in contact with bromine atoms comes out to ~ 0.35 ev.

In the formation of V_1-centers and holes, neither molecules nor atoms of halogen are dissolved in the crystal lattice. In reality, a stoichiometric excess of halogen, which can be detected by chemical analysis, arises as a result of a stoichiometric deficiency of metal atoms coming from the removal of electrons from the lattice upon introduction of holes with the attendant removal of a corresponding number of interstitial cations. The experiments of Uchida and Nakai[22], who demonstrated the possibility of obtaining V_1-centers in KI and NaI by an electro-chemical method, by the introduction of holes into the crystal from a pointed anode similarly to the way F-centers can be treated by the introduction of electrons into the crystal from the cathode, can serve as a direct corroboration of this.

---

* This value should be made more precise by independent determinations of the equilibrium concentrations of V_1-centers and of holes at various temperatures.

* The process of hole-formation becomes monomolecular, if it is considered in equilibrium with atomic bromine.

Both optical measurements and the study of the conductivity of AgBr furnish us a basis to deny the possiblity of the formation of F-centers in AgBr. Evidently, in these crystals, which have mobile holes in their makeup, V_1- and F-centers cannot simultaneously exist with the same absorption spectrum as adsorbed bromine molecules.

V. THE MECHANISM OF ADDITIVE COLORATION OF AgBr IN A BROMINE ATMOSPHERE

In the analysis of the mechanism of additive coloration we proceed from the formation in the crystal of structural defects of Frenkel type. This initial postulate is fully substantiated for the silver halides. If such a crystal is introduced into a halogen atmosphere, then the latter will be adsorbed on the facets and internal surfaces of the specimen in the form of molecules and atoms. The concentration of the latter, obviously, will depend on the partial pressure of the halogen molecules and the degree of their dissociation at the assigned temperature.

Halide ions, situated on the surface layers of the crystalline lattice, are able to give up their valence electrons to the adsorbed atoms. The probability of such an exchange is increased with the concentration of these atoms, wherewith holes arise in the crystal. They possess high mobility and therefore are able to migrate into the lattice with great speed. Such motion is restrained by the negative charge which develops on the surface. Inside the crystal, near its surface layers a considerable potential gradient arises which depends on the concentration and mobility of the holes. Under the influence of this field, interstitial cations drift to the surface, where they are joined to anions of halide and form new lattice planes. Their motion reduces the gradient of potential in the crystal and removes the charge on the surface. The crystal remains electrically neutral. The rate of additive coloration is determined by the concentration and mobility of the interstitial ions--the slowest step of additive coloration. Holes and vacant cation sites have opposite effective charges and therefore can recombine with the formation of V_1-centers, which, in their turn, exist in equilibrium with "free" holes. The motion of holes into the crystal lattice is possible only when mobile cations are present in its structure. Therefore, their maximum concentration is controlled by the presence of interstitial cations in the structure of the crystal.

Holes cannot only arise, but also disappear at the surface of a crystal. With reduction of the concentration of halogen atoms in the adsorbed layer, conditions are established favorable for the localization of holes by halide ions on the surface. Under these conditions, halogen atoms are formed which can leave the crystal. The surface acquires a positive charge, due to a stoichiometric excess of cations. The flow of holes to the surface establishes a gradient of potential inside the crystal directed from the surface into the volume. Under the influence of this field, cations travel into the lattice. Inasmuch as additive coloration is a reversible process, the original properties are restored upon bleaching.

---

[1] N. F. Mott and M. J. Littleton, Trans. Farad. Soc. 34, 485 (1938).

[2] C. Tubandt and S. Eggert, Z. anorg. Chem. 110, 196 (1920).

[3] C. Wagner and J. Beyer, Z. Physik Chem. B32, 113 (1936).

[4] C. R. Berry, Phys. Rev. 82, 422 (1951).

[5] H. D. Keith and J. W. Mitchell, Phil. Mag. 42, 334, 1331 (1951).

[6] F. Seitz, Rev. Mod. Phys. 23, 328 (1951).

[7] J. W. Mitchell (Editor), *Fundamental Mechanisms of Photographic Sensitivity*, Bristol Symposium, March 1950 (London, 1951), p. 242.

[8] C. Tubandt and E. Lorenz, Z. Physik Chem. 87, 513 (1914).

[9] H. W. Schamp, Jr., and E. Katz, Phys. Rev. 94, 828 (1954).

[10] A. N. Murin and Iu. Taush, Dokl. Akad. Nauk SSSR 80, 579 (1951).

[11] A. N. Murin, G. N. Kazakova and B. G. Lur'e, Dokl. Akad. Nauk SSSR 99, 529 (1954).

[12] J. Hedges and J. W. Mitchell, Phil. Mag. 44,223, 357 (1953); J. W. Mitchell, Z. Physik 138, 381 (1954).

[13] P. V. Meikliar and E. K. Putseiko, Dokl. Akad. Nauk SSSR 73, 63 (1950); P. V. Meikliar, Dokl. Akad. Nauk SSSR 77, 391 (1951); P. V. Meilkiar and R. S. Shimanskii, J. Exptl. Theoret. Phys. (U.S.S.R.) 27, 156 (1954).

[14] S. Golub and E. Kirillov, Trudy Odessa Univ. (Phys.) 2, 5 (1940).

[15] L. Shamovskii, Dokl. Akad. Nauk SSSR 91, 229 (1953).

[16] Landolt-Börnstein, Phys. Chem. Tab., Hw. II, 893 (1923), I Eg.-Bd., 432 (1927).

[17] E. Mollwo, Ann. Physik 29, 394 (1937).

[18] O. Honigschmidt and E. Zintl, Ann. Chemie 433, 701 (1923).

[19] F. Koch and C. Wagner, Z. phys. Chem. 38, 295 (1937).

[20] F. Seitz, Revs. Mod. Phys. 26, 7 (1954).

[21] L. Lewis and M. Randall, *Thermodynamics and Free Energy of Chemical Substances*, (New York, McGraw Hill),1923.

[22] J. Uchida and M. Nakai, J. Phys. Soc. Japan 8, 795 (1953); E. Mollwo, Gött. Nachr. H 3, 89 (1943); J. Heiland, Z. Physik 128, 144 (1950).

Translated by R. L. Eisner
134

SOVIET PHYSICS JETP VOLUME 3, NUMBER 4 NOVEMBER, 1956

The Dielectric Properties of Castor Oil at High Pressures

L. F. VERESCHAGIN, L. F. KUZNETSOV AND T. I. ALAEVA

(Submitted to JETP editor June 25, 1955)
J. Exptl. Theoret. Phys. (U.S.S.R.) 30, 661-666 (April, 1956)

The dielectric constant and tangent of the loss angle of castor oil has been measured with varying pressures up to 9000 atmospheres, and at different frequencies. It is shown that the dielectric constant and the tangent of the loss angle pass through a maximum as the pressure is increased, which is connected with a change in the viscosity upon a change in pressure.

AS is known, pressure can result in a change in the dielectric constant of liquids with polar molecules as a result of a change in the density. The equation of Debye

$$\frac{\varepsilon-1}{\varepsilon+2}\frac{M}{\rho}=\frac{4}{3}\pi N\left(\alpha_0+\frac{\mu^2}{3kT}\right)$$

where ϵ is the dielectric constant, μ is the dipole moment, M is the molecular weight, ρ is the density, N is Avogadro's number, k is the Boltzmann constant), which we can use in considering the possible influence of pressure on the dielectric constant does not include, however, the possibility of the influence of pressure upon the electric polarizability α_0 and the orientation polarizability $\mu^2/3kT$. "The internal field" to which Lorentz has ascribed the value $4\pi/3$, can also change under pressure, which leads to an uncertainty in the treatment of the results.

At the present time a number of investigations of the dielectric properties of liquids under high pressures are known. For example, Kyropulos[1] investigated the influence of pressure up to 3000 atmospheres on the change of the dielectric constant. In this work, ethyl ether, carbon disulfide, chloroform, petroleum ether, carbon tetrachloride, and pyridine were investigated. It was found that the dielectric constant increased with an increase in the pressure for all of the liquids. The Clausius-Mosotti function for non-polar liquids

$$\frac{\varepsilon-1}{\varepsilon+2}\frac{M}{\rho}=\frac{4}{3}\pi N\alpha_0$$

is approximately constant except for carbon disulfide and ethyl ether. The author considers that under high pressure the molecules become markedly complex, which leads to an anomaly in the theoretical relations.

Chang[2] and Danforth[3] continued these investigations up to a pressure of 12,000 atmospheres, during which were conducted measurements of the dielectric constants of a number of liquids such as ethyl ether, eugenol, glycerine and others. It was established that the dielectric constant increases with the pressure and that at high pressures for strongly polar liquids a significant role in the polarization of the dielectric is played by the orientation term $\mu^2/3kT$, which must depend on the viscosity. The viscosity of liquids is in turn strongly dependent on the pressure. This led to Danforth's observing anomalies in the change of the dielectric constant of glycerine and eugenol with changes of the pressure.

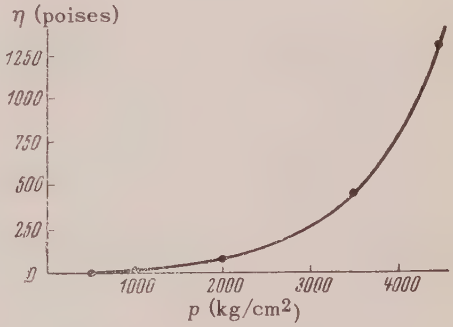

FIG. 1. Dependence of the viscosity of castor oil on the pressure, $t = 30°$.

This leads to an interest to study the influence of high pressure on the dielectric properties of polar liquids, in particular to study the influence of pressure on the tangent of the loss angle, the investigation of which can give additional knowledge about the behavior of polar molecules in fields of high frequencies under different pressures. Castor oil was the medium chosen for the study. This oil has important applications in engineering as a lubricating material and also in electrical engineering in industry as a dielectric material. The chief constituent of castor oil consists of glyceryl ricinic acid.

$$CH_3(CH_2)_5CH(OH)CH_2CH{=}CH(CH_2)_7COOH$$

The viscosity of castor oil is strongly dependent on the pressure, as is seen in Fig. 1 which we have taken from the monograph of Zhohkovaskii[4].

The presence of the dipoles of the molecules in castor oil and the strong dependence of its viscosity upon pressure give us reason to expect that

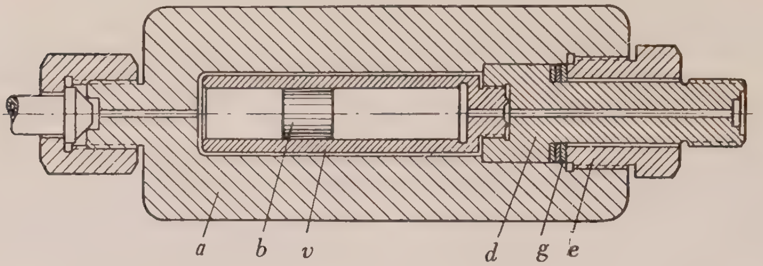

FIG. 2. Press Device: a – frame, b – plunger, v – cylinder, g – obturator, d – packing washers, e – sealing nut.

at high pressures the influence of the pressure on the dielectric constant and on the tangent of the loss angle will be especially noticeable.

EXPERIMENTAL PROCEDURE AND APPARATUS

The apparatus, with which the present investigations were carried out, consisted of a hydraulic compressor of ultra-high pressure, a reservoir, which serves to even out the changes in pressure of the system, a press device, and a high pressure vessel inside of which the measuring condenser is located. The press device permits the separation of the liquid under investigation from the oil which comes from the compressor under pressure.

From Fig. 2 we see that this press device consists a steel cylinder with a cylindrical steel plunger, tightly ground in to inner surface of the cylinder. In Fig. 3 is shown the plan of the high pressure vessel together with the measuring condenser. This steel vessel is made of steel of brand 40X, hardened to a hardness R_c 40-45. The outside diameter of this vessel is 70 mm, and the inside diameter is 10 mm. To maintain the temperature constant during the time of measurement a steel jacket is provided, through which oil was circulated controlled by an ultra-thermostat of Gepler. The temperature was maintained constant to an accuracy of ±0.3° during the time of the experiment.

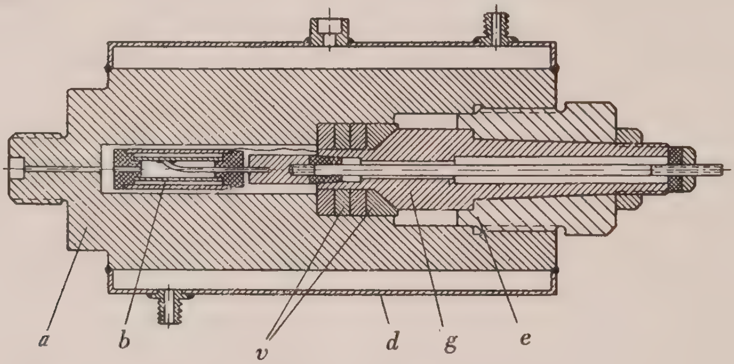

FIG. 3. High pressure vessel with the measuring condenser: a – frame, b – measuring consenser, v – jacket, g – electrode, d – nut, e – sealing washers.

The measuring condenser is shown in Fig. 4. The condenser consists of two coaxial cylinders a and b, made of steel. The inside diameter of the outside cylinder equals 8mm, the outer diameter of the inner cylinder is 7.6 mm, the length of the cylinders is 34 mm. The coaxial cylinders are secured by the use of two ebonite bushings v and g. For filling the space between the walls of condenser with the liquid dielectric being investigated the ebonite bushings have a longitudinal opening, and the outer wall is perforated so that pressure can be transmitted with the greatest possible uniformity. The outer wall of the measuring condenser is exposed to the steel vessel and grounded. A connection from the inner wall of the condenser is accomplished by an electrode. The plan of this electrode is seen in Fig. 5, where a steel core-rod a passes through a cone b of high

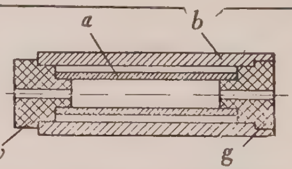

FIG. 4. Measuring condenser: a, b, – coaxial cylinders, v, g, – ebonite bushing.

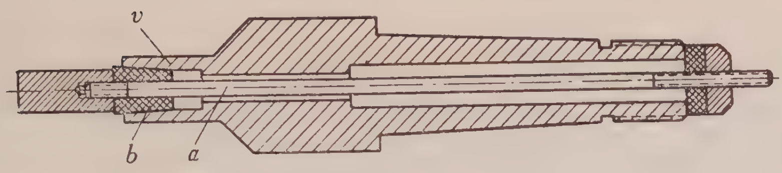

FIG. 5. Plan of the electrode: a — core-rod, b — cone v — obturator.

quality porcelain. A tight high pressure seal is accomplished by the liquid pressing the porcelain cone in a cone opening of the obturator v. Both surfaces (cone and cone mount) are carefully ground in with the aid of boron carbide.

The capacity of the electrode and conducting cable is 19.1 cm and does not depend on the pressure. Because the dielectric used is a solid, the its dielectric constant is practically unchanged with applied pressure. The conductor which is brought out through the electrode is connected to the inner plate of the condenser and by a shielded cable to a measuring instrument such as a Q-meter or dielectric meter. Upon change of the dielectric constant the dielectric meter changes; the principle of its construction is a method of comparing a beat frequency to the frequency of an auxiliary generator of constant audio frequency. The comparison of the beat frequency to the audio frequency generator is made on the screen of an electron oscillograph.

The frequencies which are compared give a Lissajou figure on the oscillograph screen(ellipse, figure eight). The measurement of dielectric constant is made up to frequencies of 1 mc.

The pressure is recorded with the aid of an indicating manometer constructed by Nagatkin with a scale up to a limiting pressure of 10, 000 kg/cm^2.

Before installing the measuring condenser and the liquid to be measured in the steel vessel, the capacity of the lead alone and the capacity of the lead together with the measuring condenser, with air as the dielectric ($\epsilon = 1.005$), was determined. Comparing the capacity of the condenser filled with oil to the capacity of the same condenser filled with air at atmospheric pressure gave the value of the dielectric constant of the oil. This measurement performed for castor oil at atmospheric pressure and temperature of 20° gave the value $\epsilon = 4.35$ which is in good agreement with values in the literature.

To be sure that during the time of the experiment the liquid being investigated does not mix with the liquid transmitting the pressure, the values of the indices of refraction for light of the investigated liquid are compared before and after the experiment. The index of refraction is determined with the aid of a refractometer.

EXPERIMENTAL RESULTS

The values of the dielectric constant of castor oil (ϵ) in relation to pressure are shown in Table 1, and the results of the measurement of the tangent of the phase angle (tanδ%) in relation to the pressure for different temperatures are given in Table 2. These data are shown in the form of curves in Figs. 6-9.

As we see in Fig. 6 where the change in the dielectric constant of castor oil with pressure at 32° is shown, the dielectric constant at first rises with rising pressure (with rise in the density of the liquid), then the curve passes through a maximum and succeeding values of ϵ begin to decrease, in spite of the fact that the pressure continues to

TABLE 1

The dependence of the dielectric constant on pressure, temperature 32°.

Pressure p in kg/cm^2	ε	Pressure p in kg/cm^2	ε	Pressure p in kg/cm^2	ε	Pressure p_2 in kg/cm	ε
1	4,35	2000	4,97	4400	5,15	6300	4,67
200	4,70	2400	5.08	4600	5,11	6800	6,55
425	4,74	2600	5,15	4900	5,04	7150	4,46
800	4,77	3050	5,22	5150	5,01	7400	4,41
1000	4,8	3450	5.25	5400	4,87	7625	4,25
1200	4,81	3650	5,25	5650	4,81	8150	4.17
1600	4,89	4050	5,22	6025	4,72	8750	4.11
						9050	4.05

TABLE 2

The dependence of the tangent of the phase angle on pressure.

$f = 464$ kc/sec, $t = 7^{\circ}$		$f = 1.48$ Nc/sec, $t = 7^{\circ}$		$f = 144$ Kc/sec, $t = 5^{\circ}$	
p in kg/cm^2	tan δ in %	p in kg/cm^2	tan δ in %	p in kg/cm^2	tan δ in %
1	3,51	1	6,44	1	2,25
700	4.71	580	7,89	600	3,60
1000	6.06	1000	10,04	1000	4,42
1550	7.56	1500	10.44	1500	6,46
2000	9,76	2000	10,64	2000	7,70
4500	8.91	2500	10,74	2600	10,50
5050	6,71	3000	9,64	3000	11,30
5300	6,31	3500	9,24	4200	9,20
6000	5.20	4000	7.74	5000	7.48
6520	4,74	4500	6,44	6000	6.36
—	—	5120	5,54	7100	4,64
—	—	5620	4.84	—	—
—	—	6050	4,49	—	—

rise. The maximum of the curve relating ϵ to pressure corresponds to a pressure of approximately 3600 atmospheres. The change of the dielectric constant with pressure is anomalous, because with an increase of the density of the liquid, ϵ should rise also. The anomaly of the change in the dielectric constant with increasing pressure, apparently can be explained by a relaxation phenomenon which becomes significant as a result of the viscosity. At such pressure the dielectric constant upon an increase in the pressure should be effected by a significant rise in the relaxation time τ. As is known, Debye[5] determined the relaxation time assuming that the molecular model could be a sphere with radius r. Then, taking Stokes' coefficient of drag $\zeta = 8\pi\eta r^3$ for rotary motion of a sphere in a viscous medium with a coefficient of viscosity η, Debye obtained the expression $\tau = (4\pi r^3/kT)$. Clearly in an investigation of the liquid, castor oil, we cannot assume that the molecule has the shape of a sphere of radius r; however we can assume a connection between the relaxation time and the viscosity of the liquid, as was established by Debye. In this way the relaxation time will rise with an increase in viscosity, which at sufficiently high frequencies of the external field should lead to the molecules not being able to reorient through a large angle, near to 180°. And at sufficiently high values of viscosity the role of the orientation polarizability $\mu^2/3kT$ becomes vanishingly small. This must lead to a diminution of the numerical value of ϵ, which was determined previously from the value of the electric polarizability α_0 and the orientation polarizability $\mu^2/3kT$. In the part of the curve of Fig. 6, where ϵ depends inversely on the pressure, clearly, the value of ϵ will be determined by only the electric polarizability. It is interesting to note that ϵ at pressures of the order of 9000 atmospheres is approximately 10% less than its value at atmospheric pressure.

Undoubtedly, measurement of the loss angle of the dielectric in the liquid investigated by us can give additional knowledge about the behavior of

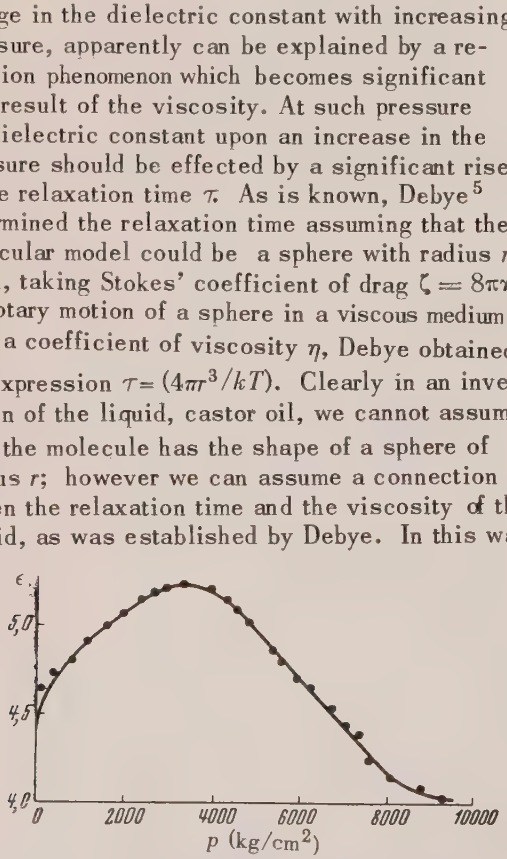

FIG. 6. The dependence of the dielectric constant of castor oil on pressure at a temperature of 32°.

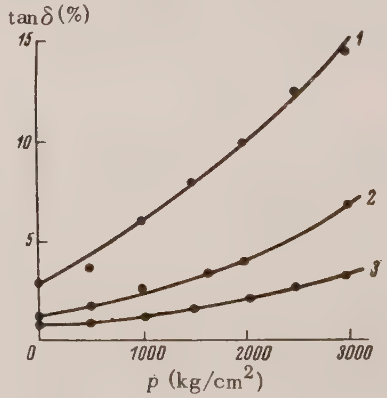

FIG. 7. The dependence of the tangent of the loss angle on pressure at a frequency of $f = 148$ mc/sec at different temperatures: $1 - t = 22.2^{\circ}$; $2 - t = 50^{\circ}$; $3 - t = 74.2^{\circ}$.

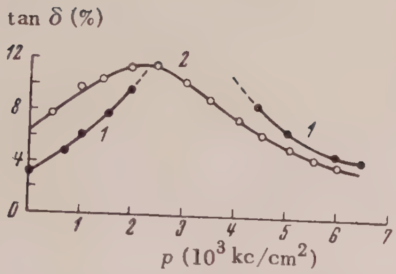

FIG. 8. The dependence of the tangent of the loss angle on pressure at different frequencies ($t = 7^\circ$) 1 – $f = 464$ kc/sec; 2 – $f = 1.48$ mc/sec.

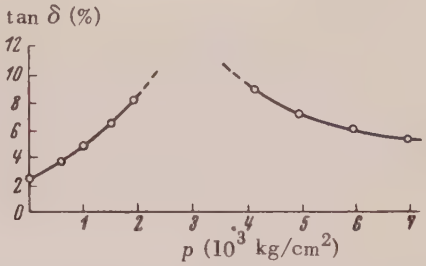

FIG. 9. The dependence of the tangent of the loss angle on pressure at temperature 5° and $f = 144$ kc/sec.

polar molecules in liquids which are under high pressure. As is seen in Figs. 8 and 9, where the dependence of tanδ on the pressure at temperatures of 5° and 7° at different frequencies is shown, the value of tanδ in relation to the pressure passes through a maximum and then at even higher pressure diminishes. It is clear that the values of the phase angle are relatively small at both low pressures and very high pressures due to the strong interactions between molecules. In this way at low pressures tanδ will be small, then the value of the tangent of the phase angle will rise with an increase in pressure and pass through a maximum beyond which it will diminish, when the strong interactions between molecules reach the value where the external high frequency electric field can not turn the polar molecules through a significant angle.

As was to be expected, at increased temperatures the measurements (see Fig. 7) lead to lower values of tanδ, which follows from the dependence of the viscosity of liquids on temperature.

We express thanks to laboratory mechanic S. J Vlasov, who made the necessary apparatus.

---

[1] S. Kyropulos, Z. Phys. Chem. **40,** 507 (1926).

[2] L. T. Chang, Chinese J. Phys. **1,** 1 (1934).

[3] W. E. Danforth, Jr., Phys. Rev. **38,** 1224 (1931).

[4] M. K. Zhokhovskii, *Technical Measurement of Pressure and Vacuum,* Mashgiz, 1952.

[5] P. Debye, *Polar Molecules.*

Translated by F. P. Dickey
136

SOVIET PHYSICS JETP VOLUME 3, NUMBER 4 NOVEMBER, 1956

Magnetic Analysis of the (d,p) Reaction Products in the Investigation of Spin and Parity of Levels of the Daughter Nucleus

IU. A. NEMILOV AND V. F. LITVIN
Radium Institute, Academy of Sciences, USSR

(Submitted to JETP editor, July 25, 1955)
J. Exptl. Theoret. Phys. (U.S.S.R.) 30, 686-689 (April, 1956)

The energy dependence of the intensity ratio of different proton groups from the reaction $Al^{27}(d,p)Al^{28}$ has been utilized to determine possible spin and parity values of some levels in Al^{28}. The obtained results give for the level at 1.625 mev; even parity, spin between 0 and 5; at 5.128 mev: odd parity, spin between 0 and 6, and at 5.435 mev: odd parity, and spin between 1 and 4.

BY observing the angular distribution of proton or neutron groups in stripping reactions it is possible to limit the possible values of spin and to determine the parity of excited states of the daughter nucleus.[1]

In this way the characteristics of excited states of light nuclei and of some low levels of heavier nuclei have been determined. However, it is not possible to employ the usual techniques of determining the angular distributions in the region of higher excitation in heavier nuclei, where the levels lie close together. The methods usually employed are energy analysis by stopping in foils or by measuring of track length in thick photographic emulsions.

The aim of the present work is to utilize the method of magnetic analysis of the reaction products which allows one to obtain a higher energy resolution. However, the immediate application of this method in angular distribution experiments meets with a number of technical difficulties. Therefore, a slightly different approach was chosen. As is well known the most probable angle with which the proton leaves the target with respect to the incoming particle direction in a stripping reaction depends on the orbital angular momentum of the captured neutron, on the reaction energy, and on the kinetic energy of the incoming deuterons. One therefore can observe at a fixed angle and vary the energy of the primary deuterons. The dependence of the intensity of a particular proton group on the primary energy therefore will have a well defined form which will depend on the characteristics of the particular excited level of the daughter nucleus.

The experimental arrangement used was similar to that described in Ref. 2. An assembly of sampleholder, defining slits, and plateholder was placed inside of the vacuum chamber of a cyclotron. The energies and intensities were determined by track counting under the microscope. The setup was calibrated by the (*d*,*p*) reaction on carbon and oxygen whose reaction energies are known with great accuracy. The first experiments were conducted with Al. This element was chosen because it is monoisotopic. Further, it is easy to make thin foils for the target; finally, the (*d*,*p*) reaction leads to Al^{28} whose complicated level scheme has been well investigated. Therefore there exists a good amount of information with which to compare the obtained results.

The angle of observation was 109° ± 3° in the laboratory system. The deuteron energy could be varied from 1 to 5.6 mev. One of the curves, showing the proton energy distribution at a primary deuteron energy of 1.71 mev is shown in Fig. 1. All told there were found 31 proton groups which agreed with the positions of levels as given in Refs. 2,3,4, although many of the levels found in Ref. 4 could not be resolved. Additionally, one new level was observed at an excitation energy of 8.24 mev.

The energy dependence of the intensities of the various proton groups can be most accurately determined relative to the intensity of an arbitrary group, preferably one with a known angular distribution. For this purpose the group p_0 was chosen which corresponds to the transition to the ground state doublet ($\Delta E \approx 31$ kev) which was not resolved in our case. It follows both from shell theory and from analysis of experimentally obtained angular distributions[6] that this transition has an orbital angular momentum $l=0$. We determined the ratio of the intensity of the proton groups corresponding to the levels of Al^{28} at 0.974, 1.015, 1.367, 1.625, 5.128, and 5.435 mev (the groups p_1, p_2, p_3, p_4, and p_5 respectively) to that of the ground state group at deuteron energies of 1.12, 1.71, 2.43, 3.15, 3.81, 4.54, 5.17, and 5.59 mev. The distributions obtained are plotted in Fig. 2. We either could not separate the remaining groups because of the rather poor energy resolution of our arrangement (≈100 kev) or could observe them with sufficient intensity only at some deuteron energies and so were not able to obtain enough points to construct the curves.

The energy dependence of different proton groups could have had arbitrary shapes if compound nucleus formation would have played an important part in the process. However, the stripping cross sections usually are much larger than the compound nucleus cross sections, and up to now no resonance phenomena have been observed in (*d*, *p*) processes in neighboring *Z* nuclei. All maxima actually observed in the intensity ratios of different groups are sufficiently broad to correspond to the shape one would expect in stripping reactions. These shapes could scarcely obtain in compound nucleus processes. We therefore shall assume that the observed intensity ratios are due exclusively to the stripping process.

For a rigorous interpretation of the obtained results one has to know the dependence of the intensity at the particular angle of observation on the deuteron energy for different values of the angular momentum *l* transferred to the nucleus in the capture of the neutron. In an accurate solution of this problem one has to take into account the influence of the coulomb interaction and the nuclear interaction and the deformation of the wave function of the deuteron in its approach to the nucleus. Such calculations have not yet been performed. An experimental determination of these dependencies could be possible in some cases. This would be so if one could find a neighboring *Z* nucleus with fewer levels which then could be investigated by the method of angular distributions. The energy dependence of the intensity of the same proton groups can then be determined with the present method. Since the *l*-values connected with these proton groups would be known having been obtained from the angular distributions, one now could use these shapes in the analysis of levels which can be studied only by means of magnetic analysis.

At present it is possible to estimate the spin and parity only for those few levels whose dependence of the intensity of their proton groups on the deuteron energy show prominent features and which can be determined using data from Refs. 1, 7. These papers give theoretical angular distributions. By means of graphical extrapolation into the region of Z,Q, and deuteron energy of interest here, it is possible to predict roughly the place at which the maximum of the intensity will occur for different l.

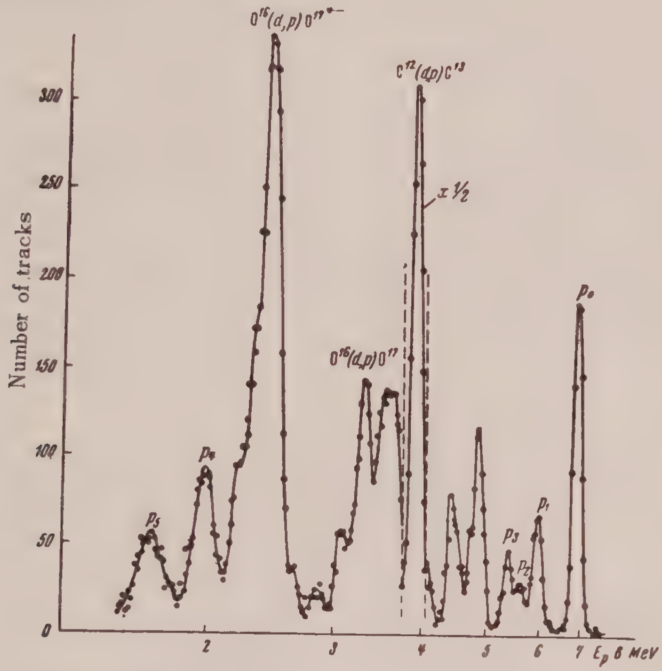

FIG. 1. Energy spectrum of protons from the reaction Al^{27} (d,p) Al^{28} at a primary deuteron energy E_d=1.71 mev. (Scale between the dotted vertical lines decreased by a factor of 2).

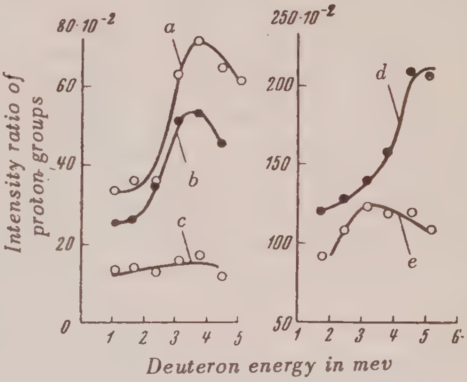

FIG. 2. Dependence of the intensity ratio of some proton groups on the primary deuteron energy.

In Ref. 6 it was found by means of angular distributions that the capture of neutrons into the states at 974 and 1015 kev, which were not resolved in their experiments, occurred with l=0 and l=2. In the present experiment these levels also were not resolved. The ratio of the intensity of this group to that of the group leading to the ground state doublet is shown as curve a in Fig. 2. From this curve we can only determine the presence of the l=2 transition, since an l=0 transition having the same l as the ground state transition would have to yield a constant value. From curve b of Fig. 2 one can see that the transition to the level at 1.625 mev in Al^{28} is also an l=2 transition. Hence its parity is even, and since the ground state spin of Al^{27} is 5/2 its spin can be between 0 and 5. Curve c of Fig. 2 shows the intensity of the proton group leading to the level at 1.37 mev of $Al.^{28}$ It is rather closely a straight line parallel to the abscissa, thus indicating an $l=0$. However, the intensity is rather low and this result is not too certain.

We furthermore could obtain similar data for the levels of Al^{28} at 5.128 and 5.435 mev (curves *d* and *e* of Fig. 2). According to Ref. 4 there are some more levels in their vicinity which could not be resolved here. However, since according to the same work[4] the intensity of the groups we observed is almost an order of magnitude larger than that of the neighboring ones, the shape of the curves is mostly determined by these two groups. According to our estimates from Refs. 1, 7 as described above it seems likely that the transition to the level at 5.128 mev (curve *d*) involves an $l=3$, and hence the parity of this state would be odd while the spin could have a value between 0 and 6. Analogously, curve *e* indicates for the level at 5.435 mev a transfer of $l=1$ and hence odd parity and a spin between 1 and 4.

---

[1] S. T. Butler, Proc. Roy. Soc. (London) A 208, 559 (1951).

[2] L. M. Khromchenko, Dokl. Akad. Nauk SSSR 94, 1037 (1954).

[3] K. K. Keller, Phys. Rev. 84, 884 (1951).

[4] H. A. Enge, W. W. Buechner, and A. Sperduto, Phys. Rev. 88, 963 (1952).

[5] D. R. Inglis, Rev. Mod. Phys. 25, 390 (1953).

[6] I. R. Holt and T. N. Marsham, Proc. Phys. Soc. (London) A66, 249 (1953).

[7] W. Tobocman and M. H. Kalos, Phys. Rev. 97, 132 (1955).

Translated by M. Danos
140

SOVIET PHYSICS JETP VOLUME 3, NUMBER 4 NOVEMBER, 1956

The Interaction of the States of Two Zones in the Single-electron Scheme

Iu. M. SEIDOV AND V. S. GALISHEV
Institute of the Physics of Metals, Ural Affiliate.
Academy of Sciences, USSR

(Submitted to JETP editor, November 15, 1954)
J. Exptl. Theoret. Phys. (U.S.S.R.) 30, 695-700 (April, 1956)

A generalization of the results of Bogoliubov [1] in the zone (single-electron) approximation is worked out for the case of the presence of an excited state. The expression obtained for the energy spectrum permits a direct judgment on the combination of two zone states.

1. INITIAL HAMILTONIAN OF THE PROBLEM

IN the well known investigations of Bogoliubov[1] on the theory of metals, the simplest case of *s* electrons was considered. The eigenfunction of the system of electrons in the crystal corresponding to this case was sought in the form of a linear combination of antisymmetrized products composed only of eigenfunctions of the lowest atomic energy level. Moreover, improvement of the accuracy of the method requires, as is well known, the consideration, along with the eigenfunctions, of the eigenfunctions of the succeeding energy levels, in particular when they are close to the ground state. Solution of a similar problem for the case of the excited state is also the purpose of the present research. In this case we limit ourselves only to the electron zone approximation, since calculation of the interaction of the electrons complicates all the considerations considerably, and requires independent consideration.

Following Bogoliubov, we consider the crystalline lattice with "frozen" positive ions, and limit ourselves to the case of monovalent metals. For such a crystalline lattice, the secular equations are written down in the monograph[1] cited above in the representation of second quantization and their detailed investigation is carried out for the case of the *s*-state. In this case the index $\lambda=(l,m)$ (the aggregate of orbital and magnetic quantum numbers) drops out everywhere in general in the Bogoliubov formula. If we calculate the *p*-state along with the *s*-state, then the index λ will have four values: (0,0), (1,1), (1,0), (1,-1), which naturally complicate all the calculations greatly. Therefore, it seems quite appropriate to consider initially the simplest possible case — nondegenerate *p*-states, i.e., to consider that the *p* electron of the free atom is described by one real eigenfunction, and not by three. In this case, let $\lambda=0$

everywhere characterize the s-state, and $\lambda=1$ the p-state. This assumption naturally simplifies the problem. For initial orientation, we find it appropriate to limit ourselves to the consideration of such an artificial case, which is a crude approximation to reality.

Thus in the approximations assumed above, the initial Hamiltonian of the problem in the representation of second quantization has the form (see Ref. 1, p. 128, Eq. 4.36);

$$H = U_0 + \Sigma L_e(f, \lambda;\ f', \lambda')\, \hat{a}^+_{f\lambda\sigma}\hat{a}_{f'\lambda'\sigma}. \qquad (1.1)$$

Here summation is carried out over all indices; U_0 is the constant potential energy of electrostatic interaction of the ions; $f=(f^1, f^2, f^3)$ are the cartesian coordinates of the ion in the crystalline lattice; $\lambda=(0.1)$ are the indices which characterize the normal and excited states; $\sigma=(+1/2, -1/2)$ are the two possible values of the spin quantum number; $\hat{a}^+_{f\lambda\sigma}$, $\hat{a}_{f\lambda\sigma}$ are the Fermi amplitude operators;

$$L_e(f, \lambda; f', \lambda') = \int \theta_{f\lambda}(q)\left\{-\frac{h^2}{2\mu}\Delta_q + V(q)\right\}\theta_{f'\lambda'}(q)\, dq,$$

where $q=(q^1, q^2, q^3)$ are the cartesian coordinates of the electron, $2\pi h$ is Planck's constant, μ is the mass of the electron, Δ is the Laplace operator, $V(q)=\sum\limits_f U_f(q)$ is the periodic potential of the ionic lattice, $\theta_{f\lambda}(q)=\{\theta_{f0}(q), \theta_{f1}(q)\}$ are the orthonormalized atomic functions of the normal and excited states of the electron. The index e in $L_e(f\lambda; f'\lambda')$ denotes that to the potential of the ionic lattice is added the potential of the mean distribution of the charge of the electrons. Summation over f in (1.1) is extended over all fundamental directions of the crystal.

For what follows, it is appropriate to rewrite the Hamiltonian (1.1) differently, removing the sums over λ and λ' in it. Then the initial Hamiltonian is written in the following form:

$$H = U_0 + \sum_{f, f', \sigma} \{L_e(f0;\ f'0)\, \hat{a}^+_{f0\sigma}\hat{a}_{f'0\sigma} + L_e(f1; f'1)\, \hat{a}^+_{f1\sigma}\hat{a}_{f'1\sigma} + L_e(f0;\ f'1)\, \hat{a}^+_{f0\sigma}\hat{a}_{f'1\sigma} + L_e(f1;\ f'0)\, \hat{a}^+_{f1\sigma}\hat{a}_{f'0\sigma}\}. \qquad (1.2)$$

Our problem now consists in the transformation of Eq. (1.2) to diagonal form.

2. DIAGONALIZATION OF THE HAMILTONIAN

The first step in the solution of the problem formulated in Sec. 1 consists in the transition from the operators $\hat{a}_{f0\sigma}$ and $\hat{a}_{f1\sigma}$ in (1.2) to the new Fermi operators $\hat{a}_{k0\sigma}$ and $\hat{a}_{k1\sigma}$. These new operators are related to the operators $\hat{a}_{f0\sigma}$ and $\hat{a}_{f1\sigma}$ by (see Ref. 1, p. 136):

$$\hat{a}_{f0\sigma} = N^{-1/2}\sum_k e^{i(kf)}\, \hat{a}_{k0\sigma};\ \hat{a}_{k0\sigma} = N^{-1/2}\sum_f e^{-i(kf)}\hat{a}_{f0\sigma};$$

$$\hat{a}_{f1\sigma} = N^{-1/2}\sum_k e^{i(kf)}\hat{a}_{k1\sigma};\ \hat{a}_{k1\sigma} = N^{-1/2}\sum_f e^{-i(kf)}\hat{a}_{f1\sigma}.$$

Making use of these relations, we obtain from (1.2):

$$H = U_0 + \sum_{k, \sigma}\{W_{00}(k)\, \hat{a}^+_{k0\sigma}\hat{a}_{k0\sigma} + W_{11}(k)\, \hat{a}^+_{k1\sigma}\hat{a}_{k1\sigma} + W_{01}(k)\, \hat{a}^+_{k0\sigma}\hat{a}_{k1\sigma} + W_{10}(k)\, \hat{a}^+_{k1\sigma}\hat{a}_{k0\sigma}\}, \qquad (2.1)$$

where $(\lambda, \lambda' = 0,1)$

$$W_{\lambda\lambda'} = \sum_f e^{-i(fk)}\int \theta_\lambda(q-f)\left\{-\frac{h^2}{2\mu}\Delta_q + V(q)\right\}\theta_{\lambda'}(q)\, dq = \sum_f e^{-i(fk)} L_e^{\lambda\lambda'}(f). \qquad (2.2)$$

To diagonalize Eq. (2.1), we turn to the method which has been applied recently in a number of researches.[2] For this purpose, we define the operators $\hat{b}_{k0\sigma}$ and $\hat{b}_{k1\sigma}$ by means of a canonical transformation [for the definition of S, see below, Eq. (2.7)]:

$$\hat{a}_{k0\sigma} = e^{-iS}\hat{b}_{k0\sigma}e^{iS};\quad \hat{a}^+_{k0\sigma} = e^{-iS}\hat{b}^+_{k0\sigma}e^{iS}; \qquad (2.3)$$

$$\hat{a}_{k1\sigma} = e^{-iS}\hat{b}_{k1\sigma}e^{iS};\quad \hat{a}^+_{k1\sigma} = e^{-iS}\hat{b}^+_{k1\sigma}e^{iS}.$$

Then the Hamiltonian (2.1) transforms into the Hamiltonian $\mathscr{H}$, so that

$$H = e^{-iS}\mathscr{H}e^{iS}, \qquad (2.4)$$

$$\mathscr{H} = U_0 + \sum_{(k, \sigma)}\{W_{00}(k)\, \hat{b}^+_{k0\sigma}\hat{b}_{k0\sigma} + W_{11}(k)\, \hat{b}^+_{k1\sigma}\hat{b}_{k1\sigma} + W_{01}(k)\, \hat{b}^+_{k0\sigma}\hat{b}_{k1\sigma} + W_{10}(k)\, \hat{b}^+_{k1\sigma}\hat{b}_{k0\sigma}\}. \qquad (2.5)$$

Further, we represent (2.4) in the form of an infinite series

$$H = \mathscr{H} - \frac{i}{1!}[S,\mathscr{H}] - \frac{1}{2!}[S,[S,\mathscr{H}]] + \frac{i}{3!}[S,[S,[S,\mathscr{H}]]] + \frac{1}{4!}[S,[S,[S,[S,\mathscr{H}]]]] + \dots, \tag{2.6}$$

where S is a generating function which we define in the following fashion:

$$S = i\sum_k \{\Phi_1(k)\,\hat b^+_{k1\sigma}\hat b_{k0\sigma} + \Phi_2(k)\,\hat b^+_{k0\sigma}\hat b_{k1\sigma}\}, \tag{2.7}$$

where the coefficients Φ, (k) and $\Phi_2(k)$ are primitive unknown functions of the propagation vector k.

With the help of lengthy, but elementary, calculations, it is now easy to find all the expressions entering successively into Eq. (2.6). Below we write the result of the appropriate series of calculations:

$$\begin{aligned} H = U_0 &+ \sum_k \{W_{00}(k) \\ &- (W_{01}(k)\Phi_1(k) - W_{10}(k)\Phi_2(k))\Lambda_1(k) \\ &+ 2(W_{00}(k) - W_{11}(k))\Phi_1(k)\Phi_2(k)\Lambda_2(k)\}\,\hat b^+_{k0\sigma}\hat b_{k0\sigma} \\ &+ \sum_k \{W_{11}(k) \\ &+ (W_{01}(k)\Phi_1(k) - W_{10}(k)\Phi_2(k))\Lambda_1(k) \\ &- 2(W_{00}(k) - W_{11}(k))\Phi_1(k)\Phi_2(k)\cdot\Lambda_2(k)\}\,\hat b^+_{k1\sigma}\hat b_{k1\sigma} \\ &+ \sum_k \{W_{10}(k) \\ &- 2(W_{01}(k)\Phi_1(k) - W_{10}(k)\Phi_2(k))\Phi_1(k)\Lambda_1(k) \\ &+ (W_{00}(k) - W_{11}(k))\Phi_1(k)\Lambda_1(k)\}\,\hat b^+_{k1\sigma}\hat b_{k0\sigma} \\ &+ \sum_k \{W_{01}(k) \\ &+ 2(W_{01}(k)\Phi_1(k) - W_{10}(k)\Phi_2(k))\Phi_2(k)\Lambda_2(k) \\ &- (W_{00}(k) - W_{11}(k))\Phi_2(k)\Lambda_1(k)\}\,\hat b^+_{k0\sigma}\hat b_{k1\sigma}, \end{aligned} \tag{2.8}$$

where $\Lambda_1(k)$ and $\Lambda_2(k)$ are given by

$$\Lambda_1(k) = 1 + \sum_{n=1}^{\infty}\frac{(4\Phi_1(k)\Phi_2(k))^n}{(2n+1)!} = \frac{\operatorname{sh} 2\sqrt{\Phi_1(k)\Phi_2(k)}}{2\sqrt{\Phi_1(k)\Phi_2(k)}};$$

$$\Lambda_2(k) = \frac{1}{2} + \sum_{n=1}^{\infty}\frac{(4\Phi_1(k)\Phi_2(k))^n}{(2n+2)!} = \frac{\operatorname{ch} 2\sqrt{\Phi_1(k)\Phi_2(k)} - 1}{4\Phi_1(k)\Phi_2(k)}. \tag{2.9}$$

If we substitute Eq. (2.9) in (2.8) and set the curly brackets equal to zero (which stand in front of the nondiagonal products of operators $b_{k\lambda\sigma}$), then it is not difficult to show that

$$\Phi_2(k) = -\frac{W_{01}(k)}{W_{10}(k)}\Phi_1(k); \tag{2.10}$$

$$\operatorname{tg} 2\Phi_1(k)\sqrt{\frac{W_{01}(k)}{W_{10}(k)}} = -\frac{2\sqrt{W_{10}(k)W_{01}(k)}}{W_{00}(k) - W_{11}(k)},$$

and the terms remaining in Eq. (2.8) in this case yield

$$\begin{aligned} H = U_0 &+ \\ &\frac{1}{2}\sum_{k,\sigma}\{W_{00}(k) + W_{11}(k) + [(W_{00}(k) - W_{11}(k))^2 \\ &\quad + 4W_{01}(k)W_{10}(k)]^{1/2}\}\,\hat b^+_{k0\sigma}b_{k0\sigma} \\ &+ \frac{1}{2}\sum_{k,\sigma}\{W_{00}(k) + W_{11}(k) \\ &\quad - [(W_{00}(k) - W_{11}(k))^2 \\ &\quad + 4W_{01}(k)W_{10}(k)]^{1/2}\}\,\hat b^+_{k1\sigma}\hat b_{k1\sigma}. \end{aligned} \tag{2.11}$$

Thus the energetic spectrum of the system under investigation will be

$$\begin{aligned} E = U_0 &+ \\ &\frac{1}{2}\sum_{k,\sigma}\{W_{00}(k) + W_{11}(k) + [(W_{00}(k) - W_{11}(k))^2 \\ &\quad + 4W_{01}(k)W_{10}(k)]^{1/2}\}\,n_{k0\sigma} \\ &+ \frac{1}{2}\sum_{k,\sigma}\{W_{00}(k) + W_{11}(k) \\ &\quad - [(W_{00}(k) - W_{11}(k))^2 \\ &\quad + 4W_{01}(k)W_{10}(k)]^{1/2}\}\,n_{k1\sigma}, \\ &n_{k1\sigma},\quad n_{k0\sigma} = 0,1;\quad \sum_{k,\sigma}(n_{k0\sigma} + n_{k1\sigma}) = N, \end{aligned} \tag{2.12}$$

and the generating function is

$$S = \frac{i}{2}\sum_k \arccos\frac{W_{00}(k) - W_{11}(k)}{[(W_{00}(k) - W_{11}(k))^2 + 4W_{01}(k)W_{10}(k)]^{1/2}} \times\left\{\sqrt{\frac{W_{10}(k)}{W_{01}(k)}}\,\hat b^+_{k1\sigma}\hat b_{k0\sigma} - \sqrt{\frac{W_{01}(k)}{W_{10}(k)}}\,\hat b^+_{k0\sigma}\hat b_{k1\sigma}\right\}.$$

3. CRITIQUE OF THE RESULTS

The quantities $W_{\lambda\lambda'}(k)$ by which the energy spectrum (2.12) is given, can be given a graphic physical interpretation. With this purpose we must first transform $W_{\lambda\lambda'}(k)$. In the Eqs. (2.2) for $W_{\lambda\lambda'}(k)$, it is appropriate to go from the orthonormal atomic functions $\theta_{f\lambda}(q)$ to the ordinary atomic functions $\varphi_{f\lambda}(q)$. The general method of such a transformation was developed by Bogoliubov[1], and can be reproduced without difficulty in our case. Therefore we give below the explicit equations for the quantities under consideration up to first order of smallness inclusively, not basing any conclusion on them:

$$W_{00}(k) = E_0 + \int \varphi_0^2(q)\,[V(q) - U(q)]\,dq + \sum_{f\neq 0} A_{00}(f)\,e^{-i(fk)}; \tag{3.1}$$

$$W_{11}(k) = E_0 + \Delta E + \int \varphi_1^2(q)\,[V(q) - U(q)]\,dq + \sum_{f\neq 0} A_{11}(f)\,e^{-i(fk)};$$

$$W_{01}(k) = \int \varphi_0(q)\,\varphi_1(q)\,[V(q) - U(q)]\,dq + \sum_{f\neq 0} A_{01}(f)\,e^{-i(fk)};$$

$$W_{10}(k) = \int \varphi_1(q)\,\varphi_0(q)\,[V(q) - U(q)]\,dq + \sum_{f\neq 0} A_{10}(f)\,e^{-i(fk)},$$

where E_0 is the energy of the s-electron in the isolated atom, ΔE is the perturbation energy of the electron in the isolated atom;

$$\begin{aligned}
A_{00}(f) = {} & \tfrac{1}{2}\int\Big\{\Big[V(q) - U(q-f) - \int \varphi_0^2(q_1 - f)\,(V(q_1) - U(q_1 - f)\,dq_1\,\Big] \\
& + \Big[V(q) - U(q) - \int \varphi_0^2(q_1)\,(V(q_1) - U(q_1))\,dq_1\Big]\Big\}\,\varphi_0(q)\,\varphi_0(q-f)\,dq; \\
A_{11}(f) = {} & \tfrac{1}{2}\int\Big\{\Big[\Delta E + V(q) - U(q-f) - \int \varphi_1^2(q_1 - f)\,(\Delta E + V(q_1) \\
& - U(q_1 - f))\,dq_1\Big] + \Big[\Delta E + V(q) - U(q) - \int \varphi_1^2(q_1)\,(\Delta E + V(q_1) \\
& - U(q_1))\,dq_1\Big]\Big\}\,\varphi_1(q)\,\varphi_1(q-f)\,dq; \\
A_{01}(f) = {} & \int [\Delta E + V(q) - U(q-f)]\,\varphi_0(q)\,\varphi_1(q-f)\,dq - \tfrac{1}{2}\Big\{\int \varphi_0^2(q)\,[V(q) \\
& - U(q)]\,dq + \int \varphi_1^2(q-f)\,[\Delta E + V(q) - U(q-f)]\,dq\Big\}\int \varphi_0(q)\,\varphi_1(q-f)\,dq; \\
A_{10}(f) = {} & \int [V(q) - U(q-f)]\,\varphi_1(q)\,\varphi_0(q-f)\,dq - \tfrac{1}{2}\Big\{\int \varphi_0^2(q-f)\,[V(q) \\
& - U(q-f)]\,dq + \int \varphi_1^2(q)\,[\Delta E + V(q) - U(q)]\,dq\Big\}\int \varphi_1(q)\,\varphi_0(q-f)\,dq.
\end{aligned} \tag{3.2}$$

Furthermore, if we limit our consideration, for example, to the case of a simple cubic lattice, then in place of Eq. (3.1) we will have:

$$W_{00}(k) = E_0 + C_0 + 2A_{00}(\cos ak^x + \cos ak^y + \cos ak^z); \tag{3.3}$$

$$W_{11}(k) = E_0 + \Delta E + C_1 + 2A_{11}(\cos ak^x + \cos ak^y + \cos ak^z);$$

$$W_{01}(k) = B + 2A_{01}(\cos ak^x + \cos ak^y + \cos ak^z);$$

$$W_{10}(k) = B + 2A_{10}(\cos ak^x + \cos ak^y + \cos ak^z).$$

Here a is the cubic lattice constant;

$$C_0=\int\varphi_0^2(q)\,[V(q)-U(q)]\,dq;\qquad(3.4)$$

$$C_1=\int\varphi_1^2(q)\,[V(q)-U(q)]\,dq;$$

$$B=\int\varphi_0(q)\,\varphi_1(q)\,[V(q)-U(q)]\,dq.$$

Thus, as might be expected, the s level E_0 of the isolated atom in the crystalline lattice is displaced by a quantity C_0 and split into a band, the width of which is determined by the value of the transfer integral A_{00}. Analogously, the perturbed p-level $(E_0+\Delta E)$ of the isolated atom is shifted in the crystalline lattice by the value C_1 and splits into a band whose width is determined by the transfer integral A_{11}. $W_{00}(k)$ and $W_{11}(k)$ are respectively the energies of the s- and p-electrons in the crystalline lattice.

It is evident that the energy spectrum of the system will be determined only by the energies $W_{00}(k)$ and $W_{11}(k)$ if we neglect the integrals $L_e(f0;f'1)$ and $L(f1;f'0)$ in Eq. (1.2). Actually,

$$E=U_0+\sum_{k,\sigma}(W_{00}(k)\,n_{k0\sigma}+W_{11}(k)\,n_{k1\sigma}),\qquad(3.5)$$

$$n_{k0\sigma},\ n_{k1\sigma}=0,1;\quad\sum_{k,\sigma}(n_{k0\sigma}+n_{k1\sigma})=N,$$

i.e., the energy spectrum of the system in this case is composed additively of $W_{00}(k)$ and $W_{11}(k)$ taken with corresponding coefficients (occupation numbers). If the integrals $L_e(f0;f'1)$ and $L_e(f1;f'0)$ are considered as small quantities, then we can expand the square root in Eq. (2.12) in a series and restrict ourselves to the second terms of the expansion. In this case we have

$$E=U_0+\sum_{k,\sigma}\left\{W_{00}(k)+\frac{W_{01}(k)\,W_{10}(k)}{W_{00}(k)-W_{11}(k)}\right\}n_{k0\sigma}$$

$$+\sum_{k,\sigma}\left\{W_{11}(k)-\frac{W_{01}(k)\,W_{10}(k)}{W_{00}(k)-W_{11}(k)}\right\}n_{k1\sigma},\qquad(3.6)$$

$$n_{k0\sigma},\quad n_{k1\sigma}=0,1;\quad\sum_{k,\sigma}(n_{k0\sigma}+n_{k1\sigma})=N.$$

Comparing (3.5) with (3.6), we conclude that in the latter case the energies of the s-and p-electrons in the crystal are changed by $W_{01}(k)\,W_{10}(k)/[W_{00}(k)-W_{11}(k)]$. This correction depends on the integrals $W_{01}(k)$ and $W_{10}(k)$. The latter in turn, in agreement with Eq. (3.3), contain the energy of transfer of the electron from the normal to the excited state at its lattice point (integral B) and the integral A_{01} and A_{10} for transitions between neighboring atoms are of the same type. Consequently, the matrix elements $W_{01}(k)$ and $W_{10}(k)$ can be treated as the energy of the "excited" and "bound" electron in the lattice.

In the general case, when the integrals $L_e(f0;f'1)$ and $L_e(f1;f'0)$ are not small, the energy spectrum of the electrons in the crystalline lattice is given by Eq. (2.12). In this case, the combination of the s- and p-states is essentially established, and we cannot neglect the energies $W_{01}(k)$ and $W_{10}(k)$ in comparison with the energies $W_{00}(k)$ and $W_{11}(k)$. Such is evidently the case, for example, in bivalent metals (alkali earths)[3] and must be taken into account in the construction of a theory of their electrical conductivity. The first case of the overlapping of the bands was considered by Blokhintsev.[4] He performed an attempt at the approximation treatment of the combination of of the s-state with degenerate p-states and obtained a series of interesting, but only qualitative results.

Finally, it seems appropriate to emphasize that in the ordinary treatment of the approximation of strong coupling in the zone theory interaction of the states of the s- and p-zones in the zeroth approximation does not in general enter into the theory at all. It appears only upon the introduction of additional, in considerable degree artificial, assumptions. In our case, the necessity for this is lacking. The interaction of the zones enters into the theory in zeroth approximation (through the quantities W_{10} and W_{01}) as a consequence of the strict treatment of the zone approximation with the help of the apparatus of second quantization.

In conclusion, the authors consider it their pleasant duty to express their gratitude to Prof. S. V. Vonsovskii for a series of critical discussions.

---

[1] N. N. Bogoliubov, *Lectures on Quantum Statistics*, Kiev, 1949.

[2] Y. Kitano and H. Nakano, Prog. Theor. Phys. 9, 370 (1953); D. Bohm and D. Pines, Phys. Rev. 82, 625 (1951); Problems of Contemporary Physics 11, 113 (1952). Russian translation .

[3] H. Bethe and A. Sommerfeld, *Electron Theory of Metals* (Russian translation) ONTI, 1938, Sec. 13.

[4] D. I. Blokhintsev, J. Exptl. Theoret. Phys. (U.S.S.R.) 3, 475 (1933); Z. Physik Sowjetunion 5, 316 (1934).

Translated by R. T. Beyer
142

SOVIET PHYSICS JETP VOLUME 3, NUMBER 4 NOVEMBER, 1956

Magnetic Analysis Study of Energy Levels of S^{33}

L. M. KHROMCHENKO
Radium Institute, Academy of Sciences, USSR

(Submitted to JETP editor July 25, 1955)
J. Exptl. Theoret. Phys. (U.S.S.R.) 30, 681-685(April, 1956)

The energy of protons from the reaction S^{32} (d,p) S^{33} has been analyzed magnetically. A total of 21 proton groups have been observed corresponding to the ground state and 20 excited levels of S^{33}. The region of excitation energies up to 9.2 mev was investigated. Besides 12 already known levels 8 new ones have been found in the region of high excitation.

THE nuclide S^{32} which has a natural abundance of 95% has a number of peculiarities. It is an even-even nucleus and has an equal number of protons and neutrons. According to the shell model it has a closed shell configuration and so its shape must be very closely spherical and it should have zero spin and even parity. One can surmise that the excitation probability of such nuclei is smaller than that of odd asymmetric nuclei. In a S^{32} (d,p) S^{33} reaction which yields information on S^{33}, one would expect at low excitation energies to reach mostly "one particle" states, i.e., such configurations where just the last odd particle is excited, leaving the core in essentially the ground state of S^{32}.

In view of the small yield of the above reaction, the spectrum of the levels of S^{33} is insufficiently known. The review article by Endt and Kluyver[1] gives data from three papers which report studies of the reaction $S^{32}(d,p)$ S^{33} in several regions of excitation energy.

In 1941 Smith and Pollard[2] found 6 proton groups corresponding to the ground state and 5 excited states of S^{33}. They used 3.1 mev deuterons. Davison[3] studied the same reaction in 1949 with greater intensity and resolution and reported 13 proton groups, one for the ground state and 12 for excited states of S^{33}. The last paper as of the time of the writing of the present paper seems to be the paper by Holt and Marsham.[4] They used a deuteron energy of 8 mev and so could reach a large range of excitation energies. However, according to the authors, the accuracy and the resolution in this work were inferior to those of Davison. Of their 13 proton groups only 6 can be said to be well established. These are listed in Ref. 1 and are due to levels of S^{33} at the following energies: 0.85, 2.90, 3.26, 4.21, 4.89, and 5.72 mev. The other levels which they found are less trustworthy. Holt and Marsham did not determine the energy of the S^{32} (d,p) S^{33} reaction but used the Q-value as given by Strait et al.[5]

For some of the proton gruups Holt and Marsham determined the angular distributions. Therefore they could give probable spins and parities of the compound states in addition to the energy. A compilation of the data on S^{33} in the literature is given in Table 1.

In all cited investigations the proton energy was determined by absorption in calibrated Al foils. Clearly this method does not allow high accuracy and resolution. In the present work the energy of the reaction products was measured by means of a magnetic spectrometer which allows a better determination of the energy of the excited states. The method used was described earlier.[6,7,8] In short it consists of a combined plate-and sample-holder (Fig. 1). A sample of the material to be studied is placed at A. It is irradiated with a collimated beam of deuterons of an energy up to 4.7 mev. The holder is placed in a magnetic field perpendicular to the plane of the drawing. The charged particles which are emitted in a nuclear reaction are bent by the magnetic field and fall on a thin emulsion plate after passing through a narrow slit at B. Discrete proton groups show up as lines C_1, C_2, . . . parallel to the slit. By determining the location of a line and knowing the magnetic field strength H one can obtain the energy of a particular particle group if its e/m is known. Thus one can determine the excitation energy of the corresponding level of the nucleus under investigation. On top of the plate there was located a filter of variable thickness. It covered the plate fully lengthwise but only half of the plate across. Its thickness increased along the plate in such a way as to absorb fully deuterons and particles of still shorter range but to transmit protons. The use of this modified wedge-filter[9] allowed us to separate the proton groups originating in the (d,p) reaction from all other charged particles.

The high intensity of the available deuteron beam allowed us to obtain exposures which showed visually observable lines on the plates.

TABLE 1.

Excited levels of S^{33}, energies in mev

Level	Results of the present work	Results of other authors		
		Smith and Pollard	Davison	Holt and Marsham
0	0	0	0	0
1	$0{,}78_{6}$	1.05	0,79	0,85
2	$1{,}86_{9}$	—	1,90	1.86
3	$2{,}22_{8}$	2,17	2,17	2.28
4	$2{,}95_{6}$	—	2,85	2.90
5	$3{,}32_{9}$	3.22	3,15	3.26
6	$4{,}02_{3}$	—	3.88	3.91
7	4.27_{9}	4.33	4,15	4.21
—	—	—	4,42	—
8	$4{,}77_{0}$	—	4,70	4.89
9	5.04_{3}	—	5.11	—
10	$5{,}46_{8}$	5,32	5,63	5.72
11	5,90	—	—	—
12	$6{,}10_{2}$	—	—	—
13	$6{,}62_{2}$	—	6.30	6,48
14	$6{,}91_{6}$	—	—	—
15	7.22_{5}	—	—	—
16	$7{,}45_{2}$	—	—	7.44
—	—	—	—	7,83
17	8.04_{7}	—	—	—
18	$8{,}28_{9}$	—	—	—
19	$8{,}85_{8}$	—	—	—
20	9.11_{8}	—	—	—

Therefore the counting of tracks under the microscope could be replaced by an analysis with a microphotometer. The high concentration of tracks necessary to obtain visual lines insured a very high statistical accuracy in the observation of particle groups.

The sample consisted of a thin layer of finely ground ZnS powder on a silver foil. As in the quoted earlier papers the results were interpreted as being due to the isotope S^{32} only. An investigation of the level schemes of Mg, Si and other elements has shown that under the conditions of the present work the influence of reactions from the low abundance isotopes on the results is unimportant. This seems to be borne out also by the comparison of our results on the spectrum of S^{33} with the data in the literature.

Figure 2 is a reproduction of one of the plates with a spectrum from sulfur. The microphotogram of this plate is shown in Fig. 3. The upper curve has been obtained from the uncovered portion of the plate, i.e., it gives the spectrum of all charged particles emerging from the sample under bombardment with deuterons. The lower curve is the microphotogram of the filtered part of the plate and contains the spectrum of protons only. The unfiltered curve shows prominently deuterons scattered from the nuclei of Ag, Zn, and S, making up the target. The energy of the primary deuterons was obtained from these groups. These intense peaks

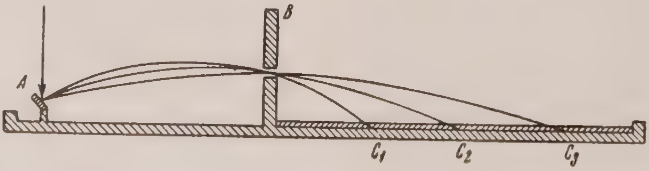

FIG. 1. Schematic diagram of the plateholder.

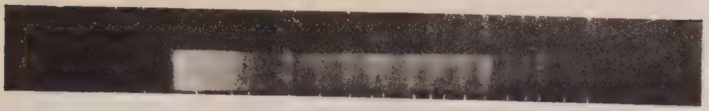

FIG. 2. Energy spectrum of the nucleus of S^{33}.

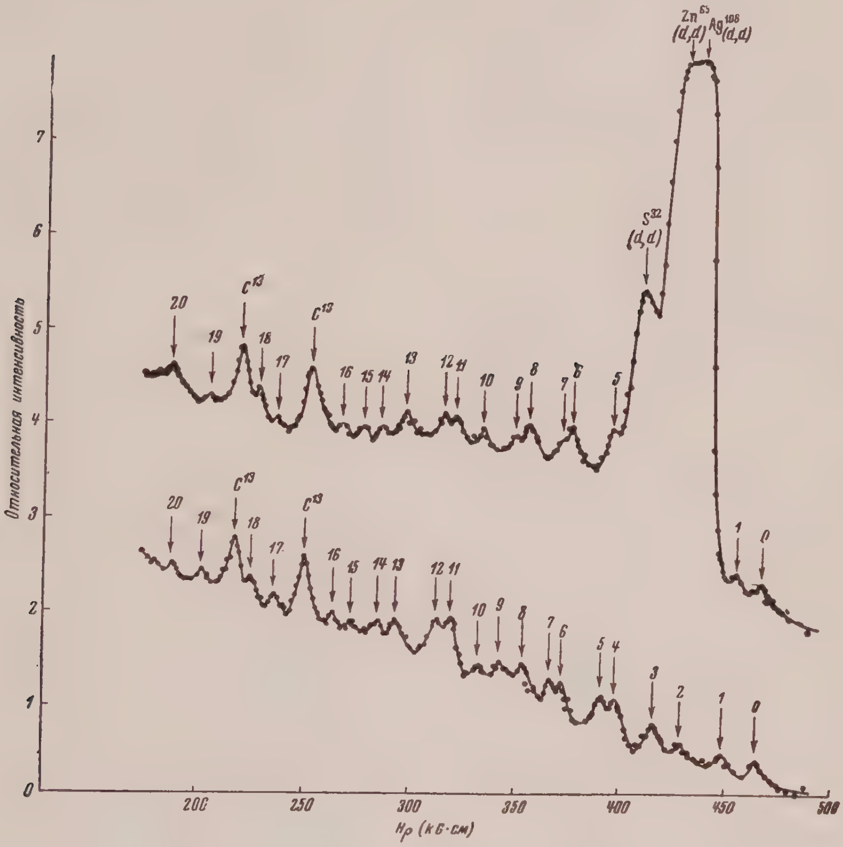

FIG. 3. Microphotogram of a plate showing the energy spectrum of S^{33}. The proton groups corresponding to states in S^{33} are marked by number only. The numbers correspond to those of Table 1. The remaining groups are identified by the reaction. The deuteron energy $E_d = 4.68$ mev. The lower curve is obtained from the filtered part, the upper from the unfiltered part of the plate.

are completely absent in the lower curve of Fig. 3 Besides the deuteron groups the curves show a large number of proton groups. These come from the (d,p) reaction on sulfur, numbered from 0 to 20, and from carbon contaminants.

A total of 5 plates were exposed. A control experiment with a PbS sample showed that the obtained proton groups did not originate in a (d,p) reaction on Zn. The data given in Table 1 are averages from all 5 plates. In order to check on the correctness of the interpretation of the proton groups, 2 primary deuteron energies were used: 3 plates were obtained at a deuteron energy of about 4.7 mev, 2 at about 3.8 mev.

In the present experiment a Q-value for the reaction S^{32} (d,p) S^{33} has been obtained:

$Q_0 = 6.633 \pm 0.020$ mev; Smith and Pollard give $Q_0 = 6.62$ mev, Davison gives $Q_0 = 6.48 \pm 0.11$ mev, Strait et al. give $Q = 6.422 \pm 0.011$ mev.

The analysis of the results, as summarized in Table 1 shows that from the 23 proton groups found in the present work only 2 are due to the reaction $C^{12}(d,p)\,C^{13}$. All the other groups are due to the (d,p) reaction on sulfur. A comparison with the data of the other workers confirms the identity of almost all levels observed earlier, except for the level of S^{33} at E=4.42 mev. This level was found only by Davison and is absent in the present work as well as in the other cited papers. We do not believe that the identity of this level is sufficiently well established.

The excitation energies of the levels at 3.32_9, 5.46_8, and 6.62_2 mev as obtained in the present study differ considerably from those obtained by the earlier workers. This difference is larger than the experimental errors. In the present experiments they were for the majority of the levels on the order of 20 kev; in a few cases where the corresponding peaks were not too pronounced they reached up to 40 kev.

We found (besides the already published levels of S^{33}) eight new ones; these are the levels 11, 12, 14, 15, 17, 18, 19, 20 of Table 1. The level at 7.83 mev found by Davison was hidden in our work by a rather strong proton group from the reaction $C^{12}\,(d,p)\,C^{13}$. Another proton group from the carbon reaction masked the energy region corresponding to an excitation energy of around 8.5 mev, between the levels 18 and 19.

It is also interesting to compare the level scheme of S^{33} as obtained from the (d,p) reaction with the data from γ-spectroscopy. The thermal neutron capture γ-rays obtained by Kinsey, Bartholomew and Walker[10] are listed in Table 2. The γ-rays C,D,E,F,G,H,I,M,O are sufficiently close in energy to the excitation energies of the levels 16, 15, 13, 11, 10, 9, 8, 5 and 4 respectively of Table 1 to suppose that they represent the ground state transitions from the respective levels of S^{33}.

The γ-rays B,J,K,L and N may be associated with transitions from the highest level to the levels corresponding to the groups 1, 6, 7, 9, and 10 respectively of Table 1. This interpretation is at variance with the level scheme proposed in Ref.10 on the basis of their results and the data of Davison. It therefore needs further confirmation.

TABLE. 2.

Thermal neutron capture γ-rays in sulfur[10]

Level	γ-ray energy in mev	Level	γ-ray energy in mev	Level	γ-ray energy in mev
A	8.64 ± 0,02	*F*	5,97 ± 0,06	*K*	4,38 ± 0,03
B	7,78 ± 0.03	*G*	5,43 ± 0.02	*L*	3,69 ± 0,05
C	7,42 ± 0.03	*H*	5.03 ± 0,06	*M*	3.36 ± 0,05
D	7,19 ± 0.03	*I*	4,84 ± 0,06	*N*	3.21 ± 0,03
E	6.64 ± 0,03	*J*	4.60 ± 0,06	*O*	2.94 ± 0.05

---

[1] P.M. Endt and J.C. Kluyver, Rev. Mod. Phys. **26**, 95 (1954).

[2] E. Smith and E. Pollard, Phys. Rev. **59**, 942, (A) (1941).

[3] P.W. Davison, Phys. Rev. **75**, 757 (1949).

[4] J.R. Holt and T.N. Marsham, Proc. Phys. Soc. (London) **A66**, 467 (1953).

[5] E.N. Strait, D.M. Van Patter, W. W. Buechner and A. Sperduto, Phys. Rev. **81**, 747 (1951).

[6] L.M.Khromchenko, Dokl. Akad. Nauk SSSR **93**, 451 (1953).

[7] L.M. Khromchenko, Dokl. Akad. Nauk SSSR **94**, 1037 (1954).

[8] L.M. Khromchenko, Dokl. Akad. Nauk SSSR **98**, 761 (1954).

[9] I.A. Nemilov, Izv. Akad. Nauk SSSR, Ser. Fiz. **14**, 319 (1950).

[10] B.B. Kinsey, G.A. Bartholomew and W. H. Walker, Phys. Rev. **85**, 1012 (1952).

Translated by M. Danos
139

SOVIET PHYSICS JETP VOLUME 3, NUMBER 4 NOVEMBER, 1956

Reflection of Slow Electrons from the Surface of Pure Tungsten and from Tungsten Covered by Thin Films

N. D. MORGULIS AND D. A. GORODETSKII
Kiev State University

(Submitted to JETP editor June 30, 1955)
J. Exptl. Theoret. Phys. (U.S.S.R.) 30, 667-674 (April, 1956)

The reflection of slow electrons from the surface of both pure tungsten and tungsten covered with adsorbed films of barium and various thicknesses, and of oxygen, is investigated. Particular attention is given to achieving a very high vacuum in the experimental tubes so that the components of residual gases ($p_{\text{eff}} \approx 10^{-10} - 10^{-11}$ mm) condensed on the surface could not have a measurable effect. The results of the experiments show an unusual dependence on the primary electron energy V_p of the coefficient of secondary emission R for pure W and O-W, and a large effect on R of the films of Ba adsorbed on W with a thickness smaller than, and of the order of a monatomic layer. The correct correlation is also obtained between the threshold of emission of the secondary electrons and the work function of the target.

THE contemporary period of development of the physical cathode electronics is characterized in part by a renewed increased interest in the problem of a solid body covered by thin and active films. This interest is connected with the fact that such systems-cathodes are again beginning to assume a serious importance as practical sources of electrons[1], and also that at the present time these investigations can be carried out on a high experimental level previously entirely unattainable. Among these systems belong first of all tungsten covered by thin adsorbed layers of electropositive barium, which appears to be a model of the contemporary porous metal-coated (L) cathodes. In this project, together with recently completed accurate investigations of the work function of similar systems[2] a great interest also encourages the study of reflection of slow electrons from such surfaces and also from tungsten covered by a film of electro-negative oxygen. This method has not been used thus far to study directly the surface potential barrier of similar film systems. These circumstances have stimulated us to undertake the present work.

As is well known, a study of elastic reflection of slow electrons is a very difficult problem from the experimental point of view. First, it is very difficult to achieve in the experimental tube such vacuum conditions that would fully guarantee a complete cleanliness and also reliabliity of the obtained results. We particularly emphasize here the role of this factor since the coefficient of elastic reflection of slow electrons R is very sensitive to changes of the surface composition entirely undetectable by other methods. From this point of view the majority of the work completed to date may not be sufficiently reliable. Since we had appropriate ionization techniques to obtain, maintain and measure very high vacuum in experimental tubes, i.e., pressures $p \lesssim 10^{-9}$ mm[3], we have decided to carry out the present investigation.

Two designs of the experimental tubes were used in the present work; the first is shown schematically in Fig. 1. The experimental target was a disk of rolled tungsten ribbon, which could be moved into two positions: 1) outside of the measuring system where it could undergo thorough cleaning by electron bombardment, and where films of Ba and Ag of the desired thickness could be evaporated on it; 2) inside of the collector (position *2*) where the measurements were made. The only disadvantage of this system was that its collector did not have a spherical form which could reflect itself on the accuracy of the interpretation (even though to only a very small degree) of the trapping curves of the reflected electrons (see below). The layer of Ag used as an additional control was always thick; the films of Ba deposited on *W* were both monatomic with various degrees of coverage Θ, and thick. The density of Ba atoms in this film could be accurately determined by a measurement of the contact potential V_k of the target relative to the tungsten cathode of the gun[2]. The contact potentials were measured in position *2* by a precisely parallel displacement of the voltampere characteristics *1-5* of the current in the target I_M, which on a semilogarithmic graph has a linear character. This led to a correct order of magnitude of temperature of the electrons $T \approx 2300°$, as is evident from Fig. 2. The accuracy of the focusing of the beam of slow electrons, very important in this case, was tested first by means of a collection of the beam on a

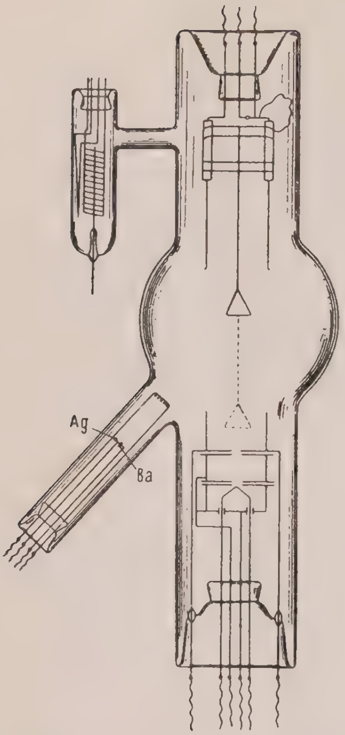

FIG. 1. Diagram of the experimental tube.

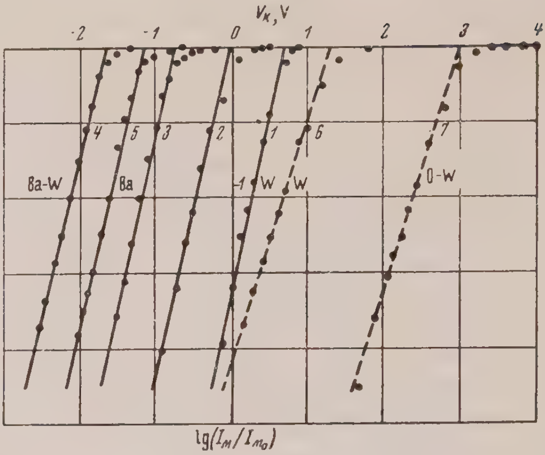

FIG. 2. Volt-ampere characteristic curves: *1*-$\Delta\varphi = 0$; *2*-$\Delta\varphi = 0.7$; *3*-$\Delta\varphi = 1.5$; *4*-$\Delta\varphi = 2.4$; *5*-$\Delta\varphi = 1.9$; *6*-$\Delta\varphi = 0$; *7*-$\Delta\varphi = 1.7$ ev.

model of our system of electrodes, whose collecting disk was divided into a set of isolated rings with individual leads. The system was pumped constantly at a pressure $p \approx 10^{-6} - 10^{-7}$ mm. This test has shown that our primary beam of electrons up to energy $V_p = 2V$ is well focused on the surface of the target and consequently, no substantial errors should originate from this surface.

Together with the tubes of the first design we have made a considerable use of tubes of a second design, which differed only in the shape of the target. In the second design the target was made in Π shape of the same tungsten ribbon, 0.06 mm thick, 4 mm wide and 6 mm long in the front end. This target was placed in a fixed position inside the collector and could be directly heated by flowing through it current of an appropriate magnitude. In this case, even without mentioning two new possibilites discussed below, we could carry out the measurements of the coefficient of reflection of electrons from W both immediately, as the target has cooled after its high temperature degassing (similarly to the bulb of the first design), and also after the degassing but still directly from a glowing target, for example, at $T \approx 1700°$ K where the films adsorbed to tungsten are basically absent. In the latter case the tungsten target was heated by an alternating current passed through a half wave rectifier to remove the magnetic field due to the large heating current through the tungsten ribbon and the potential drop caused by it across the target, and the measurements were carried out in the half period when the current was shut off. This scheme has been sucessfully used by us several times previously[4]. Furthermore, to separate out the electrons reflected from the target due to its spontaneous thermal emission as a result of the heating, the primary beam was modulated by 50 periodic square wave pulses synchronized with the shutting off of the heating current, on which was superimposed a sinusoidal signal of frequency 7.8 kc. The current of reflected electrons was amplified and was measured on an oscilloscope.

A great deal of attention was paid to achieving the proper vacuum conditions in the tubes[5]. After lengthy and very careful pumping and outgassing, spraying of Ba gas getter and finally sealing off the bulb, the initial pressure of the residual gases inside the tube was about $p_0 \approx 10^{-7}$ mm; This pressure was measured by a modified ionization gauge[6] soldered to the experimental tube (see Fig. 1). After the sealing off of the tube this ionization gauge was working constantly as an activator of ionizing gas absorption[3,6]. By these means, the pressure of the residual gases in the bulb was reduced to $p \approx 3 \times 10^{-9}$ mm and was maintained at that level. However, it can be shown that p_{eff} of that part of the residual gases which in fact can be adsorbed on the studied surface and cause deterioration of the obtained results, is still at a much lower level. This can be seen from the

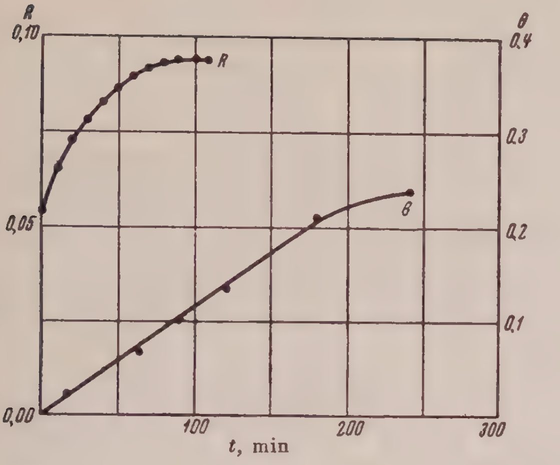

FIG. 3. The change of the quantities R and θ for a tungsten ribbon which is left cold in the tube.

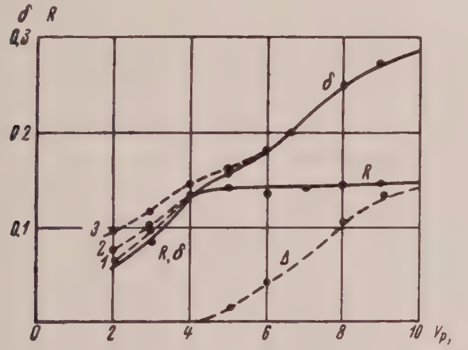

FIG. 4. The variation of the quantities δ and R for clean tungsten as a function of the energy of primary electrons.

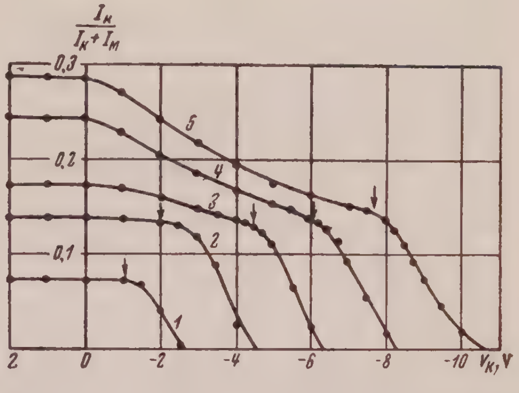

FIG. 5. The family of trapping curves for clean tungsten: 1 - $V_p = 2$; 2 - $V_p = 4$; 3 - $V_p = 6$; 4 - $V_p = 8$; 5 - $V_p = 10$ v.

analysis of the mass-spectrograms of the gas in similar glass tubes used for a long period of time[6,7], and also by a direct application to these experimental tubes of the method of "flashing"[3,8] and also from the measurement of the coefficient of elastic reflection R (see below). As an illustration of this very important circumstance we shall show that in one case where the tungsten target of the second design was flashed we obtained a result shown in Fig. 3. Here the ordinate on the right hand side is the drop in pressure in the bulb at the moment of flash, recalculated to the corresponding fraction θ of covering the target by the adsorbed gas on an assumption that a monomolecular layer has 1.25×10^{14} mol/cm^2 [8]; the abscissa is the time of the preceding adsorption. From the slope of the initial linear portion of the curve $(d\theta/dt)_{t=0}$ one can obtain $p_{\text{eff}} \gtrsim 10^{-11}$mm at a time that the ionization gauge shows $p = 3.5 \times 10^{-9}$ mm. The second curve in the same figure gives the typical time dependence of the coefficient R for tungsten at a constant $V_p = 2V$ (the scale is on the left-hand ordinate); here, from the quantity $(dR/dt)_{t=0}$ one obtains a value $p_{\text{eff}} = 10^{-10}$ mm. Thus, the value of the quantity $p_{\text{eff}} < p$ lies within these very low limits $10^{-10} - 10^{-11}$ mm. It allows us to assume that we work under sufficiently pure conditions if the measurements are made immediately after the outgassing of the target. Furthermore, one sees immediately the error in the measured quantity R that can be introduced under actual conditions. It should be noted that even for such low pressures of the residual gases in the tube there exists a slow but still noticeable increase of the reflection coefficient R with time (see Fig. 4). This may increase by a factor of two or more over its initial value. This limiting value of the quantity R at a fixed V_p may vary in different cases because of its dependence on the pressure and the composition of the residual gases in the tube. By the way, under the same conditions one observes only a small increase ($\lesssim$ 0.1 ev) in the work function of the investigated surface. The work function is determined from the changes in the contact potential. In this manner the coefficient R of elastic reflection of electrons appears to be very sensitive to the smallest changes in the composition of the surface under investigation. Therefore, all of our subsequent data refer to the initial uncontaminated values of the quantity R. The fact that the deviation from the linear dependence of R and θ on t in Fig. 3 begins at different times t_R and t_θ, where $t_R < t_\theta$, is evidently a manifestation of the entirely different physical character of the two

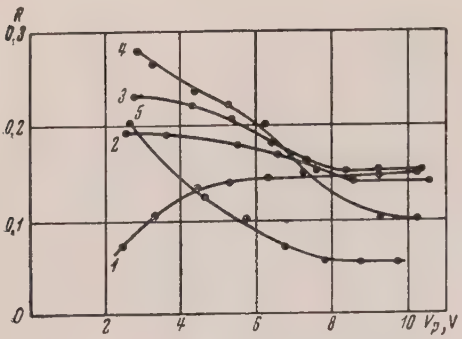

FIG. 6. The variation of the quantity R as a function of the energy of primary electrons for W and Ba-W with coverage corresponding to: 1 - $\Delta\varphi = 0$ (W); 2 - $\Delta\varphi = 0.7$; 3 - $\Delta\varphi = 1.5$; 4 - $\Delta\varphi = 2.4$; 5 - $\Delta\varphi = 1.9$ ev (Ba).

measures of the number of adsorbed molecules. Indeed, if the effective interaction separation between the gas molecules falling on the surface and those already adsorbed is simply their gas kinetic diameter $d_k \approx 3$ Å, and for impinging slow electrons is of the order of magnitude of a phase wavelength λ_e which is of the order 8 Å for $V_p = 2V$; then $\lambda_e > d_k$ to which corresponds $t_R < t_\theta$.

The determination of the coefficient of elastic reflection R of electrons from the investigated surface was carried out by the usual method based on a preliminary determination of the curve of the trapped current in the collector circuit I_k for all values of V_p. An example of such a family of curves for the case of pure tungsten is given in Fig. 5; the arrows point to those values that characterize elastic reflection and whose appropriate ordinates give us the value of the quantity R. Even though our system was not spherical, the points of inflection of the curves of Fig. 5 are sufficiently clearly apparent to enable us to separate out reliably from all electrons leaving the the target the group that was elastically reflected. Control experiments with a spherical system led to the same results.

An example of a similar determination of the coefficient of elastic reflection R of electrons as a function of the energy V_p of the primary electrons impinging on the target, taking into account contact potential difference, is shown in Fig. 4. Here, one of the two solid curves gives $R = f(V_p)$ for thoroughly cleaned tungsten surface. This curve was reproduced many times with tubes of both designs, and also using the modulation of the primary beam. The second solid curve gives the dependence on V_p of the relative number δ of all electrons leaving the target, measured in the saturated states for $V_k = +2V$ (Fig. 5). Both inelastically reflected and also secondary electrons will be included in the number δ. As is apparent from Fig. 4, both of these curves merge, in the region of small values of V_p, beginning at $V'_p \approx 4$-5 V, which may be regarded as a threshold of secondary emission from W (see below). The group of dotted curves 1, 2 and 3 give the same quantity δ measured at various times $t_1 < t_2 < t_3$, which are the periods for which the target remained cold after its high temperature cleaning. We notice that as a result of adsorption of a part of the residual gases on the target, the increase in δ is principally on the left-hand side of the curves where almost all emitted electrons are elastically reflected. This increase becomes more pronounced as V_p decreases. Thus, Fig. 4 immediately shows the effect of the adsorption of films from residual gases on the target in the regions of various values of V_p.

On a closer inspection of Fig. 4 attention is drawn to the unusual form of the curve $R = f(V_p)$ for pure W. Regardless of the detailed description of this penomenon one should expect a decrease in R with an increase in V_p, while the experiments repeated many times show here an opposite relation, particularly in the region of small V_p. On the other hand, a thick layer of silver deposited on the same W had a somewhat more normal dependence. In comparing the data for W and Ag with the data obtained by Myers[9] we have concluded that the curve $R = f(V_p)$ obtained by him for W corresponds to our W covered by an adsorbed film. For Ag, the disagreement of some degree is only in the initial part of the curve.

An attempt to explain the above facts encounters immediately great obstacles, particularly since one of the least clear facets of the problem is the role played here by the polycrystalline character of the investigated tungsten surface. This is so even though there are indications that rolled tungsten ribbon should have its surface composed of microcrystals with predominant orientation of the (100) axis[10]. We have attempted to clarify this problem for W which may be subjected to high temperature cleaning by crystallizing the tungsten ribbon through an appropriate temperature treatment. This treatment consisted of repeated turning on and off of the heating current which heated the central part to about 1800° K. Simultaneously, a very steep temperature gradient was established along the ribbon by conducting away heat through thick leads, and consequently, an elastic strain was established as well[11]. It turns out that by this means one partly succeeds in crystallizing the ribbon, obtaining crystals as large as ≈ 0.1 mm in the regions where dT/dx was maximum. We have unfortunately not succeeded in obtaining larger crystals. Of course, this amount of crystallization is still far from necessary, but nevertheless we obtained both the contact potential curves and the curve $R = f(V_p)$ in one of our tubes of the second design for very carefully cleaned tungsten both before crystallization and after crystallization. However, we could not find any noticeable difference between the two sets of curves.

With a gradual adsorption of thin films on an ordinarily (uncrystallized) clean tungsten surface ($\varphi_0 = 4.5$ ev) with various degrees of coverage θ, we obtain the results shown in Fig. 6 with curves 1-5 consecutive in time (similarly to Fig. 2). The films are characterized by the average value of the work function $\Delta V_k = \Delta\varphi$ determined from changes of the contact potential $\varphi = \varphi_0 - \Delta\varphi$. The greatest density of a monolayer of Ba corresponds to $\Delta\varphi = 2.4$ ev (curve *4*), i.e., it is somewhat smaller than the one corresponding to the optimum covering where $(\Delta\varphi)_m = 2.9$ ev[2], i.e., $\varphi_m = 1.6$ ev. The last curve *5* refers to a thick layer of Ba for which it is well known that $\varphi = 2.6$ ev. In Fig. 6 one notices that the character of the curve $R = f(V_p)$ changes sharply with a gradual adsorption of a film of Ba on tungsten even within the limits of a monatomic layer. We see that with a growth of the quantity θ the behavior of the curves deforms gradually within the limits $\theta < 1$, finally assuming the normal character of decreasing R with an increase in V_p. Finally, the curve *5* for a thick layer of Ba has a normal appearance and agrees well with the measurements of Bruining[12],

Together with an investigation of electropositive films Ba-W, we have undertaken an investigation of electronegative films O-W. We used tubes of the second design, which, after all the above-described operations and measurements with clean tungsten, were soldered to a second vacuum system by means of a special side connection. The additional vacuum system was designed to introduce various pure gases at low pressures into the tube. Pure oxygen was let into the tube at a pressure ≈ 10^{-5} mm and the ribbon was carefully heated in its atmosphere at $T \approx 1300°$ K. Oxygen was meanwhile periodically pumped out and the change in the work function was determined by the previously described method. In this manner, as is evident from the two dotted curves *6* and *7* of Fig. 2, the change in the contact potential in the reverse direction was $\Delta V_k = \Delta\varphi = -1.7$ ev, i.e., $\varphi = 6.2$ ev, which is quite close to the limiting value of $\varphi_m = 6.3$ ev[13] quoted in the literature. As this level was reached, the residual gases were pumped out very carefully and all the above described measurements were carried out. The results for the O-W system are given in Fig. 7; for comparison the data for our Ba-W system with $\Delta\varphi = 2.4$ ev are included in dotted lines which (together with Fig. 4 for pure W) give a complete picture of the problem of interest to us. We see that the data for O-W are very similar in character to the data for pure W, differing only by greater value of R and δ, but at the same time entirely different from the data for Ba-W.

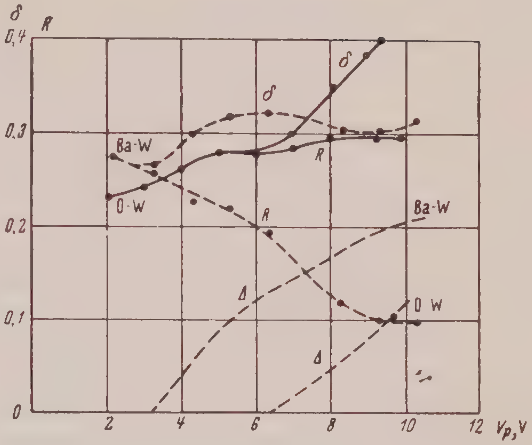

FIG. 7. The dependence of δ and R of the energy of primary electrons for Ba-W and O-W.

As has already been shown above, one of the tasks of our investigstion was the study of the structure of the surface potential barrier for monolayer systems by the method of reflection of slow electrons. In a direct utilization of our experimental data for this purpose one must be careful to a certain extent. First of all, the tungsten surface may have a polycrystalline character and then the work function may vary over its surface and thus both the height of the potential barrier $\Delta\varphi \gtrsim 0.3$ ev and also the nature of the local contact fields will vary from place to place. Secondly, a film on W with $\theta < 1$ may have a somewhat spotty character with the linear dimensions of nonuniformities a probably much greater than wavelength λ_e of the primary electrons probing the surface ($a \gg \lambda_e$). The reflection from the entire surface is then a sum of the reflection effects from the separate elements of the surface—both

System	V_p' in v	φ in ev
W	4—5	4.5
Ag	3—4	4.3
Ba	3—4	2.6
Ba — W	~3	2.1
O — W	~6	6.2

clean and covered by a film[14]. Therefore, it makes sense to compare with theory only the curves *4* and *7* for Ba-W and O-W (see Fig. 2) with a coverage close to optimum, where one can consider the tungsten base to be covered more or less continuously and uniformly. With that goal one should make a theoretical computation of the dependence $R = f(V_p)$ on the basis of well-known methods[15], selecting the appropriate form of the total potential barrier. However, in view of the reasons given above, such work would be somewhat premature at the present time, before our experiments are extended to the reflection from uniform single crystals, which will be our problem in the near future. Still, it should be noted that, for example, the increase of the quantity R with the degree of coverage θ in the region of small V_p observed in Fig. 6 is theoretically quite real since we gradually pass from a potential barrier of continuous hyperbolic shape for clean W to a barrier with more sharply defined wall formed by a superposition on the preceding barrier of a rapid potential change due to the film of Ba atoms adsorbed on W. We ascribe similar reasons to the growth of the quantity R in passage from W to O-W.

The main object of our study was the elastic reflection of electrons which takes place without noticeable losses of energy. Together with this effect one observes on the trapping curves the effect of a second group of emitted electrons with noticeably smaller energies[16] when the energy V_p of the primary electrons exceeds a particular value V_p'. This means that for $V_p > V_p'$ the number of all emitted electrons δ and the number R of elastically reflected ones will increasingly differ, as is shown in Figs. 4 and 7 by the dotted curves for the quantity $\Delta = \delta - R$. The threshold values obtained for the latter curve, i.e., the quantity V_p', and also the work function $\varphi = \varphi_0 - \Delta V_k$ of the various systems considered by us are given in the accompanying Table. It is evident from the Table (thus far only qualitatively, since we did not specifically concern ourselves with this question) that the values of V_p' correlate with the corresponding values of φ which agree with the condition $V_p' + \varphi \approx 2\varphi$. The last fact may be used to a certain extent as an argument that we deal with a threshold of the secondary emission[17] and not with the appearance of inelastic losses, and that therefore the curve $\Delta = f(V_p)$ characterizes a purely secondary emission. However, we cannot prove this fact, since our work is only of a qualitative nature.

---

[1] N. Morgulis, Usp. Fiz. Nauk **53**, 504 (1954).

[2] V. Gavriliuk, Trudy. Inst. Phys., Acad. Sci., USSR 5, 87 (1954).

[3] N. Morgulis, J. Tech. Phys. (U.S.S.R.) **25**, 1667 (1955).

[4] P. Marchuk, Trudy. Inst. Phys., Acad. Sci., USSR **7**, 3 (1956).

[5] N. Morgulis and V. Gavriliuk, J. Exptl. Theoret. Phys. (U.S.S.R.) **30**, 149 (1956); Soviet Phys. JETP **3**, 159 (1956).

[6] D. Alpert, J. Appl. Phys. **24**, 860 (1953); D. Alpert and R. S. Buritz, J. Appl. Phys. **25**, 202 (1954).

[7] N. Morgulis and G. Pikus, Dokl. Akad. Nauk SSSR **102**, 1103 (1955).

[8] J. Becher and C. Hartmann, J. Phys. Chem. **57**, 153 (1953); H. D. Hagstrum, Rev. Sci. Instr. **24**, 1135 (1953).

[9] H. Myers, Proc. Roy. Soc. (London) **A215**, 329 (1952).

[10] C. Herring and M. Nichol, *Thermoelectric emission*, IIL, 1950, p. 91 (Russian translation).

[11] V. Kuznetsov, *Crystals and Crystallization*, GITTL, 1953, p. 365.

[12] H. Bruining, Physica **5**, 913 (1938).

[13] A. L. Reimann, Proc. Roy. Soc. (London) **A163**, 499 (1937).

[14] N. Morgulis and M. Bernadiner, J. Exptl. Theoret. Phys. (U.S.S.R.) **9**, 998 (1939).

[15] L. A. MacColl, Phys. Rev. **56**, 699 (1939); Bell Syst. Techn. J. **30**, 888, (1951).

[16] Iu. Nemilov and E. Fedorova, Collected Papers in Television Techniques **5**, 64 (1951) (in Russian); A. Shul'man and E. Miakinin, Dokl. Akad. Nauk SSSR **91**, 1075 (1953).

[17] N. Morgulis, J. Tech. Phys. (U.S.S.R.) **10**, 1714 (1940).

Translated by M. J. Stevenson
137

SOVIET PHYSICS JETP VOLUME 3, NUMBER 4 NOVEMBER, 1956

Investigation of the Dependence of the Dielectric Constant and the Tangent of the Dielectric Loss Angle of Barium Titanate on the Strength of a High Frequency Electric Field

E. V. SINAKOV AND V. V. GALPERN
Dnepropetrovsk State University

(Submitted to JETP editor July 15, 1955)
J. Exptl. Theoret. Phys. (U.S.S.R.) 30, 675-680 (April, 1956)

A method of measurement of dielectric constants and the tangent of the dielectric loss angle of ferroelectrics in strong high frequency (10^6 cps) fields is described. The results of measurements of the dependence of capacity and the tangent of the dielectric loss angle on the strength of electric field at various temperatures are presented and evaluated for a barium titanate sample.

1. INTRODUCTION

AT the present time the nonlinear properties of ferroelectrics are widely used in various radio installations[1].

To utilize a ferroelectric material in frequency and amplitude modulation equipment as well as in capacitative amplifiers one must know the dependence of the dielectric constant and of the tangent of the dielectric loss angle on the intensity of high frequency electric field. Thus far, the nonlinear properties of ferroelectrics are insufficiently known at high frequencies because of the considerable experimental difficulties encountered in measurements of dielectric constants and the tangent of the dielectric loss angle in strong electric fields of high frequency. These difficulties are caused by the heating of samples due to large dielectric losses. Since ϵ and $\tan\delta$ of ferroelectrics strongly depend on temperature, it is necessary to maintain the temperature of the sample constant during the investigation of their dependence on the strength of the electric field.

Kambe[2] has used the pulse technique to study the hysteresis loops of barium titanate in strong high frequency fields at various temperatures. From the analysis of the hysteresis loops the authors concluded that the maximum polarization decreases with increasing frequency. Only qualitative conclusions are possible in the cited work about the dielectric losses. Zavelskii[3] has also observed a decrease of the dielectric constant with a decrease in the duration of the charging of condenser made of $BaTiO_3$ and an increase of the dielectric constant with an increase in the electric field intensity.

The experimental technique used by Kambe[2] and Zavelskii[3] is not convenient for the measurement of the smooth variation $\epsilon = f(E)$ and $\tan\delta = \varphi(E)$. The investigation of the mentioned dependences at high frequency is important both for the theory

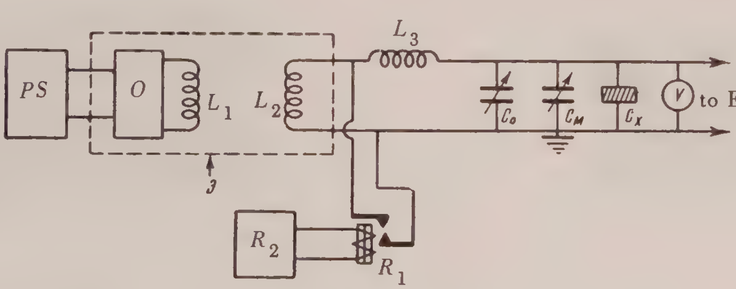

FIG. 1. Block diagram of the experimental apparatus. *PS*-stabilized power supply; *O*-Oscillator; L_1-induction coil of the oscillator; L_2-coupling coil; L_3-induction coil of the measuring circuit; C_0-standard condenser; C_M-modulating condenser; C_x-condenser containing the dielectric under investigation; *V*-vacuum tube voltmeter of the type VKS-7 (used with a voltage divider); R_1-relay; R_2-a system of control relays.

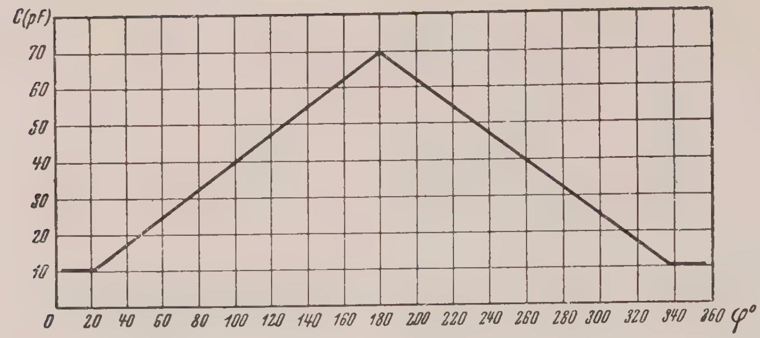

FIG. 2. The dependence of the capacity of the modulating condenser on the angle of rotation of its rotor.

of the ferroelectric phenomena and for its technical utilization. Hence, it is necessary to develop a method of measurement of the continuous dependence of $\epsilon = f(E)$ and $\tan\delta = \varphi(E)$ at high frequency. Such is the purpose of the present work.

EXPERIMENTAL TECHNIQUE

The basis of employed means of determination of ϵ and $\tan\delta$ is the resonance method of varying capacitance in which changes were introduced to permit measurements on ferroelectric samples in strong fields of high frequency. The block diagram of the apparatus is given in Fig. 1.

The special feature of the method employed is a modulation of the natural resonance frequency of the measuring circuit. This was accomplished by means of the modulation capacitor C_M. The axis of the capacitor was attached to the rotor of

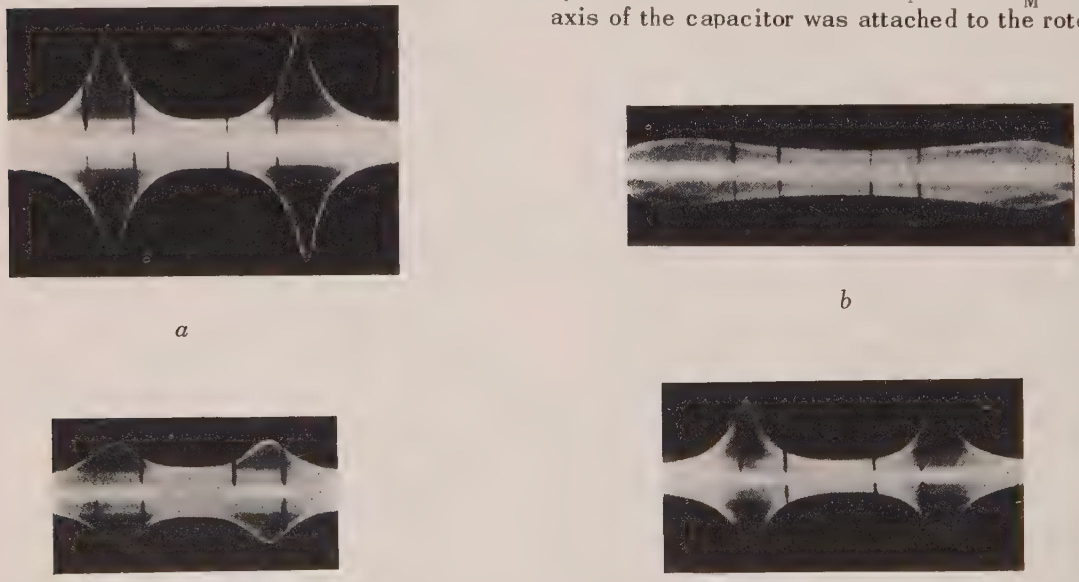

a

b

c

d

FIG. 3. Oscillograms of the resonance curves: a-without a sample; b-for a sample of $BaTiO_3$ ($T = 82°$); c-for a sample of $BaTiO_3$ ($T = 167°$); d-for a KTK type condenser.

an electrical motor rotating with an angular velocity of 1500 rpm. The dependence of the capacity of the modulating condenser on the angle of rotation is given in Fig. 2. At a particular value of the total capacitance a resonance takes place in the measuring circuit, the resonance capacitance occuring twice during the time of a single revolution of the capacitor C_M. Two resonance curves are then presented on the screen of the oscilloscope (Fig. 3). With a change of capacitance in the measuring circuit the separation between the resonance maxima changes. Therefore, it is possible to evaluate the change of capacity of the investigated sample from the separation of the two resonance peaks. The oscilloscope screen is first calibrated by means of a standard condenser C_0.

The tangent of the dielectric loss angle calculated from the formulas of Bogoroditskii[4] and Skanavi[5] is:

$$\tan\delta = \frac{\Delta c}{2}\,\frac{(U - U_x)}{U_x \cdot C_x}, \qquad (1)$$

where U is the resonance intensity in the measuring circuit without a sample, C_x is the capacitance of the sample, U_x is the resonance intensity in the measuring circuit with a sample, Δc the so-called distortion of the contour: $\Delta c = C_0'' - C_0'$ where C_0' and C_0'' are the values of the capactiance in the measuring circuit without a sample corresponding to an intensity $\sqrt{2}$ times smaller than the resonance intensity (taken on both sides of the resonance curve peak).

The values Δc, U and U_x are determined from the resonance curves. For this purpose the oscilloscope screen was calibrated for measurements of intensity by a vacuum tube voltmeter V. The determination of Δc directly from the resonance curve assured a greater accuracy than a measurement of that quantity by variation of the circuit capacity by the condenser C_0.

From the above it follows that for a determination of the dependence $\epsilon = f(E)$ and $\tan\delta = \varphi(E)$ it is necessary to photograph the resonance curves without and with the sample in the circuit at various intensities of the electric field. In order to prevent the heating of the ferroelectric samples due to dielectric losses the voltage was applied to the sample for the period of time $t = 0.1$ sec, during which the photographs were taken. For such a duration of the electric field the sample practically did not heat at all (it is also necessary to take into account that the time of action of the full resonance intensity on the sample is still shorter).

As is evident from the diagram of Fig. 1, the emf induced in the coupling coil L_2 by the oscillator 0 is passed through the measuring circuit only if the relay R_1 is open. The opening of the relay R_1 for the period of time $t = 0.1$ sec was made by a system of control relays R_2.

To stabilize the presentation of the resonance curves on the oscilloscope screen, synchronization by pulses of constant intensity was employed. The pulses were introduced on the external synchronization terminals of the EO-7 oscilloscope from the terminals of a storage battery through contacts that were periodically broken by a cam attached to the axis of the motor driving the modulating condenser.

The analysis of errors has shown that the maximum calculated error in measurements by our apparatus did not exceed 2% for the capacity and

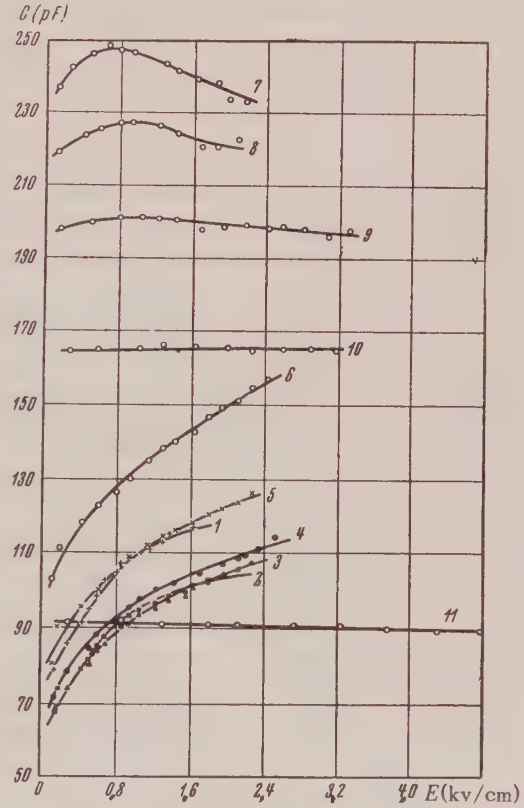

FIG. 4. The dependence of capacity of sample of $BaTiO_3$ on the electric field intensity at high frequency and various temperatures: *1* - $T = 19°$; *2* - $t = 38°$; *3* - $t = 60°$; *4* - $t = 82°$; *5* - $t = 98°$; *6* - $t = 116°$; *7* - $t = 123°$; *8* - $t = 127°$; *9* - $t = 132°$; *10* - $t = 142°$; *11* - $t = 167°$.

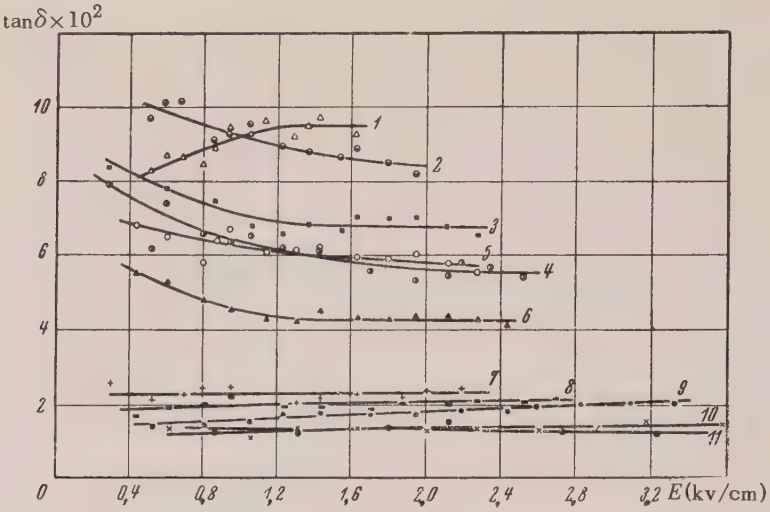

FIG. 5. The dependence of the tangent of the dielectric loss angle of $BaTiO_3$ on the intensity of high frequency electric field for various temperatures: *1* - $t = 19°$; *2* - $t = 38°$; *3* - $t = 60°$; *4* - $t = 82°$; *5* - $t = 98°$; *6* - $t = 116°$; *7* - $t = 123°$; *8* - $t = 127°$; *9* - $t = 132°$; *10* - $t = 142°$; *11* - $t = 167°$.

25% for the tangent of the dielectric loss angle. This is entirely satisfactory for the resonance methods.

EXPERIMENTAL RESULTS AND THEIR EVALUATION

By means of the above discussed method the dependence on the electric field intensity of the capacity and of the tangent of the dielectric loss angle of a sample of polycrystalline $BaTiO_3$ was investigated at a frequency 10^6 cps and at various temperatures (Figs. 4 and 5). On the basis of this data the curves for the temperature dependence of the capacity and of tan δ were prepared for several values of the electric field intensity (Fig. 6). To verify the employed technique further we measured the dependence of $C = f(E)$ and $\tan\delta = \varphi(E)$ for ceramic condensers of the KTK type (Fig. 7).

The results of measurements show that at a high frequency and strong fields one observes a nonlinear dependence $C = f(E)$ characteristic for the ferroelectric region of $BaTiO_3$ and the capacity-temperature curve has a sharply defined maximum.

The temperature dependence of tan δ in strong fields of high frequency is similar to the analogous dependence in weak fields: in the region of a sharp increase of ϵ the value of tan δ sharply decreases. Saturation in the curve $C = f(E)$ was observed for the given field intensities only for temperatures lying in the region of the Curie point, and with an approach to the Curie point the maximum of the curve $C = f(E)$ shifts to the region of the weaker fields.

A comparison of the values of the dielectric constant of $BaTiO_3$ at high frequency and strong fields with the dielectric constant of samples of the same batch measured at frequency 50 cps at the same values of field intensity and temperature shows that the dielectric constant is smaller at high frequency than at 50 cps. From a similar comparison it also follows that the nonlinear properties of barium titanate are less pronounced at high frequencies. As is evident from Fig. 5, the tangent of the dielectric loss angle depends on the electric field intensity weakly at high frequency. The fact that the nonlinear properties of barium titanate manifest themselves most significantly in the region of the Curie point can be explained qualitatively by saying that in the temperature range the rotation of the electrical moments of the spontaneous polarization domains is made easier by the action of an external field. The decrease in the value of the dielectric constant and weaker manifestation of the nonlinear properties at a high frequency in comparison with the corresponding data for a frequency of 50 cps are apparently due to the fact that at a high frequency the duration of the action of the electric field within one half period decrease relative to the time needed

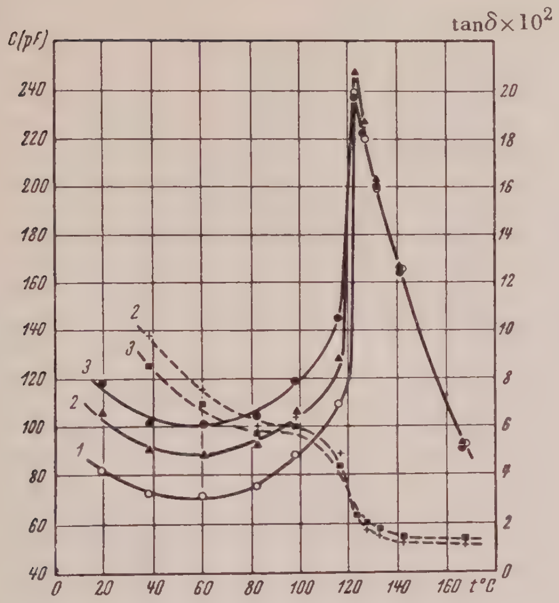

FIG. 6. The dependence of the capacity (solid curves) and tanδ (dotted curves) of $BaTiO_3$ sample on temperature at high frequency and for various field intensities: *1* - $E = 0.2$; *2* - $E = 0.8$; *3* - $E = 1.7$ kv/cm.

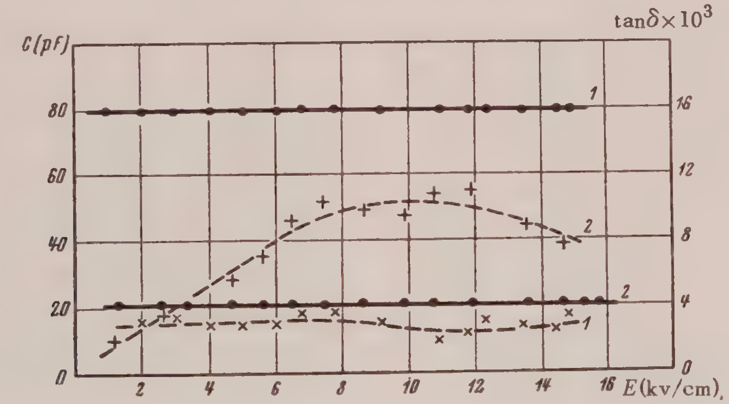

FIG. 7. The dependence of capacity (solid curves) and tanδ (dotted curves) of ceramic condensers on field strength of high frequency: *1* - KTK, orange, 82 ± 10% *μμf*; *2* - KTK, red, 20 ±5% *μμf*.

to establish polarization. (This is in the nature of polarization determined by rotation of the domain moments.)

CONCLUSIONS

In the studied range of electric field intensities:

1. The nonlinear properties of barium titanate are less pronounced at a high frequency (10^6 cps) than at a low frequency (50 cps).

2. The most significant nonlinear properties of barium titanate at high frequency take place in the temperature range close to the Curie point.

3. The tangent of the dielectric loss angle of barium titanate at high frequency depends weakly on the intensity of the electrical field.

---

[1] D. M. Kazarnovskii, Elektrichestvo 2, 40 (1954).

[2] Kambe, Nakada and Takahasi, J. Phys. Soc. Jap. 8, 9 (1953).

[3] F. S. Zavelskii, J. Exptl. Theoret. Phys. (U.S.S.R) 25, 479 (1953).

[4] N. P. Bogoroditskii, V. V. Pasynkov and B. N. Tareev, *Electrotechnical Materials*, Gosenergoizdat, 1950.

[5] G. I. Skanavi, *Dielectric polarization and losses in glasses and ceramic materials with a high dielectric constant*, Gosenergoizdat, 1952.

Translated by M. J. Stevenson
138

SOVIET PHYSICS JETP VOLUME 3, NUMBER 4 NOVEMBER, 1956

Scattering of 250 mev Photons by Free Electrons

L. V. KURNOSOVA, L. A. RAZORIONOV AND P. A. CHERENKOV
P. N. Lebedev Physical Institute, Academy of Sciences, USSR

(Submitted to JETP editor, June 29, 1955)
J. Exptl. Theoret. Phys. (U.S.S.R.) 30, 690-694 (April, 1956)

The paper reports measurements of the ratio of the scattering cross section for photons of 250 mev by free electrons in a Be target to the pair production cross section. The apparatus counted the recoil electrons and the pair electrons and positrons in the energy intervals 235-247 and 222-233 mev.

The observed ratios agree within the accuracy of the experiment with those deduced from the Bethe-Heitler formula for pair production and the Klein-Nishina-Tamm theory for Compton scattering.

IT is well known that the Klein-Nishina-Tamm formula for the differential cross section for the scattering of photons by free electrons has been verified by numerous experiments[1] in the region of incident photon energies up to 20 mev, with an accuracy of about 10%. Recently, measurements of the total cross section of Compton scattering at energies of the order of hundreds of mev have also been reported.[2] In the present paper we report on measurements of the Compton cross section using the photon beam of the 250 mev synchrotron, selecting particularly those scattering events in which the photon gave up nearly the whole of its energy to the recoil electron.

The pair electrons and positrons, as well as the Compton electrons emitted by the Be target passed through an analyzing magnet. The apparatus registered simultaneously the number of positrons, $N_+=N_\mathrm{P}$, and the total number of electrons (from pairs and recoil) $N_-=N_\mathrm{P}+N_\mathrm{C}$. The number of recoil electrons was then determined as the difference $N_\mathrm{C}=N_- - N_+$. The ratio of this number to the number of pairs (i.e., the number of observed positrons) was compared with the theoretical value calculated from the formulas for pair creation and Compton scattering. The apparatus used for this experiment (Fig. 1) consisted of a collimator, cleaning magnets, the target, the analyzing magnet, and the counting devices.

The beam from the synchrotron was collimated by means of a lead block of 15 cm thickness, with an aperture of 5 mm diameter. The collimator was placed at a distance of 13 meters from the synchrotron. The measuring instruments were placed in a separate room, which was separated from the synchrotron by a 1.5 meter concrete wall. The whole passage of the beam from the collimator to the target was enclosed in a vacuum chamber. On entering the vacuum chamber the beam passed for 40 cm through a cleaning magnetic field of 7000 oersteds. This field removed all charged particles created in the beam on the way to the collimator and within the collimator. However, photons scattered in the collimator walls and traveling at an angle to the axis of the beam could also produce charged particles in the walls of the vacuum chamber, which could be recorded. For this reason a second cleaning field, of strength 3000 oersteds and 10 cm length was provided near the exit of the vacuum chamber.

The field of the analyzing magnet used in the apparatus had axial symmetry. The strength of the field could be varied over a wide range; in the center it could reach 13,200 oersteds over an aperture of 10 cm.

Electrons and positrons of high energy, traveling nearly in the direction of the beam, were deflected in such a way that on leaving the field they were moving along a straight line through the center of the magnet forming an angle α with the beam direction. This angle α depends on the strength and shape of the magnetic field, and the particle energy. From the knowledge of the variation of the field intensity with the distance from the axis one can calculate the orbit of an electron of given energy, and hence the final deflection α. Figure 2 shows the variation of this angle with the electron energy.

The electrons and positrons emitted by the target and deflected appropriately by the magnet were recorded in a counter telescope using twofold coincidences.

In the course of the measurements the field of the analyzing magnet was reversed systematically, so that each measurement was carried out with the field in both directions. This eliminated any inaccuracy in the alignment of the counter telescopes with the axis of the magnet and also any individual variation between the counters or the counting channels. The telescopes were placed in such a way as to count electrons and positrons of a high energy close to the maximum energy of the beam. In this way one therefore measures not the integral cross section, but the partial cross section for the production of a recoil electron with an energy in a fixed interval. Such a cross section,

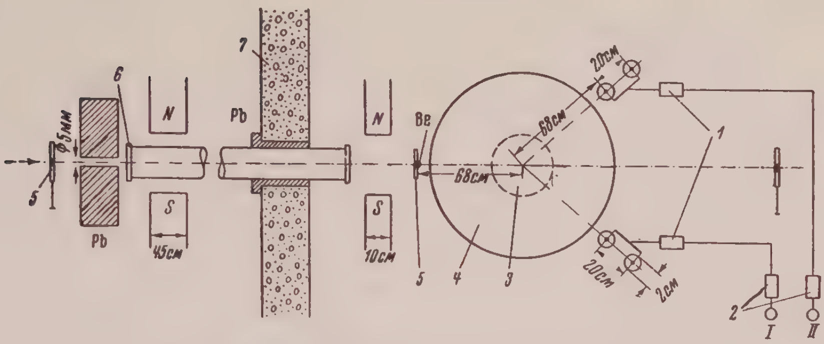

FIG. 1. Sketch of apparatus: *1*-coincidence selectors, *2*-output scalers, *3*-pole pieces, *4*-magnet coil, *5*-X-ray films, *6*-thin transparent window, *7*-concrete wall of 1.5 meters.

in contrast to the total cross section which includes all final energies, will be called "semi-integral".

For a very small energy interval this "semi-integral" cross section goes over into the differential cross section. If we allow for the inhomogeneity of the incident photon beam, characterized by a function $f(\gamma)$ (where γ is the photon energy in units of mc^2) the measured cross section can therefore be expressed by the relation

$$\int_{\gamma_{20}}^{\gamma_{21}} \int_{\gamma_2+0.5}^{\gamma_{\max}} f(\gamma)\, \sigma_C\, d\gamma_2\, d\gamma = \sigma_C^*,$$

where the upper limit of integration with respect to γ is the maximum energy of the photons in the incident spectrum, σ_C the differential cross section, γ_2 the energy of the recoil electron, and γ_{20} and γ_{21} the limits of the energy interval selected by the apparatus.

The "semi-integral" cross section for pair electrons can be expressed similarly:

$$\int_{\gamma_{20}}^{\gamma_{21}} \int_{\gamma_2+1}^{\gamma_{\max}} f(\gamma)\, \sigma_p\, d\gamma_2\, d\gamma = \sigma_p^*,$$

where σ_P is the differential cross section for pair creation, γ_2 the energy of the electron (or positron) in the pair, and γ_{20} and γ_{21} have the same meaning as before.

The determination of the absolute value of this "semi-integral" cross section meets with difficulties which arise from the fact that both the number of incident photons and their spectrum are not sufficiently accurately known. We therefore chose to determine the ratio of the "semi-integral" cross section for Compton scattering to the "semi-integral" cross section for pair creation. This method is particularly effective if both the observed recoil electron and one of the pair electrons has an energy very close to the maximum energy of the incident photons. At high photon energies the total cross section for Compton scattering is much less than the cross section for pair creation. The

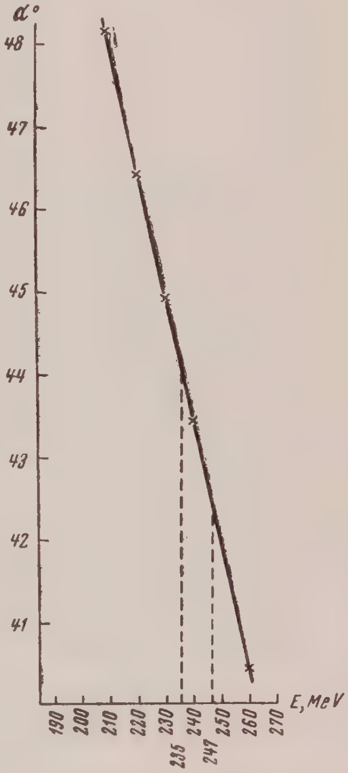

FIG. 2. Variation of the angle of deflection for particles in the magnetic field with energy.

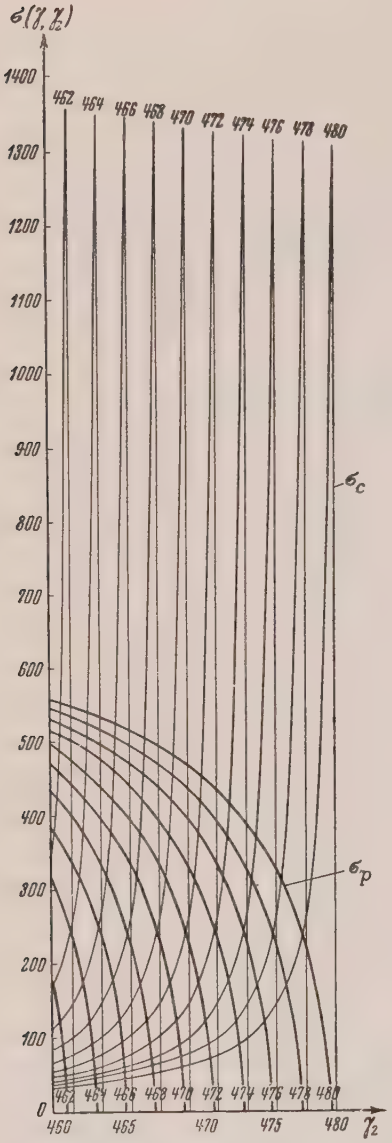

FIG. 3. Variation of the differential cross section σ_C for Compton scattering, and σ_P for pair creation with electron energy, for different values of the incident photon energy γ. The values of γ are indicated on the curves. The unit for the cross sections is 0.78×10^{-30} cm^2.

differential cross sections of the two processes are of the same order when the energy γ_2 of the observed electron or positron lies in a certain interval close to the energy of the incident photon. (Cf. Fig. 3). This fact makes it possible to obtain the number of recoil electrons by subtraction from the total number of electrons with energies close to the energy of the incident photons.

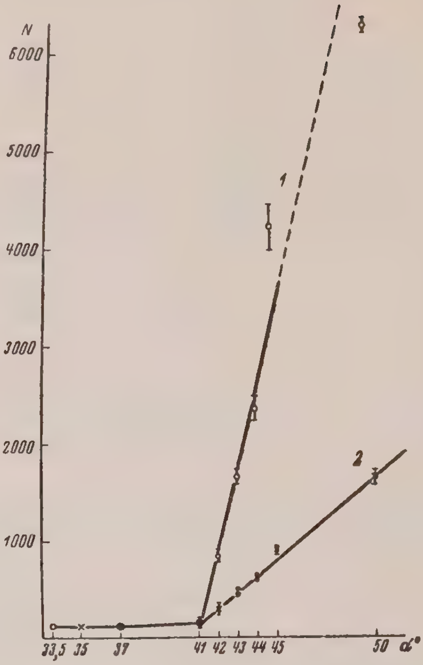

FIG. 4. Counting rate of electron telescope against angle of deflection in the magnetic field. Curve 1-with, Curve 2-without beryllium target.

One of the main factors in setting up the cross section measurements was the accurate placing of the telescopes in space, and their adjustment for the selected electron and positron energy. If the target is removed from the photon beam, then ideally the counter should not record any particles at any angle. In practice, some charged particles are always produced in the air near the beam, and some scattered photons will create charged particles in parts of the apparatus; in addition, the beam may still contain some charged particles which have got through the cleaning fields. Therefore there will be a certain counting rate in the absence of a target. This background count of charged particles was always determined and subtracted. When the target was placed in the beam, the counting rate increased by a large factor. Figure 4 shows the counting rate N_- of the counter telescope as a function of the angle α, the deflection of the electrons in the magnetic field. The electrons and positrons of the maximum energy were deflected by a certain angle α_{max}. At telescope angles less than α_{max}, the counting rate diminished sharply. The break in the curve for the counting rate determines the maximum energy of the electrons and positrons, and hence also the maximum energy of the photons in the beam. The maximum photon energy in the beam was found by this method to lie between 249 and 254 mev, which agrees with the nominal value (250 mev) of the maximum energy of the photons from the synchrotron.

In order to check the performance of the apparatus, the ratio of the cross sections for pair creation and Compton scattering was measured for different target materials. The results obtained for targets of elements with low Z agree with the Z dependence of this ratio calculated from the Bethe-Heitler formula for pair creation. For high Z , when the Bethe-Heitler formula is not applicable, one has to use for the pair creation cross section formulas obtained in references,[3,4] and to allow for the fact that the pair occurrenceof an electron or a positron of given energy has different probability.

For the calculation of the ratio of the ''semi-integral'' cross sections for Compton scattering and pair creation from the theoretical formulas it turned out to be important to know the spectrum of the incident photons. The magnitude of this ratio is, however, not very sensitive to the shape of the spectrum (different calculations of the ratio for a Schiff spectrum and a $1/\gamma$ spectrum differed only by about 20%). In our case, when the synchrotron pulse is spread out in time, the spectrum is in the neighborhood of the maximum, in good approximation proportional to $1/\gamma$, as can be seen from the measured numbers of positrons in the intervals 222-233 and 235-247 mev.

Calculations of the required ratio between the cross sections for a spectrum of this form gave for the energy intervals 235-247 and 222-233, to which the measurements relate, the values 2.01 and 0.85, respectively.

The results of the measurements of the ratio between the ''semi-integral'' cross sections for the intervals 235-247 and 222-233 mev are 1.84 ±0.18 and 0.71 ±0.08, respectively. Thus we find a good agreement between the calculated and measured ratios of the ''semi-integral'' cross sections for Compton scattering and pair creation.

Since the validity of the formula for the pair production cross section (for low Z) in the energy region of 200 to 300 mev has been established experimentally,[5] our results may be taken as confirming the validity of the Klein-Nishina-Tamm formula at incident photon energies of 220 to 250 mev.*

The authors express their gratitude to D. B. Skobel'tsyn, V. I. Veksler, V. L. Ginsburg, N. A. Dobrotin, M. A. Markov, M. I. Podgoretskii, and V. I. Gol'danskii for taking part in the discussions on this work, and to M. I. Fradkin, N. S. Il'ina and B. D. Kuz'minov, who took part in the measurements.

---

*In a short communication[6], measurements of the cross section for Compton scattering with photons of 250 mev have been reported. The results of these measurements are also in agreement with the theoretical formula for the scattering of photons by free electrons.

[1] D. V. Skobel' tsyn, Comptes rendus (Paris) 194, 1914, (1932); Nature, 123, 411 (1929); Z. Physik 65, 773 (1930). L. A. Delsasso,W. A. Fowler and C. C. Lauritsen, Phys. Rev. 51, 391 (1937). W. G. Cross and N. F. Ramsey, Phys. Rev. 80, 929, (1950).

[2] J. L. Lawson, Phys. Rev. 75, 433 (1949); J. W. DeWire, A. Ashkin and L. Beach, Phys. Rev. 83, 505 (1951).

[3] H. A. Bethe snd L. C. Maximon, Phys. Rev. 93, 768 (1954).

[4] H. Davies, H. A. Bethe and L. C. Maximon, Phys. Rev. 93, 788 (1954).

[5] C. R. Emigh, Phys. Rev. 86, 1028 (1952).

[6] F. H. Coensgen, Phys. Rev. 93, 948 (1954).

Translated by R. Peierls
141

SOVIET PHYSICS JETP VOLUME 3, NUMBER 4 NOVEMBER, 1956

Application of Singular Integral Equation Theory to Problems of the Scattering of Particles in an External Field*

N. P. KLEPIKOV

Institute of Nuclear Problems, Academy of Sciences, USSR

(Submitted to JETP editor December 18, 1954)
J. Exptl. Theoret. Phys. (U.S.S.R.) 30, 701-706 (April, 1956)

The possible application of singular integral equation theory to the calculation of the scattering phases of particles in an external field is given. The case of scattering by a δ-potential is considered as an example.

IT has been shown in a series of cases relating the scattering of particles in an external field, for example, the scattering of electrons by heavy nuclei, that, on the one hand, the Born approximation for the external field is quite inadequate, and on the other hand, radiation corrections do not yet exist. For phase calculations in this case, one must use numerical integration of the differential equation for the wave function of the scattered particles. However, determination of the phases by this method requires a great deal of work on very accurate calculation of the wave functions for a considerable distance from the scatterer, and the computation must be repeated for each value of the momentum and energy of the particles. Much simpler calculations are obtained by application of the method of Drukarev[1], where an auxiliary function approaches the phase monotonically. However, even in this case, the calculation must be repeated for each value of the energy and momentum. It is therefore desirable to point out a method in which the amplitude (or phase) of the scattering would be found without calculation of the auxiliary function, and would be found for a considerable energy interval at one stroke.

Such a possibility is presented in a series of cases in the use of integral equations of scattering investigated by several authors[2-4]. For direct derivation of the integral equation of scattering, we consider the equation for the S matrix under the condition that the interaction is initiated at $t = 0$:

$$i\partial S(t)/\partial t = H(t)\,S(t) + i\delta(t), \qquad (1)$$

where $H(t) = \exp(iH_0t)\,H\exp(-iH_0t)$ is the interaction operator in the interaction representation (if the energy spectrum of all states is continuous, then we can take the initial time at $t=-\infty$ and omit $\delta(t)$ in the equation). Having in view those problems in which there are only diverging waves in the final state, we shall look for the solution in the form

$$S(t) = \frac{i}{2\pi}\int_{-\infty}^{\infty} e^{-i(E-H_0)t} \times [1 + \xi(E-H_0)\,U(E)]\,\frac{dE}{E-H_0+(i/2)\,\Gamma(E)}, \qquad (2)$$

where $\Gamma(E)$ is a diagonal operator and $U(E)$ is nondiagonal, and

$$\xi(x) = \frac{1}{i}\int_0^{\infty} e^{itx}\,dt = \frac{P}{x} - \pi i\delta(x) = -2\pi i\delta_+(x) \qquad (3)$$

(P = principal value). Here $x\xi(x) = 1$ and

$$-\frac{1}{2\pi i}\int_{-\infty}^{\infty} e^{itx}\xi(x)\,dx = \eta(t) = \begin{cases}1, & t>0,\\ 0, & t<0.\end{cases} \qquad (4)$$

With the aid of Eq. (4), we can put Eq. (2) in the form

$$S(t)=\eta(t)-\frac{1}{2\pi i}\int_{-\infty}^{\infty} e^{-i(E-H_0)t}\,\xi(E-H_0) \times \left[U(E)-\frac{i}{2}\Gamma(E)\right]\frac{de}{E-H_0+(i/2)\,\Gamma(E)}\,. \qquad (5)$$

We substitute Eq. (5) on the left hand side of Eq. (1) and Eq. (2) on the right. Then

$$-\frac{1}{2\pi i}\int_{-\infty}^{\infty} e^{-i(E-H_0)t} \times \left[U(E)-\frac{i}{2}\Gamma(E)-H-H\xi(E-H_0)\,U(E)\right] \times \frac{dE}{E-H_0+(i/2)\,\Gamma(E)} = 0 \qquad (6)$$

for arbitrary $t > 0$, whence

$$U-(i/2)\,\Gamma-H-H\xi U=0. \qquad (7)$$

The diagonal terms give

$$\Gamma = 2i\,(H+H\xi U)_d, \qquad (8)$$

and the nondiagonal terms,

---

* This paper is an account of researches carried out by the author in 1953 and 1954 and written up earlier in the Reports of the Institute of Nuclear Problems of the Academy of Sciences, USSR.

$$U = (H + H\xi U)_{n,d}\,. \tag{9}$$

The probability of transition from state i to state f in this case is

$$W_{fi} = |\,S_{fi}(\infty)\,|^2 \tag{10}$$

$$= \frac{|\,\dot{U}_{fi}(E_f)\,|^2}{\{E_f - E_i - {}^1/_2\,\mathrm{Im}\Gamma_{ii}(E_f)\}^2 + \{{}^1/_2\,\mathrm{Re}\,\Gamma_{ii}(E_f)\}^2}\,.$$

Equation (9) serves as a fundamental equation for finding the operator U. As is shown in Ref. 3, it has the operator solution

$$U = \frac{1}{1 - H\xi}\left\{H - \left[\left(\frac{1}{1 - H\xi}\right)_d\right]^{-1}\left(\frac{1}{1 - H\xi}H\right)_d\right\}, \tag{11}$$

wherein $Re\Gamma(E) = 2\pi[U^+(E)\delta(E - H_0)U(E)]_d$. In the transition to a continuous spectrum $\Gamma \to 0$, we get the simplification:

$$U = H + H\xi U, \tag{12}$$

$$U = (1 - H\xi)^{-1}H. \tag{13}$$

In this case, the transition probability per unit time is

$$W = \sum_f \lim_{t\to\infty}\frac{\partial}{\partial t}|\,S_{fi}(t)\,|^2 \tag{14}$$

$$= 2\pi\sum_f \delta(E_f - E_i)\,|\,U_{fi}(E_f)\,|^2.$$

Carrying out a formal expansion of Eqs. (11) and (13) in powers of H, we can show the complete identity of the solution (2) of Eq. (1) with the usual solutions in the form of series. It was shown in Ref. 3 that $S(t) = 0$ for $t < 0$ and $\lim\limits_{t\to 0+0} S(t) = 1$, whence the unitary character of $S(t)$ follows for arbitrary $t > 0$.

Computing the matrix elements of the operators on the right and left sides of Eq. (12), we find

$$U_{fi} = H_{fi} + H_{ff'}\,\xi(E - E_{f'})\,U_{f'i}, \tag{15}$$

where the summation over f' is carried out over all states whose wave functions form a complete set of functions of the operator H_0 and of operators that associated with it in obtaining a complete set of operators.

Since, according to Eq. (3), the integral in Eq. (15) enters in the sense of a principal value, this equation is a linear singular integral equation. The theory of such equations was worked out by Muskhelishvili and his coworkers[5,6].

We consider the scattering of the particle without spin on a central field, where $H(\mathbf{r}) = (g^2/r_0)\,\Phi(r/r_0)$. We represent the solution of Eq. (15) in the form

$$U(E,\theta) \tag{16}$$

$$= \frac{4\pi g^2 r_0^2}{L^3}\,\frac{1}{x\sqrt{x^2 - 1}}\sum_{l=0}^{\infty}\frac{2l+1}{2}P_l(\cos\theta)\,\psi_l(x),$$

where $x = E/mc^2$, and decompose the matrix element H_{if} in Legendre polynomials. Then we get the following equations:

$$\psi_l(x)\frac{1}{x\sqrt{x^2 - 1}} = f_l(x,x) + \lambda\int_1^{\infty}\psi_l(y) \tag{17}$$

$$\times\left\{\frac{1}{x - y} - \pi i\delta(x - y)\right\}f_l(x,y)\,dy,$$

$$f_l(x,y) = \frac{1}{r_0 k_0}[(x^2 - 1)(y^2 - 1)]^{-1/4} \tag{18}$$

$$\times\int_0^{\infty}J_{l+1/2}(k_0 r_0\rho\sqrt{x^2 - 1})\,J_{l+1/2}$$

$$\times\;(k_0 r_0\rho\sqrt{y^2 - 1})\,\Phi(\rho)\,\rho\,d\rho,$$

where $\lambda = (g^2/\hbar c)(r_0 k_0)^2$ $(k_0 = mc/\hbar)$, and $J_{l+1/2}$ is a Bessel function.

If the solution of this equation is known, then, from a comparison of Eqs. (16) and (14) with the formulas of the general theory of scattering, we obtain

$$f(\theta) = \frac{\lambda}{k_0\sqrt{x^2 - 1}}\sum_{l=0}^{\infty}(2l + 1)P_l(\cos\theta)\,\psi_l(x), \tag{19}$$

$$\sigma = \frac{4\pi}{k_0^2}\,\frac{\lambda^2}{x^2 - 1}\sum_{l=0}^{\infty}(2l + 1)\,|\,\psi_l(x)\,|^2. \tag{20}$$

Comparison of Eq. (19) with the expression $f(\theta)$ through the phase of the scattering gives

$$\delta_l = \frac{1}{2}\,\mathrm{arctg}\,\frac{2\lambda\,\mathrm{Re}\,\psi_l}{\sqrt{1 - (2\lambda\,\mathrm{Re}\,\psi_l)^2}}, \tag{21}$$

where use is made of the relation

$$\mathrm{Im}\,\psi_l(x) = \lambda\,|\,\psi_l(x)\,|^2, \tag{22}$$

which follows from the unitary nature of the S matrix, and which guarantees the real nature of the phases and satisfaction of the equation

$$\sigma = (4\pi/k_0)(x^2 - 1)^{-1/2}\,\mathrm{Im}\,f(0). \tag{23}$$

In the more general case, Eq. (15) separates into individual equations which correspond to definite values of the total moment and total isotopic spin, or also to their projections (depending on the type of interaction).

As an example of the application of singular integral equation theory, let us consider the scattering of a particle without spin on a point potential. Let $H(\mathbf{r}) = g^2 r_0{}^2 \delta(\mathbf{r})$. Then $f_l(x,y) = g^2 r_0{}^2 L^{-3} \delta_{l0}$ and, in terms of the variables

$$x = \frac{E}{mc^2}, \qquad U(x) = \frac{\varphi(x)}{x\sqrt{x^2-1}} \, \frac{g^2 r_0^2}{L^3}$$

Eq. (17) takes the form ($l = 0$)

$$\frac{\varphi(x)}{x\sqrt{x^2-1}} - \lambda \int_1^\infty \left(\frac{1}{x-y} - \pi i \delta(x-y)\right) \varphi(y)\, dy = l, \tag{24}$$

where $\lambda = (1/2\pi^2)(g^2/\hbar c)(k_0 r_0)^2$. For the limiting case $m = 0$, we get (for $x = (E/g^2) r_0$)

$$\varphi(x) \frac{1}{x^2} - \lambda \int_0^\infty \left(\frac{1}{x-y} - \pi i \delta(x-y)\right) \varphi(y)\, dy = 1, \tag{25}$$

where $\lambda = (1/2\pi^2)(g^2/\hbar c)^3$.

Equations (24) and (25) belong to a type of equation considered in Ref. 5:

$$A(z)\varphi(z) + \frac{1}{\pi i} \int_L \frac{K(z,\zeta)\varphi(\zeta)\, d\zeta}{\zeta - z} = f(z), \tag{26}$$

where $K(z, e)$ does not become zero or infinite for $z = e$, L is a certain line in the complex plane e and z lies on this line. It was shown in Ref. 5 that the solution of the equation

$$A(x)\varphi(x) + \frac{B(x)}{\pi i} \int_L \frac{\varphi(y)}{y-x}\, dy = f(x), \tag{27}$$

if $A(x) \pm B(x) \neq 0$ on the line L, has the form

$$\varphi(x) = \frac{A(x)}{A^2(x) - B^2(x)} - \frac{1}{\pi i} \frac{B(x)}{A^2(x) - B^2(x)} \int_L \frac{f(t)\, dt}{t-x} \frac{Z(x)}{Z(t)}, \tag{28}$$

$$Z(x) = \sqrt{A^2(x) - B^2(x)} \times \exp\left\{\frac{1}{2\pi i} \int_L \frac{d\tau}{\tau - x} \ln \frac{A(\tau) - B(\tau)}{A(\tau) + B(\tau)}\right\}. \tag{29}$$

In accordance with this theory, the solution of Eq. (24) has the form

$$\frac{\varphi(x)}{x\sqrt{x^2-1}} = \frac{1 + \pi i \lambda x \sqrt{x^2-1}}{1 + 2\pi i \lambda x \sqrt{x^2-1}} - \frac{\lambda}{(1 + 2\pi i \lambda x \sqrt{x^2-1})^{1/2}} \times \int_1^\infty \frac{t\sqrt{t^2-1}\, dt}{(t-x)(1 + 2\pi i \lambda t \sqrt{t^2-1})^{1/2}} \times \exp\left\{\frac{t-x}{2\pi i} \int_1^\infty \frac{\ln(1 + 2\pi i \lambda \tau \sqrt{\tau^2-1})}{(\tau - x)(\tau - t)}\, d\tau\right\}, \tag{30}$$

and the solution of Eq. (25) is given in the form $\varphi(x) = x^2 f(\pi\lambda x^2)$, where

$$f(z) = \frac{1 + iz}{1 + 2iz} - \frac{iz}{\sqrt{1 + 2iz}} \times \exp\left\{-\frac{1}{2\pi i} \int_0^\infty \frac{\ln(1 + 2iz\tau^2)}{\tau(\tau - 1)}\, d\tau\right\} \times \frac{1}{\pi i} \int_0^\infty \frac{t^2\, dt}{(t-1)\sqrt{1 + 2izt^2}} \times \exp\left\{\frac{1}{2\pi i} \int_0^\infty \frac{\ln(1 + 2izt^2\tau^2)}{\tau(\tau - 1)}\, d\tau\right\}. \tag{31}$$

For our case, when the interval of integration is infinite, the solutions of the two possible classes (with indices 0 and –1) coincide, and all the solutions of the homogeneous equation are equal to zero.

It is easy to show that the convergence in Eqs. (30) and (31) is uniform, and is determined only by the presence of the integral in the exponent. Therefore it is appropriate to consider the integrals in Eq. (31) and show that they converge. It is easy to show that

$$F(2zt^2) \equiv \frac{1}{2\pi i} \int_0^\infty \frac{\ln(1 + 2izt^2\tau^2)}{\tau(\tau - 1)}\, d\tau = -\frac{\pi}{4} \frac{1}{2\pi i} \times \int_{-1/2 - i\infty}^{-1/3 + i\infty} \frac{ds}{s} \frac{\operatorname{ctg} \pi s}{(2zt^2)^{s/2}} \left(\sec \frac{\pi}{4} s + i \operatorname{cosec} \frac{\pi}{4} s\right). \tag{32}$$

Completing, for $z > 0$, $2zt^2 > 1$, the contour on the right, and carrying out the calculation only for

$s = 0$, we obtain the asymptotic expression for $F(2zt^2)$ as $t \to \infty$:

$$F(2zt^2) \sim -\frac{1}{4} \ln t \sqrt{2z} + i\left(\frac{1}{2\pi} \ln^2 t \sqrt{2z} - \frac{31}{96}\pi\right). \tag{33}$$

Then the outer integral in Eq. (31) converges for $z > 0$, since the integral

$$\int_1^\infty \exp\left\{-\frac{1}{4}\ln x + \frac{i}{2\pi}\ln^2 x\right\} dx = \pi \sqrt{\frac{i}{2}}\, e^{9\pi i/32}\left(1 - \Phi\left(\frac{3}{8}\sqrt{2\pi i}\right)\right), \tag{34}$$

converges. Here $\Phi(x) = 2\pi^{-1/2}\int_0^x e^{-t^2}dt$. For this reason, the solutions (30) and (31) of Eqs. (24) and (25) exist, though they cannot be expanded in powers of $g^2/\hbar c$. This is particularly clear in the example (31), since Eq. (31) depends only on the product $\pi\lambda x^2$, and cannot be decomposed into powers of this quantity without disrupting the convergence of the integral. This coincides with the fact that the integral in (31), in correspondence with (33), is proportional to $z^{-1/2} \sim (g^2/\hbar c)^{-3/2}$ and is not analytic in g^2/hc as $g^2/hc \to 0$. Furthermore, this also agrees with the result of the application of perturbation theory where, for the case $m \neq 0$,

$$U(x) = \frac{g^2 r_0^2}{L^3}\left\{1 + \lambda\int_1^\infty \left[\frac{1}{x-y} - \pi i\delta(x-y)\right] \times y\sqrt{y^2-1}dy + \lambda^2\int_1^\infty \left[\frac{1}{x-y} - \pi i\delta(x-y)\right] \times y\sqrt{y^2-1}dy \int_1^\infty \left[\frac{1}{y-t} - \pi i\delta(y-t)\right] \times t\sqrt{t^2-1}dt + \dots\right\} \tag{35}$$

and all the integrals diverge.

It is easy to see that the Fredholm theory of scattering gives the same result as perturbation theory. Hence, it is also inapplicable to such a singular potential as the δ-potential. Thus the theory of the solution of singular integral equations according to Muskhelishvili makes it possible to obtain solutions without decomposition in the coupling parameter, which is especially important when this solution is not expanded in such a series (but this, according to the Fredholm theory, always takes place when the potential is sufficiently singular at zero, and consequently its Fourier components diminish too slowly with an increase in energy).

In the case of a more complicated potential, the singular equations will not achieve as clear a description of the solution, as in the case considered, but, with the help of the operation of regularization reported in Ref. 5, these equations can be converted into Fredholm equations with regular kernels which can, in turn, be solved numerically.

For quantized fields there arise infinite sets of equations of the type (15). In this case, on the one hand, it is fundamental to assume as fruitful the application of the theory of systems of singular integral equations to obtain solutions without decomposition in powers of the coupling parameter but, on the other hand, the mathematics for infinite systems is still insufficiently worked out to draw more fundamental conclusions.

---

[1] G. F. Drukarev, J. Exptl. Theoret .Phys. (U.S.S.R.) 19, 247 (1949).

[2] W. Heitler and S. T. Ma, Proc. Roy. Irish Acad. 52, 109 (1949).

[3] E. Arnous and S. Zienau, Helv. Phys. Acta **24**, 279 (1951).

[4] B. A. Lippman and J. Schwinger, Phys. Rev. **79**, 469 (1950).

[5] N. I. Muskhelishvili, *Singular integral equations*, Moscow, 1947, Ch. 4.

[6] N. P. Vekua, *Systems of singular integral equations*, Moscow, 1950.

[7] A. Salam and P. T. Matthews, Phys. Rev. **90**, 690 (1953).

[8] J. Hamilton, Phys. Rev. **91**, 1524 (1953).

Translated by R. T. Beyer
143

SOVIET PHYSICS JETP VOLUME 3, NUMBER 4 NOVEMBER, 1956

On the Singularity of the Electromagnetic Potential in the Higher Approximations of Perturbation Theory

IU. M. LOMSADZE
P. N. Lebedev Physical Institute, Academy of Sciences, USSR

(Submitted to JETP editor June 14, 1954)
J. Exptl. Theoret. Phys. (U.S.S.R.) 30, 707-712 (April, 1956)

It is shown that the singularity at the origin in the potential of the electromagnetic interaction of two electrons (or of an electron with a positron), taken in any, arbitrarily high, approximation of perturbation theory, involving the nth power of the charge, is not of higher order than $(1/r)\ \ln^{(n-2)/2}r$.

IT is known that the potential of the electromagnetic interaction* of two spinor particles in the second approximation of perturbation theory behaves like $1/r$ (r is the three-dimensional distance between the particles) at the origin, which theoretically allows the possibility of bound stationary states of a system of two oppositely charged particles, as actually observed in nature (for example, the hydrogen atom, and also the recently discovered positronium). The question naturally arises as to the character of the singularity at the origin in the potential in higher approximations of the theory.

Calculations with nonrelativistic quantum electrodynamics give a strengthening of the singularity in the potential (to $1/r^3$) in the fourth approximation. Such a strong singularity of the potential is brought about, for example, by the term $e^2[A_\mu^2(\mathbf{x}_1) + A_\mu^2(\mathbf{x}_2)]$, which appears on the introduction of the electromagnetic field into the Schröedinger equation for two particles ($\mathbf{x}_1$ and $\mathbf{x}_2$ are the space coordinates of the particles). Calculations with relativistic nonquantum theory[1] give an analogous strengthening (to $1/r^3$) of the singularity of the potential in fourth approximation.

With regard to relativistic quantum electrodynamics, here, because of the well-known fundamental difficulties with infinities, up until recent years it has not appeared possible, without violating the consistency of the theory, to obtain the potential in an approximation higher than the first nonvanishing one (i.e., the second), and the question of the singularity of the potential in higher approximations has remained open. At the present time, owing to the appearance of consistent methods for the removal of infinities, relativistic quantum electrodynamics can to a certain extent be regarded as a completed, consistent theory, and the answer to this question would be of great interest. It it were to turn out that also in the relativistic quantum electrodynamics the singularity of the potential at the origin were essentially strengthened (becoming stronger than $1/r^2$) in higher approximation, as occurs in the nonrelativistic and nonquantum approximations, this would mean a new difficulty in principle, as the possibility of bound stationary states, which follows from the second approximation, would become fictitious--the theory would obviously be in contradiction with observed facts.

The purpose of the present paper is to show that the interaction potential of two spinor particles (for concreteness we shall call them electrons), calculated in relativistic quantum electrodynamics with known methods of removing infinities, has a singularity at the origin not higher than $1/r^{1+\epsilon}$ (with ϵ an arbitrarily small positive number), in any arbitrarily high (but of course finite) order of perturbation theory.

In this paper "natural" units are used ($\hbar = c = 1$). In addition, in applying the summation convention, the fourth term of a sum over a "dummy" index is taken with the minus sign.

It is well known that the singularity at the origin in the interaction potential of two particles can be determined from the asymptotic behavior of the S-matrix for the scattering of the particles at high momenta. For this prupose it suffices to take into account in the calculation of the S-matrix only those of its elements that correspond to Feynman diagrams that form an irreducible representation (see Bethe and Salpeter[2]). Besides this, the S-matrix must be calculated without use of the law of conservation of energy for the initial and final states.

The essence of the proof consists of showing that in passing from the nth approximation, which is assumed reduced to finite form, to the next [obviously, the $(n+2)$nd], after the removal of all infinities in the $(n+2)$nd approximation, the asymptotic approach to zero of the S-matrix with increasing momenta is weakened by a factor not stronger than logarithmic.

---

* Here and in what follows we shall have in mind the ordinary electrodynamics with the interaction part of the Hamiltonian not containing derivatives of the field operators.

If we denote the initial momenta of the electrons by p_μ and q_μ, and the final momenta by p'_μ and q'_μ, then the element of the S-matrix in the first nonvanishing (the second) approximation, corresponding (apart from "exchange") to the single diagram in this approximation

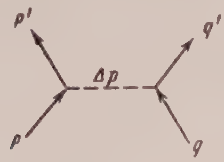

(I)

is given by

$$S_2 = -\frac{(2\pi)^4 ie^2}{2} \tag{1}$$

$$\times\frac{1}{(\Delta p_\mu)^2}\cdot\Psi^+_{p'}\gamma_\mu\Psi_p\cdot\Psi^+_{q'}\gamma_\mu\Psi_q\cdot\delta(p_\nu+q_\nu-p'_\nu-q'_\nu).$$

Here $\Delta p_\mu \equiv p'_\mu - p_\mu$; Ψ_p, Ψ_q and so on denote the amplitudes of plane waves with the indicated momenta; $\Psi^+ \equiv \Psi^* \gamma_4$, where the sign * denotes the complex conjugate and transposed quantity. It follows from (1) that for $\Delta p_\mu \to \infty$, S_2 behaves like $1/(\Delta p_\mu)^2$, which corresponds to a potential with a $1/r$ singularity at the origin.

We shall show that the passage from any arbitrary approximation to the following one can be accomplished either by the "connecting" of any two electron lines (solid lines in the diagram), which may in particular be coincident lines, by a photon (dotted) line, or else by the "insertion" in any photon line of a closed electron loop (consisting of two electron lines). In this way one can immediately obtain from diagram (I) all the diagrams of the fourth approximation, of which only the first is reducible:

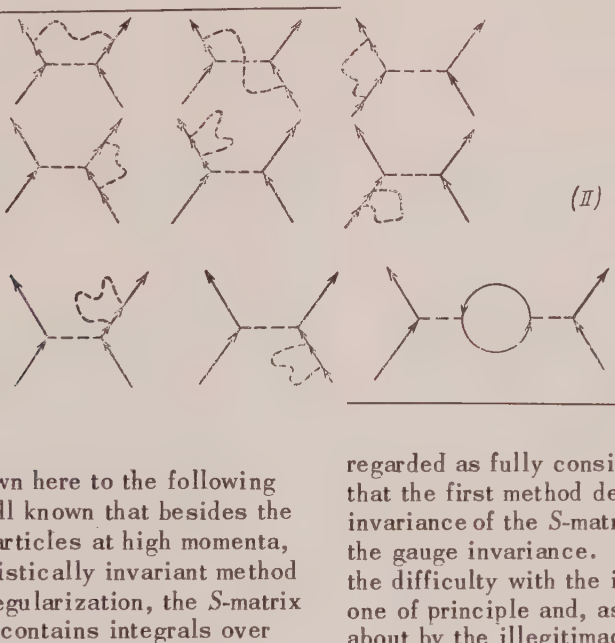

(II)

Attention must be drawn here to the following circumstance. It is well known that besides the divergences of virtual particles at high momenta, removable by the relativistically invariant method of renormalization and regularization, the S-matrix of electrodynamics also contains integrals over the momenta l_μ of virtual photons that diverge at zero (the "infrared catastrophe"). This divergence can be removed in two well-known ways: 1) "cutting off" near zero in the l-space, or 2) assigning to the photon a certain finite rest mass[*]. It is true that, even if we omit consideration of the ambiguity of these methods, they cannot be regarded as fully consistent in view of the fact that the first method destroys the relativistic invariance of the S-matrix and the second destroys the gauge invariance. The fact is, however, that the difficulty with the infrared catastrophe is not one of principle and, as is well known, is brought about by the illegitimacy of the expansion of the S-matrix in the series of perturbation theory. The exactly calculated S-matrix is free from this difficulty.

In what follows it will be assumed that all occurring integrals over virtual momenta have, if divergent at zero, been brought to finite form by one of the known methods; we shall suppose, however, that no inconsistency in principle is thus introduced.

We consider the following types of passages from the nth approximation to the $(n+2)$nd, shown in diagrams (*III*)-(*VII*) [or to the $(n+4)$th, in case (*VIII*)].

---

[*] It must be noted that the possibility of removing the infrared catatrophe by the introduction of real photons is excluded by the very statement of our problem.

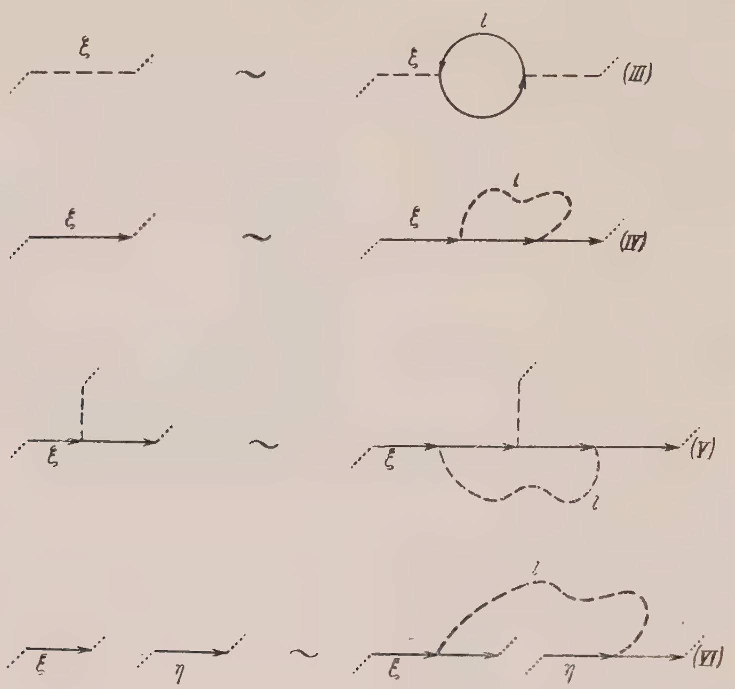

The diagonally directed series of dots represent certain entirely arbitrary parts of the diagram. In case (*VI*) it is assumed that 1) if the ξ and η lines belong to one succession of electron lines, then between the ends of the line l (along the succession of electron lines) there are at least two points, and 2) if one (or both) of the lines ξ and η belongs to a closed loop of electron lines, then in the left-hand part of (*VI*) this loop must consist of not fewer than four (electron) lines.

The necessity of special consideration of cases (*VII*) and (*VIII*), passages from closed loops of two electron lines directly to loops of four lines, is occasioned by our wish to exclude from consideration diagrams with loops of three electron lines, because of the unremovable infinities appearing in the element of the *S*-matrix corresponding to each such diagram. The exclusion of these cases is, of course, permissible, as by Furry's theorem[3] the sum of the elements of the *S*-matrix corresponding to all such diagrams is equal to zero.

It is obvious that by means of alterations (*III*)-(*VIII*) one can obtain from the collection of diagrams of any arbitrary approximation all possible diagrams (with nonvanishing total contributions) of any higher approximation.

We note that ξ_μ, η_μ and ζ_μ are algebraic sums of some number (which may, in particular, be zero) of virtual momenta l_μ, over which integration is to be performed, and one of the terms $-\Delta p_\mu$, $\Delta p_\mu - p_\mu$, $\Delta p_\mu - q_\mu$, p_μ, q_μ (or of virtual momenta only), i.e., symbolically

$$\xi \equiv \xi(p,\ l),\quad \eta \equiv \eta(p,\ l),\quad \zeta \equiv \zeta(p,\ l).$$

In the passage from the nth approximation, assumed reduced to finite form, to the $(n+2)$nd, or in case (*VIII*) to the $(n+4)$th, there occurs in the integrand of the expression for the *S*-matrix a replacement of a factor $M_i(\xi_\mu)$* by another: $M_i(\xi_\mu) \rightarrow M_i'(\xi_\mu)$; the latter is in general infinite, but reducible to finite form: $M_i'(\xi_\mu) \rightarrow M_i''(\xi_\mu)$. Comparison of these two factors M_i and M_i'' makes possible a decision about the change of asymptotic behavior of the *S*-matrix with increasing order of approximation. First of all we can convince ourselves that in all of cases (*III*)-(*VII*) the asymptotic behavior of $M_i''(\xi_\mu)$ for $\xi_\mu \rightarrow \infty$ can differ from that of $M_i(\xi_\mu)$ by nothing stronger than a

---

* For case (*VI*) $M_i(\xi_\mu, \eta_\mu)$, and for case (*VIII*) $M_i(\xi_\mu, \eta_\mu, \zeta_\mu)$, respectively.

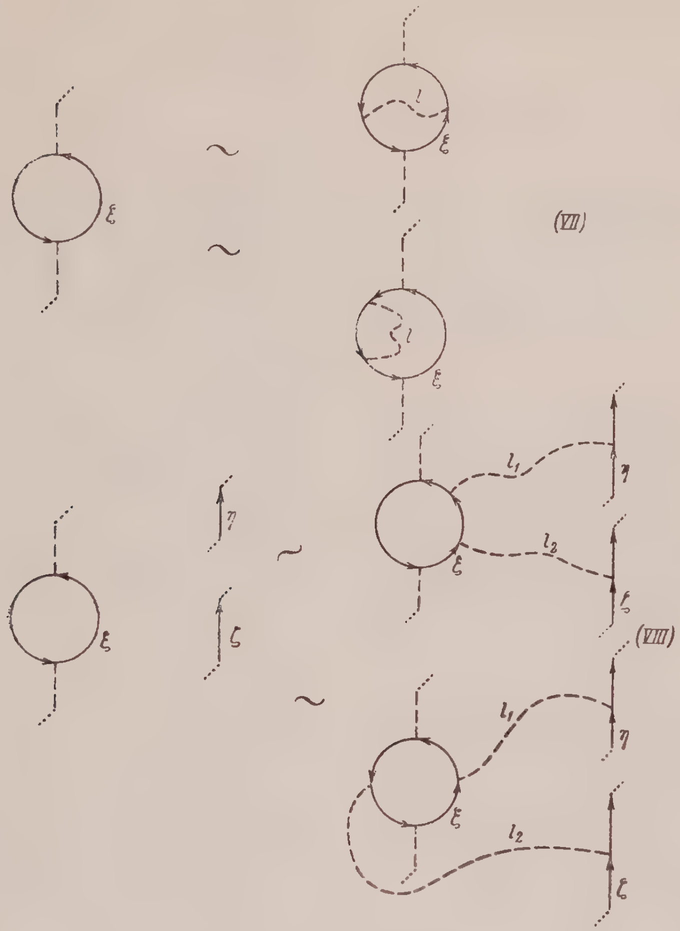

logarithmic factor, and in case (*VIII*) by nothing stronger than its square, i.e.,

$$\underset{\xi_\mu\to\infty}{M_i''(\xi_\mu)} \sim M_i(\xi_\mu)\cdot\underset{\xi_\mu\to\infty}{\Lambda_i(\xi_\mu)}, \qquad (2)$$

where for $\xi_\mu\to\infty$, $\Lambda_i(\xi_\mu)$ approaches infinity in cases (*III*)-(*VII*) no more strongly than $\ln\xi_\mu^2$, and in case (*VIII*) not more strongly than $\ln^2\xi_\mu^2$. (Incidentally, as is easily seen, there follows from this the full renormalizability of electrodynamics.)

We present as an example the factors M_1 and M_1'' for case (*III*):

$$M_1 = \delta_{\mu\nu};\ M_1'' = \frac{e^2}{4(2\pi)^2}(\xi_\mu\xi_\nu - \xi^2\delta_{\mu\nu}) \qquad (3)$$

$$\times\int_0^1 dx\,\frac{x^2(1-{}^1\!/_3x^2)}{m^2+(\xi^2/_4)(1-x^2)};$$

$$\underset{\xi_\mu\to\infty}{M_1\sim}\,\mathrm{const};\ \underset{\xi_\mu\to\infty}{M_1''\sim}\,\mathrm{const}\ln(\xi_\mu^2/m^2). \qquad (4)$$

In deriving the asymptotic behavior of the factors M_i'' in the more complicated cases (*VI*) and (*VIII*) it is necessary to use the general formulas (for arbitrary integers l, n, k, m):

$$\frac{1}{a_1\ldots a_l} = (l-1)!\int_0^1 dx_1\ldots \qquad (5)$$

$$\times\int_0^{x_{l-2}} dx_{l-1}\cdot[a_1x_{l-1}+a_2(x_{l-2}-x_{l-1})+\ldots$$

$$\ldots+a_l(1-x_1)]^{-l};$$

$$\int_{(\infty)} d^4l\cdot\overbrace{l_\mu l_\xi\ldots l_\eta l_\nu}^{2n}\cdot f(l^2) \qquad (6)$$

$$= 4^{-n}\int_{(\infty)} d^4l\,(l_\mu)^{2n} f(l^2)\cdot\sum\overbrace{\delta_{\mu\xi}\ldots\delta_{\alpha\nu}}^{n}$$

[for half-integral n integral (6) is equal to zero],

$$\int_{(\infty)} d^4 l \quad \frac{l^{2k}}{(l^2+\lambda)^m} \tag{7}$$

$$= \frac{\pi^2 i}{\lambda^{m-k-2}} \Big[\frac{1}{(m-k-2)\,(m-k-1)}$$

$$- C_1^k \frac{1}{(m-k-1)(m-k)}$$

$$(m-k-2 \geqslant 1).$$

$$+ \ldots + (-1)^k \frac{1}{(m-2)(m-1)} \Big].$$

The summation in (6) is taken over all permutations of the indices $\mu, \xi, \ldots, \alpha, \nu$. Equation (6) can be proved from general considerations of relativistic invariance.

Furthermore, on the basis of (2) it is not difficult to prove the following assertion: if the integral

$$S_n = \int_{(l)} f[l, p, \xi(p, l)]\, M[\xi(p, l)] \quad \text{for} \quad p_\mu \to \infty$$

approaches zero (just this approach to zero is essential) like some function $J_n(p_\mu)$, then

$$S_{\substack{n+2\\n+4}} = \int_{(l)} f[l, p, \xi(p, l)]\, M''[\xi(p, l)] \text{ for } p_\mu \to \infty$$

will approach zero in cases (*III*)-(*VII*) no more weakly than $J_n(p_\mu) \ln(p_\mu)^2$ and in case (*VIII*) no more weakly than $J_n(p_\mu) \ln^2(p_\mu)^2$. In other words, in the passage from the nth approximation to the $(n+2)$nd the asymptotic approach to zero of the scattering S-matrix for $p_\mu \to \infty$ is weakened by nothing stronger than a logarithmic factor; and this means that the singularity at the origin in the (electromagnetic) interaction potential of two electrons, and consequently, of the system electron-positron, in any arbitrarily high nth (in powers of the charge) approximation of perturbation theory cannot be stronger than*

$$(1/r) \ln^{(n-2)/2} r.$$

Furthermore, it is not hard to see that in nonrelativistic approximation for $p_\mu \to \infty$ the main term of the S-matrix in an arbitrary approximation will be, generally speaking, of the nature of a constant, which corresponds to a potential with a singularity of the form r^{-3}. But this need not appear strange, as a consideration of the interaction potential at the origin (which is equivalent to a consideration of the scattering S-matrix at large momenta) in the nonrelativistic approximation (i.e., in the approximation of small momenta) is internally self-contradictory.

In conclusion, the writer expresses his gratitude to M. A. Markov for suggesting the problem and for his aid in the work.

---

* This result of course does not mean that the asymptotic behavior of the sum of the whole infinite series of perturbation theory will differ from $1/r$ by only a (finite) power of the logarithm of r. A discussion of the question arising in this connection, and also of the question in general of the convergence of the whole series of perturbation theory, which has given rise to doubts, particularly for large momenta (i.e., for small r), is beyond the scope of this paper.

[1] Zh. S. Takibaev, Dissertation, Phys. Inst. Acad. Sci. USSR, 1952.

[2] E. E. Salpeter and H. A. Bethe, Phys. Rev. 84, 1232 (1951).

[3] W. H. Furry, Phys. Rev. 51, 125 (1937).

Translated by W. H. Furry
144

SOVIET PHYSICS JETP VOLUME 3, NUMBER 4 NOVEMBER, 1956

Explanation of the Transition Effect for "Stars" in the Stratosphere

ZH. S. TAKIBAEV
Physico-Technical Institute, Kazakh SSR

(Submitted to JETP editor October 11, 1954)
J. Exptl. Theoret. Phys. (U.S.S.R.) 30, 713-718 (April, 1956)

An explanation based on cascade multiplication of nucleons is given for the transition curves of nuclear "stars". It is shown that significant transition effects for stars should be observed at heights exceeding 15 km above sea level even when heavy element absorbers are used; this prediction is in agreement with experimental results. In the case of absorbers consisting of heavy elements, the neutron excess in the nucleus must be taken into account.

THE basic experimental data, obtained (the first results were published in the papers of Ref. 1) from investigations of transition effects for nuclear "stars" during the period from 1950 to 1954, lead to the following conclusions:

1. The transition effect for stars with three or more prongs (i.e., the increase in number of stars in an emulsion exposed under an absorber above the number of the same type of star in an emulsion exposed in air without absorber) even for π-mesons depends essentially on the atomic number of the absorber and on the altitude above sea level at which the experiment is done.

2. In the experiments on transition effects for stars, lead, graphite and paraffin absorbers were used down to thicknesses of 10, 30 and 50 cm, respectively. In all experiments at altitudes of 22-29 km, we observed an increase in the number of stars in photographic plates under lead (compared with the number of stars in plates without absorber) by 30-50% (depending on the altitude of observation, as well as on the thickness and the arrangement of the lead blocks).

3. In the case of light element absorbers (graphite and paraffin), at an altitude of 22 km no significant increase was observed in the number of stars in plates under absorber compared with the number of stars in plates exposed in air, without absorber. Only at an altitude of ~27-28 km did we observe an increase in number of stars (by approximately 10-20%) upon entering a graphite absorber 30 cm in thickness.

4. It was shown experimentally that the transition effect both in heavy element absorbers (lead) and in absorbers consisting of light elements (graphite and paraffin) is due mainly to stars with 3-7 prongs. This indicates that a considerable number of star-producing particles of low energy (from 60 to 500 mev) are generated in the absorbers.

5. The altitude dependence of number of stars in the range 20-27 km was explained.

6. We obtained the altitude dependence of slow π-mesons stopping in emulsions. The transition effect for π-mesons in lead, graphite, paraffin and copper absorbers was explained. We explained the energy spectrum of slow π-mesons in air, and the spectrum of π-mesons generated in the various absorbers.

While omitting all the details of the various experiments and of the processing of plates exposed in the stratosphere, we shall here try to explain the experimental results, which have been briefly cited in points 1-5, starting from the general picture of the passage of the nucleonic component of cosmic rays through matter.

We shall assume that the investigation of star transition effects is carried out at some definite depth ϑ_B in the atmosphere. We set ourselves the problem of finding the total number N of particles with energy greater than E, at depth ϑ_A in the absorber, which are capable of producing stars. We assume, in accordance with accepted notions, that the star-producing particles are neutrons, protons and π-mesons of sufficient energy. Consequently, each of the particles which enters the absorber, can produce a definite number of neutrons, protrons and π-mesons via cascade multiplication in the course of reaching the depth ϑ_A. We shall denote by $N_{1n}(E_n, E, \vartheta_A)$, $N_{1p}(E_n, E, \vartheta_A)$, and $N_{1\pi}(E_n, E, \vartheta_A)$, respectively, the numbers of neutrons, protons and π-mesons with energy greater than E at depth ϑ_A, due to a single neutron which enters the absorber from air, with energy E_n. Then

$$N_1(E, \vartheta_A) = \sum_{i,k} N_{1i}(E_k, E, \vartheta_A)$$

denotes the total number of particles of all three types, with energy greater than E at depth ϑ_A, due to a neutron, proton and π-meson incident on the surface of the absorber with energies E_n, E_p and E_π, respectively. The total number of all such particles, due to neutrons, protons and π-mesons with energies greater, respectively, than E_n, E_p and E_π, will be

$$N(E,\ \vartheta_A^1,\ E_n,\ E_p,\ E_\pi,\ \vartheta_B) \tag{1}$$

$$= \sum_{i,k} \int_{E_k}^{\infty} N_{1i}(E_k',\ E,\ \vartheta_A)\, K(E_k',\ \vartheta_B)\, dE_k',$$

where the subscripts i and k take on three values for neutron, proton and π-meson, while $K\ (E_k', \vartheta_B')\, dE_k'$ denote the differential spectrum of the particles at depth ϑ_B.

Treatment of the problem in this general form requires the solution of a system of three integro-differential equations (including energy loss by ionization). Janossy, Messel and others[2], using the method of Bhabha and Chakrabarty[3], have solved the equation, not including mesons, i.e., they treated the nucleon cascade in the atmosphere. They assumed that the effective nucleon-nucleon interaction cross section is a uniform function of the energy of the particles after collision. Our initial attempt[1] at explaining the transition effects for stars was phenomenological in character, since the energy spectrum of the particles was essentially taken from experimental data. In the present paper we present a general scheme for solving the problem of transition curves, based on a treatment of the cascade multiplication of a flux of nucleons passing through matter, using the methods developed in Ref. 2. Since our experiments as well as those of other observers show that the number of stars due to π-mesons is small, the calculation will be made only for the nucleonic component.

If we neglect ionization losses of the proton, then neutrons and protons will behave in the same way, and the number of nucleons (i.e., neutrons plus protons) with energy greater than E, at depth ϑ_A, due to a nucleon incident on the absorber surface with energy greater than E_0, will be

$$N_1(E_0,\ E,\ \vartheta_A) \tag{2}$$

$$= \frac{1}{2\pi i} \int_{s_0'-i\infty}^{s_0'+i\infty} \left(\frac{E}{E_0}\right)^{-s'} \exp\{-\ \vartheta_A \cdot f(D_A \alpha_{s'})\}\, \frac{ds'}{s'},$$

where $f(x) = 1 - 2x^{-2}[1-(1+x)e^{-x}]$, D_A is the number of collisions of the initial nucleon with nucleons in the nucleus, when it traverses the diameter of a nucleus of atomic weight A. The function α_s depends on the nature of the nucleon-nucleon interaction, i.e.,

$$\alpha_s = \int_0^1 \int_0^{1-\varepsilon_2} (1 - \varepsilon_1^s - \varepsilon_2^s)\, W(\varepsilon_1, \varepsilon_2)\, d\varepsilon_1 d\varepsilon_2 \tag{3}$$

$$\text{and } \epsilon_1 = \frac{E_1}{E_0},\quad \varepsilon_2 = \frac{E_2}{E_0},$$

where E_1 and E_2 are the energies, after collision, of the nucleons, one of which was at rest while the other had energy E_0 before the collision, $W(\epsilon_1, \epsilon_2)\, d\epsilon_1 d\epsilon_2$ is the probability that after the collision of the incident nucleon with energy E_0 and the nucleon at rest, they have energies E_1 and E_2, respectively.

We shall assume that $K(E_0, \vartheta_B)\, dE_0$ is the number of nucleons with energy in dE_0 at E_0 at the depth ϑ_B in the atmosphere. Then the number of nucleons with energy greater than E at a depth of absorber equal to ϑ_B, which were formed by initial particles with energies in dE_0 at E_0, is $N_1(E_0,\ \vartheta_A,\ E)\, K(E_0,\ \vartheta_B)\, dE_0$. The total number of nucleons with energy greater than E at depth ϑ_A, due to initial nucleons with energy greater than E_0, is given by

$$N(E_0,\ \vartheta_A,\ E,\ \vartheta_B) \tag{4}$$

$$= \int_{E_0}^{\infty} N_1(E_0,\ \vartheta_A,\ E)\, K(E_0, \vartheta_B)\, dE_0$$

$$= \frac{1}{2\pi i} \int_{E_0}^{\infty} \int_{s_0-i\infty}^{s_0+i\infty} K(E_0, \vartheta_B) \left(\frac{E}{E_0}\right)^{-s}$$

$$\times \exp\{-\vartheta_A f(D_A \alpha_s) \vartheta_A\} \frac{ds}{s}\, dE_0.$$

If we use the initial conditions

$$K(E_0,\ 0) = \begin{cases} \gamma E_c^\gamma / E_0^{\gamma+1} & \text{for } E_0 > E_c \\ 0 & \text{for } E_0 < E_c. \end{cases}$$

then

$$N(E_0, E_c, \vartheta_B) \tag{5}$$

$$= \frac{\gamma}{2\pi i} \int_{s_0 - i\infty}^{s_0 + i\infty} \left(\frac{E_0}{E_c}\right)^{-s} e^{-\vartheta_B f(D_B \alpha_s)} \frac{ds}{s(\gamma - s)}$$

$$= \int_{E_0}^{\infty} K(E_1, E_c, \vartheta_B)\, dE_1;$$

$$K(E_0, E_c, \vartheta_B) = -\frac{\partial N(E_0, E_c, \vartheta_B)}{\partial E_0} \tag{6}$$

$$= \frac{\gamma}{2\pi i} \int_{s_0 - i\infty}^{s_0 + i\infty} \left(\frac{E_0}{E_c}\right)^{-s} e^{-\vartheta_B f(D_B \alpha_s)} \frac{ds}{E_0(\gamma - s)}.$$

Then

$$N(E_0, \vartheta_A, E, E_c, \vartheta_B) \tag{7}$$

$$= \frac{\gamma}{4\pi^2 i^2} \int_{E_0}^{\infty} \int_{s_0 - i\infty}^{s_0 + i\infty} \int_{s'_0 - i\infty}^{s'_0 + i\infty} \frac{(E_0/E_c)^{-s}}{E_0(\gamma - s)}$$

$$\times e^{-\vartheta_B f(D_B \alpha_s)} \frac{(E/E_0)^{-s'}}{s'} e^{-\vartheta_A f(D_A \alpha_{s'})}\, ds\, dE_0\, ds',$$

where $s > s'$. After integrating with respect to E_0 and setting the lower limit equal to E, and using the relation

$$\frac{1}{2\pi i} \int_{s'_0 - i\infty}^{s'_0 + i\infty} \frac{e^{-\vartheta_A f(D_A \alpha'_s)}}{s'(s - s)}\, ds' \tag{8}$$

$$= \frac{1}{s} \exp\{-\vartheta_A f(D_A \alpha_s)\},$$

we get

$$N = \frac{\gamma}{2\pi i} \int_{s_0 - i\infty}^{s_0 + i\infty} \frac{(E/E_c)^{-s}}{(\gamma - s)s} \tag{9}$$

$$\times \exp\{-\vartheta_B f(D_B \alpha_s) - \vartheta_A f(D_A \alpha_s)\}\, ds,$$

where $\gamma > s_0$. The location of the maximum of the transition curve is found from the conditions

$$\partial N(\vartheta_A, E, E_c, \vartheta_B) / \partial \vartheta_A = 0 \quad \text{or}$$

$$f(D_A \alpha_s) = 0, \text{ i.e., } \alpha_s = 0.$$

We calculate the values of the function N by the saddle point method:

$$N = \frac{\gamma}{2\pi i} \int_{s_0 - i\infty}^{s_0 + i\infty} e^{S(s)}\, ds \tag{10}$$

$$= \gamma (2\pi)^{-1/2} [-S''(s_0)]^{-1/2} e^{-S(s_0)},$$

where

$$-S(s) = -s \ln \varepsilon \tag{11}$$

$$-\ln s(\gamma - s) - \vartheta_B f(D_B \alpha_s) - \vartheta_A f(D_A \alpha_s),$$

$$-S'(s) = -\left.\frac{\partial S}{\partial s}\right|_{s=s_0} = -\ln \varepsilon - \frac{\gamma - 2s_0}{s_0(\gamma - s_0)}$$

$$-\vartheta_B f'(D_B \alpha_s) - \vartheta_A f'(D_A \alpha_s) = 0.$$

Then

$$\vartheta_A\big|_{\max} = \frac{-\ln \varepsilon - \dfrac{\gamma - 2s_0}{s_0(\gamma - s_0)} - \vartheta_B \dfrac{2}{3} \alpha'_{s_0} D_B}{{}^2/_3\, \alpha'_{s_0} D_A}, \tag{12}$$

where $\alpha' = (\partial \alpha_s / \partial S)_{s=s_0}$. Using $E = 50$ mev, $E_c = 2 \times 10^3$ mev, $\gamma \approx 1.3$, $D_{Pb} = 8.7$, $D_B \approx 3.6$, and the α_s from the most recent work of Messel, we obtained

$$\vartheta_{Pb} = 0.578 - 0.414\, \vartheta_B, \tag{13}$$

where ϑ_B is measure in units of 65 gm/cm^2, and ϑ_{Pb} in units of 160 gm/cm^2. The dependence of $X_{Pb} \approx 160\, \vartheta'_{Pb}$ on X_B is shown in Fig. 1.

One is not able experimentally to establish accurately the position of the maximum of the transition curve. Despite this, the general behavior of the curve and its dependence on the altitude of observation, as obtained from examination of plates exposed in the stratosphere at various altitudes under absorbers (of lead, graphite and paraffin) of different thicknesses, lead to the following conclusions: 1) the maximum transition effect is observed at the highest altitude (27-29 km); 2) the effect decreases with decreasing altitude, and below 15 km is not observed (within the limits of experimental error);

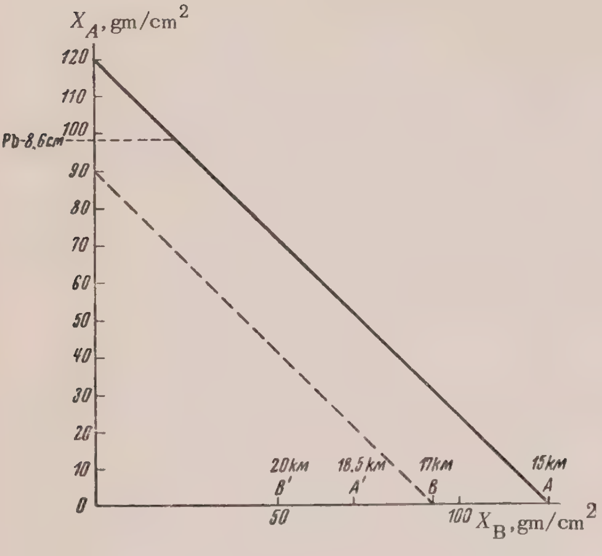

FIG. 1. Dependence of the position X_A on the maximum of the transition curve for stars on depth X_B in the atmosphere.

3) the position of the maximum apparently also depends on altitude.

The experimental data mentioned are entirely in accord with the general theoretical picture of the passage of the nucleonic component through matter. In fact, from the graph shown in Fig. 1, it follows that below 15 km there should be no transition effect (i.e., no increase in number of stars) under a lead absorber, and in addition, the position of the maximum should depend on the altitude of observation, which is also in accord with our data obtained from flights during 1953; according to Fig. 1, the position of the maximum shifts to smaller thicknesses with increasing depth in the atmosphere.

We should mention that the general conclusions are not essentially changed if, instead of $W(\epsilon_1\epsilon_2) = 15(1-\epsilon_1)\epsilon_2^2$ (the solid line), we use $W(\epsilon_1\epsilon_2) = 120\,\epsilon_1\epsilon_2(1-\epsilon_1-\epsilon_2)$ (the dotted line). Therefore, these conclusions are probably also changed only slightly for the actual W, which cannot be predicted at present.

We should point out that the points A and B are shifted to the left (to points A' and B') if we consider the total intensity of nucleons by using Gross's transformation.

The calculations carried out above explain the altitude dependence of the transition effect for stars, as well as the dependence of the maximum of the transition curve on the altitude of observation, but they do not explain the magnitude of the transition effect (this can be shown from estimates using the saddle point method). For example, the transition effect for a graphite absorber is calculated to be somewhat greater (5%) than for a lead absorber, whereas experiment gives the opposite result (cf. the beginning of the paper).

It appears that to explain the magnitude of the transition effect for a lead absorber we must take into account the neutron excess in the nucleus of a heavy element (lead) as compared to nuclei of light elements where the numbers of neutrons and protons are the same; the point is that the majority of small stars, for which the transition effect is a maximum, are formed precisely by neutrons. To get this result, we solve the equations

$$\frac{\partial S^{ik}_{(E,\,\theta)}}{\partial\theta} + S^{ik}_{(E,\,\theta)} = F(A,k) \tag{14}$$

$$\times \int\limits_0^\infty \{S^{i,\,k}_{(E',\,\theta)} + S^{i,\,3-k}_{(E',\,\theta)}\}\, V\left(\frac{E}{E'}\right)\frac{dE'}{E'} + \delta_{ik}\beta\frac{\partial}{\partial E}S^{i,\,k}_{(E,\,\theta)},$$

which reduce to the usual equations of cascade multiplication of nucleons passing through the atomsphere if we set $F(A,k) = ½$ (cf. Messel[3]), since for air (and in general for light elements),

$$F(A,k) = Z/A \approx (A-Z)/A = 1/2.$$

In the case of passage of nucleons through a heavy element absorber:

$$k=1:\ \frac{\partial S^{i,1}_{(E,\,\theta)}}{\partial\theta} + S^{i,1}_{(E,\,\theta)} \tag{15}$$

$$= \frac{Z}{A}\int\limits_0^\infty \{S^{i,1}_{(E',\theta)} + S^{i,2}_{(E',\theta)}\}\, V\left(\frac{E}{E'}\right)\frac{dE'}{E'} + \beta\frac{\partial}{\partial E}S^{i,1}_{(E,\,\theta)},$$

$$k=2:\ \frac{\partial S^{i,2}_{(E,\,\theta)}}{\partial\theta} + S^{i,2}_{(E,\,\theta)}$$

$$= \frac{A-Z}{A}\int\limits_0^\infty \{S^{i,2}_{(E',\,\theta)} + S^{i,1}_{(E',\,\theta)}\}\, V\left(\frac{E}{E'}\right)\frac{dE'}{E'},$$

where i refers to the initial nucleon ($i = 1$ for a proton, $i = 2$ for a neutron). $S^{i,k}_{(E,\theta)}$ is the average number of protons or neutrons (depending on the value of the index k) in dE at energy

E, at depth ϑ in a lead absorber, due to an initial particle incident on the surface of the absorber with energy greater than E_0. Then

$$N^{i,k}(E_0, E, \vartheta_A) \approx \frac{1}{2\pi i} \tag{16}$$

$$\times \int\limits_{s_0'-i\infty}^{s_0'+i\infty} \left(\frac{E_0}{\beta_A}\right)^{s'} \left(\frac{\beta}{E + \beta_A g^{i,k}_{(s'+1,\,\theta A)}}\right)^{s'} f_0^{i,k}(s'+1, \theta_A)\,\frac{ds'}{s'},$$

where

$$f_0^{i,k}(s'+1, \theta_A) = \frac{\delta_{ik}}{V_{s'}}[(V_{s'} - 1$$

$$+ A_{3-k}(s')\,e^{-\theta(1-V_{s'})} - (A_{3-k}(s') - 1)\,e^{-\vartheta}]$$

$$- \frac{(1-\delta_{ik})\,B_k(s')}{V_{s'}}[e^{-\theta(1-V_s)} - e^{-\theta}];$$

$$A_1(s') = 1 - (Z/A)\,V_{s'};$$

$$A_2'(s') = 1 - V_{s'}(A - Z)/A;$$

$$B_1(s') = -(Z/A)\,V_{s'};$$

$$B_2(s') = V_{s'}(A - Z)/A.$$

These expressions reduce to those given by Messel if $Z/A \sim (A - Z)/A \sim ½$. If we now apply to (16) all the considerations made for the case of equal numbers of protons and neutrons, and make use of the initial conditions, then the number of neutrons is given by the formula

$$N_n(E, \vartheta_A, \vartheta_B) \tag{17}$$

$$= \frac{\gamma}{4\pi^2 i^2} \int\limits_{E}^{\infty} \int\limits_{s_0'-i\infty}^{s_0'+i\infty} \int\limits_{s_0-i\infty}^{s_0+i\infty} \left(\frac{E_0}{E}\right)^{s'} f_0^{j,2}(s'+1, \vartheta_A)$$

$$\times \frac{1}{s'}\left(\frac{E_c}{E_0}\right)^{s} \frac{1}{\gamma - s} f_0^{1,j}(s+1, \vartheta_B)\,\frac{dE, ds'\,ds}{E_0}.$$

Here we have neglected ionization loss, i.e., $\beta_A = \beta_B \to 0$. Since almost all the low-energy stars are formed by neutrons, we correctly explain only the increase in number of neutrons under lead, so we shall calculate only $N_n(E, \vartheta_A, \vartheta_B)$. As we see from Fig. 2, such a calculation, for altitudes ~ 28-30 km, gives an increase in number of stars under lead of 20%, compared to the case where the neutron excess in heavy nuclei is not taken into account. This number agrees approximately with the experimental data obtained in our laboratory.

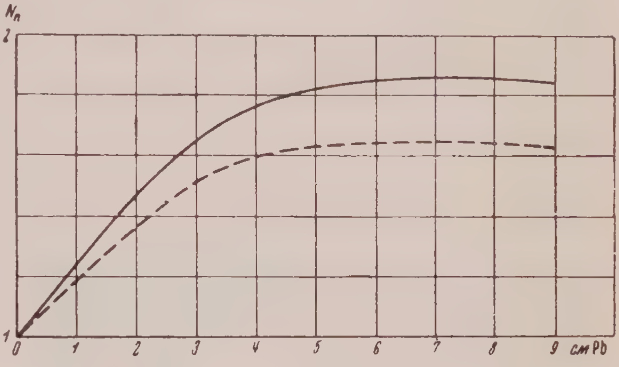

FIG. 2. Dependence of number N_n of star-producing neutrons with energy greater than 50 mev on thickness of lead absorber at altitude 27 km above sea level. The solid curve shows the intensity calculated, including the effect of neutron excess, the dotted curve is calculated without including this effect.

Thus, on the basis of the generally accepted picture of the passage of the nucleonic component through matter we are able to explain (at least approximately) the experimental data presented in brief summary at the beginning of this paper.

In conclusion, the author thanks P. A. Usik, who carried out the numerical computation using formula (17).

---

[1] Zh. S. Takibaev, Dokl. Akad. Nauk SSSR 78, 457 (1951); J. Exptl. Theoret. Phys. (U.S.S.R.) 23, 543 (1952).

[2] W. Heitler and L. Jánossy, Proc. Phys. Soc. (London) A62, 374, 669 (1949); G. Thomson and P. Hodgson, Phil. Mag. 42, 978 (1951); H. Messel and D. Ritson, Proc. Phys. Soc. (London) A63, 1359 (1950); L. Jánossy, Proc. Roy. Irish Acad. A53, 181 (1950); Proc. Phys. Soc. (London) A63, 241 (1950); L. Jánossy and H. Messel, Proc. Phys. Soc. (London) A64, 1 (1951); H. Messel, Phys. Rev. 83, 21, 26, 1279 (1951).

[3] H. Messel, Progress in Cosmic Ray Physics, 2, Amsterdam (1954).

Translated by M. Hamermesh
145

The Free Path Length of a Nonlocalized Exciton in a Polar Crystal

A. I. ANSEL'M AND IU. A. FIRSOV
Leningrad Physico-technical Institute, Academy of Sciences, USSR

(Submitted to JETP editor December 31, 1954)
J. Exptl. Theoret. Phys. (U.S.S.R.) 30, 719-723 (April, 1956)

The free path length of a nonlocalized exciton in a polar crystal is calculated for high and low temperatures, taking into account the interaction of the electron and hole, which form the exciton, with the thermal vibrations of the lattice.

INTRODUCTION

IN an earlier article by the present authors[1], devoted to the free path length of a nonlocalized exciton in an atomic crystal, the general question of the existence of excitons was considered, and experimental results supporting this existence were presented. In the present article we give results concerning the calculation of the free path length of a nonlocalized exciton in a polar crystal at high and low temperatures, omitting the details of the computation, since they are similar to the calculations of the earlier article.

We shall, as before, consider a nonlocalized exciton as a hydrogenlike formation, made up of an electron and a hole, described by the wave function

$$\psi_{\text{ex}} = V^{-1/2} e^{i\mathbf{kR}} (\pi a_{\text{ex}}^3)^{-1/2} \exp\{-r/a_{\text{ex}}\}. \qquad (1)$$

Here V is the elementary volume of the crystal, **k** is the wave vector of the forward motion of the exciton, **R** and **r** are radius vectors of the center of inertia of the exciton and of the electron relative to the hole, that is,

$$\mathbf{R} = (\mu_1\mathbf{r}_1 + \mu_2\mathbf{r}_2)/(\mu_1 + \mu_2), \quad \mathbf{r} = \mathbf{r}_1 - \mathbf{r}_2, \qquad (2)$$

where μ_1, μ_2 and $\mathbf{r}_1$, $\mathbf{r}_2$ are the effective masses and radius vectors of the electron and hole (we shall continue to use the index 1 to refer to the electron and 2 to refer to the hole). The "Bohr radius of the exciton" is

$$a_{\text{ex}} = \varkappa\hbar^2/\mu e^2, \qquad (3)$$

where $\varkappa$ is the optical dielectric constant and $\mu = \mu_1\mu_2/(\mu_1 + \mu_2)$ is the reduced mass. The energy corresponding to the state (1) of the exciton is

$$E_0 = (\hbar^2 k^2/2\mu_{\text{ex}}) - \mu e^4/2\varkappa\hbar^2 = \varepsilon - \Delta E, \qquad (4)$$

where the mass of the exciton is $\mu_{\text{ex}} = \mu_1 + \mu_2$.

Dykman and Pekar[2] have shown that localized excitons are formed in polar crystals only under the conditions $\mu_1/\mu_2 > 10$ (or $\mu_2/\mu_1 > 10$). In the treatment which follows we shall suppose that the ratio of the effective masses of the electron and hole does not reach such large values, that is, that we have to do with a nonlocalized exciton. It should also be noted that, apart from the slow decrease of the Coulomb field with distance, the application of the hydrogenlike exciton model[3] is justified, from our point of view, to the same extent to which the application of the method of effective masses to electrons and holes in kinetic phenomena is allowed.

The interaction of an exciton in a polar crystal with the thermal vibrations of the lattice is dependent on the interaction of the electron and hole with the optical branch of the vibrations. We shall, in what follows, concern ourselves only with those collisions of excitons with phonons in which an internal excitation or dissociation of the exciton does not occur. For collisions of an exciton with a phonon of the optical branch of the vibrations, for minimum excitation of the exciton, the conservation laws give

$$\mathbf{k} \pm \mathbf{q} = \mathbf{k}', \qquad (5)$$

$$\frac{\hbar^2 k^2}{2\mu_{\text{ex}}} \pm \hbar\omega_0 = \frac{\hbar^2 k'^2}{2\mu_{\text{ex}}} + E_1. \qquad (6)$$

Here **q** is the wave vector of the phonon, ω_0 is the frequency of the optical branch of the vibrations (we shall consider ω_0 as independent of **q**) and $E_1 = 3/4\,\Delta E$ is the minimum energy of excitation of the exciton.

From (5) and (6) it is easy to show that the condition of nonexcitation of the exciton during a collision with a phonon of the optical branch has the form:

$$\gamma = \varepsilon/(E_1 - \hbar\omega_0) < 1. \qquad (7)$$

For an overwhelming number of excitons we may replace ϵ by $3/2\, k_0 T$ in this expression; thus,

$$\bar{\gamma} = 3k_0T/2(E_1 - \hbar\omega_0) < 1. \tag{7a}$$

Since in polar crystals $\varkappa^2 \sim 5$, we have $E_1 \sim \mu/m_e$ ev. The energy $\hbar\omega_0$ is of the order of hundredths of an electron volt. Hence, if the ratio μ/m_e is not very small, then the inequality (7a) will be fulfilled up to high temperatures, of the order of thousands of degrees.

By substituting $E_1 = 0$ (the exciton is not excited) into (6), it is easy to determine the lowest and highest values of q for high and low temperatures. For high temperatures ($k_0T \gg \hbar\omega_0$):

$$q_{\min} = 0, \quad q_{\max} = 2k. \tag{8}$$

For low temperatures ($k_0T \ll \hbar\omega_0$):

$$q_{\min} = \sqrt{2\mu_{\rm ex}\omega_0/\hbar + k^2} - k, \tag{8a}$$
$$q_{\max} = \sqrt{2\mu_{\rm ex}\omega_0/\hbar + k^2} + k.$$

In calculating the free path length of the exciton we shall make the assumption that the average time of the free path between two successive collisions with the lattice vibrations is much less than the average lifetime of the exciton.

PROBABILITY $W_{\mathbf{kk}'}$ FOR AN EXCITON TRANSITION DURING ABSORPTION AND EMISSION OF A PHONON

As the energy of excitation U for the interaction of an exciton with the vibrations of a polar lattice we take the energy of interaction of the electron and the hole with the optical branch of the vibrations[4]:

$$U = -e\sum_{\mathbf{q}} \varphi_{1\mathbf{q}}(\mathbf{r}_1) + e\sum_{\mathbf{q}} \varphi_{2\mathbf{q}}(\mathbf{r}_2), \tag{9}$$

$$\varphi_{1\mathbf{q}}(\mathbf{r}_1) = -\frac{2\pi i Z e C_1}{\sqrt{MNa_0^3}\,q}\left(a_{\mathbf{q}} e^{i\mathbf{q}\mathbf{r}_1} - \overset{*}{a}_{\mathbf{q}} e^{-i\mathbf{q}\mathbf{r}_1}\right). \tag{9a}$$

Here Z is the charge number of the ions, $M = M_1M_2/(M_1 + M_2)$ is the reduced mass of the ions, a_0 is the lattice constant, N is the number of cells in the fundamental volume of the crystal V, C_1 is a constant of the order of unity, taking account of the deformation of the electron shells during collisions of the ions, the $a_{\mathbf{q}}$ are the normal coordinates of the lattice vibrations. An analogous expression, depending on $\mathbf{r}_2$, may be written for $\varphi_{2\mathbf{q}}(\mathbf{r}_2)$, that is, for a hole. The constant C_2 will be different from C_1, since the electron and the hole are in different quantum states.

The wave function for the zeroth approximation of the system, consisting of exciton and crystal, has the form

$$\Psi(\mathbf{R}, r_1 a_{\mathbf{q}}) = V^{-1/2} e^{i\mathbf{k}\mathbf{R}} (\pi a_{\rm ex}^3)^{-1/2} \times \exp\{-r/a_{\rm ex}\} \prod_{\mathbf{q}} \Phi_{N_{\mathbf{q}}}(a_{\mathbf{q}}), \tag{10}$$

where $\Phi_{N_{\mathbf{q}}}(a_{\mathbf{q}})$ is the oscillator wave function of the normalized vibration $a_{\mathbf{q}}$.

Calculating the matrix element of the transition by the general rule

$$U_{\mathbf{kk}'} = \int \Psi^*(\mathbf{R}, r, a_{\mathbf{q}})\, U \Psi(\mathbf{R}, r, a_{\mathbf{q}})\, d\mathbf{R}\, d\mathbf{r}\, da_{\mathbf{q}}, \tag{11}$$

we obtain for the transition probability associated with the absorption and emission of phonons the expressions:

$$W_{\mathbf{kk}'}^{+} = wN_{\mathbf{q}}Q(q)\,\delta(\varepsilon_{\mathbf{k}'} - \varepsilon_{\mathbf{k}} - \hbar\omega_0), \tag{12}$$
$$W_{\mathbf{kk}'}^{-} = w(N_{\mathbf{q}} + 1)\,Q(q)\,\delta(\varepsilon_{\mathbf{k}} - \varepsilon_{\mathbf{k}} + \hbar\omega_0).$$

Here $w = 8\pi^3 Z^2 e^4 C_1^2/VMa_0^3\omega_0 q^2$, $N_{\mathbf{q}}$ is the quantum number of the normal vibrations, δ is a delta function expressing the law of conservation of energy and

$$Q(q) = [(1 + \beta_1^2 q^2)^{-2} - s(1 + \beta_2^2 q^2)^{-2}]^2, \tag{12a}$$

where $\beta_1 = \varkappa\hbar^2/2\mu_1 e^2$, $\beta_2 = \varkappa\hbar^2/2\mu_2 e^2$ and $s = C_2/C_1$. In order of magnitude β_1 and β_2 are equal to $a_{\rm ex}$.

FREE PATH LENGTH OF AN EXCITON AT HIGH AND LOW TEMPERATURES

The free path length of an exciton is $l = \tau v$. The velocity of the exciton is $v = \hbar k/\mu_{\rm ex}$, while at high temperatures ($k_0T \gg \hbar\omega_0$) the relaxation time τ is determined by the formula[5]

$$\frac{1}{\tau} = -\sum_{\mathbf{q}} \frac{\Delta k_x}{k_x}\left(W_{\mathbf{kk}'}^{+} + W_{\mathbf{kk}'}^{-}\right). \tag{13}$$

Calculation gives

$$l = l_1 F(x), \quad l_1 = \frac{a_0}{2\pi}\left(\frac{\hbar\omega_0}{C_1 Z e^2/a_0}\right)^2 \frac{M}{\mu_1}\frac{\varepsilon}{k_0 T}. \tag{14}$$

Here l_1 is the free path length of an electron with energy ϵ equal to the energy of the forward motion of the exciton. The function $F(x)$, depending on the dimensionless variable $x = a_{ex}^2 k^2 = 2\mu_{ex} a_{ex}^2 \epsilon / \hbar^2$, determines the deviation of the free path length of the exciton from the free path length of an electron of the same kinetic energy:

$$\frac{1}{F(x)} = \frac{\alpha_1+\alpha_2}{\alpha_1 x}\left[\frac{s^2}{3\alpha_1^2}\left(1-\frac{1}{(1+\alpha_1^2 x)^3}\right) + \frac{1}{3\alpha_2^2}\left(1-\frac{1}{(1+\alpha_2^2 x)^3}\right) - \frac{2s}{1-(\alpha_1/\alpha_2)^2}\left(\frac{2/\alpha_2^2}{1-(\alpha_2/\alpha_1)^2}\ln\frac{1+\alpha_2^2 x}{1+\alpha_1^2 x} + \frac{x}{1+\alpha_2^2 x} + \left(\frac{\alpha_1}{\alpha_2}\right)^4 \frac{x}{1+\alpha_1^2 x}\right)\right], \tag{14a}$$

where $\alpha_1 = \mu_1/\mu_{ex}$ and $\alpha_2 = \mu_2/\mu_{ex}$. Thus, the function $F(x)$ depends only on two parameters: $s = C_2/C_1$ and $g = \mu_2/\mu_1$.

In the special cases when $g = 1$ or $g \gg 1$ or $s = 1$, the function (14a) becomes simpler. In order to obtain a more visual representation of the change of the free path length of the exciton with the change in its energy, curves (Figs. 1 and 2) were drawn up. The dimensionless kinetic energy $a = a_{ex}^2 k^2$ is plotted as abscissa and the function $F(x; s, g)$ is plotted as ordinate. In Fig. 1, $g = 10$ for all the curves, while the parameter s ranges in value from 0.3 to 2. In Fig. 2 g ranges from 1.2 to 10, while s varies within the narrower interval from 0.85 to 1.1. The general aspect of the curves in Figs. 1 and 2 shows that the function $F(x; s, g)$ has a maximum in those cases where for $g > 1$ the ratio of the corresponding polarization constants $s < 1$. In such cases, the nearer s is to unity, that is, the smaller the difference between C_2 and C_1, the smaller is the value of x at which the maximum occurs. If g and s are both larger (smaller) than unity, then the function $F(x; s, g)$ decrease monotonically with increasing x and decreases more steeply the closer s is to unity. It must be kept in mind, however, that, in accordance with (7), the theory applies for such times as

$$x < (2\mu_{ex} a_{ex}^2 / \hbar^2)(E_1 - \hbar\omega_0). \tag{15}$$

In thermal equilibrium $\epsilon = \bar{\epsilon} = 3/2 k_0 T$ for the overwhelming number of excitons; hence, for them the factor l_1 does not depend on the temperature, and the curve $F(x; s, g)$ gives directly, in relative units, the dependence of the free path length

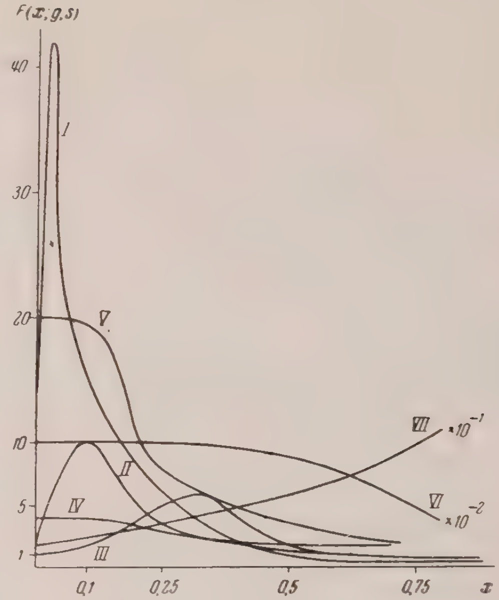

FIG. 1. $g = \mu_2/\mu_1 = 10$ for all the curves. $s = 0.9$ for curve *I*, $s = 0.8$ for curve *II*, $s = 0.7$ for curve *III*, $s = 1.15$ for curve *IV*, $s = 1.07$ for curve *V*, $s = 2.0$ for curve *VI*, $s = 0.3$ for curve *VII*.

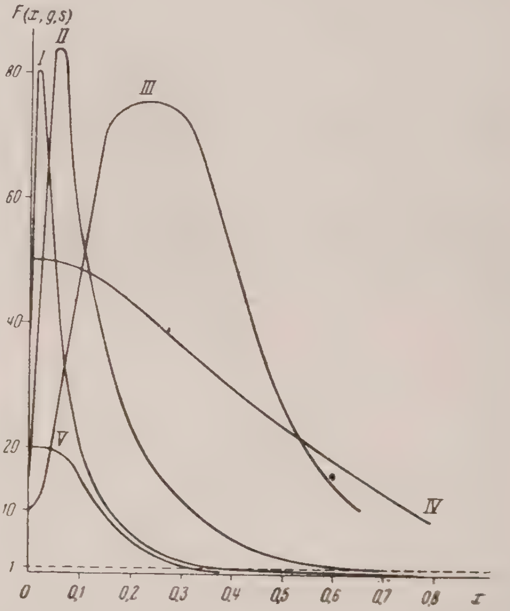

FIG. 2. $g = 10$, $s = 0.95$ for curve *I*; $g = 5$, $s = 0.9$ for curve *II*; $g = 3$, $s = 0.85$ for curve *III*; $g = 1.2$, $s = 1.1$ for curve *IV*; $g = 5$, $s = 1.1$ for curve *V*.

of the exciton on the temperature. On the other hand, it must be kept in mind that if we consider the free path length as a function of the average energy $\overline{\epsilon}$ of the exciton, then the change in x has not only an upper limit but also a lower limit:

$$x > (3\mu_{\mathrm{ex}} a_{\mathrm{ex}}^2 / \hbar^2)\, \hbar\omega_0. \tag{15a}$$

If we consider $\mu_1 = \mu_2 = m_e$ and $\varkappa^2 \approx 5$, then the order of the interval in which x lies is from 0.01 to 1.

For low temperatures ($k_0 T \ll \hbar\,\omega_0$) the possible values of q for phonons interacting with excitons lie in the narrow interval (8a). Thus, the magnitude of $\beta_{1,2}^2 q^2$ in $Q(q)$ [see Eq. (12a)] is equal, in order of magnitude, to

$$\beta_{1,2}^2 q^2 \approx \beta_{1,2}^2 \frac{2\mu_{\mathrm{ex}}\omega_0}{\hbar} = \frac{m_e(\mu_1+\mu_2)\varkappa^2}{4\mu_{1,2}^2} \frac{\hbar\omega_0}{V_i}. \tag{16}$$

where $V_i = 13.5$ ev is the ionizing energy of a hydrogen atom. Since $\hbar\,\omega_0$ is of the order of a few hundredths of an electron volt, while the factor $m_e(\mu_1+\mu_2)\varkappa^2/4\mu_{1,2}^2$ is of the order of unity, then (16) is of the order of 10^{-3}.

If, on the other hand, the absolute magnitude of the difference $(1-s)$ is not less than 10^{-2}, that is, if it is larger in order of magnitude than $\beta_{1,2}^2 q^2$, then we may put

$$Q(q) = (1-s)^2. \tag{17}$$

In this case the transition probabilities (12) and (12a) differ from the usual ones only in the constant factors $(1-s)^2$; hence, the calculated free path length of the exciton is equal to[4]:

$$l = \frac{a_0 M}{2\pi\mu_{\mathrm{ex}}} \left(\frac{\hbar\omega_0}{C_1 Ze^2/a_0}\right)^2 e^{\hbar\omega_0/k_0T} \sqrt{\frac{\varepsilon}{\hbar\omega_0}} \frac{1}{(1-s)^2} \tag{18}$$

$$= l_1 \frac{\mu_1}{\mu_1+\mu_2} \frac{1}{(1-s)^2}.$$

Here l_1 is the free path length of an electron with energy equal to the energy of forward movement of the exciton ϵ. If $|1-s| \sim 0.1$ and $\mu_1/(\mu_1+\mu_2) \sim 1$, then l is 100 times as large as l_1. We do not consider the more complicated case where $Q(q)$ may not be replaced by the constant value (17).

It should be noted that for sufficiently low temperatures the free path length of an exciton will probably be determined not by the interaction with the thermal vibrations of the lattice, but by scattering from impurities and defects in the crystal.

We make a remark concerning a localized exciton in a polar crystal, an exciton which is formed, according to Dykman and Pekar[2], only for a large ratio μ_2/μ_1 (or μ_1/μ_2). As these authors have remarked, a heavy particle here acts like a polaron, but a light particle acts like an F-center electron. An analysis of the question indicates that the free path length of such an exciton coincides in order of magnitude with the free path length of a polaron, corresponding to a heavy particle.

---

[1] A. I. Ansel'm and Iu. A. Firsov, J. Exptl. Theoret. Phys. (U.S.S.R.) 28, 151 (1955); Soviet Phys. JETP **1**, 139 (1955).

[2] I. M. Dykman and S. I. Pekar, Trudy Inst. Phys. Acad. Sci., USSR 3, 92 (1952).

[3] G. H. Wannier, Phys. Rev. **52**, 191 (1937).

[4] V. I. Davydov and I. M. Shmushkevich, J. Exptl. Theoret. Phys.(U.S.S.R.) 10, 1043 (1940).

[5] H. Fröhlich, *Elektronentheorie der Metalle*, 1936.

Translated by M. G. Gibbons
146

SOVIET PHYSICS JETP VOLUME 3, NUMBER 4 NOVEMBER, 1956

Phase Diagram for the Liquid-Vapor System of Helium Isotopes (He^3-He^4). I.

B. N. ESEL'SON AND N. G. BEREZNIAK

Physico-technical Institute, Academy of Sciences, Ukrainian SSR

(Submitted to JETP editor, September, 1955)

J. Exptl. Theoret. Phys. (U.S.S.R.) 30, 628-639 (April, 1956)

The temperature dependence of the vapor pressure of twenty solutions of helium isotopes has been measured, with He^3 content varying from 0.4 to 90.8%. Measurements have also been made of the pressure corresponding to initiation of condensation for eight mixtures with He^3 content from 1.9 to 82.4%. The phase diagram of the liquid-vapor system of He^3-He^4 is constructed, and the temperature dependence of the partition of He^3 between liquid and vapor and the concentration of the liquid phase have been determined.

1. INTRODUCTION

HE availability in comparatively large quantities of helium mixtures that are rich in the light isotope[1] has made possible the study of the thermodynamic properties of mixtures of the helium isotopes. In particular, it is possible to obtain data which are necessary to construct phase diagrams for the liquid-vapor system of helium isotopes. Such a diagram is naturally of great interest, not only because it characterizes the properties of binary mixtures of the isotopes, but also because the properties of each of the pure components are associated with quantum effects.[2,3] The adherence of He^3 and He^4 to different statistics, the presence of superfluidity in He^4 and its absence in He^3 accentuates this interest. In addition, knowledge of the phase diagram has great significance for the technology of the separation of He^3 and He^4 [1], and makes possible the calculation of the change of concentration of the liquid phase, due to the transition of part of the He^3 into the vapor phase, in the quantitative investigation of the properties of this system.

Numerous attempts[4-13] at the measurement of the dependence on concentration of the vapor pressure of the mixtures and the distribution coefficient of He^3 between liquid and vapor have not led to sufficiently accurate and complete data. Consequently, they do not permit the construction of the desired phase diagram. This is explained by the fact that, up to the present, only small quantities of the isotopic mixture have been used, the presence of equilibrium between vapor and liquid has not been maintained, and the effect of the HeII film has not been removed.

Having obtained an appreciable amount of mixtures of the helium isotopes with known content of He^3, we set up a series of experiments to obtain sufficiently accurate data, which are necessary for the construction of the phase diagram.

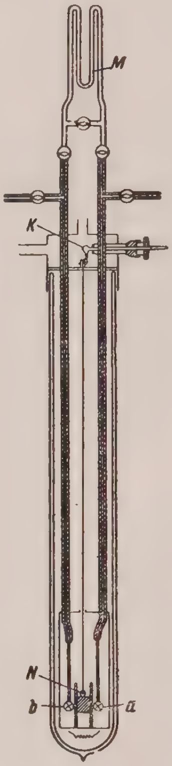

FIG. 1. Apparatus for measuring the vapor pressure of solutions of He^3 in He^4

2. APPARATUS AND METHOD OF MEASUREMENT

Inasmuch as we are discussing the liquid-vapor phase diagram, we must set up the dependence between the vapor pressure and the composition of the liquid and gaseous phases. Such data were obtained by the measurement of the vapor pressure of mixtures with different He^3 content in the liquid in a series of experiments, and by the measurement of the pressure at initial condensation of mixtures with various contents of He^3

in the gaseous phase in another series of experiments.

Measurements of the vapor pressure were carried out with the aid of the apparatus shown in Fig. 1.[14] The mixture of isotopes with known He^3 content and ordinary helium (He^4) were condensed in the two glass globules *a* and *b*, equipped with light iron vanes. These vanes were put into vibratory motion by vertical displacement of the magnet *N*, which is accomplished by means of the crankshaft *K*, rotated by an electric motor at a speed of 12 rpm. The resulting agitation of the liquid led to a rapid establishment of equilibrium between the liquid and the vapor. With the aid of a differential manometer *M*, the difference in the vapor pressure Δp between the solution with known concentration of He^3 and the He^4 was measured. For work with mixtures with He^3 content up to 6.3%, the manometer was filled with oil, while mercury was used for the higher concentrations of He^3. Measurement of the difference in vapor pressure in the manometer was obtained by the cathetometer KM-5, which enabled readings to be made to 0.001 mm. Before condensation, both the mixture of isotopes and the He^4 were led through coils submerged in liquid hydrogen, in which possible impurities were frozen out,so that both gases were completely pure upon entrance into the apparatus.

All parts of the apparatus, located above the globule with the mixture, had sufficiently small volume so that the space occupied by the vapor amounted to about 5 cm.[3] Usually, 350-400 cm^3 of gas were condensed in the research with mixtures with content of He^3 up to 52.7 % and about 200cm^3 in research with richer mixtures. Under such conditions, the impoverishment of the mixture due to the transition of part of the He^3 to the vapor state was inconsiderable and,consequently, one could assume in these experiments that the concentration of He^3 in the liquid was equal to the known concentration of He^3 in the gas up to its condensation. This circumstance was specially controlled by the saturation curves which were recorded at the time of condensation of the mixture of the isotopes, and which represented the dependence of Δp on the quantity *q* of the condensed gas, As the quantity of the mixture increases, a smooth increase in Δp was first observed; however, beginning approximately at 50 cm^3 for low temperatures and with 150-200 cm^3 at high temperatures, Δp is practically unchanged with further increase in *q*. Thus the quantity of the mixture ordinarily used guaranteed the small dependence of Δp on *q*, i.e., the insignificant impoverishment of the mixture with respect to the light isotope.

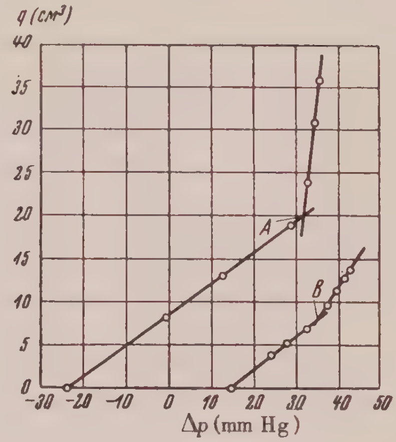

FIG. 2. Dependence of the pressure difference on the quantity of gaseous mixture supplied. The lower part ,of the graphs (up to the break) corresponds to gaseous state, the upper to the liquid. Point *A*: $T = 3{,}229°$ K, $X = 11{,}6\%$ $\Delta p = 31.4$; point *B*: $T = 1{,}865°$K, $X = 73{,}4\%$, $\Delta p = 35.9$

Establishment of equilibrium between the liquid and the vapor was achieved, as already pointed out, by the agitation of the liquid, and was also controlled by the method of reducing the dependence of Δp on time at constant temperature. Such an equilibrium was quickly established both in He II (3 – 4 min.)and in He I (10-15 min.). In addition to the presence of equilibrium between vapor and liquid, one noted the absence of hysteresis in going through the temperature interval above and below. In this case the data obtained in one experiment and on different days agreed very well.

The results obtained with mixtures of different content of He^3, and in a wide temperature interval, made possible the establishment of the relation between the vapor pressure and the concentration of the liquid phase.

The connection between the vapor pressure and the composition of the gas phase was obtained by measurement of the pressure for initial condensation of the gas mixture with known content of the light isotope (dew point).[15] These experiments were carried out with apparatus similar to that already described, adapted for the measurement of the vapor pressure. As before, two vessels were used, but now a definite portion of gas mixture of the isotopes was put in one of them, and liquid He^4 was put in the other. The pressure difference Δp was measured between these two vessels after introduction of each portion of the gas mixture

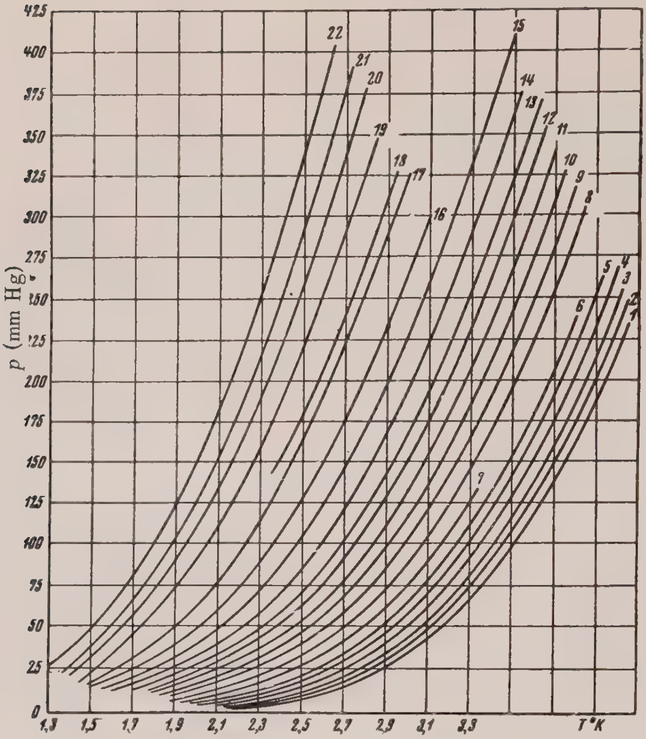

FIG. 3. Temperature dependence of vapor pressure for mixtures of isotopes of helium with different content of He^3. Percent composition of He^3 in the mixture: *1* — 0; *2* — 0,4; *3* — 0,8; *4* — 1 9; *5* — 3,0; *6* — 4,0; *7* — 6,3; *8* — 8,3; *9* — 11.1; *10* — 13.4; *11* — 16,7; *12* — 19,2; *13* — 22,6; *14* — 23.9; *15* — 30.2; *16* — 38,3; *17* — 52.7; *18* — 56.3; *19* — 73,4; *20* — 82,4; *21* — 90,8; *22* — 100,0%

and the dependence of Δp on the amount of the given mixture q was constructed. The sharp break on the curve $\Delta p - q$ makes possible a precise determination of the dew point. It is natural that the measured pressure of onset of condensation is related to the mixture, supplied in the apparatus, for which the He^3 content is known, and it makes no sense to speak of what change there is in the concentration in this case. Two such typical curves are plotted in Fig. 2; one characterizes the mixture with He^3 content 11.6% ($T = 3.229°$ K), and the second, 73.4% ($T = 1.865°$K). Usually, some amount of gas is supplied in the reservoir for the mixture until the pressure is close to the pressure for onset of condensation and only after this is the desired dependence recorded. Thus q in the graphs characterizes not the total amount of the mixture, but only part of it.

The vessel for the measurement of the dew point was changed depending on the concentration of the mixture investigated, since, as the concentration increased, i.e., with higher pressure for onset of condensation, the consumption of the mixture increased greatly. In experiments with mixtures with small amounts of He^3, the volume of the vessel amounted to several cubic centimeters, but for

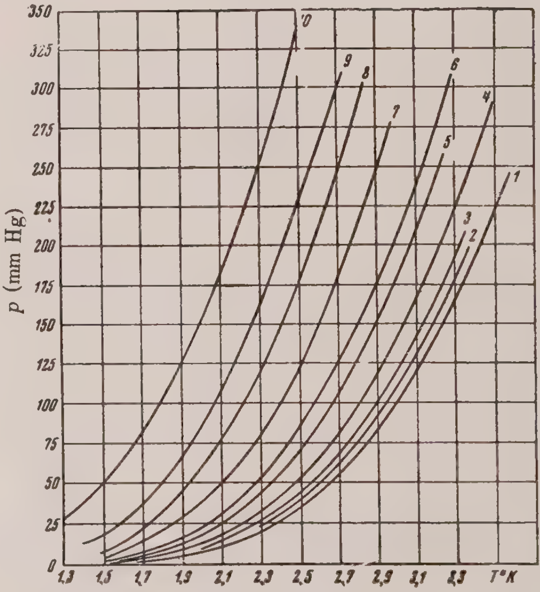

FIG. 4. Temperature dependence of the pressure at onset of condensation of mixtures of helium isotopes with different content of He^3. Percent composition of He^3 in the mixture :

1 — 0; *2* — 1,9; *3* — 4,0; *4* — 11,6; *5* — 29,0; *6* — 35,4; *7* — 57,6; *8* — 73,4; *9* — 82,4; *10* — 100,0%

work with concentrated mixtures--about 1 cm.[3] The data obtained for a given gas mixture at a particular temperature, with the use of reservoirs of different volumes, agreed well with one another.

The manometer for the measurement of Δp was filled with oil for work with low concentrations of the mixtures, and with mercury for rich He^3 mixtures. The measurement was carried out with the same cathetometer KM-5. In order to exclude the effect of the position of the level of liquid helium in the dewar on the pressure in the vessel with the gas mixture, a tube, which joined this vessel with the manometer was embedded in the vacuum jacket.

The gaseous mixture of isotopes was brought into the apparatus by means of a calibrated Toepler pump. In these experiments, the mixture of isotopes and He^4 were run through coils immersed in liquid hydrogen.

The temperature in the dewar was determined by the vapor pressure of the liquid helium with the use of the 1949 tables.[14] Determination of the pressure by the manometer was also carried out in this case with the aid of a cathetometer, which is essential in the region of low temperatures, i.e., for small values of the vapor pressure. During the experiment, the pressure was kept constant with great accuracy, by means of an automatic regulator.[17]

3. RESULTS

By means of the above methods, the temperature dependence of the vapor pressure of twenty mixtures with He^3 content from 0.4 to 90.8% was measured. The pressure at the onset of condensation of eight mixtures with He^3 content ranging from 1.9% to 82.4% was also measured as a function of the temperature. The measurements were carried out in the interval 1.35-3.2°K for mixtures with He^3 content up to 30.2%, and in the interval 1.35-2.7°K for the richer mixtures.

Part of the results obtained, which relate to the dependence of the vapor pressure of the mixture on temperature for different composition X_{liq} of the liquid are represented in the form of Table 1 and in Fig. 3. The analogous dependence for various compositions X_v of the vapor are shown in Table 2 and in Fig. 4 [the concentration was determined as $X = N_3/(N_3 + N_4)$]. For convenience of observation, the curves in Figs. 3 and 4 are successively displaced to the right by 0.04°, except for curve 13 (Fig. 3) which is displaced by 0.08° relative to curve 14. The dependencies for pure He^4 [16] and He^3 [18] have also been drawn in on the same curves for comparison purposes.

The accuracy of measurement of the difference in the vapor pressure was within 0.5% for small values of Δp and was appreciably larger for higher values of Δp. In experiments on the determination of the dew point, Δp was measured with less accuracy (2-3%). The concentrations of the isotope mixtures were known within 1.5-4% of the measured values.

The resultant data permit us to construct the phase diagram for the vapor-liquid system He^3–He^4. Such a diagram is shown in Fig. 5 with the coordinates pressure-concentration. In this drawing, a number of isotherms between 1.4 and 2.6°K are plotted. These isotherms have been displaced arbitrarily along the ordinate axis relative to one another, preserving the scale along this axis (one division corresponds to 25 mm Hg). For each isotherm the pressures for pure He^3 and He^4 are indicated. The reduced diagram, which is essentially the first detailed phase diagram of isotopic mixtures has a cigar shape like the diagrams of

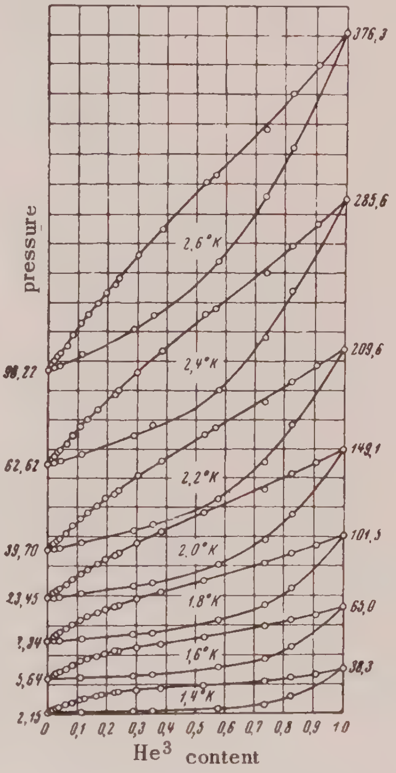

FIG. 5. Liquid-vapor phase diagram for the system of helium isotopes. Pressure in mm Hg.

the majority of ordinary liquid mixtures. In this case, as is seen in Fig. 5, the difference between the content of He^3 in the vapor and in the liquid increases with decrease in temperature.

Among the data in the literature on the vapor pressure and pressure at onset of condensation of He^3-He^4 mixtures, the most complete are those of Sommers,[18] in which measurements were carried out in the interval 1.25-2.15°K for a He^3 content in the liquid phase up to 13%, and in the vapor up to 78%. In Fig. 6 is shown a comparison of the results of the present work with the data of Sommers (crosses) which relate to the dependence of the vapor pressure on the composition of the liquid phase, and in Fig. 7, on the composition of the vapor. In this and in other cases, there is completely satisfactory agreement. Along with this it is necessary to note that the formula assumed by Sommers for the calculation of the concentration of the gaseous phase from the known vapor pressure

$$X_v = (\Delta p / p)[1 + 0{,}080 \times \{T - 1{,}100 + 0{,}600(\Delta p / p)^3\}^2], \qquad (1)$$

provides an inadequate description of the experimental data.

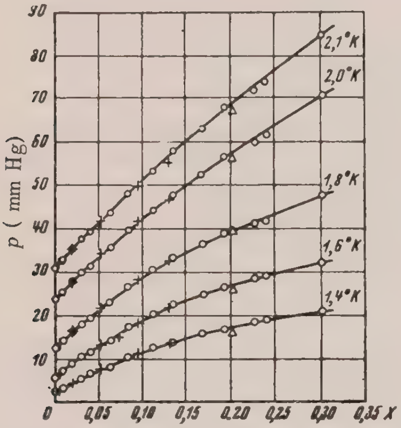

FIG. 6. Dependence of the vapor pressure on the composition of the liquid phase: o= results of the present research, += results of Sommers[19], Δ= results of Weinstock, Osborne and Abraham.[7]

Figure 6 shows the results of measurement of the vapor pressure of mixtures of the isotopes of helium with a He^3 content of 20.3%, carried out by Weinstock, Osborne and Abraham.[7] These results also agree well with ours.

Laying out the phase diagram, one can obtain data which characterize the distribution of He^3 between the vapor and the liquid. Such a distribution is described by the ratio X_v/X_l of the He^3 concentration respectively in the vapor and in the liquid. The dependence of this ratio on the tempera-

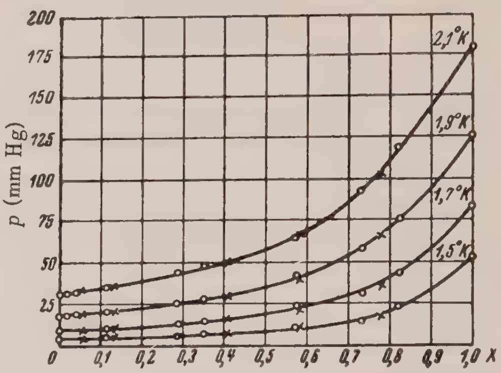

FIG. 7. Dependence of the vapor pressure on the composition of the gaseous phase: o= results of the present research, += results of Sommers.[19]

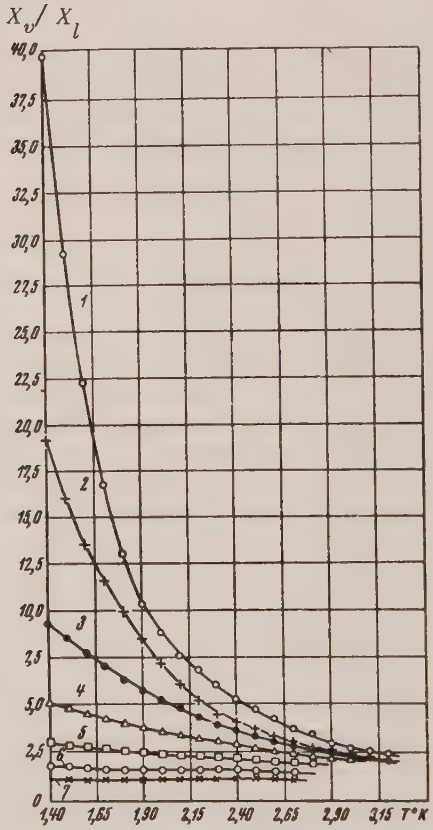

FIG. 8. Temperature dependence of the distribution of He^3 between the vapor and the liquid for different X_l. Curve 1 – X_l = 0.4; 2 – 3.0; 3 – 8.3; 4 – 16.7; 5 – 30.2; 6 – 52.7; 7 – 90.8.

ture for different X_l and on X_l for different temperatures is shown in Figs. 8 and 9. The computed values are given in Table 3. Inasmuch as these data were obtained, not by direct measurement, but from the diagram, the accuracy of the determination of X_v/X_l is not very great. It follows from the drawings that X_v/X_l decreases with rising temperature and with increase in X_l.

It follows directly from the form of the diagram that it differs appreciably from that for an ideal solution. In the entire region of concentration investigated, the vapor pressure is larger than would follow from the generalized rule of Raoult:*

$$p = X_l\ (p_3^0 - p_4^0) + p_4^0, \qquad (2)$$

where p_3^0 and p_4^0 are the vapor tensions of pure He^3 and He^4 respectively.

In the region of low concentrations of He^3, Henry's law is satisfied

$$p_3 = aX_l\ , \qquad (3)$$

where p_3 is the partial pressure of He^3.

For the linear portion of the curve showing the dependence of the vapor pressure on X_l (for small X_l), we can write

$$p = X_l\ (a - p_4^0) + p_4^0 \qquad (4)$$

and we can determine the constant a and its temperature dependence from the tangent of the curve p–X_l. The ratio a/p_3^0 characterizes the departure of the solution from the ideal, inasmuch as this ratio is equal to unity for an ideal solution. The dependence of a/p_3^0 on temperature is shown in Fig. 10, from which it follows that the maximum deviation from ideal is observed at low

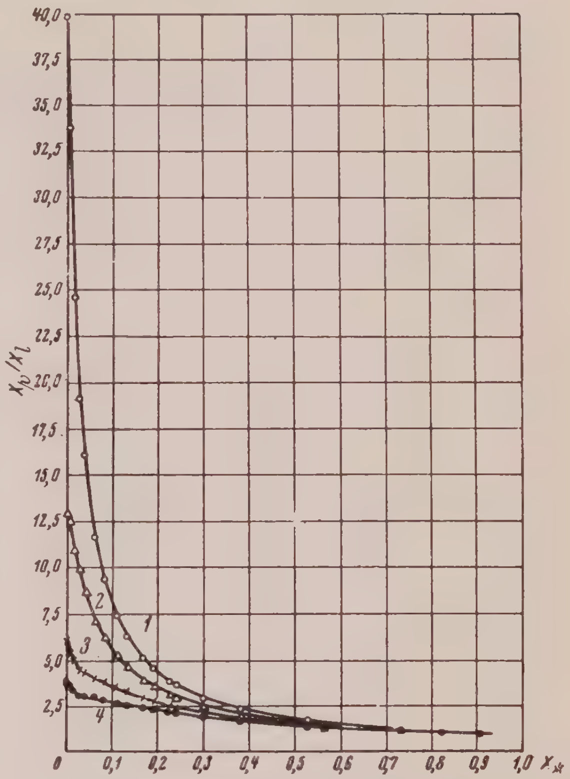

FIG. 9. Dependence of the distribution of He^3 between the vapor and the liquid in the composition of the liquid phase X_l for different temperatures. Curve 1 – T=1.4; 2 – 1.8; 3 – 2.3; 4 – 2.7 °K

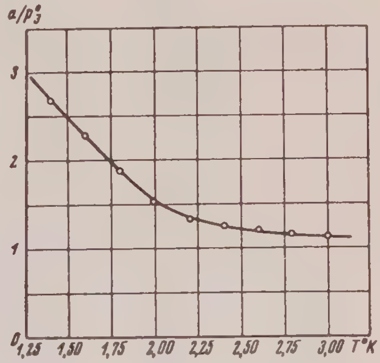

FIG. 10. Temperature dependence of the ratio of the Henry's law constant to the vapor pressure of He^3.

---

*In the earlier works, incorrect concentrations were given (not the fault of the authors). This led to erroneus conclusion of the positive and negative deviations from Raoult's law. We take this occasion to list the correct values:

Published, in %	Corrected concentrations, in %	Literature references
0,49	0,4	[14]
1,00	0,8	[14, 20]
2,40	1,9	[14, 15, 20, 21]
4,23	3,0	[14, 20]
5,18	4,0	[14, 15]
8,08	6,3	[14]

Published, in %	Corrected concentrations, in %	Literature references
14,5	11,6	[15]
31,7	25,8	[21]
34,7	29,0	[15]
37,0	31,2	[21]
41,8	35,4	[15]
63,8	57,6	[15, 21]

TABLE I

Temperature dependence of the vapor pressure (p, mm Hg) for different compositions of the liquid phase (X_l %)

X_l	T	p
0,4	1.377	2,22
	1,387	2,35
	1,489	3,84
	1,594	6.01
	1.675	8,26
	1,755	11,12
	1,836	14.68
	1,918	19,04
	1,993	23.80
	2.070	29,36
	2.124	33.67
	2,172	38,00
	2.201	40.94
	2.301	51.56
	2,406	64.80
	2.554	87.05
	2,694	112.15
	2.793	133.11
	2,902	158,09
	3,051	197,55
	3.104	213.54
	3,202	243.60
	3.211	246.60
0,8	1,358	2.46
	1,563	5,87
	1,634	7,71
	1,763	12,21
	1,815	14.50
	1,927	20,46
	2.008	25.76
	2,105	33.03
	2.126	34.85
	2,153	37.15
	2,165	38.26
	2,171	38,86
	2,175	39,17
	2,181	39.78
	2,188	40,74
	2.208	42,83
	2,248	46,89
	2.380	62,66
	2,449	72,32
	2,548	87.58
	2,748	125,10
	2.815	139.69
	2,900	159,38
	2.902	160.04
	3,003	186,35
	3,050	199,43
	3.052	199.82
	3.167	234.73
	3.202	245.97
1,9	1.358	3,53
	1,377	3,75
	1,495	5.86
	1,572	7,73
	1,668	10.59
	1.743	13,33
	1,815	16,61
	1,877	19 88
	1,978	26,16
	2,037	30,26
	2.102	35,36
	2,149	39,39
	2.163	40,59
	2,177	41,91
	2,203	44,98
	2,223	47,13
	2.298	55.41
	2.424	71,83
	2,533	88.68
	2.608	101,76
	2.696	118.59
	2,740	127,95
	2.790	138.89
	2,914	168,08
	3.073	211.98
	3,217	257,23
3.0	1,377	4,79
	1,387	4,90
	1,549	8,36
	1,572	9,23
	1.644	11.34
	1.721	14,23
	1,836	19,62
	1,977	28,23
	2.053	33,84
	2,093	36.94
	2.102	37,80
	2.144	41,16
	2,175	44,10
	2,197	46,72
	2,249	52.30
	2,348	64,50
	2.460	80,45
	2.513	88,93
	2,635	110,63
	2,752	134.73
	2.850	157,33
	2,979	190.23
	3,124	233,17
	3.197	256,64
4.0	1.358	5.32
	1,358	5,31
	1.495	8,16
	1.559	9.79
	1,655	12.91
	1.745	16.56
	1.855	22,06
	1.939	27,23
	2,039	34.42
	2.120	40,89
	2,169	45,47
	2,191	48,07
	2,202	49,34
	2,254	55,06
	2,397	73,81
	2,468	84,34
	2,485	87,29
	2,549	97,93
	2,671	120,46
	2,799	148,66
	2,950	186,04
	3,105	231,36
6,3	1,358	6,96
	1,489	10,11
	1,618	14,30
	1,718	18,42
	1,828	24,08
	1,958	32,30
	2,008	35,92
	2,159	48,91
	2,183	51,49
	2,194	53,08
	2,258	60,30
	2,336	70,54
	2,428	84,13
	2,525	100,11
	2,603	114,57
	2,665	126,88
	2,701	134,60
8.3	1,352	8,10
	1,358	8,88
	1,483	12,55
	1,598	16,77
	1,696	21,05
	1,851	29,48
	1,983	38,52
	2,085	46,53
	2,107	48,71
	2,144	52,49
	2,172	55,67
	2,187	58,40
	2,207	60,45
	2,248	65,67
	2,402	87,77
	2,565	116,39
	2,720	148,91
	2,881	189,59
	3,023	230,39
	3,206	291,15
	3,219	296,01
11,1	1,354	10,32
	1,363	10,94
	1,461	14,19
	1,467	14,58
	1,542	17,27

TABLE I (continued)

x_l	T	p	x_l	T	p	x_l	T	p
11,1	1,635	21,32		2.384	106.13		3,136	333,87
	1,730	26,16		2.530	134.41		3,211	363,31
	1.842	32.96		2,656	162.07			
	1,936	39,42		2,805	200.80	23,9	1,336	15,54
	2,015	44.96		2,900	228,16		1,362	16,39
	2,020	45,62		3,028	269.00		1,406	18,21
	2,086	51.88		3.155	314.27		1,498	22,65
	2,125	56,13		3,219	339,33		1,579	27,15
	2,148	58.71					1,710	35,07
	2,180	62,49	19,2	1,360	14,61		1,806	41,82
	2.200	65,97		1,379	15,59		1,826	43,10
	2.298	79.37		1,474	19,19		1.873	47,81
	2,476	108.64		1,558	23.60		1,908	51,12
	2,699	154,57		1,650	28,57		1,948	54,97
	2,796	178,77		1,706	32,10		2,038	65,46
	2,904	207.62		1.752	35,06		2,149	80,07
	3,023	243,69		1,839	41,04		2,184	85,28
	3,215	309,33		1,883	44,91		2,198	88,61
				1.930	48,58		2,279	100,87
13,4	1.342	11,63		1,974	53,62		2,458	138,48
	1.399	12,74		2,027	59.13		2,601	171,54
	1,469	15,99		2.081	65.43		2,754	213,45
	1,553	19.64		2,128	71,07		2,885	253,67
	1,628	23,15		2.175	77.42		3,035	305,70
	1,725	28,48		2,233	87,67		3,206	372,35
	1.807	33,34		2,278	94,66			
	1.844	35,89		2.376	111,85	30,2	1,316	16,23
	1,944	42,87		2.469	129,86		1,341	17,11
	1,995	46,88		2,571	152,18		1,380	18,70
	2,045	51,43		2.688	180,74		1.423	21,59
	2,087	56.30		2,799	211,32		1,485	24.60
	2,122	60,15		2,900	241,21		1,537	27,80
	2,156	64.07		2,999	273,69		1,597	31,24
	2,181	67,19		3,107	312,17		1,649	34,40
	2,199	70,59		3,202	348.09		1.722	39,73
	2,301	85,25					1.735	40,71
	2,409	103,12	22,6	1,336	15,14		1,784	45,58
	2,501	119,52		1,353	15.68		1,830	49,96
	2,600	140,17		1,460	20,74		1.911	58,94
	2,701	163,41		1,502	22,80		1,972	66,74
	2,802	189,58		1,554	25,64		1,992	69,14
	2,884	212,07		1,646	30,52		2,069	79,85
	3,063	267,83		1.704	33.99		2,126	88,03
	3,215	321,79		1,802	40.58		2,170	95,37
				1,831	42,53		2,202	102,22
16,7	1,388	14,86		1,864	45.14		2,218	105,97
	1,463	17,84		1,905	48,88		2,302	121,12
	1.496	19,23		1,968	55,53		2,375	135,95
	1,596	23,86		2,007	59.75		2,508	166,50
	1,701	29.80		2,068	66,98		2,655	205,91
	1,771	34,01		2,101	71,32		2,773	241,97
	1,849	39.14		2,126	74,71		2,878	276,70
	1,896	42.53		2,173	81.47		3,004	322,59
	1,930	45.06		2,202	86,68		3,102	361,65
	1,955	47.15		2,294	101,82		3,205	404,75
	1,980	49,79		2,414	124,29			
	2,037	55,60		2,474	136,54	38,3	1,331	18,99
	2,107	63,35		2,552	154,02		1,334	18.95
	2,138	67.25		2.611	168.17		1,389	21,76
	2,174	71.79		2,719	196,36		1,422	23,21
	2,189	75,00		2,809	222,64		1,471	25,80
	2,213	78,15		2,906	252,03		1,543	30,11
	2,298	90,91		3,052	301,99		1,570	32.27

TABLE I (continued)

X_e	T	p	X_e	T	p	X_e	T	p
38,3	1,641	37.91		2,163	127.30		2,710	340,66
	1,715	44,94		2,193	136,18			
	1.757	49,06		2.254	150,86	82,4	1,380	28.56
	1,804	53,89		2.330	171.00		1,392	30.15
	1,857	60,38		2.390	186,91		1.490	41.09
	1,949	72,69		2,474	211.68		1,595	53,71
	2.046	86,79		2,540	232.01		1,694	68.86
	2,090	94,65		2,617	257,47		1,808	88,66
	2.141	102,24		2,669	275.95		1,894	105,38
	2.170	107.71		2.737	301,49		1,996	128.22
	2,194	113,66		2,786	320,42		2,085	149,67
	2,199	114.78					2,176	172.34
	2,253	125.72					2,199	182,17
	2,306	137,19	56,3	2,255	157,26		2,256	199,37
	2,331	142,88		2,352	181,33		2,308	216,63
	2,408	161,34		2.448	208,82		2,400	248,31
	2.488	181,52		2.535	235.80		2,504	287.36
	2,554	199,62		2.629	267,32		2,603	328.42
	2,604	213,13		2,703	294,96		2,695	369.74
	2,680	237,15		2.774	322,21			
	2,757	262,36						
	2,856	296.94	73,4	1.400	27.27	90,8	1,392	31.26
				1,411	26,52		1.405	32.49
52,7	1,350	21,06		1,422	26.89		1.507	45.32
	1,356	21,83		1,515	38.52		1.601	58.41
	1,437	26,70		1,596	48.30		1,678	70,71
	1.471	28,94		1,691	61.06		1.809	94,55
	1.519	34.15		1,806	79,06		1,906	115.67
	1.562	36.58		1.897	95.09		2.004	138,61
	1.592	40.29		2,007	117.08		2,097	163,04
	1.652	45,84		2,108	140.19		2.139	175,30
	1,686	49.87		2,152	150.56		2.182	186,34
	1,728	54,79		2.177	157,95		2.193	192,94
	1,803	64,71		2,194	162.98		2.259	214.74
	1,877	75.24		2,257	181.08		2.303	229,99
	1,944	85,94		2,306	195,48		2,395	263,90
	2,009	97,14		2,404	226,82		2,507	309,00
	2,054	105,32		2,499	259,30		2,586	343,55
	2,106	115.41		2,606	298,89		2,648	371,96

temperatures.

There is great interest in the comparison of the experimental results with the dependence of the equilibrium vapor pressure p on the composition of the liquid and gaseous phases obtained from purely thermodynamic considerations under the assumption of an ideal vapor:[22]

$$X_l = X_v - X_{\text{п}}(1 - X_{\text{п}})\,\partial \ln p / \partial X_{\text{п}}. \qquad (5)$$

The results of such a comparison are shown in Fig. 11. These results are plotted for the isotherms 1.8 and 2.6°K by means of a calculation (according to the above formula) of the dependence of the vapor pressure on the composition of the gaseous phase X_v (the corresponding points are marked with crosses). For low temperatures and small concentrations, satisfactory agreement is observed with experiment, while for high concentrations and higher temperatures, a divergence is observed, occasioned by the non-ideal character of the vapor.[23]

In conclusion, let us take this occasion to express our appreciation to N. E. Alekseevskii and his co-workers for carrying out a great deal of work connected with the determination of the content of He^3 in the helium isotope mixtures that were used. We also thank L. D. Landau and I. M. Lifshitz for their criticism of the results and B. G. Lazarev and E. S. Borovik for their advice.

TABLE 2

Temperature dependence of the pressure for onset of condensation (ρ, mm Hg) for mixtures with different content of He^3 (X_v, %)

X_v	T	p	X_v	T	p	X_v	T	p
1.9	2,037	26,4		1,986	31,5		1,998	51.4
	2.166	37,2		2,349	78.4		2.101	66.5
	2,369	59.7		2.533	112,7		2,444	137,4
	2,520	81,5		2,676	146,3		2,652	204,4
	2,776	129,3		2.826	187,0		2,825	267,4
	3,033	193,5		3,012	248,3			
						73.4	1,451	9,5
4,0	1.748	10,4	35.4	1,404	3,3		1.691	29,6
	2,077	30,2		1,836	21,9		1,865	51,3
	2,411	66,4		2,044	40,2		2,254	127,1
	2,732	122,3		2,159	54,4		2.489	199,3
	3,040	198,7		2,298	76,4		2,731	294,8
				2.516	121,1			
11,6	1,350	1,9		2,706	167,6	82,4	1,412	16,1
	1,795	14,0		2,808	197,0		1,611	30,3
	2,131	38,0		2,899	225,7		1,818	59.0
	2,309	58,7		3,100	299,7		2,106	119.7
	2,628	111,8		3,355	418,6		2,283	173,7
	2,853	164,2					2,404	210.5
	3,229	281,6	57,6	1,433	5,7		2,640	296.3
				1,581	13,8			
29,0	1,410	3,3		1,811	31,5			
	1,768	15,5		1,963	47.8			

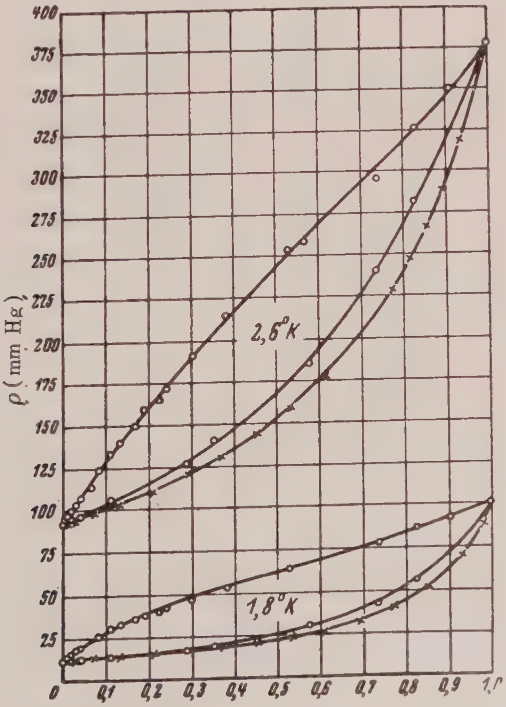

FIG. 11. Phase diagram for liquid-vapor of $He^3 - He^4$. Comparison of the experimental results with Eq. 5. The points obtained by calculation are denoted by crosses.

TABLE 3

Distribution of He^3 between vapor and liquid (X_v/X_l) for different compositions of the liquid phase X_l and for different temperatures.

X_l	X_v $X_П$																		
	1,4° K	1,5° K	1,6° K	1,7° K	1,8° K	1,9°	2,0° K	2,1° K	2,2° K	2,3° K	2,4° K	2,5° K	2,6° K	2,7° K	2,8° K	2,9° K	3,0° K	3,1° K	3,2° K
0.004	39,75	29.25	22.25	16.75	13.00	10.25	8.75	7,50	6.75	6,00	5,25	4.75	4,25	3,75	3,50	3.00	2,75	2,62	2,50
0.008	33.75	25.62	20,00	15.87	12.62	10.12	8.37	6,87	6.00	5.37	4.75	4.37	4.00	3.62	3.25	3.00	2,75	2.62	2.50
0.019	24.53	19.63	16,05	13.26	11.00	9.21	7.79	6.68	5.74	5,05	4.42	4.05	3.68	3.37	3.05	2.84	2.63	2.47	2.26
0.030	19,17	16.03	13.53	11,57	9,93	8.43	7.10	6.00	5.10	4.43	4.03	3.70	3,30	3,10	2,87	2.67	2,47	2.27	2,07
0.040	16.10	13.82	11,92	10.22	8,67	7.47	6,42	5,50	4.80	4.25	3,97	3.62	3,20	3,07	2,82	2.57	2,40	2,22	—
0,063	11.67	10,43	9,24	8,11	7,11	6.35	5,75	5.21	4.59	3,98	3.75	3,44	3.17	3.00	—	—	—	—	—
0.083	9,34	8.52	7,76	7,04	6.24	5.70	5.22	4.77	4,30	3.87	3,54	3,25	3,04	2.89	2,73	2,54	2.37	2,20	2,06
0.111	7,32	6.76	6,29	5.79	5.33	4,90	4.57	4.19	3,85	3.61	3,31	3,05	2,86	2.71	2.60	2,45	2,31	2,17	2,04
0.134	6.22	5,79	5,42	5,04	4,68	4,36	4.07	3,79	3,51	3.33	3,11	2,90	2,72	2,59	2,48	2,36	2,25	2,14	2,04
0,167	5,12	4,82	4,53	4.24	3,96	3,74	3,53	3,32	3,12	2,99	2,84	2,66	2.52	2,43	2,33	2,19	2,10	—	—
0,192	4.53	4,28	4,03	3,80	3.58	3,39	3,22	3,04	2.87	2,79	2,66	2,50	2,39	2,33	2.23	—	—	—	—
0,226	3,91	3,71	3,52	3,34	3.15	3,01	2,88	2,73	2.61	2,54	2,44	2,33	2,24	2,19	2,10	—	—	—	—
0,239	3,72	3.53	3,36	3.19	3.02	2,89	2.76	2,64	2.53	2,46	2.37	2,27	2.19	2.14	2.05	—	—	—	—
0,302	3,00	2.87	2,75	2,64	2,53	2,44	2,35	2,27	2.20	2,15	2,08	2,03	1.96	1,93	1,87	—	—	—	—
0,383	2,39	2.31	2,24	2.17	2,11	2,05	1,99	1.94	1.90	1,86	1,81	1,78	1,73	1,71	1,68	—	—	—	—
0,527	1,78	1,73	1.69	1,66	1,63	1,61	1,58	1,55	1,53	1,51	1,48	1,47	1,44	1,43	1,41	—	—	—	—
0,563	—	—	—	—	—	—	—	—	1,46	1,44	1,42	1,41	1,39	1,37	1.36	—	—	—	—
0,734	1.31	1,29	1.28	1,26	1,26	1,24	1.23	1.22	1,21	1.20	1.20	1,19	1,18	1,17	—	—	—	—	—
0,824	1,18	1,17	1,16	1,15	1,15	1,14	1,14	1,13	1,12	1.12	1.12	1,11	1,11	1,10	—	—	—	—	—
0,908	1.09	1.08	1,08	1.07	1,07	1,07	1.06	1,06	1,06	1.06	1,05	1,05	1.05	1,05	—	—	—	—	—

[1] B. N. Esel' son and B. G. Lazarev, J. Exptl. Theoret. Phys. (U.S.S.R.) 20, 742 (1950).

[2] L. D. Landau, J. Exptl. Theoret. Phys. (U.S.S.R.) 11, 592 (1941).

[3] I. Ia. Pomeranchuk, J. Exptl. Theoret. Phys. (U.S.S.R.) 20, 919 (1950).

[4] H. A. Fairbank, C. A. Reynolds, C. T. Lande, B. B. McInteer, L. T. Aldrich and A. O. Nier, Phys. Rev. 74, 345 (1948).

[5] K. W. Taconis, J. J. M. Beenakker, A. O. Nier and L. T. Aldrich, Physica 15, 733 (1949).

[6] B. N. Esel'son, B. G. Lazarev and N. E. Alekseevskii, J. Exptl. Theoret. Phys. (U.S.S.R.) 20, 1055 (1950).

[7] B. Weinstock, D. W. Osborne and B. M. Abraham, Phys. Rev. 77, 400 (1950).

[8] J. G. Daunt and C. V. Heer, Phys. Rev. 86, 205 (1952).

[9] H. A. Fairbank, C. T. Lane, L. T. Aldrich and A. O. Nier, Phys. Rev. 71, 911 (1947).

[10] H. A. Fairbank, C. T. Lane, L. T. Aldrich and A. O. Nier, Phys. Rev. 73, 729 (1948).

[11] B. V. Rollin and J. Hatton, Phys. Rev. 74, 508 (1948).

[12] J. G. Daunt, R. E. Probst and S. R. Smith, Phys. Rev. 74, 495 (1948).

[13] Lane, Fairbank, Aldrich and Nier, Phys. Rev. 75, 46 (1949).

[14] B. N. Esel' son, J. Exptl. Theoret. Phys. (U.S.S.R.) 26, 744 (1954).

[15] B. N. Esel'son and N. G. Berezniak, J. Exptl. Theoret. Phys. (U.S.S.R.) 27, 648 (1954).

[16] H. Van D

[16] H. van Dijk and D. Shoenberg, Nature 164, 151 (1949).

[17] N. E. Alekseevskii and A. I. Shal'nikov, J. Exptl. Theoret. Phys. (U.S.S.R.) 16, 361 (1946).

[18] Abraham, Osborne and Weinstock, Phys. Rev. 80, 366 (1950).

[19] H. S. Sommers, Phys. Rev. 88, 113 (1952).

20

[18] Abraham, Osborne and Weinstock, Phys. Rev. 80, 366 (1950).

[19] H. S. Sommers, Phys. Rev. 88, 113 (1952).

[20] B. N. Esel'son and N. G. Berezniak, Dokl. Akad. Nauk SSSR 98, 569 (1954).

[21] B. N. Esel'son and B. G. Lazarev, Dokl. Akad. Nauk SSSR 97, 61 (1954).

[22] L. D. Landau and E. M. Lifshitz, *Statistical Physics*, Gostekhteoretizdat, 1951, p. 301.

[23] Kilpatrick, Keller and Hammel, Phys. Rev. 94, 1103 (1954).

Translated by R. T. Beyer
133

SOVIET PHYSICS JETP VOLUME 3 NUMBER 4 NOVEMBER, 1956

Point Charge Interaction Energy in Ionic Crystals

T. I. LIBERBERG-KUCHER
Zhitomir Pedagogical Institute

(Submitted to JETP editor January 15, 1955)
J. Exptl. Theoret. Phys. (U.S.S.R.) 30, 724-733 (April, 1956)

The interaction energy of two charges located in an ionic crystal is calculated in a macroscopic way. The ions are considered fixed at the lattice points; only the noninertial polarization component of the crystal is taken into account. The result depends on the sign of the charges and for large separations the interaction is of the Coulomb type. If the charges are localized on neighboring ions, the result differs in the mean from the Coulomb energy by 17-20%. The polarization energy of the crystal due to the field of a point charge located at one of the lattice points is calculated in this same approximation for KCl.

IN the works of Pekar and his colleagues[1-3] on the investigation of the local states of the electron in ionic crystals, consideration of the polarization of the crystal in the field of a point charge or ionic vacancy (at an *F*-center) plays a great role. A macroscopic expression for the electronic polarization[1] is determined with the help of the coefficient $C = (1/n^2) - 1/\epsilon$ which appears as the basic parameter of the theory. Since the results are subsequently applied to states with effective radii comparable with the lattice constant or even equal to it, there is interest in an estimate of the admissibility of such a method. This is the more essential, that the basic contribution in the polarizing field is made precisely by the near ions, to the determination of the polarization of which the macroscopic method is less applicable.

The author, on the suggestion of K. B. Tolpygo, has considered the problem of the electrostatic interaction energy of two charges which are located in a crystal, and its dependence on the distance between them. The ions are assumed to be fixed at the lattice points (noninertial polarization). The calculations are carried out by a macroscopic method. The extra electron (or hole), in accordance with the chosen approximation, is considered to be localized on the ions of corresponding sign.

Mott and Littleton[4], and also DuPre and others[5] have computed the work of noninertial polarization, performed in transporting a point charge into the ionic crystal, and also the potential which arises at the point where the charge is located. These authors have shown the great role of these quantities in the theory of electrolytic conductivity[5], absorption spectra, color centers and electron emission. However, the method of successive approximations of Mott and Littleton is not successful in our case. Results computed with accuracy to 10th order do not permit us to determine the limit to which they converge.

In the present work, there is given another, completely independent method for the determination of the above-mentioned quantities, which can also be applied to the calculation of the dipole moments of the ions of the polarized crystal. For numerical calculation, the crystal KCl was chosen, for which all the necessary parameters are known, and which is frequently employed in experimental researches.

1. ARRANGEMENT OF THE PROBLEM AND METHOD OF CALCULATION

We introduce two point charges q_1 and q_2 in the ionic crystal; as a result, the crystal is polarized. If the ions are fixed at the lattice points then only non inertial polarization results, which is connected with deformations of the electron shells of the ions and with the appearance of the electric field E of the polarized ions.

The dipole moment p_s^l of an ion of type s located in the lth cell of the crystal can be represented approximately as the sum

$$\mathbf{p}_s^l = \mathbf{p}_{1s}^l + \mathbf{p}_{2s}^l \tag{1}$$

of the dipole moments associated with the charges q_1 and q_2 separately. We represent the field similarly:

$$\mathbf{E}(\mathbf{r}) = \mathbf{E}_1(\mathbf{r}) + \mathbf{E}_2(\mathbf{r}). \tag{2}$$

The total electrostatic energy U of the crystal as a function of the distance $\mathbf{R}$ between the charges q_1 and q_2, with consideration of Eqs. (1) and (2), will be equal to

$$U(\mathbf{R}) = U_1 + U_2 + U_{1,2}(\mathbf{R}), \tag{3}$$

where

$$U_1 = \sum_s \sum_l \left\{ \frac{(\mathbf{p}_{1s}^l)^2}{2\alpha_s} - \mathbf{p}_{1s}^l \left[\frac{1}{2} \mathbf{E}_1(\mathbf{r}_s^l) + \frac{q_1 \mathbf{r}_{1s}^l}{r_{1s}^l} \right] \right\} \tag{4}$$

is the characteristic energy of the charge q_1 (the

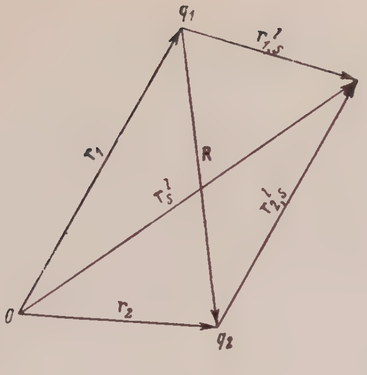

FIG. 1

energy necessary to insert q_1 in the crystal). A similar expression exists for U_2;

$$U_{1,2}(\mathbf{R}) = \frac{q_1 q_2}{R} + 2\sum_s \sum_l \left\{ \frac{(\mathbf{p}_{1s}^l \mathbf{p}_{2s})}{2\alpha_s} - \mathbf{p}_{1s}^l \left[\frac{1}{2}\mathbf{E}_2(\mathbf{r}_s^l) + \frac{q_2 \mathbf{r}_{2s}^l}{r_{2s}^l} \right] + \mathbf{p}_{2s}^l \left[\frac{1}{2}\mathbf{E}_1(\mathbf{r}_s^l) + \frac{q_1 \mathbf{r}_{1s}^l}{r_{1s}^l} \right] \right\} \tag{5}$$

is the interaction energy of charges q_1 and q_2, α_s = polarizability of the ion of type s; for the vector notation, see Fig. 1. Summation in l is carried out over all cells of the fundamental region of the crystal, the number of which we set equal to M. The aim of the present work is the calculation of the energies of Eqs. (4) and (5).

For further calculations, we expand all quantities in Fourier series:

$$\mathbf{p}_s^l = \sum_{\mathbf{k}} \mathbf{p}_{s,\mathbf{k}} \exp\{i\mathbf{k}\mathbf{r}_s^l\}; \tag{6}$$

$$\mathbf{E}(r_s^l) = \sum_{\mathbf{k}} \mathbf{E}_{s,\mathbf{k}} \exp\{i\mathbf{k}\mathbf{r}_s^l\};$$

$$\frac{q}{r_s^{l\,3}}\mathbf{r}_s^l = \sum_{\mathbf{k}} \vec{\rho}_{s,\mathbf{k}} \exp\{i\mathbf{k}\mathbf{r}_s^l\}.$$

Evidently*,

$$\mathbf{p}_s^l = \alpha_s \left[\mathbf{E}(\mathbf{r}_s^l) + \frac{q}{r_s^{l3}} \mathbf{r}_s^l \right]. \tag{7}$$

It also follows from Eqs (5) and (7) that

$$\mathbf{p}_{s,\mathbf{k}} = \alpha_s [\mathbf{E}_{s,\mathbf{k}} + \vec{\rho}_{s,\mathbf{k}}]. \tag{8}$$

Substituting Eq. (6) in Eqs. (4) and (5), and considering that

$$\sum_l e^{i(\mathbf{k}+\mathbf{k}')\mathbf{r}_s^l} = M\delta_{\mathbf{k},\,-\mathbf{k}'}, \tag{9}$$

we find U_1 and $U_{1,2}$, expanded in Fourier series.

2. DETERMINATION OF THE FIELD E AND $\vec{\rho}$

The field created by the dipole plane wave

$$\mathbf{p}_s^l = \mathbf{p}_s \exp[i\mathbf{k}\mathbf{r}_s^l - i\omega t],$$

was represented by Ewald[7] in the form of two rapidly converging series which we write out here in view of the presence of a misprint in Ref. 7. The **k**th component of the field **E** in Eq. (6) is

$$\mathbf{E}_{\mathbf{k}} = \operatorname{grad}\operatorname{div}\mathfrak{P}_{\mathbf{k}} - \frac{1}{c^2}\ddot{\mathfrak{P}}_{\mathbf{k}}, \tag{10}$$

where $\mathfrak{P}_{\mathbf{k}}$ is the Hertz vector[8]:

$$\mathfrak{P}_{\mathbf{k}}(\mathbf{r}_s^l, t) = \sum_{s'} \sum_{l'}{}' \frac{\mathbf{p}_{s'\mathbf{k}}^{l'}}{|\mathbf{r}_s^l - \mathbf{r}_{s'}^{l'}|} \times \exp\left\{ i\omega\left(t - \frac{1}{c}|\mathbf{r}_s^l - \mathbf{r}_{s'}^{l'}|\right) + i\mathbf{k}\mathbf{r}_{s'}^{l'} \right\} = e^{i\omega t}\{e^{i\mathbf{k}\mathbf{r}_s}\mathbf{p}_{s,\mathbf{k}}\overline{S}_l(\mathbf{r}_s^l - \mathbf{r}_s) + e^{i\mathbf{k}\mathbf{r}_{s'}} S(\mathbf{r}_s^l - \mathbf{r}_{s'})\}. \tag{11}$$

Here

$$S \equiv S_{\mathbf{k}}(\mathbf{r}) = \sum_{l'} \frac{1}{|\mathbf{r}^{l'} - \mathbf{r}|} \times \exp\{i\frac{\omega}{c}|\mathbf{r} - \mathbf{r}^{l'}| + i\mathbf{k}\mathbf{r}^{l'}\}, \tag{12}$$

and $\overline{S}_l$ differs from S by the absence of a term with $l' = l$. Ewald transformed S and $\overline{S}_l$ into the rapidly converging series:

$$S(\mathbf{r}) = \frac{2}{\sqrt{\pi}} \times \sum_l e^{i\mathbf{k}\mathbf{r}^l} \int_\varepsilon^\infty \exp\left\{ -|\mathbf{r} - \mathbf{r}^l|^2 x^2 + \frac{K_0^2}{4x^2} \right\} dx + \frac{4\pi}{\Delta} \sum_l \frac{\exp\{-(\mathbf{K}_l^2 - K_0^2)/4\varepsilon^2 + i(\mathbf{K}_l\mathbf{r})\}}{\mathbf{K}_l^2 - K_0^2} \tag{13}$$

where the following notation is used: $K_0 = \omega/c$, $\mathbf{K}_l = 2\pi\mathbf{h}_l + \mathbf{k}$, $\mathbf{h}_l$ is the arbitrary vector of the inverse lattice;

---

* This same relation was proved in Ref. 6 by considering the crystal as a polyelectron problem in the approximation of Heitler-London-Heisenberg.

$$S_l(\mathbf{r}) = S(\mathbf{r}) - i\frac{\sin(K_0|\mathbf{r}-\mathbf{r}^l|)}{|\mathbf{r}-\mathbf{r}_l|} \tag{14}$$

$$- \frac{1}{2|\mathbf{r}-\mathbf{r}^l|}\left\{e^{iK_0|\mathbf{r}-\mathbf{r}^l|}\,\Phi\left(|\mathbf{r}-\mathbf{r}^l|\varepsilon+\frac{iK_0}{\varepsilon}\right)\right.$$

$$\left.+\,e^{-iK_0|\mathbf{r}-\mathbf{r}^l|}\,\Phi\left(|\mathbf{r}-\mathbf{r}^l|\varepsilon-\frac{iK_0}{\varepsilon}\right)\right\},$$

Φ = proability integral:

$$\Phi(x) = \frac{2}{\sqrt{\pi}}\int_0^x e^{-t^2}\,dt.$$

The result is independent of the choice of ϵ, $\Delta = d^3/4$ is the volume of the elementary cell.

After substitution of Eq. (13) and (14) in Eq. (11), and the result in Eq. (10), we find the components of the expansion of the field E in a Fourier series in the wave numbers k:

$$\mathbf{E}_\mathbf{k}(r_s^l) = e^{-i\omega t+i\mathbf{k}\mathbf{r}_s^l}\left\{\frac{4}{3\sqrt{\pi}}\varepsilon^3\mathbf{p}_s - \frac{4}{\sqrt{\pi}}p_s\sum_{l'\neq l}\int_\varepsilon^\infty x^2\exp\{-|\mathbf{r}^l-\mathbf{r}^{l'}|^2x^2+i\mathbf{k}[\mathbf{r}^{l'}-\mathbf{r}^l]\}\,dx\right.$$

$$+\frac{8}{\sqrt{\pi}}\sum_{l'\neq l}{}'(\mathbf{p}_s[\mathbf{r}^l-\mathbf{r}^{l'}])(\mathbf{r}^l-\mathbf{r}^{l'})\int_\varepsilon^\infty x^4\exp\{-|\mathbf{r}^l-\mathbf{r}^{l'}|^2x^2+i\mathbf{k}(\mathbf{r}^{l'}-\mathbf{r}^l)\}\,dx$$

$$-\frac{4\pi}{\Delta}\sum_{l'}\frac{(\mathbf{p}_s\mathbf{K}_{l'})\mathbf{K}_{l'}}{\mathbf{K}_{l'}^2-K_0^2}\exp\{-(\mathbf{K}_{l'}^2-K_0^2)/4\varepsilon^2\}$$

$$-\frac{4}{\sqrt{\pi}}p_{s'}\sum_{l'}\exp\{i(\mathbf{k}[\mathbf{r}_{s'}^{l'}-\mathbf{r}_s^l])\}\int_\varepsilon^\infty x^2\exp\{-|\mathbf{r}_s^l-\mathbf{r}_{s'}^{l'}|^2x^2\}\,dx \tag{15}$$

$$+\frac{8}{\sqrt{\pi}}\sum_{l'}(\mathbf{p}_{s'}[\mathbf{r}_s^l-\mathbf{r}_{s'}^{l'}])(\mathbf{r}_s^l-\mathbf{r}_{s'}^{l'})\int_\varepsilon^\infty x^4\exp\{-x^2|\mathbf{r}_s^l-\mathbf{r}_{s'}^{l'}|^2+i\,\mathbf{k}(\mathbf{r}_{s'}^{l'}-\mathbf{r}_s^l)\}\,dx$$

$$-\frac{4\pi}{\Delta}\sum_{l'}\exp\{-(\mathbf{K}_{l'}^2-K_0^2)/4\varepsilon^2+i\mathbf{q}_{l'}(\mathbf{r}_s-\mathbf{r}_{s'})\}\frac{(\mathbf{p}_{s'}\mathbf{K}_{l'})\mathbf{K}_{l'}}{\mathbf{K}_{l'}^2-K_0^2}$$

$$\left.+\frac{4\pi}{\Delta}\frac{\omega^2}{c^2}\frac{(\mathbf{p}_s+\mathbf{p}_{s'})}{(\mathbf{k}^2-K_0^2)}\exp\{-(\mathbf{k}^2-K_0^2)/4\varepsilon^2\}\right\}.$$

If, in accordance with the above, we set $\epsilon = \sqrt{2\pi}/d$, the lattice vectors $\mathbf{a}_1 = (d/2)(j+\mathbf{k})$, $\mathbf{a}_2 = (d/2)(\mathbf{i}+\mathbf{k})$, $\mathbf{a}_3 = (d/2)(\mathbf{i}+\mathbf{j})$, choose the origin of the coordinates in ion K^+, and the radius vectors $\mathbf{r}_s$ and $\mathbf{r}_{s'}$ equal to $\mathbf{r}_1 = 0$, $\mathbf{r}_2 = (d/2)\times(\mathbf{i}+\mathbf{j}+\mathbf{k})$, then, substituting these in Eq. (15), we obtain the expansion coefficients of E in the Fourier series in k:

$$\mathbf{E}_\mathbf{k} = a^{-3}\Phi_\mathbf{k}\mathbf{P}_\mathbf{k} = 8d^{-3}\Phi_\mathbf{k}\mathbf{P}_\mathbf{k}, \tag{16}$$

where $\Phi_\mathbf{k}$ is a symmetric matrix of 6th order with elements $\Phi_{ss'xy}$ and $\mathbf{E}_\mathbf{k}$ and $\mathbf{P}_\mathbf{k}$ are six-dimensional vectors with components $E_{\mathbf{k}sx}$ and $p_{\mathbf{k}sx}$ ($s = 1,2$; $x = x, y, z$) which are the totality of two corresponding three-dimensional vectors of the field and the dipole moment, which correspond to the two types of ions.

The elements of the matrix $\Phi_\mathbf{k}$ were considered in Ref. 8 only for eight points of k, which is quite insufficient for further calculations. Therefore, the author has again calculated the matrix $\Phi_\mathbf{k}$ for 29 values of the wave vector k, which makes possible the calculation of the field $\mathbf{E}_{s,\mathbf{k}}$ and the dipole moments $\mathbf{p}_{s,\mathbf{k}}$ at 729 points of the cell of the inverse lattice. The results are given in Table I.

The Fourier components $\vec{\rho}\,^{(j)}_{s,\mathbf{k}}$ of the field of a point charge localized on the ion of type j in the place where an ion of type s is located are considered in similar fashion. Since this calculation has not been performed earlier, we carry it out in some detail.

We obtain from Eq. (6) the kth coeefficient of the series expansion of the field of the point charge q in the usual way. For convenience we temporarily set q at an arbitrary point $\mathbf{r}$ (not at a lattice point). Then

TABLE I. The matrices $\Phi_k \cdot 10^3$

№	$\varkappa_x$	$\varkappa_y$	$\varkappa_z$	φ_{ssxx}	φ_{ssyy}	φ_{sszz}	φ_{ssxy}	φ_{ssxz}	φ_{ssyz}	$\varphi_{ss'xx}$	$\varphi_{ss'yy}$	$\varphi_{ss'zz}$	$\varphi_{ss'xy}$	$\varphi_{ss'xz}$	$\varphi_{ss'yz}$
1	0	0	1/4	1954	1954	—3908	0	0	0	2331	2331	—4662	0	0	0
2	0	0	1/2	1605	1605	—3210	0	0	0	2912	2912	—5825	0	0	0
3	1/4	1	1	—2479	1240	1240	0	0	0	7017	—3509	—3509	0	0	0
4	0	0	1	1083	1083	—2167	0	0	0	3760	3760	—7520	0	0	0
5	0	1/4	1/4	1780	—890	— 890	0	0	—2938	2598	—1299	—1299	0	0	—2576
6	0	1/4	1/2	1343	676	—2019	0	0	—2035	3260	1122	—4382	0	0	—1498
7	0	1/4	3/4	878	934	—1812	0	0	— 991	3948	2270	—6218	0	0	— 592
8	0	1/4	1	677	935	—1612	0	0	0	4242	2650	—6891	0	0	0
9	0	1/2	1/2	669	—335	— 335	0	0	—2132	4140	—2070	—2070	0	0	—1328
10	1/4	1/2	1	— 479	547	— 68	—1222	0	0	4556	526	—5082	618	0	0
11	0	1/2	1	— 394	788	— 394	0	0	0	5493	0	—5493	0	0	0
12	1/8	1/8	1/8	0	0	0	—2052	—2052	—2052	0	0	0	—1943	—1943	—1943
13	1/4	1/4	1/4	0	0	0	—1950	—1950	—1950	0	0	0	—1503	—1503	—1503
14	3/8	3/8	3/8	0	0	0	—1849	—1849	—1849	0	0	0	— 822	— 822	— 822
15	1/2	1/2	1/2	0	0	0	—1808	—1808	—1808	0	0	0	0	0	0
16	1/8	1/8	3/8	1251	1251	—2502	— 559	—1565	—1565	1971	1971	—3941	— 407	—1292	—1292
17	1/8	1/8	5/8	1181	1181	—2363	— 273	— 843	— 843	2955	2955	—5910	— 49	— 555	— 555
18	1/8	1/8	7/8	973	973	—1946	— 219	— 272	— 272	3519	3519	—7039	62	— 148	— 148
19	1/8	3/8	3/8	1096	—548	— 548	— 928	— 928	—2492	2772	—1386	—1386	— 535	— 535	—1803
20	1/8	3/8	5/8	639	456	—1094	— 621	— 689	—1741	3756	510	—4265	— 29	— 258	—1004
21	1/8	3/8	7/8	235	730	— 964	— 556	— 251	— 608	4439	1448	—5886	203	— 60	— 288
22	3/8	3/8	5/8	209	209	— 418	—1495	—1560	—1560	1524	1524	—3047	124	— 402	— 402
23	1/8	5/8	5/8	— 248	124	124	— 602	— 602	—1470	4963	—2481	—2481	77	77	— 669
24	1/4	1/4	1/2	638	638	—1276	—1068	—1720	—1720	1668	1668	—3335	— 387	—1040	—1040
25	1/4	1/4	3/4	640	640	—1281	— 810	— 928	— 928	2766	2766	—5531	149	— 411	— 411
26	1/4	1/4	1	566	566	—1132	— 774	0	0	3167	3167	—6334	315	0	0
27	1/4	1/2	1/2	327	—163	— 163	—1313	—1313	—1966	2876	—1438	—1438	— 230	— 230	— 913
28	1/4	1/2	3/4	— 204	409	— 204	—1206	— 867	—1206	4055	0	—4055	385	0	— 385

$$\rho^{(r)}_{j,\,\mathbf{k}} = \frac{1}{M}\sum_{l'}\frac{\mathbf{r}_j^{l'}-\mathbf{r}}{|\mathbf{r}_j^{l'}-\mathbf{r}\,|^3}\,e^{-i\mathbf{k}\mathbf{r}_j^{l'}} \tag{17}$$

$$= \frac{1}{M}e^{-i\mathbf{k}\mathbf{r}_j}\,\nabla\sum_{l'}\frac{e^{-i\mathbf{k}\mathbf{r}^{l'}}}{|\mathbf{r}^{l'}-(\mathbf{r}-\mathbf{r}_j)|^3}\,.$$

But the latter, according to Eq. (12) is equal to

$$\frac{1}{M}\,e^{-i\mathbf{k}\mathbf{r}_j}\,\nabla S\,(\mathbf{r}-\mathbf{r}_j)$$

for $K_0 = 0$ (for a static field). Thence, we obtain

$$\vec{\rho}^{\,j}_{j,\mathbf{k}} = q\,\frac{\exp\{-i\,\mathbf{k}\mathbf{r}_j\}}{M}\;\nabla\bar{S}\,(\mathbf{r}-\mathbf{r}_j), \tag{18}$$

$$\vec{\rho}^{\,j}_{j',\,\mathbf{k}} = q\,\frac{\exp\{-i\mathbf{k}\mathbf{r}_j\}}{M}\,\nabla S\,(\mathbf{r}-\mathbf{r}_j),$$

where the upper index refers to the type of ion on which the charge q is placed, and the lower, as usual, denotes the type of ion for which the field is calculated. Carrying out the indicated operations, we get

$$\vec{\rho}^{\,j'}_{j,\,\mathbf{k}} = \frac{q}{M}\,\frac{4}{\sqrt{\pi}} \tag{19}$$

$$\times\sum_{l}\Big\{\mathbf{r}^{l}+\mathbf{r}_j\,\beta_{jj'}\exp\Big\{-i\,\mathbf{k}\mathbf{r}^{l}-i\,\mathbf{k}\mathbf{r}_j\,\beta_{jj'}\Big\}$$

$$\times\int_{\varepsilon}^{\infty}x^2\exp\Big\{-\,|\mathbf{r}^{l}+\mathbf{r}_j\,\beta_{jj'}|^2\,x^2\Big\}\,dx$$

$$+\frac{4\pi i}{\Delta}\sum_{l}\frac{\mathbf{K}_l}{K_l^2}\exp\Big\{-\mathbf{K}_l^2/4\varepsilon^2+i\mathbf{q}_l\,\mathbf{r}_j\,\beta_{jj'}\Big\}\Big\},$$

where $\beta_{jj'} = 1 - \delta_{jj'}$, q_l is the arbitrary vector of the reciprocal lattice, $\mathrm{K}_l = q_l + \mathrm{k}$. As already noted above, ϵ is arbitrary; here we set $\epsilon = \sqrt{2\pi}/d$. The series in Eq. (19) converge rapidly. The charge q was located at the origin of the coordinate system. If the same q were located at a point $\mathbf{R}$, then (see Fig. 1) the entire expression (18) would be multiplied by $e^{i\mathbf{k}\mathbf{R}}$[*].

It is also easy to see that the case of holes differs from that of the excess electron by a change of order and also of the signs for $\vec{\rho}_j$: $\rho^{(1)}_{1\mathbf{k}} = -\vec{\rho}^{\,(2)}_{2\mathbf{k}}$ and $\vec{\rho}^{\,(1)}_{2\mathbf{k}} = -\vec{\rho}^{\,(2)}_{1\mathbf{k}}$.

We replace $\rho_{j\mathbf{k}}$ by the dimensionless quantity $\vec{\Psi}_{j\mathbf{k}}$. Then, setting the origin of the coordinates on the ion at which the charge is localized, we get:

1) Field of the extra electron:

$$\vec{\rho}_{j\mathbf{k}} = (8ie/Md^2)\,\vec{\Psi}_{j\mathbf{k}}, \tag{20}$$

2) Field of the hole:

$$\vec{\rho}_{j\mathbf{k}} = -\,(8ie/Md^2)\vec{\Psi}_{j'\mathbf{k}}, \tag{21}$$

where e is the electronic charge.

The value of Ψ for the 29 values of k were computed by the author and appear in Table II.

3. FOURIER COMPONENTS OF THE IONIC DIPOLE MOMENTS AND THE ENERGY OF THE CHARGES

Substituting Eq. (16) in Eq. (8), we get a system of six equations for the determination of the Fourier coefficients of the dipole moments $p_{j\mathbf{k}}$ of the ions in the external field $\vec{\rho}_{\mathbf{k}}$. In the resultant equations, it is appropriate to transform to the dimensionless quantities $\pi_{j\mathbf{k}}$ and A_j, writing

$$p_{j\mathbf{k}} = (ied/M)\,\pi_{j\mathbf{k}}\,, \tag{22}$$

and

$$\alpha_j = (d^3/8)\,A_j \qquad (j = 1,2):$$

For KCl: $A_1 = 0.02569$ and $A_2 = 0.1087$.

Substituting $\mathrm{p}_{j\mathbf{k}}$ and α_j from Eq. (22) in our set of equations, we finally get

$$C_{\mathbf{k}}\,\vec{\pi}_{\mathbf{k}} = -\,\vec{\Psi}_{\mathbf{k}}\ \ \text{(extra electron)} \tag{23}$$

$$C_{\mathbf{k}}\,\vec{\pi}_{\mathbf{k}} = \quad\vec{\Psi}_{\mathbf{k}}\ \ \text{(hole)}$$

where $C_{\mathbf{k}}$ is a 6th order matrix which differs from $\Phi_{\mathbf{k}}$ only in the diagonal elements:

$$-\,c_{ss'xy} = \varphi_{ss'xy} - (1/A_s)\,\delta_{ss'}\,\delta_{xy} \tag{24}$$

$$(s = 1, 2;\ \ x = x,\ y,\ z),$$

$\vec{\pi}_{\mathbf{k}}$ and $\vec{\Psi}_{\mathbf{k}}$ are six-dimensional (dimensionless) vectors.

For the determination of the dipole moments $\vec{\pi}_{\mathbf{k}}$ the inverse matrices $C_{\mathbf{k}}^{-1}$ were found by the author for 28 values of the wave vector k. Their values are listed in Table III.

For long waves (limiting case k → 0), the vectors $\vec{\rho}_{\mathbf{k}}$ and the matrix $\Phi_{\mathbf{k}}$ were expanded in a series in k by Tolpygo. The $\vec{\pi}_{\mathbf{k}}$ were determined by him for small k. With accuracy up to terms of order k^2, inclusively.

---

[*] All the $\mathrm{p}_{j\mathbf{k}}$ are multiplied by the same factor, which follows from the linearity of Eqs. (8) and (16).

TABLE II. The vectors $\vec{\Psi}_j \cdot 10^4$

№	Ψ_{1x}	Ψ_{1y}	Ψ_{1z}	Ψ_{2x}	Ψ_{2y}	Ψ_{2z}
1	0	0	—37065	0	0	—39138
2	0	0	—14470	0	0	—17451
3	5613	0	0	— 7756	0	0
4	0	0	0	0	0	0
5	0	—17042	—17042	0	—19341	—19341
6	0	— 5024	—10483	0	— 7901	—13809
7	0	— 1192	— 4466	0	— 4696	— 6873
8	0	— 235	0	0	— 4015	0
9	0	— 4569	— 4569	0	— 8790	— 8790
10	2196	1086	0	— 5299	— 6301	0
11	0	0	0	0	— 5658	0
12	—25165	—25165	—25165	—26345	—26345	—26345
13	—10308	—10308	—10308	—12909	—12909	—12909
14	— 4222	— 4222	— 4222	— 8828	— 8828	— 8828
15	0	0	0	— 7749	— 7749	— 7749
16	— 5738	— 5738	—17515	— 7162	— 7162	—20408
17	— 1426	— 1426	— 8188	— 3224	— 3224	—11145
18	— 210	— 210	— 2367	— 2295	— 2346	— 3612
19	— 2554	— 8277	— 8277	— 4373	—11804	—11804
20	— 469	— 2534	— 4912	— 2925	— 7050	— 8574
21	448	— 208	— 1498	— 2524	— 5498	— 3058
22	— 456	— 456	— 2533	— 6888	— 6888	— 7495
23	703	— 1599	— 1599	— 2881	— 6394	— 6394
24	— 3495	— 3495	— 7749	— 6892	— 6892	—11555
25	— 459	— 459	— 3476	— 4759	— 4759	— 6266
26	409	409	0	— 4301	— 4301	0
27	— 745	— 3149	— 3149	— 5591	— 8257	— 8257
28	1384	0	— 1384	— 5248	— 6657	— 5248

$$\vec{\pi}_j = \frac{A_j}{1 - 2\pi A/3}\left\{\vec{\Psi}_j - \frac{2\pi}{3} A_j (\vec{\Psi}_j - \vec{\Psi}_{j'}) \right. \quad (25)$$

$$\left. - \frac{2\pi}{1 + 4\pi A/3} \frac{[A_j \vec{\Psi}_j + A_{j'} \vec{\Psi}_{j'}]\,\vec{\varkappa}}{\vec{\varkappa}^2}\,\vec{\varkappa} \right\},$$

$$\vec{\Psi}_1 = -\frac{\vec{\varkappa}}{\vec{\varkappa}^2} + 1{,}200\,\vec{\varkappa}, \quad (26)$$

$$\vec{\Psi}_2 = -\frac{\vec{\varkappa}}{\vec{\varkappa}^2} + 0{,}295\,\vec{\varkappa}.$$

Here $\vec{\varkappa}$ is the nondimensional wave vector

$$\mathbf{k} = 2\pi(\varkappa_1 \mathbf{b}_1 + \varkappa_2 \mathbf{b}_2 + \varkappa_3 \mathbf{b}_3) = (2\pi/d)\,\vec{\varkappa}, \quad (27)$$

where b_1, b_2 and b_3 are the vectors of the reciprocal lattice of the crystal; $A = A_1 + A_2$. The interval of variation of the components of $\vec{\varkappa}$ runs from $-½$ to $+½$. In the entire work the points of k are designated by $(\varkappa_1, \varkappa_2, \varkappa_3)$ or $(\varkappa_x, \varkappa_y\ \varkappa_z)$. The expansion was carried out for the points $\vec{\varkappa}(1/8, 1/8, 1/8)$ and $\vec{\varkappa}(1/4, 1/4, 1/4)$. The deviation from the computed point values did not exceed 2%.

The dipole moments of all ions can now be calculated at will by simple summation of the Fourier series of the three variables.

In Sec. 1 we obtained Eqs. (4) and (5) for the energy of the charges in the crystal. We substitute p and $\vec{\rho}$ in them. It is easy to show that all the coefficients $\mathbf{E}_\mathbf{k}$, $\mathbf{p}_\mathbf{k}$ and $\vec{\rho}_\mathbf{k}$ are odd in k, i.e., they change sign upon replacement of k by $-$k. Keeping this in mind, we obtain, after substitution of Eqs. (23), (19)-(21) and (16) in the expression for U_1, U_2 and $U_{1,2}$ and some simple transformations:

1) Eigenvalue of the energy of each charge $\pm e$:

$$U = -\frac{4e^2}{Md} \sum_s \sum_k (\vec{\pi}_{s,\,\mathbf{k}} \vec{\Psi}_{s,\,\mathbf{k}}); \quad (28)$$

2) Interaction energy of the two charges ($q \equiv e$ = electronic charge):

a) of the same kind

$$U_{1,2}(\mathbf{R}_{1,2}) \equiv U_{1,2}(\mathbf{R}) \quad (29)$$

$$= \frac{e^2}{R} - \frac{8e^2}{Md} \sum_\mathbf{k} \cos(\mathbf{kR}) \sum_s (\vec{\pi}_{s,\,\mathbf{k}} \vec{\Psi}_{s,\,\mathbf{k}});$$

TABLE III. Inverse matrices $C^{-1} \cdot 10^4$

№	C^{-1}_{11xx}	C^{-1}_{11yy}	C^{-1}_{11zz}	C^{-1}_{11xx}	C^{-1}_{22yy}	C^{-1}_{22zz}	C^{-1}_{11xy}	C^{-1}_{11xz}	C^{-1}_{11yz}	C^{-1}_{22xy}	C^{-1}_{22xz}	C^{-1}_{22yz}	C^{-1}_{12xy}	C^{-1}_{12xz}	C^{-1}_{12yz}	C^{-1}_{12yx}	C^{-1}_{12xz}	C^{-1}_{12zy}	C^{-1}_{12xx}	C^{-1}_{12yy}	C^{-1}_{12zz}
1	276	276	243	1408	1408	793	0	0	0	0	0	0	0	0	0	0	0	0	89	89	—86
2	276	276	254	1357	1357	862	0	0	0	0	0	0	0	0	0	0	0	0	106	106	—119
3	269	277	277	953	1310	1310	0	0	0	0	0	0	0	0	0	0	0	0	162	—122	—122
4	277	277	277	1291	1291	1001	0	0	0	0	0	0	0	0	0	0	0	0	128	128	—183
5	276	257	257	1381	1098	1098	0	0	—16	0	0	—309	0	0	—60	0	0	—60	97	—11	—11
6	276	265	256	1320	1236	973	0	0	—11	0	0	—221	0	0	—40	0	0	—24	114	46	—94
7	276	268	269	1264	1244	1005	0	0	—5	0	0	—115	0	0	—19	0	0	—2	131	76	—151
8	277	269	277	1242	1237	1037	0	0	0	0	0	0	0	0	0	0	0	0	138	86	—176
9	276	259	259	1237	1116	1116	0	0	—11	0	0	—238	0	0	—22	0	0	—22	134	—50	—50
10	268	261	276	1111	1177	1162	—6	0	0	—147	0	0	1	0	0	12	0	0	126	14	—151
11	276	262	276	1133	1188	1133	0	0	0	0	0	0	0	0	0	0	0	0	158	0	—158
12	263	263	263	1203	1203	1203	—12	—12	—12	—216	—216	—216	—48	—48	—48	—48	—48	—48	27	27	27
13	261	261	261	1186	1186	1186	—12	—12	—12	—205	—205	—205	—37	—37	—37	—37	—37	—37	20	20	20
14	259	259	259	1169	1169	1169	—12	—12	—12	—195	—195	—195	—20	—20	—20	—20	—20	—20	10	10	10
15	258	258	258	1162	1162	1162	—11	—11	—11	—191	—191	—191	0	0	0	0	0	0	0	0	0
16	271	271	251	1319	1319	932	—4	—9	—9	—63	—166	—166	—12	—35	—35	—12	—26	—26	77	77	—76
17	273	273	262	1296	1296	948	—2	—4	—4	—36	—94	—94	—4	—18	—18	—4	—6	—6	103	103	—132
18	274	274	274	1267	1267	1008	—2	—1	—1	—32	—32	—32	—2	—6	—6	—2	0	0	118	118	—173
19	272	257	257	1291	1114	1114	—6	—6	—14	—99	—99	—265	—18	—18	—38	—11	—11	—38	98	—23	—23
20	273	261	262	1232	1190	1056	—4	—4	—9	—74	—73	—194	—7	—12	—25	—2	0	—10	121	21	—106
21	274	264	274	1188	1198	1081	—3	—1	—3	—72	—27	—72	—3	—4	—8	2	2	1	136	46	—159
22	261	261	261	1176	1176	1121	—10	—9	—9	—167	—166	—166	—3	—15	—15	—3	1	1	48	48	—82
23	274	263	263	1142	1154	1154	—3	—3	—8	—66	—66	—176	—5	—5	—6	5	5	—6	144	—71	—71
24	265	265	257	1234	1234	1044	—7	—10	—10	—121	—182	—182	—14	—30	—30	—14	—16	—16	61	61	—75
25	268	268	268	1217	1217	1048	—5	—5	—5	—104	—102	—102	—4	—15	—15	—4	1	1	89	89	—141
26	269	269	276	1203	1203	1072	—5	0	0	—104	0	0	—1	0	0	—1	0	0	98	98	—169
27	267	258	258	1198	1140	1140	—8	—8	—11	—140	—140	—213	—14	—14	—16	—2	—2	—16	91	—35	—35
28	268	260	268	1140	1175	1140	—7	—5	—7	—139	—91	—139	—3	—8	—8	8	8	3	116	0	—116

b) of opposite kind

$$U_{1,2}(\mathbf{R}) = -\frac{e^2}{\mathbf{R}} - 4\frac{e^2}{Md}\sum_{\mathbf{k}} \cos(\mathbf{kR}) \qquad (30)$$

$$\times \sum_{s} \{(\vec{\pi}_{e,s,\mathbf{k}} \vec{\Psi}^{*}_{q,s,\mathbf{k}}) + (\vec{\pi}_{q,s,\mathbf{k}} \vec{\Psi}^{*}_{e,s,\mathbf{k}})\},$$

where the indices q and e refer, respectively, to the hole and to the electron.

In the expression for the energy (29) and (39) there occurs summation over the wave vector k or, what amounts to the same thing, over the nondimensional wave vector $\vec{\varkappa}$. The summation is carried out over the interval $\varkappa_i = \pm \frac{1}{2}$, in which it has $N = M^{1/3}$ values: $\varkappa_i = 0; \pm 1/N; \pm 2/N; \ldots \pm \frac{1}{2}$. In view of the large value of N, the summation over $\vec{\varkappa}$ can be replaced by integration over $d\varkappa_1$, $d\varkappa_2 d\varkappa_3$. The integral can be computed by any approximation method. We made use of Simpson's rule.

4. RESULTS OF THE CALCULATION

In view of the tedious nature of the calculation, all the quantities have been found for the minimal R--closest approach of the charges. Like charges are placed on neighboring like ions, with $|\mathbf{R}| = |\mathbf{a}_3| = 2^{-\frac{1}{2}} d$; unlike charges on neighboring ions with $|\mathbf{R}| = d/2$. The results are given in Table IV.

Mott[4] has computed the potential of the field created at the point when the point charge q is located in the crystal polarized by it, and DuPre[5] gave the energy U_q of the charge q in this field.

As would also be expected, on the basis of Eqs. (21) and (22):

$$U_q = qV_q = -q\sum_{s,l} \frac{(\mathbf{p}_s^l \mathbf{r}_s^l)}{r_s^{l3}} \qquad (31)$$

$$= -\frac{8e^2}{Md}\sum_{s,\mathbf{k}} (\vec{\pi}_{s,\mathbf{k}} \vec{\Psi}^{*}_{s,\mathbf{k}}),$$

i.e., U_q differs only by the coefficient 2 from the eigen energy (28) in the case $q = \pm e$.

The eigen energy (28) was computed, as also $U_{1,2}$, and the results obtained for $d = 6.27 \times 10^{-8}$ cm are given in Table V.

Correspondingly, the potential V_q is expressed by the nondimensional quantity V_q/V_0, for the case $V_0 = (q/4\pi d)(1 - n^{-2})$ is equal to

$$\frac{V_q}{V_0} = -\frac{16\pi}{1 - n^{-2}}\sum_{s}\sum_{\mathbf{k}} (\vec{\pi}_{s,\mathbf{k}} \vec{\Psi}^{*}_{s,-\mathbf{k}}). \qquad (32)$$

If we set $n^{-2} = 0.4600$ (for KCl), then we get the results of Table VI. It is easy to verify that, when the charges are entirely separated ($R \to \infty$), we get the Coulomb expression

$$U_{1,2}(\mathbf{R}) = e^2 / Rn^2.$$

The author considers it his pleasant duty to express his gratitude to K. B. Tolpygo for suggesting the theme and for his lively interest in the work.

TABLE IV. Interaction energy $U_{1,2}(\mathbf{R})$

Charges	Interaction Energy		
	in units of $e^2\sqrt{2}/d$	in ev	in % of Coulomb's law
Electron-electron	0.512	1.665	111
Electron-hole	—0.779	—2.553	120
Hole-hole	0.540	1.756	117
Coulomb's law	0.460	1.469	100

TABLE V. Eigenenergy

Charges	according to Mott, in ev	According to the Author	
		cgs units	in ev
Electron	—2.02	—0.2090(4 e^2/d)	—1.922
Hole	—1.44	—0.1470(4e^2/d)	—1.325

TABLE VI. Potential (in arbitrary units)

Charges	According to DuPre et al.				According to the Author
	macroscopic	first approximation	second approximation	third approximation	
Electron	18.96	20.60	20.44	20,27	19.45
Hole	—	—14.69	—	—	—13.69

---

[1] S. I. Pekar, *Investigations on the Electronic Theory of Crystals*, Gostekhizdat, Leningrad-Moscow, 1951, Sec. 5.

[2] M. F. Deigen, J. Exptl. Theoret. Phys. (U.S.S.R.) 18, 818 (1948).

[3] G. E. Zil'berman, J. Exptl. Theoret. Phys. (U.S.S.R.) 19, 135 (1949).

[4] N. F. Mott and M. J. Littleton, Trans. Faraday Soc. 34, 485 (1938).

[5] E. S. Rittner, R. A. Hutner and F. K. DuPre, J. Chem.Phys. 17, 198 (1949).

[6] T. I. Liberberg and K. B. Tolpygo, J. Exptl. Theoret. Phys. (U.S.S.R.) 26, 35 (1954).

[7] P. P. Ewald, Ann. Physik 64, 253 (1951).

[8] I. G. Zaslavskaia and K. B. Tolpygo, Trudy Inst. Fiz. Akad. Nauk, Ukrainian SSR 4, 71 (1953).

[9] M. Born and M. Goeppert-Mayer, *Theory of Solids* (Russian translation) ONTI, Moscow-Leningrad, 1938.

Translated by R. T. Beyer
147

SOVIETPHYSICS JETP VOLUME 3, NUMBER 4 NOVEMBER, 1956

Relativistic Spherical Functions

A. Z. Dolginov
Leningrad Physico-Technical Institute, Academy of Sciences, USSR

(Submitted to JETP editor January 19, 1955)
J. Exptl. Theoret. Phys. (U.S.S.R.) 30, 746-755 (April, 1956)

The finite-dimensional representations of the rotation groups in four-dimensional pseudo-Euclidian and Euclidean spaces are considered. The basis functions which are constructed are eigenfunctions of the four-dimensional angular momentum operator. The Clebsch-Gordon coefficients are calculated. Spinors which are eigenfunctions of the four-dimensional angular momentum operator are determined. The possibility of separating variables in the relativistic two-body problem is discussed briefly.

---

1. STATEMENT OF THE PROBLEM

FOR the nonrelativistic description of the bound state of a two-particle system we choose as wave functions the basis functions of the irreducible representations of the three-dimensional rotation group. These functions are also the eigenfunctions of the angular momentum operator. By analogy with the three-dimensional case, we can construct a system of eigenfunctions of the four-dimensional angular momenta operator, which form the basis for irreducible representations of the Lorentz group, and try to use them for solving the equation of a system of relativistic particles.

If the relativistic equation admits of analytic continuation into the region of pure imaginary values of the relative time, its solution is greatly simplified. In this case one can use the basis functions of the rotation group in Euclidean space. The possibility of analytic continuation for the relativistic two-body equation (equation of the Bethe-Salpeter type) was pointed out by Wick[1]. The four-dimensional spherical functions of a Euclidean space are well known, and were used by Fock[2] for the solution of the problem of the hydrogen atom in momentum representation. They have the form

$$\psi_{nlm}(\alpha, \vartheta, \varphi) = i^l Y_{lm}(\vartheta\varphi) \frac{\sin^l \alpha}{M_l} \frac{d^{l+1} \cos n\alpha}{d(\cos\alpha)^{l+1}}, \quad (1)$$

where α, ϑ, φ are the angles describing the four-dimensional radius vector, and

$$M_l = [n^2(n^2-1^2)\ldots(n^2-l^2)]^{1/2}, \qquad n = 0, 1, 2, \ldots$$

These functions are eigenfunctions of the square of the four-dimensional angular momentum operator L^2 (L^2 is the angular part of the d'Alembertian operator) and can be used as basis functions.

The irreducible finite-dimensional representations of the group can be obtained from the irreducible representations of the group of rotations of four-dimensional Euclidean space by going over to pure imaginary values of the angle α. If in Eq. (1) we simultaneously replace α by $i\alpha$ and n by in, where $0 \leq n \leq \infty$, we get one of the infinite-dimensional representations of the Lorentz group. The infinite-dimensional representations were investigated in general form by Gel'fand and Naimark[3]. A detailed survey of the linear representations of the Lorentz group is contained in a paper of Naimark[4]. According to this work, the representations can be classified by the assignment of two numbers k_0, c. The number k_0 determines the smallest weight of representation of the three-dimensional subgroup which is contained in the (k_0, c) representation of the Lorentz group. The explicit form of the basis functions for one special case with $k_0 \neq 0$ was obtained in a paper of Ginzburg and Tamm[5].

Since we are interested in representations which contain a scalar among the basis functions, we shall consider the case of $k_0 = 0$.

In order to make use of the invariance of equations describing a system of relativistic particles with respect to the choice of the reference system (i.e., with respect to Lorentz transformations), we must know the explicit form of the expansion of a wave function in terms of irreducible representations (Clebsch-Gordan series). The Clebsch-Gordan coefficients for the three-dimensional case are well known[6]. They are obtained for the four-dimensional case in the present paper. If the basis functions are chosen in the form of Eq. (1), then the expansion turns out to be extremely complicated. However, we can make use of the fact that L^2 and l^2 commute with one another, and take our basis functions to be linear combinations of the ψ_{nlm}. Linear combinations for which the Clebsch-Gordan expansion is particularly simple are obtained in a natural way, if we construct the basis functions starting from the spinor representations of the four-dimensional rotation group. These new basis functions prove to be suited for the description of systems of relativistic particles.

2. THE MATRICES OF THE IRREDUCIBLE REPRESENTATIONS OF THE FOUR-DIMENSIONAL ROTATION GROUP

We first construct the finite-dimensional, irreducible representations of the Lorentz group and determine the coefficients in the Clebsch-Gordan expansion. A special feature of this case is the need to consider timelike and spacelike functions separately. If we replace α by $i\alpha$, both of them give equivalent representations of the Euclidean group of four-dimensional rotations.

We introduce, in the four-dimensional pseudo-Euclidean space, the coordinates

$$t = \rho \cosh \alpha, \; r = \rho \sinh \alpha \text{ for } t^2 - r^2 > 0, \tag{2}$$

$$t = \rho \sinh \alpha, \; r = \rho \cosh \alpha \text{ for } r^2 - t^2 > 0. \tag{3}$$

The Lorentz transformation is a rotation of the four-dimensional coordinate system in the pseudo-Euclidean space. Let ϵ, ζ and ϵ', ζ' be the two components of a spinor in the initial and rotated coordinate systems, respectively. We denote the complex-conjugate spinors by $\dot{\epsilon}$, $\dot{\zeta}$, $\dot{\epsilon}'$, $\dot{\zeta}'$. In Ref. 7 it is shown that the $(2J+1)(2j+1)$ quantities

$$u^{Jj}_{M\mu} = [(J+M)!\,(J-M)!]^{-1/2} \varepsilon^{J+M} \zeta^{J-M} \times [(j+\mu)!\,(j-\mu)!]^{-1/2} \dot{\varepsilon}^{j+\mu} \dot{\zeta}^{j-\mu} \tag{4}$$

transform according to an irreducible representation of the Lorentz group. We apply to $u^{Jj}_{M\mu}(\alpha', \vartheta', \varphi')$, where α', ϑ', φ' are the "polar angles" in the new system, a four-dimensional rotation operator $\hat{R}$, which rotates the system back to its initial position

$$\hat{R} u^{Jj}_{M\mu}(\alpha', \vartheta', \psi') \equiv u^{Jj}_{M\mu}(\alpha, \vartheta, \varphi) = \sum_{M',\mu'} D^{Jj}_{M\mu M'\mu'}(\psi, \theta, \phi)\, u^{Jj}_{M'\mu'}(\alpha', \vartheta', \varphi'). \tag{5}$$

The coefficients D are the components of the $(2J+1)(2j+1)$-dimensional matrix of the transformation, $J > M > -J$; $j > \mu > -j$; θ and ϕ are the Euler angles of the three-dimensional rotation (cf. Fig. 1). The rotation about the new position of the z axis (through the third Euler angle) is not of interest, since a point in space is determined by a pair of angles. Tanh $\psi = v$ is the velocity of the new reference system. The z axis is chosen along the direction of the velocity.

Under a four-dimensional rotation of the reference system, spinors transform according to the law $\epsilon = \delta\epsilon' - \beta\zeta'$, $\zeta = -\gamma\epsilon' + \alpha\zeta'$. The quantities α, β, γ, δ form a binary transformation matrix:

$$\begin{aligned} \alpha &= \cos\frac{\theta}{2} \exp\{(i\phi - \psi)/2\}; \\ \beta &= -i \sin\frac{\theta}{2} \exp\{-(i\phi + \psi)/2\}; \\ \gamma &= -i \sin\frac{\theta}{2} \exp\{(i\phi + \psi)/2\}; \\ \delta &= \cos\frac{\theta}{2} \exp\{-(i\phi - \psi)/2\}. \end{aligned} \tag{6}$$

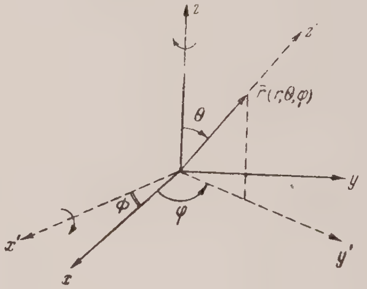

Upon substituting the explicit expressions (4) and (6) in (5), we get

$$D^{Jj}_{M\mu M'\mu'}\left(\psi, \theta, \varphi - \frac{\pi}{2}\right) = D^{J*}_{M'M}\left(-\frac{\pi}{2}, \theta, \varphi\right) D^{j}_{\mu'\mu}\left(-\frac{\pi}{2}, \theta, \varphi\right) e^{(M'+\mu')\psi}, \tag{7}$$

where $D^J_{M'M}(-\pi/2, \theta, \varphi)$ and $D^j_{\mu'\mu}(-\pi/2, \theta, \varphi)$ are the matrices of the irreducible $(2J+1)$ and $(2j+1)$-dimensional representations of the three-dimensional rotation group:

$$D^J_{M'M}(\gamma, \theta, \varphi) = \sum_k (-1)^k \frac{[(J+M)!\,(J-M)!\,(J+M')!\,(J-M')!]^{1/2}}{(J+M-k)!\,k!\,(M'-M+k)!\,(J-M'-k)!} \times e^{iM'\gamma} \left[\cos\frac{\theta}{2}\right]^{2J+M-M'-2k} \left[\sin\frac{\theta}{2}\right]^{2k-M-M'} e^{iM\varphi}. \tag{8}$$

Making use of the equality

$$D^{J*}_{M'M}(\gamma, \theta, \varphi) = (-1)^{M-M'} D^J_{-M'-M}(\gamma, \theta, \varphi) \tag{9}$$

and the Clebsch-Gordan expansion[6]

$$D^{J}_{-M'-M}D^{j}_{\mu'\mu}=\sum_{l=|J-j|}^{l=J+j}C^{lm'}_{J-M'j\mu'}C^{lm}_{J-Mj\mu}D^{l}_{m'm}, \tag{10}$$

we obtain

$$D^{Jj}_{M\mu M'\mu'}\left(\psi,\theta,\varphi-\frac{\pi}{2}\right) \tag{11}$$

$$=(-1)^{M-M'}e^{(M'+\mu')\psi}$$

$$\times\sum_{l}C^{lm'}_{J-M'j\mu'}C^{lm}_{J-Mj\mu}D^{l}_{m'm}\left(-\frac{\pi}{2},\theta,\varphi\right).$$

By using (10) and (11) we can get the Clebsch-Gordan expansion for the matrices in the four-dimensional space

$$D^{Jj}_{M\mu\alpha\beta}D^{Ll}_{\Lambda\lambda\gamma\delta} \tag{12}$$

$$=\sum_{K=|J-L|}^{J+L}\sum_{N=|j-l|}^{j+l}C^{K\varkappa}_{JML\Lambda}C^{N\nu}_{j\mu l\lambda}C^{K\sigma}_{J\alpha L\gamma}C^{N\omega}_{j\beta l\delta}D^{KN}_{\varkappa\nu\sigma\omega}.$$

The orthogonality relations

$$\sum_{\mu_1}C^{j\mu}_{j_1\mu_1j_2\mu-\mu_1}C^{j'\mu}_{j_1\mu_1j_2\mu-\mu_1}=\delta_{jj'} \tag{13}$$

enable us to obtain the expansion which is reciprocal to (12):

$$D^{KN}_{\varkappa\nu\sigma\omega} \tag{14}$$

$$=\sum_{\substack{\alpha,\beta,\gamma,\delta\\ M,\Lambda,\mu,\lambda}}C^{K\varkappa}_{JML\Lambda}C^{N\nu}_{j\mu l\lambda}C^{K\sigma}_{J\alpha L\gamma}C^{N\omega}_{j\beta l\delta}D^{Jj}_{M\mu\alpha\beta}D^{Ll}_{\Lambda\lambda\gamma\delta}.$$

If the rotation ψ, θ, ϕ can be represented as two successive rotations ψ'', θ'', ϕ'' and ψ', θ', ϕ', then

$$D^{Jj}_{M\mu M'\mu'}(\psi,\theta,\phi) \tag{15}$$

$$=\sum_{\varkappa,\varkappa'}D^{Jj}_{M\mu\varkappa\varkappa'}(\psi',\theta',\phi')D^{Jj}_{\varkappa\varkappa'N'\mu'}(\psi'',\theta'',\phi'').$$

3. CONSTRUCTION OF RELATIVISTIC SPHERICAL FUNCTIONS

In the four-dimensional pseudo-Euclidean space, we select an aggregate of functions $Z^{Jj}_{M\mu}(\alpha,\vartheta,\varphi)$ which transform according to the $(2J+1)(2j+1)$-dimensional representation of the Lorentz group, and for which $Z^{Jj}_{M\mu}(0, 0, \pi/2)=\delta_{M\mu}$. According to Eq. (11), such a choice is possible. In view of (5), we obtain

$$Z^{Jj}_{M\mu}(\alpha,\vartheta,\varphi)=\sum_{k}D^{Jj}_{M\mu kk}\left(\alpha,\vartheta,\varphi-\frac{\pi}{2}\right). \tag{16}$$

If we substitute in (16) the expansion (11) and the equality

$$Y_{lm}(\vartheta\varphi)=\sqrt{\frac{2l+1}{4\pi}}(-1)^{m}D^{l}_{om}(\gamma,\vartheta,\varphi), \tag{17}$$

where $Y_{lm}(\vartheta,\varphi)$ is the three-dimensional spherical function [Y_{lm} is here defined as in Ref. 8, and differs by a factor $(-1)^m$ from the definition of Y_{lm} in, say, Ref. 9], we get:

$$Z^{Jj}_{M\mu}(\alpha,\vartheta,\varphi)=\sum_{lk}(-1)^{\mu-k} \tag{18}$$

$$\sqrt{\frac{4\pi}{2l+1}}C^{lm}_{J-Mj\mu}Y_{lm}(\vartheta\varphi)C^{l0}_{J-kjk}e^{2k\alpha}.$$

It is known that the representations of the four-dimensional rotation group are determined by a pair of invariants, which can be constructed from the components of the infinitesimal rotation operator. If M is the space, and N the time part of the four-dimensional angular momentum operator J, then $J^2=M^2+N^2$ and M•N will be invariants. We consider a Z-function which depends only on the coordinates of the point and not on the spin variables. The operators M and N which act on it do not contain spin matrices and can be represented in the form

$$\mathbf{M}\equiv\mathbf{l}=-i[\mathbf{n}\nabla^{\omega}],$$

$$\mathbf{N}\equiv\mathbf{g}=\mathbf{n}\left(t\frac{\partial}{\partial r}+r\frac{\partial}{\partial t}\right)+\frac{t}{r}\nabla^{\omega},$$

where $\mathbf{n}$ is a unit vector along $\mathbf{r}=\mathbf{n}r$, and ∇^{ω} is the angular part of the gradient. Obviously $\mathbf{g}\cdot\mathbf{l}=0$. In this case, the group representation is determined (in the notation of Ref. 4), by assigning the pair of numbers $k_0=|J-j|=0$, $c=2J+1$. The functions $Z^{JJ}_{M\mu}\equiv Z^{J}_{M\mu}$ transforms according to an irreducible representation of the Lorentz group. It is an eigenfunction of $L^2=g^2+l^2$, and can be chosen as a basis function. In the special case of $J=½$ we have

$$Z^{1/2}_{1/2\,1/2}=\cosh\alpha+\sinh\alpha\cos\vartheta; \tag{19}$$

$$Z^{1/2}_{1/2\,-1/2}=\sinh\alpha\sin\vartheta\, e^{-i\varphi};$$

$$Z^{1/2}_{-1/2\,1/2}=\sinh\alpha\sin\vartheta\, e^{i\varphi};$$

$$Z^{1/2}_{-1/2\,-1/2}=\cosh\alpha-\sinh\varkappa\cos\vartheta,$$

i.e., the components $Z^{1/2}_{M\mu}$ form a timelike four-dimensional vector with components:

$$t+z=\rho Z^{1/2}_{1/2\,1/2};\qquad t-z=\rho Z^{1/2}_{-1/2\,-1/2};\qquad (20)$$
$$x+iy=\rho Z^{1/2}_{-1/2\,1/2};\qquad x-iy=\rho Z^{1/2}_{1/2\,-1/2}.$$

The definition of the rotation angles in (6), so that $\tanh\psi = v$, limits us to the case where $t^2 - r^2 > 0$. Therefore the $Z^{Jj}_{M\mu}$ function defined by (18) may be called a timelike Z-function.

The connection between the spherical functions of the form (1) and the Z-functions can be established with the help of the relation

$$\psi_{nlm}=\sqrt{\frac{2J+1}{2l+1}}\sum_k(-1)^{l-J-k}C^{l0}_{J-kJk}\,e^{2k\alpha}\qquad (21)$$
$$=\frac{\sinh^l\alpha}{M_l}\,\frac{d^{l+1}\cosh n\alpha}{d(\cosh\alpha)^{l+1}},$$

where $n = 2J + 1$. The validity of (21) can be checked by expanding the right side in series and comparing with the expansion of the left side. By using (21), we put $Z^J_{M\mu}$ in the form

$$Z^J_{M\mu}=\frac{\sqrt{4\pi}}{2J+1}\sum_l\sqrt{2l+1}\,C^{JM}_{J\mu l-m}\,\psi_{nlm}.\qquad (22)$$

If in (21) we replace α by $i\alpha$, then the right side coincides with (1), so the expression (22) will determine the Z-function for a Euclidean space.

If we rotate through $\pi/2$ in the (z,t) plane of the Euclidean space, a vector which became timelike when we replaced α by $-i\alpha$, will become spacelike. This enables us to construct spacelike basis functions of a finite-dimensional representation of the Lorentz group. Again, they will have the form (22), but now we must choose for ψ_{nlm}, not (21), but rather

$$\sqrt{\frac{2J+1}{2l+1}}\sum_k(-1)^{J-l}C^{l0}_{J-kJk}\,e^{2k\alpha}\qquad (23)$$
$$=i\,\frac{\cosh^l\alpha}{M_l}\,\frac{d^{l+1}\cos n\left(i\alpha+\frac{\pi}{2}\right)}{d(\sinh\alpha)^{l+1}}$$

The factor $(-1)^J$ has been inserted in (23) so that the Z-function will be real for arbitrary J. In analogy to (19), the components of the spacelike $Z^{1/2}_{M\mu}$ form a spacelike four-vector. The relations (2) remain valid, but we must use (3) for x, y, z, t instead of (2). According to (12) and (16), the expansion

$$Z^J_{M\mu}Z^L_{\Lambda\lambda}=\sum_{N=|J-L|}^{J+L}C^{NM+\Lambda}_{JML\Lambda}\,C^{N\mu+\lambda}_{J\mu L\lambda}\,Z^N_{M+\Lambda,\,\mu+\lambda};\qquad (24)$$

$$Z^N_{M+\Lambda,\,\mu+\lambda}=\sum_{M,\,\Lambda,\,\mu,\,\lambda}C^{NM+\Lambda}_{JML\Lambda}\,C^{N\mu+\lambda}_{J\mu L\lambda}\,Z^J_{M\mu}\,Z^L_{\Lambda\lambda}.\qquad (25)$$

exists for timelike Z-functions. The expansion (24) is valid for spacelike Z-functions, except that we must add a factor $(-1)^{N-J-L}$ on the right. This factor appears because we have introduced $(-1)^J$ in defining the functions.

By using (22) and (24), we obtain

$$\psi_{n_1l_1m_1}\psi_{n_2l_2m_2}=\sum C^{JM}_{J_1M_1J_2M_2}\,C^{J\mu}_{J_1\mu_1J_2\mu_2}\,C^{lm}_{J-MJ\mu}\qquad (26)$$
$$C^{l_1m_1}_{J_1-M_1J_1\mu_1}\,C^{l_2m_2}_{J_2-M_2J_2\mu_2}\,\psi_{nlm};$$
$$n_i=2J_i+1.$$

The summation runs over J, l, M_1, M_2, μ_1, μ_2; it can be partially carried out using the Wigner 9-j symbols:

$$\psi_{n_1l_1m_1}\psi_{n_2l_2m_2}=\sum_{J,\,l}(-1)^{J-J_1-J_2}C^{lm}_{l_1m_1l_2m_2}\qquad (27)$$
$$\chi(J_1J_1J_2J_2;\ l_1l_2,\,JJ,\,J)\,\psi_{nlm},$$

where χ is related[10] to the 9–j symbols and is a complicated function of J_1, J_2, l_1, l_2, J.

Comparison of (24) and (26), (27) shows that for problems where we have to use the expansion in irreducible representations, it is more convenient to choose the $Z^J_{M\mu}$ as basis functions, and not ψ_{nlm}.

Differentiation of the Z-function can be carried out, using (22) and the explicit form of ψ_{nlm}. However, this does not enable us directly to get the result in the form of an expansion in terms of irreducible representations (i.e., in terms of Z-functions). Such an expansion is frequently needed, and can be gotten as follows. We shall agree to denote the covariant components of the gradient by the symbol $\partial_{\propto\beta}$, where $\propto$ and β refer to the component $Z^{1/2}_{\propto\beta}$ which transforms like the associated differential operator

$$\partial_{\pm1/2,\,\pm1/2}=\partial/\partial t\mp\nabla_0;\qquad (28)$$
$$\partial_{\mp1/2,\,\pm1/2}=\mp\sqrt{2}\,\nabla_{\pm1},$$

where ∇_0, ∇_1, ∇_{-1} are the cyclic components of ∇. The cyclic components of a vector $\mathbf{a}$ are related to its Cartesian components by the relations $a_0 = a_z$,

$a_{\pm 1} = \pm 2^{-1/2}(a_x \pm i a_y)$. The contravariant components of the gradient are $\partial^{\alpha\beta} = (-1)^{\alpha+\beta+1} \times \partial_{-\alpha-\beta}$.

Making use of the transformation law for $\partial_{\alpha\beta}$ and the equality (24), we get

$$\partial_{\alpha\beta}\, G_J(\rho)\, Z^J_{M\mu} \tag{29}$$

$$= \sum_l A_{Jl}(\rho)\, C^{lM+\alpha}_{1/2\alpha JM}\, C^{l\mu+\beta}_{1/2\beta J\mu}\, Z^l_{M+\alpha,\,\mu+\beta},$$

where $G_J(\rho)$ depends only on ρ, and $A_{Jl}(\rho)$ is a quantity which can be found by starting from the explicit form of the operator $\partial_{\alpha\beta}$.

If $t^2 - r^2 > 0$, then

$$\partial_{\pm 1/2\, \pm 1/2} = Z^{1/2}_{\pm 1/2\, \pm 1/2} \frac{\partial}{\partial\rho} \tag{30}$$

$$- \frac{1}{\rho}[\sinh\alpha \pm \cosh\alpha \cos\vartheta] \frac{\partial}{\partial\alpha} \mp \frac{\overset{\omega}{\nabla}_0}{\rho \sinh\alpha};$$

$$\partial_{-1/2\, 1/2} = \overset{*}{\partial}_{1/2\, -1/2} = Z^{1/2}_{-1/2\, 1/2} \frac{\partial}{\partial\rho}$$

$$- \frac{\sqrt{2}}{\rho}\left[n_1 \cosh\alpha \frac{\partial}{\partial\alpha} - \frac{\overset{\omega}{\nabla}_1}{\sinh\alpha}\right].$$

If $r^2 - t^2 > 0$, then

$$\partial_{\pm 1/2\, \pm 1/2} = - Z^{1/2}_{\pm 1/2\, \pm 1/2} \frac{\partial}{\partial\rho} \tag{31}$$

$$+ \frac{1}{\rho}[\cosh\alpha \pm \sinh\alpha \cos\vartheta] \frac{\partial}{\partial\alpha} \mp \frac{\overset{\omega}{\nabla}_0}{\rho \cosh\alpha};$$

$$\partial_{-1/2\, 1/2} = \overset{*}{\partial}_{1/2\, -1/2} = - Z^{1/2}_{-1/2\, 1/2} \frac{\partial}{\partial\rho}$$

$$+ \frac{\sqrt{2}}{\rho}\left[n_1 \sinh\alpha \frac{\partial}{\partial\alpha} - \frac{\overset{\omega}{\nabla}_1}{\cosh\alpha}\right].$$

In eqs. (30) and (31), $n_1 = 2^{-1/2} \sin\vartheta e^{i\varphi}$.

In order to go the case of a Euclidean space (with coordinates $r = R\sin\alpha$ and $\tau = it = R\cos\alpha$), we need only change α to $i\alpha$ and ρ to $-iR$ in (30).

Since the coefficient of $\partial/\partial\rho$ in $\partial_{\alpha\beta}$ is $Z^{1/2}_{\alpha\beta}$, the equalities (24) and (29) enable us to present $A_{Jl}(\rho)$ in the form

$$A_{Jl}(\rho) = \pm\left[\frac{\partial G_J(\rho)}{\partial\rho} - B_{Jl}\frac{G_J(\rho)}{\rho}\right], \tag{32}$$

where B_{Jl} does not depend on ρ; the ± signs apply to the cases $t^2 - r^2 > 0$, and $t^2 - r^2 < 0$, respectively; B_{Jl} is the same for both $t^2 - r^2 \gtrless 0$. In order to determine B_{Jl}, we integrate both sides of (29) over the angles ϑ, φ and use (30) or (31). If we then compare terms on right and left, we get

$$B_{Jl} = 2\varkappa(2J - 2\varkappa + 1), \tag{33}$$

$$l = J + \varkappa, \quad \varkappa = \pm 1/2.$$

Performing the operation (29) twice gives

$$L^2 Z^J_{M\mu} = 4J(J+1) Z^J_{M\mu}, \tag{34}$$

where, for the case of $t^2 - r^2 > 0$,

$$L^2 = \frac{\partial^2}{\partial\alpha^2} + 2\coth\alpha \frac{\partial}{\partial\alpha} - \frac{\hat{l}^2}{\operatorname{sh}^2\alpha}, \tag{35}$$

$$\frac{\partial^2}{\partial t^2} - \nabla^2 = \frac{\partial^2}{\partial\rho^2} + \frac{3}{\rho}\frac{\partial}{\partial\rho} - \frac{L^2}{\rho^2},$$

while for $r^2 - t^2 > 0$,

$$L^2 = \frac{\partial^2}{\partial\alpha^2} + 2\tanh\alpha \frac{\partial}{\partial\alpha} + \frac{\hat{l}^2}{\operatorname{ch}^2\alpha}, \tag{36}$$

$$\nabla^2 - \frac{\partial^2}{\partial t^2} = \frac{\partial^2}{\partial\rho^2} + \frac{3}{\rho}\frac{\partial}{\partial\rho} - \frac{L^2}{\rho^2}.$$

The Lorentz group is noncompact, and its total volume is infinite, so that it is impossible to carry out the operation of group integration using only finite-dimensional representations. It is therefore impossible to pose the question of orthogonality of Z-functions in pseudo-Euclidean space. In Euclidean space, the Z-functions are orthonormal:

$$\int_0^\pi d\alpha \int_0^\pi d\vartheta \int_0^{2\pi} d\varphi \sin^2\alpha \sin\vartheta Z^J_{M\mu} Z^{J*}_{M\mu} = \frac{2\pi^2}{2J+1}. \tag{37}$$

This enables us to expand an arbitrary function of coordinates in series in terms of the $Z^J_{M\mu}$. For example, we have for exp (ikx)

$$e^{ikx} = \sum_{JM\mu} (2J+1)(-1)^J \tag{38}$$

$$\times R_J(k\rho) Z^{J*}_{M\mu}(\beta\theta\phi) Z^J_{M\mu}(\alpha\vartheta\varphi),$$

or

$$e^{ikx} = \sum_{Jlm} 4\pi(-1)^J R_J(k\rho)\, \psi^*_{nlm}(\beta\theta\phi)\, \psi_{nlm}(\alpha\vartheta\varphi), \tag{39}$$

$$R_J(k\rho) = (2/k\rho)\, J_{2J+1}(k\rho),$$

where $J_n(k\rho)$ is a Bessel function, k and x are vectors in the four-dimensional Euclidean space whose directions are defined by the angles β, θ, ϕ and α, ϑ, φ: $kx = |k|\rho \cos\omega$;

$$\cos\omega = \cos\beta\cos\alpha + \sin\beta\sin\alpha\cos\gamma; \tag{40}$$

$$\cos\gamma = \cos\theta\cos\vartheta + \sin\theta\sin\vartheta\cos(\varphi - \phi);$$

$$\left\{\frac{\partial^2}{\partial\rho^2} + \frac{3}{\rho^2}\frac{\partial}{\partial\rho} - \frac{L^2}{\rho^2} + k^2\right\} R_J(k\rho)\, Z^J_{M\mu}(\alpha\vartheta\varphi) = 0.$$

The $Z^J_{M\mu}$-functions play the same role in four-dimensional space as do the Y_{lm} in three-space.

If we carry out the transformation $\alpha \to -\alpha$ or $\mathbf{r} \to -\mathbf{r}$ on $Z^{Jj}_{M\mu}(\alpha, \vartheta, \varphi)$, then according to (18), for the case $t^2 - r^2 > 0$

$$Z^{Jj}_{M\mu}(-\alpha, \vartheta, \varphi) \tag{41}$$

$$= (-1)^{J+j-2\mu} Z^{Jj}_{M\mu}(\alpha, \pi - \vartheta, \pi + \varphi)$$

$$= (-1)^{\mu-M} Z^{Jj*}_{-M-\mu}(\alpha, \vartheta, \varphi),$$

and for the case $t^2 - r^2 < 0$,

$$Z^{Jj}_{M\mu}(-\alpha, \vartheta, \varphi) \tag{42}$$

$$= (-1)^{J+j} Z^{Jj}_{M\mu}(\alpha, \pi - \vartheta, \pi + \varphi)$$

$$= (-1)^{\mu+M} Z^{Jj*}_{-M-\mu}(\alpha, \vartheta, \varphi).$$

4. CONSTRUCTION OF RELATIVISTIC SPHERICAL SPINOR AND VECTOR FUNCTIONS.

If $\psi^{KN}_{\alpha\beta}$ transforms according to the irreducible $(2K + 1)(2N + 1)$-dimensional representation of the four-dimensional rotation group in Euclidean or pseudo-Euclidean space, then according to (12) we have the expansion

$$\psi^{KN}_{\alpha\beta} = \sum_{M,\Lambda,\mu,\lambda} C^{K\alpha}_{JML\Lambda}\, C^{N\beta}_{j\mu l\lambda}\, \psi^{Jj}_{M\mu}\, \psi^{Ll}_{\Lambda\lambda}, \tag{43}$$

$$\psi^{Jj}_{M\mu}\, \psi^{Ll}_{\Lambda\lambda} = \sum_{K,N} C^{K\alpha}_{JML\Lambda}\, C^{N\beta}_{j\mu l\lambda}\, \psi^{KN}_{\alpha\beta}.$$

For the case $L = 0$ and $l = ½$, $l = 0$ and $L = ½$, the functions $\psi^{Ll}_{\Lambda\lambda}$ become ordinary contravariant or covariant spinors.

$$\psi^{0\,1/2}_{0\sigma'}(\sigma) = \delta_{\sigma\sigma'}, \quad \psi^{1/2\,0}_{\sigma' 0}(\sigma) = (-1)^{\sigma'+1/2}\,\delta_{-\sigma'\sigma}. \tag{44}$$

Substituting $Z^J_{M\mu}\psi^{0\,½}_{0\sigma}$ for $\psi^{Jj}_{M\mu}\psi^{Ll}_{\Lambda\lambda}$ in (43), we form a contravariant spherical spinor function $P^{Jl}_{M\lambda}$, consisting of a pair of components ($\sigma = \pm ½$)

$$[P^{Jl}_{M\lambda}]_\sigma = \sqrt{2J+1}\,(-1)^J\, C^{l\lambda}_{J\mu-\sigma\,1/2\,\sigma}\, Z^J_{M\mu}. \tag{45}$$

The factor $\sqrt{2J + 1}\,(-1)^J$ is included in (45) to make the use of Eqs. (46) and (47) more convenient.

If we substitute $\psi^{½\,0}_{-\sigma 0}$ in (43), we get a covariant spherical spinor function $R^{Jl}_{M\lambda}$. This function is conveniently chosen so that the following equations are valid:

$$\left[\frac{\partial}{\partial t} - \vec{\sigma}\nabla\right] G_{Jl} P^{Jl}_{M\lambda} \tag{46}$$

$$= \pm i\left[\frac{\partial G_{Jl}}{\partial\rho} - 2\varkappa\,\frac{2J - 2\varkappa + 1}{\rho}\, G_{Jl}\right] R^{Jl}_{M\lambda};$$

$$\left[\frac{\partial}{\partial t} + \vec{\sigma}\nabla\right] G_{Jl} R^{Jl}_{M\lambda} \tag{47}$$

$$= \mp i\left[\frac{\partial G_{Jl}}{\partial\rho} + 2\varkappa\,\frac{2l + 2\varkappa + 1}{\rho}\, G_{Jl}\right] P^{Jl}_{M\lambda}$$

(where $l = J + \varkappa$).

The transition to a Euclidean space is made in the same way as for Eq. (30).

With the help of (29) it is not difficult to verify that

$$[R^{Jl}_{M\lambda}]_\sigma = \sqrt{2l+1}\,(-1)^{l+\sigma-1/2}\, C^{JM}_{l\Lambda\,1/2\,-\sigma}\, Z^l_{\Lambda\lambda}. \tag{48}$$

We shall show that the bispinor $\psi^{Jl}_{M\lambda}$ made up of $R^{Jl}_{M\lambda}$ and $P^{Jl}_{M\lambda}$, is an eigenfunction of the total four-dimensional angular momentum $\hat{J}$ of a particle with spin ½. If $\psi(\mathrm{r}, t)$ is the wave function of such a particle, then the operation of infinitesimal rotation gives

$$\psi'(\mathbf{r}+\delta\mathbf{r}, t+\delta t) \tag{49}$$

$$=\left\{1+i\vec{\delta}\left[1+\frac{1}{2}\vec{\sigma}_{\text{Д}}\right]-\vec{\delta}_0\left[\mathbf{g}-\frac{1}{2}\vec{\alpha}_{\text{Д}}\right]\right\}\psi(\mathbf{r}, t),$$

where $\vec{\delta}$ is the infinitesimal angle of the three-dimensional rotation, $\vec{\delta}_0$ is the infinitesimal velocity of the new reference system, $\vec{\sigma}_D$ and $\vec{\alpha}_D$ are the Dirac matrix vectors. We shall use the representation of the Dirac matrices in which γ^5 is diagonal. In this representation $\hat{J}^2 = L^2 + (\mathbf{l}\cdot\vec{\sigma}_D) - (\mathbf{g}\cdot\vec{\alpha}_D) + {}^3/_2$ breaks up into two two-row matrices situated along the diagonal. Their eigenvalues are identical:

$$\hat{J}^2\psi^{Jl}_{M\lambda}=\left[4Jl+2J+2l+\frac{1}{2}\right]\psi^{Jl}_{M\lambda}. \tag{50}$$

Along with the spherical spinor functions, it is possible, by using (43), to introduce the concept of four-dimensional spherical vector functions. We shall define the contravariant and covariant spherical vectors by the relations:

$$[\mathbf{Z}^{Jl}_{M\lambda}]^{\sigma_1\sigma_2}=C^{l\lambda}_{J\mu 1\sigma}\,C^{1\sigma}_{{}^1/_2\sigma_1{}^1/_2\sigma_2}\,Z^J_{M\mu}; \tag{51}$$

$$[\mathbf{Z}^{LJ}_{\Lambda\mu}]_{\sigma_1\sigma_2}=(-1)^{\sigma+1}C^{L\Lambda}_{JM1-\sigma}\,C^{1\sigma}_{{}^1/_2\sigma_1{}^1/_2\sigma_2}\,Z^J_{M\mu}. \tag{52}$$

Formulas (51) and (52) are a generalization of the definition[11] of spherical vectors to the four-dimensional case.

5. AN EXAMPLE OF THE USE OF THE Z-FUNCTION FOR SEPARATING VARIABLES IN A RELATIVISTIC EQUATION

As an example of the use of the relativistic spherical functions, we shall consider the problem of separation of variables in the Bethe-Salpeter equation for the case of a bound state of two scalar particles. This equation can be expressed in the form

$$(\Box_1-\mu^2)(\Box_2-\mu^2)\psi(x_1, x_2) \tag{53}$$

$$=\hat{I}(x_1x_2x_3x_4)\psi(x_3, x_4),$$

where $\hat{I}$ is an integral operator. We shall denote by D and ∂ the operators of differentiation with respect to the coordinates of the center of mass of the system $X = (x_1 + x_2)/2$ and with respect to the relative coordinates $x = x_1 - x_2$. For (53), we get

$$\{{}^1/_{16}D^4+{}^1/_2D^2\partial^2+\partial^4 \tag{54}$$

$$-{}^1/_2\mu^2D^2-2\mu^2\partial^2+\mu^4-(D\partial)^2\}\psi(X, x)$$

$$=\hat{I}(X, x, Y, y)\psi(Y, y).$$

Making use of Wick's[1] observation concerning the possibility of analytic continuation of the Bethe-Salpeter equation, we shall solve the problem in four-dimensional Euclidean space. We shall represent the wave function of a state in which the four-dimensional angular momentum of the total system has a definite value (the operator $\hat{J}^2$ is diagonal) in the form

$$\psi^J_{M\mu}=\sum_{L,\,l}g^J_{Ll}(R,\rho)\psi^J_{M\mu\,(L,\,l)}; \tag{55}$$

$$\psi^J_{M\mu\,(L,\,l)}$$

$$=\sum_{\Lambda_1\lambda_1\Lambda_2\lambda_2}C^{JM}_{L\Lambda_1l\lambda_1}\,C^{J\mu}_{L\Lambda_2l\lambda_2}\,Z^L_{\Lambda_1\Lambda_2}(\beta\theta\phi)\,Z^l_{\lambda_1\lambda_2}(\alpha\vartheta\varphi),$$

where l is the relative angular momentum of the two particles; L is the angular momentum of the center of inertia relative to the origin of coordinates; R, β, θ, ϕ and ρ, α, ϑ, φ are the polar coordinates of X and x; $g^J_{Ll}(R, \rho)$ is the "radial" part of the wave function. Substituting (55) in (54), we take Fourier components with respect to the coordinate X. We then get an equation analogous to (54), in which D is replaced by the total momentum P of the system, and where $G^J_{Ll}(P, \rho)\,Z^L_{\Lambda_1\Lambda_2}(\beta_p, \theta_p, \phi_p)$ appears in (55) in place of $g^J_{Ll}(R, \rho)\,Z^L_{\Lambda_1\Lambda_2}(\beta, \theta, \phi)$; β_p, θ_p, ϕ_p are the angles of the momentum 4-vector.

The presence of the term $(P\partial)^2$ makes the equation noninvariant with respect to four-dimensional rotations in the space of the relativistic coordinates. Applying $(P\partial)^2$ to $\psi^J_{M\mu}$ gives

$$(P\partial)^2\psi^J_{M\mu}=P^2\sum_{Ll}\sum_{nk}B^{Ll}_{nk}\psi^J_{M\mu\,(L+n,\,l+k)} \tag{56}$$

$$\times\left[\frac{\partial^2}{\partial\rho^2}+\frac{3-2k(2L+k+1)}{\rho}\frac{\partial}{\partial\rho}-\frac{4l(l+1)}{\rho^2}(1-2k^2)\right]$$

$$\times G^J_{Ll}(P, \rho),$$

where $n, k = 0, \pm 1$; the coefficient B_{nk}^{Ll} contains all the factors which depend only on L, l, n, k. B_{nk}^{Ll} can be expressed rather simply if we make use of Racah's formula[12] for the summation of Clebsch-Gordan coefficients.

Since the $\psi_{M\,\mu(L,l)}^{J}$ are eigenfunctions of ∂^2, and since the coordinate x appears in the integral operator $\hat{I}$ only in an exponential factor we can, by using the orthogonality of the Z-functions, obtain an infinite system of coupled equations depending on a single parameter ρ, for determining $G_{Ll}^{J}(P, \rho)$. In certain cases this system may prove to be more convenient than the initial equation (53).

Problems of separation of variables in relativistic two-body equations and possible methods for their solution will be considered in more detail in a separate paper.

I express my thanks to K. A. Ter-Martirosian for discussion of the questions touched upon here.

---

[1] G. C. Wick, Phys. Rev. 96, 1124 (1954)

[2] V. A. Fock, Z. Physik 98, 145 (1935).

[3] I. M. Gel'fand and M. A. Naimark, Izv. Akad. Nauk SSR, Ser. Mat. 11, 411 (1947).

[4] M. A. Naimark, Usp. Matem. Nauk 9, 19 (1954).

[5] V. L. Ginzburg and I. E. Tamm, J. Exptl. Theoret. Phys. (U.S.S.R.) 17, 227 (1947).

[6] E. Wigner, *Gruppentheorie und ihre Anwendung auf die Quantenmechanik der Atomspektren*, Braunschweig, 1931.

[7] B. L. van der Waerden, *Die Gruppentheoretische Methode in der Quantenmechanik*, Berlin, 1932.

[8] H. Bethe, *Ein und Zwei-Elektron Probleme*, Handb. d. Physik, vol. 24/1.

[9] E. Condon and G. Shortley, *Theory of Atomic Spectra, 1949.*

[10] H. A. Jahn and J. Hope, Phys. Rev. 93, 318 (1954).

[11] V. B. Berestetskii, A. Z. Dolginov and K. A. Ter-Martirosian , J. Exptl. Theoret. Phys. (U.S.S.R.) 20, 527 (1950).

[12] G. Racah, Phys. Rev. 62, 438 (1942).

Translated by M. Hammermesh
149

SOVIET PHYSICS JETP VOLUME 3, NUMBER 4 NOVEMBER, 1956

Cerenkov Radiation in Anisotropic Ferrites

V. E. Pafomov
P. N. Lebedev Physical Institute, Academy of Sciences, USSR

(Submitted to JETP editor February 9, 1955)
J. Exptl. Theoret. Phys. (U.S.S.R.) 30, 761-765 (April, 1956)

This work considers the radiation of electromagnetic waves by a charge moving in an anisotropic ferrite with a velocity greater than the phase velocity of light. Such radiation differs from that occurring in the case of an anisotropic dielectric, both with respect to the intensity distribution in the generatrices of the cones and with respect to the energy of the radiation.

SOME years ago Ginzburg[1] considered the question of the field and the radiated energy of an electron in an anisotropic dielectric (see also the works of Kolomenskii[2,3] and Kaganov[4]). As compared with the case of an anisotropic dielectric, the Cerenkov effect in the case of an anisotropic magnetic material possesses certain special effects, the consideration of which will, we believe, prove interesting. Such consideration might even be considered essential in connection with the possible use of the Cerenkov effect in isotropic and anisotropic ferrites for the generation of microwaves. The method used here for the investigation of the Cerenkov radiation in anisotropic ferrites is also applicable to the solution of other electrodynamic problems in ferrites.

In the present article we also derive formulas for the Cerenkov effect in an anisotropic dielectric which are more general than those which have previously been known.

1. THE HAMILTONIAN METHOD IN THE ELECTRODYNAMICS OF AN ANISOTROPIC FERRITE

In order to solve the problem under consideration we shall use the Hamiltonian method in a manner similar to that in which Ginzburg used it in the solution of the problem of the Cerenkov radiation in an anisotropic dielectric[1-5].

We shall assume that

$$\mathbf{D} = \varepsilon\mathbf{E}; \quad B_x = \mu_x H_x, \qquad (1)$$
$$B_y = \mu_y H_y, \quad B_z = \mu_z H_z.$$

We shall set the conductivity of the medium equal to zero. The extent to which this approximation is justified for ferrites, which are semiconductors, is well known. Using the additional condition

$$\operatorname{div} \mathbf{A} = 0, \qquad (2)$$

introduced by Ginzburg[6], and resolving the vector potential **A** into a Fourier series

$$\mathbf{A}(\mathbf{x}, t) = \sum_{\lambda, i} q_{\lambda i}(t)\, \mathbf{A}_{\lambda i}(\mathbf{x}), \qquad (3)$$
$$\mathbf{A}_{\lambda i} = \sqrt{4\pi}\, c\, \mathbf{a}_{\lambda i} e^{i\mathbf{k}_\lambda \mathbf{x}},$$

we obtain, by a method analogous to that used in Ref. 5,

$$\ddot{q}_{\lambda i} + \omega_{\lambda i}^2 q_{\lambda i} = \sqrt{4\pi}\, e\, (\mathbf{v}\mathbf{a}_{\lambda i})\, e^{-i\mathbf{k}_\lambda \mathbf{x}(e)}, \qquad (4)$$

provided the conditions

$$(\mathbf{a}_{\lambda i}\mathbf{a}_{\lambda i}) = 1; \quad (\mathbf{a}_{\lambda i}\mathbf{k}_\lambda) = 0;$$
$$(\mathbf{a}_{\lambda i}\mathbf{a}_{\lambda j}) = 0; \quad (\mathbf{h}_{\lambda i}\mathbf{b}_{\lambda j}) = 0. \qquad (5)$$

are fulfilled. The indices i and j take on the values 1 and 2 corresponding to the different polarizations. In the last two equations of (5) $i \neq j$. Here $\mathbf{a}_{\lambda i}$ is the normalized electric field intensity vector of the polarization wave of type i; $\mathbf{a}_{\lambda i}$ is the electric induction vector; $\mathbf{h}_{\lambda i}$ is the magnetic field vector ; $\mathbf{b}_{\lambda i}$ is the magnetic induction vector.

Conditions (5) differ from the corresponding conditions in Ref. 5, the physical meaning of which does not require explanation.

The method considered can be used for the solution of various electrodynamic problems. For example, we may consider the radiation from an oscillator in an anisotropic ferroelectric.

2. CERENKOV RADIATION IN A UNIAXIAL FERRITE CRYSTAL

We restrict ourselves in the present work to uniaxial crystals.

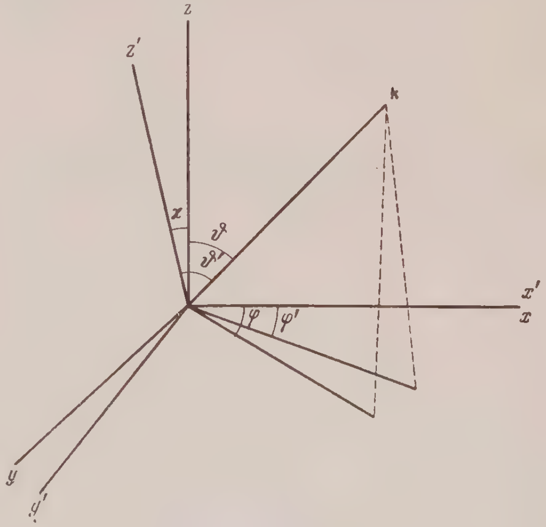

The formula for the radiation energy of the waves with type i polarization has the form*:

$$H^{i}_{\text{rad}} = \frac{e^2vt}{2\pi c^2} \times \int \left| \frac{(\mathbf{a}_{\lambda i})^2_v n^3_{\lambda i}}{n_{\lambda i} - (\partial n_{\lambda i}\ \partial\vartheta)\operatorname{ctg}\vartheta} \right|_{\vartheta=\vartheta_0} \omega_{\lambda i} d\omega_{\lambda i} d\varphi, \tag{6}$$

where $(\mathbf{a}_{\lambda i})_v$ is the projection of the normalized electric field intensity vector in the direction of the forward motion of the electron; $n_{\lambda i}$ is the index of refraction for waves with type i polarization; φ is the azimuthal angle; ϑ is the angle between the normal to the wave front and the velocity of the charged particle. In formula (6) all the magnitudes are taken for $\vartheta = \vartheta_0$, where ϑ_0 is the angle between $\mathbf{k}_\lambda$ and $\mathbf{v}$ for the radiated waves. It is found from the usual condition for the Cerenkov radiation, $(\mathbf{k}_\lambda \mathbf{v}) = \omega_{\lambda i}$, and the integration is carried out over the region where this condition is fulfilled.

For convenience in what is to follow, we introduce two systems of coordinates. We choose our basic system, that in which we shall write our final formulas, such that the z axis coincides with the direction of motion of the electron. We call it system Σ. We will let the z' axis of the auxiliary coordinate system Σ' be directed along the optic axis of the uniaxial crystal. The yz and $y'z'$ surfaces of these two systems coincide, as do the x and x' axes. In other words system Σ' is obtained by rotating system Σ, like an hour hand on a clock, by an angle $\varkappa$ about the x axis, where $\varkappa$ is the angle between the crystal axis and the direction of motion of the electron. The equations for the transformation of coordinates have the form

$$x' = x; \quad y' = y\cos\varkappa + z\sin\varkappa; \quad z' = -y\sin\varkappa + z\cos\varkappa. \tag{7}$$

The transformation equations for the trigonometric functions which will be needed below may be found from (7). They are

$$\cos^2\vartheta' = (\cos\vartheta\cos\varkappa - \sin\vartheta\sin\varphi\sin\varkappa)^2; \tag{8}$$

$$\cos^2\varphi' = \frac{\cos^2\varphi\sin^2\vartheta}{\cos^2\varphi\sin^2\vartheta + (\sin\varphi\sin\vartheta\cos\varkappa + \cos\vartheta\sin\varkappa)^2}. \tag{9}$$

We shall suppose that the dielectric constant is isotropic and different from unity. In this case the equations for the indices of refraction for the ordinary (o) and extraordinary (e) waves will be, respectively, as follows:

$$n_o^2 = \mu_o\varepsilon; \quad \frac{\varepsilon}{n_e^2} = \frac{\cos^2\vartheta'}{\mu_o} + \frac{\sin^2\vartheta'}{\mu_e}, \tag{10}$$

where $\mu_{x'} = \mu_{y'} = \mu_o$ and $\mu_{z'} = \mu_e$.

The projections of the normalized electric field vectors along $\mathbf{v}$ can be found from conditions (5):

$$\varepsilon(a_o)^2_v = (\cos\vartheta'\sin\varphi'\sin\varkappa - \sin\vartheta'\cos\varkappa)^2; \tag{11}$$

$$\varepsilon(a_e)^2_v = \sin^2\varkappa\cos^2\varphi'.$$

The conditions for radiation have the form

$$n_o^2\beta^2\cos^2\vartheta = 1; \quad n_e^2\beta^2\cos^2\vartheta = 1, \tag{12}$$

$$\beta^2 = v^2/c^2.$$

where $\beta^2 = v^2/c^2$.

In the isotropic case Eq. (6) gives

$$H_{\text{rad}} = \frac{e^2vt}{c^2}\int \mu\left(1 - \frac{1}{\beta^2\varepsilon\mu}\right)\omega d\omega, \tag{13}$$

i.e., the result obtained by Sitenko*[7]. For $\mu = 1$ we have the well-known formula of Frank and Tamm[10] We note that in (16), and also in the formulas derived below for the radiation from a charge moving faster than light in anisotropic media, μ enters as a factor, and hence the index of refraction of the radiated energy is μ times as great as it is in the case of nonmagnetic media. Unfortunately, in the centimeter region in the known ferrites $\mu < 2$ and the gain is small. However, the possibility of obtaining larger values of μ is not excluded, and then the use of ferrites for the generation of radio waves would be preferable to the use of dielectrics[11].

In what follows we shall designate the energy of radiation for the ordinary and extraordinary waves in an anisotropic magnetic medium (anisotropic μ, isotropic ϵ) as H^{o}_{ex} and H^{e}_{ex}, respectively, and the energy of radiation of the ordinary and extraordinary waves in an anisotropic dielectric (anisotropic ϵ, isotropic μ), as ${}_{\partial}H^{o}_{ex}$ and ${}_{\partial}H^{e}_{ex}$, respectively. For the calculations we use the formulas (6) and the corresponding expressions from (10) and (11).

---

* See Ref. 3. Equation (6) is valid for any type of anisotropy, since in its derivation Eq. (4), which is derived by means of a corresponding choice of conditions imposed on $\mathbf{a}_{\lambda i}$, is used.

Equation (6) does not take into account the optical activity of the medium. We note that we must separate the integral sign from the modulus of the expression under the integral.

* Equation (13) for the intensity of Cerenkov radiation in an isotropic magnetic material was also obtained by Watson and Jauch[8], but in a more complicated manner than in Ref. 7. The question of the losses of energy in isotropic magnetic materials has been considered especially in Ref. 9. However, erroneous results were there obtained (see Ref. 7).

When the specifications of (8) and (9) are used, the result takes the following form:

$$H^{o}_{ex} = \frac{e^2tv}{2\pi c^2} \times \int \mu_o (\cos\vartheta_0' \sin\varphi' \sin\varkappa - \sin\vartheta_0' \cos\varkappa)^2 \omega d\omega d\varphi; \tag{14}$$

$$H^{e}_{ex} = \frac{e^2tv}{2\pi c^2} \times \int \left| \frac{\mu_o\mu_e \sin^2\varkappa \cos^2\varphi'}{\mu_o + (\mu_e - \mu_o)(\sin\varphi\sin\varkappa - \cos H \operatorname{ctg}\vartheta_o)\sin\varphi\sin\varkappa} \right| \times \omega d\omega d\varphi, \tag{15}$$

where ϑ_0 is found from the corresponding condition of radiation (12), and the integration is taken over the region where the condition

$$n^2_{o,e}\,\beta^2 > 1. \tag{16}$$

is fulfilled.

In order to make a comparison with the case of an anisotropic dielectric, we write two formulas which may be obtained from the equations derived in Ref. 1:

$${}_{\partial}H^{e}_{ex} = \frac{e^2tv}{2\pi c^2} \int \mu \sin^2\varkappa \cos^2\varphi' \omega d\omega d\varphi; \tag{17}$$

$${}_{\partial}H^{e}_{ex} = \frac{e^2tv}{2\pi c^2} \times \int \left| \frac{\mu(\varepsilon_e \sin\varphi' \cos\vartheta_o' \sin\varkappa - \varepsilon_o \sin\vartheta_o' \cos\varkappa)^2}{[\varepsilon_o + (\varepsilon_e - \varepsilon_o)\cos^2\vartheta_0'][\varepsilon_o + (\varepsilon_e - \varepsilon_o)(\sin\varphi\sin\varkappa - \cos\varkappa \operatorname{ctg}\vartheta_o)\sin\varphi\sin\varkappa]} \right| \omega d\omega d\varphi. \tag{18}$$

The specifications of (8) and (9) have been taken into account in these formulas. In the case of an anisotropic dielectric, $\epsilon_{x'} = \epsilon_{y'} = \epsilon_o$, $\epsilon_{z'} = \epsilon_e$ (isotropic μ), and the equations for the indices of refraction are:

$$n_o^2 = \mu\varepsilon_o; \quad \frac{\mu}{n_e^2} = \frac{\cos^2\vartheta'}{\varepsilon_o} + \frac{\sin^2\vartheta'}{\varepsilon_e}. \tag{19}$$

From formulas (15) and (17) it is clear that for the motion of an electron along the optic axis of a uniaxial crystal ($\varkappa = 0$), in an anisotropic magnetic material only the ordinary waves are radiated, and in an anisotropic dielectric only the extraordinary waves are radiated.

Using the relations (8)-(12), (14), (18), we obtain for $\varkappa = 0$:

$$H^{o}_{ex} = \frac{e^2tv}{c^2} \int \left(\mu_o - \frac{2}{\varepsilon\beta^2} \right) \omega d\omega; \tag{20}$$

$${}_{\partial}H^{e}_{ex} = \frac{e^2tv}{c^2} \int \left| \left(\mu - \frac{1}{\varepsilon_o\beta^2} \right) \right| \omega d\omega. \tag{21}$$

The region of integration can be found from Eq. (16), which can be written in the form $\beta^2\mu_o\epsilon > 1$ for Eq. (20) and in the form $(\epsilon_e/\epsilon_o)(\beta^2\mu\epsilon_o - 1) > 0$ for Eq. (21).

For motion of the electron perpendicular to the optic axis ($\varkappa = \pi/2$), we obtain

$$H^{o}_{ex} = \frac{e^2tv}{2\pi c^2} \int \frac{(\mu_o - 1/\varepsilon\beta^2)\sin^2\varphi\, \omega d\omega d\varphi}{\beta^2\varepsilon\mu_o \cos^2\varphi + \sin^2\varphi}; \tag{22}$$

$$H^{e}_{ex} = \frac{e^2tv}{2\pi c^2} \times \int \left| \frac{\mu_o^2(\beta^2\varepsilon\mu_o - 1)\cos^2\varphi}{[\beta^2\varepsilon\mu_o \cos^2\varphi + \sin^2\varphi]\,[\mu_o + (\mu_e - \mu_o)\sin^2\varphi]} \right| \times \omega d\omega d\varphi; \tag{23}$$

$${}_{\partial}H^{o}_{ex} = \frac{e^2tv}{2\pi c^2} \int \frac{\mu(\beta^2\varepsilon_o\mu - 1)\cos^2\varphi\, \omega d\omega d\varphi}{\beta^2\varepsilon_o\mu\cos^2\varphi + \sin^2\varphi}; \tag{24}$$

$${}_{\partial}H^{e}_{ex} = \frac{e^2tv}{2\pi c^2} \times \int \left| \frac{(\beta^2\varepsilon_e\mu - 1)\sin^2\varphi}{\beta^2(\beta^2\varepsilon_o\mu\cos^2\varphi + \sin^2\varphi)\,[\varepsilon_o + (\varepsilon_e - \varepsilon_o)\sin^2\varphi]} \right| \times \omega d\omega d\varphi. \tag{25*}$$

The difference between Cerenkov radiation in media which are anisotropic in their magnetic properties from that in media which are anisotropic in their dielectric properties is clear from Eqs. (22)-(25). For example, the maximum intensity in a magnetically anisotropic medium corresponds to zero intensity in a medium which is anisotropic in its dielectric properties, and conversely, and this is true both for the ordinary and the extraordinary waves.

---

* For $\mu = 1$, Eq. (24) coincides with the corresponding equation in Ref. 1. Equations (21) and (25) for $\mu = 1$ do not coincide with the corresponding equations in Ref. 1 because of an error made in this reference in carrying out an integration.

The case of double anisotropy is also interesting. For the simplest medium of this type we choose a system of coordinates in which both the dielectric constant tensor and the magnetic permeability tensor are diagonal. The conditions imposed on $a_{\lambda i}$ and leading to Eq. (4) have the form

$$(d_{\lambda i}\, a_{\lambda i}) = 1; \quad (d_{\lambda i}\, k_{\lambda}) = 0; \tag{26}$$

$$(d_{\lambda i}\, a_{\lambda j}) = 0; \quad (h_{\lambda i}\, b_{\lambda j}) = 0$$

and for $\mu_x = \mu_y = \mu_z = 1$ coincide with the results of Ginzburg[5].

In a uniaxial crystal with a double anisotropy, both polarizations correspond to extraordinary waves. Equation (18), and consequently (21) and (25), but with μ_o in place of μ, holds for one polarization. The energy of radiation of the waves of the other polarization is determined by Eq. (15), but with ϵ_0 in place of ϵ. The extraordinary waves corresponding to the second polarization [Eq. (15)] are not radiated for a motion of the charge along the optic axis.

In conclusion, the author takes the opportunity of expressing his sincere gratitude to Prof. V.L. Ginzburg for proposing the problem and for valuable suggestions.

---

[1] V. L. Ginzburg, J. Exptl. Theoret. Phys. (U.S.S.R.) 10, 608 (1940).

[2] A. Kolomenskiĭ, Dokl. Akad. Nauk SSSR **86**, 1097 (1952).

[3] A. Kolomenskiĭ, J. Exptl. Theoret. Phys. (U.S.S.R.) 24, 167 (1953).

[4] M. I. Kaganov, J. Tech. Phys. (U.S.S.R.) **23**, 507 (1953).

[5] V. L. Ginzburg, J. Exptl. Theoret. Phys. (U.S.S.R.) **10**, 601 (1940)

[6] V. L. Ginzburg, J. Exptl. Theoret. Phys. (U.S.S.R.) 10, 601 (1940).

[7] A. G. Sitenko, Dokl. Akad. Nauk SSSR **98**, 377 (1954).

[8] K. M. Watson and J. M. Jauch, Phys. Rev. 75, 1249 (1949)

[9] D. Ivanenko and V. Gurgenidze, Dokl. Akad. Nauk SSSR **67**, 997 (1949).

[10] I. Frank and I. G. Tamm, Compt. rend. Acad. Sci. USSR **14**, 109 (1937)(in English).

[11] V. L. Ginzburg, Dokl. Akad. Nauk SSSR **56**, 253 (1947).

Translated by M. G. Gibbons
151

SOVIET PHYSICS JETP VOLUME 3, NUMBER 4 NOVEMBER, 1956

The Dynamics of Ionic Lattices of Ferroelectric Crystals in Limiting Cases

V. KH. KOZLOVSKII
Institute of Silicate Chemistry, Academy of Sciences, USSR

(Submitted to JETP editor February 21, 1955)
J. Exptl. Theoret. Phys. (U.S.S.R.) 30, 766-779 (April, 1956)

In this article a method is proposed for the investigation of the motion of the ions of a ferroelectric which is not limited by the magnitude of the anharmonic forces. A ferroelectric is considered whose ferroelectric ions vibrate as a rigid lattice, and coupled vibrations of two rigid lattices are also considered. The temperature dependence of the displacements and of their dispersions is obtained in qualitative agreement with experiment. Criteria are established for the number of phase transitions and their nature. Results of the investigation of a model anharmonic vibrator are made more precise, in which a possibility of a transition of the first kind is demonstrated. A model study is proposed of a ferroelectric which contains diatomic ferroelectric molecules. Criteria are established for the number and nature of phase transitions.

THE existing theories of ferroelectricity, except for the early work of Slater[1], assume that the motions of ferroelectric ions in the absence of polarization take place statistically independently of one another, so that the phase integral of the translational lattice breaks up into a product of the phase integrals of the ions. In studying problems of the polarization of liquids such theories are referred to as model theories. In a solid state there exists a greater correlation between the motions of the ions, so that it is useful to investigate another limiting case in which the ferroelectric ions form a rigid lattice (infinite wavelength). To this case belong inorganic crystals of simple structure, whose ferroelectric ions are situated relatively near to one another and the predominant wavelengths of whose vibrations are much larger than the interatomic distances. The theory of melting based on the analysis of the vibrations of a rigid lattice has turned out to be satisfactory[2]. The realization of model representations may be expected to occur in complex organic crystals with relatively large distances between ferroelectric ions, for example, in Rochelle salt.

An important role in the phenomena of ferroelectricity is played by the anharmonicity of the forces acting on the ferroelectric ions. It makes it possible to introduce normal coordinates not coupled to one another, and to define space-time trajectories of ions as is done in Born's theory[3]. Statistical methods of the determination of observed average characteristics of the motion are also complicated, and up to the present time have been applied only on the assumption of the smallness of the anharmonic terms, which imposed certain limitations. In this article we start out by assuming that the randomness in the motion of the ions of a solid is relatively small, and that it is not necessary, in order to take it into account, to utilize the apparatus of statistical mechanics which is more suitable for the treatment of liquids and gases[4]. The observed average characteristics of motion can be determined from certain dynamic principles without computing space-time trajectories. Inasmuch as the deBroglie wavelength of the ion of a solid is of the order 0.1-0.5 A, one can consider that space-time trajectories do not exist. In the present article we examine by a similar method of averaged parameters the vibrations of the rigid lattice of a ferroelectric, model theories, coupled vibrations of two rigid lattices and a model theory of a ferroelectric with diatomic ferroelectric molecules. The last case is realized in the case of Rochelle salt whose ferroelectric ions-protons are located in the lattice in pairs relatively distant from one another, so that a correlation exists only between the motion of the ions of a single pair.

1. THE BASIS OF THE METHOD OF AVERAGED PARAMETERS

Hamilton's variational principle is written in the form

$$\delta\left(\frac{1}{t_2-t_1}\int_{t_1}^{t_2} L\,dt\right)=0 \qquad (1.1)$$

under the condition $\delta q(t_1) = \delta q(t_2) = 0$. In the case of statistical equilibrium it is useful to work with the limit of the expression being varied under the condition $t_1 \to -\infty$, $t_2 \to \infty$ which exists in the case of bounded motion, and which is equal to the average value of the Lagrangian function $\bar{L}$. If we demand that the variations in the coordinates and the velocities should be bounded functions of time, and if we take into account the fact that the motion is bounded, we may go over from (1.1) to Hamilton's principle in the form[5] $\delta\overline{L} = 0$.

We shall apply this principle using Ritz's method. The true and quite complicated dependence of the coordinates on time we shall represent in the form of functions which contain parameters which define the average characteristics of the motion. The values of these parameters are found from the conditions that $\overline{L}$ should be an extremum. As such parameters we shall take the average value of the coordinate af the ion and its dispersion:

$$\overline{q}_k = s_k, \quad \overline{(q - \overline{q}_k)^2} = u_k^2. \tag{1.2}$$

Representing q_k in the form

$$q_k = s_k + u_k\theta_k(t), \tag{1.3}$$

we shall obtain on the basis of (1.2):

$$\overline{\theta}_k = 0, \quad \overline{\theta_k^2} = 1. \tag{1.4}$$

The manifold of bounded functions which satisfy conditions (1.4) represents the manifold of microscopic motions with the same average coordinate and dispersion. The relationship to the temperature is given by the relation $\overline{w}_k = kT/2$, where $\overline{w}_k$ is the average kinetic energy associated with some one generalized coordinate.

A less general method is obtained if one starts out from Hamilton's equations

$$\dot{p}_k = -\partial H/\partial q_k, \quad \dot{q}_k = \partial H/\partial p_k. \tag{1.5}$$

Averaging these equations over an infinite time interval we shall obtain

$$\overline{\partial H/\partial q_k} = 0, \quad \overline{\partial H/\partial p_k} = 0. \tag{1.6}$$

From (1.5) it follows that

$$\dot{p}_k q_l + \dot{q}_l p_k = \frac{d}{dt}(p_k q_l) = -q_l\frac{\partial H}{\partial q_k} + p_k\frac{\partial H}{\partial p_l}.$$

Averaging over time we obtain

$$\overline{q_l \partial H/\partial q_k} = \overline{p_k \partial H/\partial p_l}. \tag{1.7}$$

Expressions (1.6) and (1.7) form the required group of equations. The connection with the temperature is given in the same way as before.

2. ONE-DIMENSIONAL ANHARMONIC VIBRATIONS OF A RIGID LATTICE

The Lagrangian function of a single ion of the rigid lattice is equal to

$$L = \frac{m}{2}\left(\dot{\xi}^2 - \omega_0'^2\xi^2 - \frac{a^2}{2}\xi^4\right), \tag{2.1}$$

where $\omega_0'^2 = c'/m$, $a^2 = b/m$. Using (1.3) and (1.4) we find

$$\overline{\xi^4} = s^4 + 6s^2u^2 + 4su^3\overline{\theta^3} + u^4\theta^4.$$

We shall take $\overline{\theta^3} = 0$, assuming that the function $\theta(t)$ takes on with equal probability both the value $+\theta$, and the value $-\theta$. In view of the condition $\overline{\theta^2} = 1$, we may consider that $\overline{\theta^4}$ is equal to unity in order of magnitude. Averaging (2.1) we obtain

$$\frac{2}{m}\overline{L} = u^2\overline{\dot{\theta}^2} - \omega_0'^2(s^2 + u^2) - \frac{a^2}{2}(s^4 + 6s^2u^2 + u^4\overline{\theta^4}). \tag{2.2}$$

Using the extremal conditions $\partial\overline{L}/\partial s = 0$, $\partial\overline{L}/\partial u = 0$ and eliminating $\overline{\dot{\theta}^2}$ by means of the relationship $mu^2\overline{\dot{\theta}^2} = kT$ we shall obtain two equations:

$$s(a^2s^2 + \omega_0'^2 + 3a^2u^2) = 0, \tag{2.3}$$

$$\overline{\theta^4}a^2u^4 + 3a^2s^2u^2 + \omega_0'^2u^2 - kT/m = 0. \tag{2.4}$$

From (2.3) it follows that if $\omega_0'^2 > 0$, then only a single real solution $s = 0$ is possible which corresponds to the absence of spontaneous polarization. If $\omega_0'^2 < 0$, then for a sufficiently small u spontaneous polarization is possible. Since the dispersion u is certainly an increasing function of temperature, then above a certain temperature only the solution $s = 0$ will turn out to be possible. In the case $\omega_0'^2 < 0$, the substance is a ferroelectric. Equation (2.4) with $s = 0$ determines the dispersion of the oscillations of an ion of a paraelectric or a ferroelectric at high temperature.

In the case of a paraelectric we obtain

$$u^2 = \frac{2kT}{m\omega_0'^2}\left[1 + \sqrt{1 + \frac{4\overline{\theta^4}a^2}{m\omega_0'^4}kT}\right]^{-1} \tag{2.5}$$

For a ferroelectric (2.4) gives

$$u^2 = -\frac{2kT}{m\omega_0'^2}\left[\sqrt{1+\frac{4\overline{\theta^4}a^2}{m\omega_0'^4}kT}-1\right]^{-1} \qquad (2.6)$$

We now proceed to investigate a ferroelectric at temperatures which correspond to the existence of spontaneous polarization. Eliminating s^2 from Eqs. (2.3) and (2.4) we obtain the equation for the dispersions

$$(9-\overline{\theta^4})\,a^2u^4 + 2\omega_0'^2u^2 + kT/m = 0. \qquad (2.7)$$

From this we obtain, choosing in front of the radical that sign which gives $u^2 = 0$ at $T = 0$,

$$u^2 = -\frac{kT}{m\omega_0'^2}\left[1+\sqrt{1-\frac{(9-\overline{\theta^4})\,a^2}{m\omega_0'^4}kT}\right]^{-1}. \qquad (2.8)$$

At low temperatures we obtain the formula for the dispersion of a harmonic vibrator

$$u^2 = -kT/2m\omega_0'^2 = -kT/2c'$$

with the coefficient of elasticity equal to $-2c'$. This is the coefficient of elasticity in the region of the minimum of the curve (Fig. 1) where the ion is located at low temperatures. As the temperature increases the dispersion grows faster than in accordance with a linear law. The formula (2.8) is not applicable for temperatures $T > T' = m\omega_0'^4/(9-\overline{\theta^4})ka^2$.

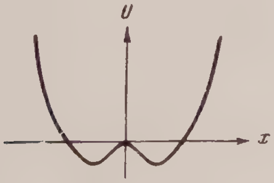

FIG. 1

On the basis of (2.3) and (2.8) we obtain the spontaneous displacement

$$s^2 = -\frac{\omega_0'^2}{a^2}\left\{1-\frac{3a^2kT}{m\omega_0'^4}\times\left[1+\sqrt{1-\frac{(9-\overline{\theta^4})\,a^2}{m\omega_0'^4}kT}\right]^{-1}\right\}. \qquad (2.9)$$

This equation may cease to hold at temperatures less than T', if its right-hand side becomes negative at $T = T'$. Making this substitution we obtain

$$s_{T'}^{(2)} = -(\omega_0'^2/a^2)\,[1-3/(9-\overline{\theta^4})]. \qquad (2.10)$$

The right-hand side is positive if $\overline{\theta^4} < 6$. In the case of sinusoidal vibrations, $\theta(t) = \sqrt{2}\sin(\omega t+\psi)$ and $\overline{\theta^4} = 1.5$, which is appreciably less than 6.

In the case of anharmonic vibrations $^2/_3\ \overline{\theta^4}$ apparently exceeds unity by only a small amount, and consequently,

$$T' = m\omega_0'^4/(9-\overline{\theta^4})ka^2 \qquad (2.11)$$

is the temperature of a phase transition of the first kind.

We then find other quantities of interest. The spontaneous displacement at absolute zero is

$$s^2_{T=0} = -\omega_0'^2/a^2. \qquad (2.12)$$

The limit of the displacement, when $T \to T'$ from below is

$$s^2_{T'-0} = -(\omega_0'^2/a^2)\,(6-\overline{\theta^4})/(9-\overline{\theta^4}). \qquad (2.13)$$

The limit of the dispersion, when $T \to T'$ from below is

$$u^2_{T'-0} = -(\omega_0'^2/a^2)/(9-\overline{\theta^4}). \qquad (2.14)$$

The limit of the dispersion, when $T \to T'$ from above is

$$u^2_{T'+0} = -\frac{2}{9-\overline{\theta^4}}\left[\sqrt{1+\frac{4\overline{\theta^4}}{9-\overline{\theta^4}}}-1\right]^{-1}\frac{\omega_0'^2}{a^2}. \qquad (2.15)$$

Assuming $\overline{\theta^4} = 2$, we obtain

$$T' = 0.143\,m\omega_0'^4/ka^2; \qquad (2.16)$$

$$s_{T'-0} = 0.75\,|\omega_0'|/a;$$

$$u_{T'-0} = 0.38\,|\omega_0'|/a;$$

$$u_{T'+0} = 0.78\,|\omega_0'|/a.$$

Figure 2 shows the variations of s and u with temperature. Analogous relationships had been established experimentally by Könzig[6] for $BaTiO_3$ by methods of X-ray analysis. Although in the case of $BaTiO_3$ two lattices are displaced, and moreover they oscillate in space, the qualitative dependences remain fundamentally analogous to those of Fig. 2.

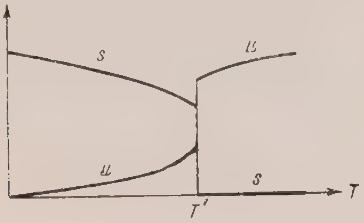

FIG. 2

We note that $m\omega'^4_0/4a^2 = U_m$ is the height of the potential barrier which separates the minima of the curve of Fig. 1. In accordance with (2.16), $kT' = 0.57\ U_m$. The quantity kT is, roughly speaking, the total energy of the oscillator at the transition point if one equates the average values of the kinetic and potential energies. It is evident that the equality $kT' = \gamma U_m$, where $\gamma \approx 1$, must hold for a barrier of arbitrary shape, and not only for that special shape which has been investigated above. The existence of the dependence of the phase transition point on the height of the potential barrier distinguishes the theory outlined above from the model theory of local minima[7]. Another difference is the existence of a discontinuity in the temperature dependence of the displacement. This also distinguishes the theory of the rigid lattice from the model theory of the anharmonic oscillator.

Let us make some numerical estimates. From (2.11) and (2.12) we have

$$kT' = bs^4_{T-0}/(9 - \overline{\theta^4}).$$

For $BaTiO_3$ it is known that $T' = 400°$, $s_{T=0.1}$A. Assuming $\overline{\theta^4} = 2$ we shall obtain $b = 4 \times 10^{23}$, $c' = 4 \times 10^5$. Values close to these can be obtained by a direct calculation using the known parameters of the ions.

3. PHASE TRANSITIONS IN A FERROELECTRIC WITH TWO LATTICES CAPABLE OF DISPLACEMENT

The present investigation can be applied to certain ferroelectrics which have more than two transitional lattices. In particular, one should note the field of solid solutions of ferroelectric components. Restricting ourselves to one-dimensional vibrations we shall characterize the positions of the ions of the two lattices by the coordinates ξ_1 and ξ_2, which are measured from the symmetrical positions in which the forces acting on the ions are equal to zero. The Lagrangian function for a molecule has the form

$$L = \frac{m_1}{2}\dot{\xi}_1^2 + \frac{m_2}{2}\dot{\xi}_2^2 - \frac{c'_1}{2}\xi_1^2 - \frac{c'_2}{2}\xi_2^2 - c'_{12}\xi_1\xi_2 - \frac{b_1}{4}\xi_1^4 - \frac{b_2}{4}\xi_{4.}^2 \quad (3.1)$$

Terms of the form $\xi_1^3\xi_2, \ldots$ are omitted. The coefficients c'_1, c'_2, c'_{12} are the direct and the mutual coefficients of elasticity which take into account the polarization of the ions. The coefficients b_1 and b_2 are taken to be positive.

Averaging (3.1), we obtain

$$\overline{L} = \frac{m_1}{2}u_1^2\overline{\dot{\theta}_1^2} + \frac{m_2}{2}u_2^2\dot{\theta}_2^2 - \frac{c'_1}{2}(s_1^2 + u_1^2) - \frac{c'_2}{2}(s_2^2 + u_2^2) - c'_{12}s_1s_2 - \frac{b_1}{4}(s_1^4 + 6\,s_1^2u_1^2 + \overline{\theta_1^4}u_1^4) - \frac{b_2}{4}(s_2^4 + 6s_2^2u_2^2 + \overline{\theta_2^4}u_2^4). \quad (3.2)$$

Equating to zero the derivatives with respect to s_1, s_2, u_1, u_2 and introducing temperature into these equations, we shall obtain

$$s_1^3 + 3s_1u_1^2 + (c'_1/b_1)s_1 + (c'_{12}/b_1)s_2 = 0; \quad (3.3)$$

$$s_2^3 + 3s_2u_2^2 + (c'_2/b_2)s_2 + (c'_{12}/b_2)s_1 = 0; \quad (3.4)$$

$$3s_1^2 + \overline{\theta_1^4}u_1^2 + c'_1/b_1 - kT/b_1u_1^2 = 0; \quad (3.5)$$

$$3s_2^2 + \overline{\theta_2^4}u_2^2 + c'_2/b_2 - kT/b_2u_2^2 = 0. \quad (3.6)$$

It is not possible to solve this system in the general case, and we shall undertake a qualitative investigation of it. From (3.3) and (3.4) it follows that if $s_1 = 0$, then also $s_2 = 0$, and conversely, so that the displacements may appear and disappear only simultaneously. Since the dispersions increase indefinitely with increasing temperature it may be shown that at sufficiently high temperature, $s_1 = s_2 = 0$. Indeed, if we assume the converse, and factor s_1 and s_2 outside the brackets in (3.3) and (3.4), we rewrite these equations in the form

$$s_1\varphi_1(T) + (c'_{12} / b_1)\, s_2 = 0;$$
$$(c'_{12} / b_2)\, s_1 + s_2\varphi_2(T) = 0,$$

where φ_1 and φ_2 increase indefinitely with temperature. The determinant of this system $\varphi_1\varphi_2 - c'^2_{12}/b_1b_2$ is positive at sufficiently high temperature, which is incompatible with the assumption that $s_1 \neq 0$ and $s_2 \neq 0$. Thus, if the substance is not a pyroelectric for which the melting point lies lower than the temperature of disappearance of spontaneous polarization, then at high temperature only the nonpolar phase exists. In this phase the dispersions are determined by the equation

$$u_1^2 + c'_1 / \overline{\theta_1^4} b_1 - kT / \overline{\theta_1^4} b_1 u_1^2 = 0. \tag{3.7}$$

in agreement with (3.5) and (3.6) (and similarly for u_2^2); conversely, the fulfillment of one of these equations characterizes the nonpolar phase. The solution of (3.7) has the form

$$u_1^2 = \frac{2kT}{|c'_1|}\left[\frac{c'_1}{|c'_1|} + \sqrt{1 + \frac{4\,\overline{\theta_1^4}\,b_1}{c'^2_1} kT}\,\right]^{-1}. \tag{3.8}$$

Let us suppose that we have the polar phase. Multiplying (3.5) by s_1, (3.3) by 3, subtracting term by term and carrying out the same operations on (3.6) and (3.4), we shall obtain the system of equations:

$$[(9 - \overline{\theta_1^4})\, u_1^2 + 2c'_1 / b_1 + kT / b_1 u_1^2]\, s_1$$
$$+ 3\,(c'_{12} / b_1)\, s_2 = 0;$$
$$3\,(c'_{12} / b_2)\, s_1 + [(9 - \overline{\theta_2^4})\, u_2^2$$
$$+ 2\,c'_2 / b_2 + kT / b_2 u_2^2]\, s_2 = 0.$$

From this it follows that the determinant

$$\Delta = \left[(9 - \overline{\theta_1^4})\, u_1^2 + 2\,\frac{c'_1}{b_1} + \frac{kT}{b_1 u_1^2}\right] \tag{3.9}$$
$$\times\left[(9 - \overline{\theta_2^4})\, u_2^2 + 2\,\frac{c'_2}{b_2} + \frac{kT}{b_2 u_2^2}\right] - 9\,\frac{c'^2_{12}}{b_1 b_2}$$

is equal to zero.

Let us for the sake of brevity denote the manifold of all those values of the temperature for which $s_1 = s_2 = 0$ by the term paramanifold. Let us denote the left-hand parts of (3.7) by D_1 and D_2; they are equal to zero everywhere within the paramanifold, and differ from zero outside it. The determinant Δ is equal to zero everywhere outside the paramanifold and, conversely, where $\Delta \neq 0$, there we have the paramanifold. Let us denote by the manifold M that submanifold of those points of the paramanifold in which $\Delta = 0$, and let us show that the manifold M is not generally empty. Over this manifold the following conditions hold: $D_1 = 0$, $D_2 = 0$, $\Delta = 0$. Substituting (3.8) into the equation $\Delta = 0$, we shall obtain for the temperature an irrational equation, the solutions of which are roots of a certain algebraic equation. From this it follows that the manifold M is finite. Let us investigate the question as to the kind of points of which this manifold may be composed. Let the point A be an isolated point of the paramanifold (Fig. 3); consequently, as T approaches T_A $s_1 \to 0$, $s_2 \to 0$. Transposing [in Eqs. (3.3) and (3.4)] s_1^3 and s_2^3 into the right-hand side and solving the equations with respect to s_1 and s_2 as linear equations, we obtain

$$s_1 = -\frac{(3u_2^2 + c'_2 / b_2)\, s_1^3 - (c'_{12} / b_2)\, s_2^3}{(3u_1^2 + c'_1 / b_1)(3u_2^2 + c'_2 / b_2) - c'^2_{12} / b_1 b_2} \tag{3.10}$$

and similarly for s_2. The determinant of this system vanishes at the point A. As may be seen from (3.7) and (3.9) it is equal to the value of Δ over the paramanifold reduced ninefold, and consequently, Δ vanishes at isolated points of the paramanifold, and these points belong to the manifold M.

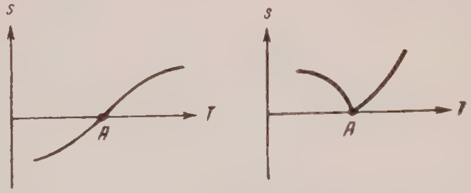

FIG. 3

Let the point C be the upper or the lower bound of the paramanifold, or the Curie point (Fig. 4). By reasoning similar to the above, but letting s_1 and s_2 approach zero from one side, we conclude that the bounds of the paramanifold belong to the manifold M. In addition to the bounds of the paramanifold and the isolated points one may also have points of discontinuity, but these are outside the scope of the present investigation. We shall deal with them only indirectly.

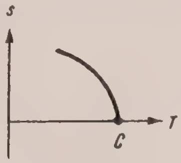

FIG. 4

Let us now proceed to a geometrical investigation of the Eqs. (3.3) and (3.4). We note that Eqs. (3.3)-(3.6) are satisfied if one replaces s_1 and s_2 by $-s_1$ and $-s_2$. The change of sign of c'_{12} leads to a change of sign of one of the displacements. Since the dispersions are monotonic, although possibly discontinuous functions of the temperature, the dependence of the solutions of the Eqs. (3.3) and (3.4) on the parameters u_1^2 and u_2^2 qualitatively represents their dependence on the temperature. Without loss of generality one may take $c'_{12} < 0$ and distinguish the following three cases: 1) $c'_1 > 0$, $c'_2 > 0$; 2) $c'_1 > 0$, $c'_2 < 0$; 3) $c'_1 < 0$; $c'_2 < 0$.

We shall consider the rigid lattice to be ferroelectric only in the case when its own coefficient of elasticity is negative. The usual stability conditions at the temperature of absolute zero

$$\frac{\partial^2 \overline{U}}{\partial s_1^2} > 0; \quad \frac{\partial^2 \overline{U}}{\partial s_2^2} > 0; \quad \frac{\partial^2 \overline{U}}{\partial s_1^2}\,\frac{\partial^2 \overline{U}}{\partial s_2^2} - \left(\frac{\partial^2 \overline{U}}{\partial s_1 \partial s_2}\right)^2 > 0$$

show that the state $s_1 = s_2 = 0$ is stable only in the first case if

$$c'^2_{12} < c'_1 c'_2 . \qquad (3.11)$$

First Case. Neither of the two lattices is ferroelectric.

The graphs of Eqs. (3.3) and (3.4) are shown in Fig. 5. As the temperature is increased the point C approaches the origin, and at sufficiently high temperature the curves intersect only at the origin.

However, it is possible that the curves intersect only at the origin at all temperatures; in such a case the substance is paraelectric. In this case the criterion for ferroelectric behavior is the inequality

$$(ds_2 / ds_1)_3 \, (ds_1 / ds_2)_4 < 1 \quad \text{for} \quad u_1 = u_2 = 0,$$

which leads to the inequality

$$|c'_{12}| > \sqrt{c'_1 c'_2}. \qquad (3.12)$$

The spontaneous polarization in this case is entirely due to the interaction of the lattices, while each lattice separately does not have any tendency for a spontaneous displacement.

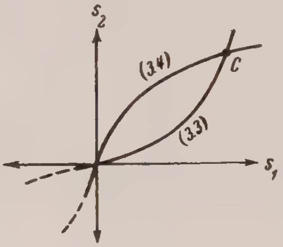

FIG. 5

Second Case. Only one of the two lattices is ferroelectric.

The corresponding graphs for a low and for a somewhat higher temperature are shown in Fig. 6. In this case the substance is a ferroelectric.

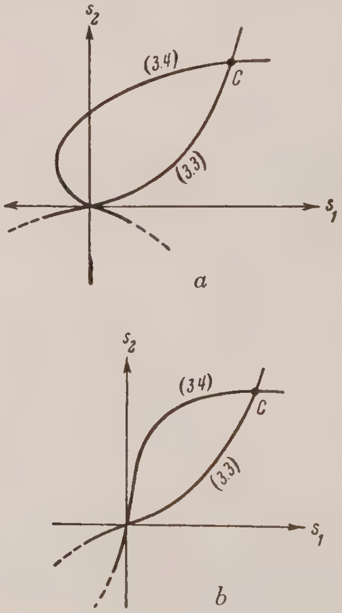

FIG. 6. a-$3u_2^2 + c'_2/b_2 < 0$, b-$3u_2^2 + c'_2/b_2 > 0$.

Third Case. Both lattices are ferroelectric ones.

The corresponding graphs for increasing temperatures are shown in Fig. 7. In this case at low temperatures not one but two nonzero intersections and two phase transitions are possible at low temperatures, but for this, the fulfillment of condition (3.11) is necessary. Thus, if the interaction between lattices is small, then at low temperatures such spontaneous displacements are established which correspond to the "natural" tendencies of the ferroelectric lattices for the production of spontaneous displacements. At still higher temperature the spontaneous displacements are determined by the interaction of the lattices. With a still further increase of temperature the spontaneous displacements disappear.

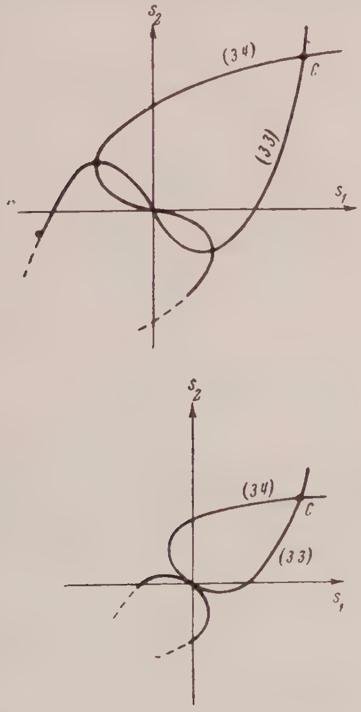

FIG. 7

We now proceed to the investigation of the nature of the phase transitions in all cases and for this we shall determine the corresponding Curie points or the isolated points. If the corresponding temperatures turn out to be negative, then even though phase transformations may occur, nevertheless they must be discontinuous. We equate expression (3.9) to zero, using (3.7), which yields the following equation:

$$\left(\frac{c_1'|c_1'|}{6b_1}+kT_C\Bigg/\left[\sqrt{1+\frac{4\overline{\theta_1^4}b_1}{c_1'^2}kT_C}+\frac{c_1'}{|c_1'|}\right]^{-1}\right)$$
$$\times\left(\frac{c_2'|c_2'|}{6b_2}+kT_C\Bigg/\left[\sqrt{1+\frac{4\overline{\theta_2^4}b_2}{c_2'^2}kT_C}+\frac{c_2'}{|c_2'|}\right]^{-1}\right)$$
$$=\frac{c_{12}'^2|c_1'||c_2'|}{36b_1b_2}. \tag{3.13}$$

The solutions of this irrational equation can be found from the solutions of the complete algebraic equation of the fourth degree. Since we are seeking only the qualitative relationships we shall assume for simplicity

$$b_1=b_2=b;\ |c_1'|=|c_2'|=c'; \tag{3.14}$$
$$\overline{\theta_1^4}=\overline{\theta_2^4}=\overline{\theta^4}.$$

First Case. Using the notation $c'^2/6b=a$; $4\overline{\theta^4}b/c'^2=\varkappa$; $c'^2_{12}c'^2/36b^2=m$, $kT_c=\chi$, (3.13) may be written in the form

$$a+\chi/(\sqrt{1+\varkappa\chi}+1)^2=m. \tag{3.15}$$

Setting $1+\varkappa\chi=y^2$ with the condition $y>0$, we obtain

$$y=-(a\varkappa-1)\pm\varkappa\sqrt{m} \tag{3.16}$$
$$=1-{}^2/_3\,\overline{\theta^4}\,(1\mp|c_{12}'|/c').$$

Since ${}^2/_3\ \overline{\theta^4}\geq 1$, we must take the upper sign in (3.16) in order to obtain $y>0$.

The Curie temperature is equal to

$$T_C=\frac{c'^2}{3bk}\left(\frac{|c_{12}'|}{c'}-1\right) \tag{3.17}$$
$$\times\left[1+\frac{1}{3}\overline{\theta^4}\left(\frac{|c_{12}'|}{c'}-1\right)\right].$$

It is positive if the condition (3.12) is satisifed, i.e., if in the first case a phase transition is possible at all, then it will be a phase transition of the second kind.

Second Case. Equation (3.13) has the form

$$\left(a+\frac{\chi}{\sqrt{1+\varkappa\chi}+1}\right)\times\left(-a+\frac{\chi}{\sqrt{1+\varkappa\chi}-1}\right)=m. \tag{3.18}$$

In analogy with the preceding we shall obtain $y^2 = m\varkappa^2 + (a\varkappa - 1)^2$ and

$$kT_{\mathrm{C}}=\frac{\overline{\theta^4}}{9b}c'^2\left[\left(\frac{c'_{12}}{c'}\right)^2+1-\frac{3}{\overline{\theta^4}}\right].$$

We have a phase transition of the first kind if the mutual coefficient of elasticity is small in comparison with the direct ones, and of the second kind if this coefficient is large.

Third Case. Equation (3.13) has the form

$$(-a+\chi/[\sqrt{1+\varkappa\chi}-1])^2=m. \tag{3.19}$$

From this we obtain

$$y=a\varkappa-1\pm\varkappa\sqrt{m}={}^2/_3\,\overline{\theta^4}\,(1\pm|c'_{12}|/c')-1.$$

If condition (3.11) is not satisfied, i.e., if only one transition exists, then $y > 0$ only corresponding to the upper sign. For sufficiently small $|c'_{12}|/c'$ the lower sign is also possible,

Further,

$$\varkappa\chi=y^2-1=\frac{2}{3}\overline{\theta^4}\left(1\pm\frac{|c'_{12}|}{c'}\right)\left[\frac{2}{3}\overline{\theta^4}\left(1\pm\frac{|c'_{12}|}{c'}\right)-2\right]. \tag{3.20}$$

If condition (3.11) is satisfied then (3.20) does not have any positive values, and both phase transitions are of the first kind. If condition (3.11) is not fulfulled, then the phase transition is of the second kind with a Curie temperature:

$$T_{\mathrm{C}}=\frac{c'^2}{3bk}\left(\frac{|c'_{12}|}{c'}+1\right)\times\left[\frac{\overline{\theta^4}}{3}\left(\frac{|c'_{12}|}{c'}+1\right)-1\right]. \tag{3.21}$$

On the basis of the above one may establish the general regularity that the domination of the mutual coefficient of elasticity over the direct ones leads to a phase transition of the second kind. The dependence of the displacements and of the total polarization on the temperature in the first and in the second cases is quite evident; one should only note that the total polarization determined by both displacements may be equal to zero, and in such a case the polar phase will be antiferroelectric. The thermodynamic theory of antiferroelectrics was developed in Ref. 8. The dependence of the displacements and of the polarization on the temperature in the third case in the presence of two phase transitions is shown in Fig. 8.

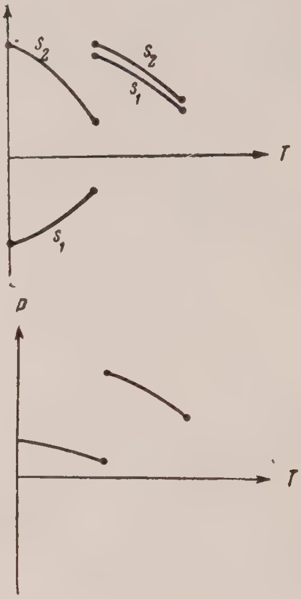

FIG. 8

We note that after the lower phase transition one of the displacements changes sign, so that in a special case one may have here a transition from a ferroelectric state into an antiferroelectric state.

4. MODEL INVESTIGATION OF THE ANHARMONIC VIBRATOR IN A SPHERICALLY SYMMETRIC POTENTIAL WELL

The calculations of this section are applicable to a vibrator both with a positive coefficient of elasticity (the model of Ginzburg-Devonshire) and also with a negative coefficient of elasticity which corresponds to the local minima model of Pauling-Slater. In this work we improve the results which were obtained not quite rigorously in Ref. 9, as it was assumed there that the effective field has no effect on the dispersion of the ion. The potential energy for a single anharmonic vibrator has the form

$$U = \frac{c}{2}(\xi^2 + \eta^2 + \zeta^2) \tag{4.1}$$

$$+ \frac{b}{4}(\xi^2 + \eta^2 + \zeta^2)^4 - \frac{1}{2} e^*A(\xi s_x + \eta s_y + \zeta s_z).$$

The coefficient ½ in front of the last term is introduced in order that the interaction of the ions will not be taken into account twice when the average potential energy of the whole lattice $N\bar{U} = -\frac{1}{2}Ne^*As^2 + \ldots$ is being calculated.

The Lagrangian function of a given ion is

$$L = \frac{m}{2}(\dot{\xi}^2 + \dot{\eta}^2 + \zeta^2) - U. \tag{4.2}$$

Averaging (4.2), we shall obtain a system of equations for the average values of the coordinates of the ion s_x, s_y, s_z and of their dispersions u_x, u_y, u_z.

$$s_x[s_x^2 + s_y^2 + s_z^2 + 3u_x^2 \tag{4.3}$$

$$+ u_y^2 + u_z^2 + (c - e^*A)/b] = 0;$$

$$3s_x^2 + s_y^2 + s_z^2 + \overline{\theta_x^4}u_x^2$$

$$+ \overline{\theta_x^2\theta_y^2}u_y^2 + \overline{\theta_x^2\theta_z^2}u_z^2 + c/b = kT/bu_x^2;$$

$$s_y[s_x^2 + s_y^2 + s_z^2 + 3u_y^2$$

$$+ u_z^2 + u_x^2 + (c - e^*A)/b] = 0;$$

$$3s_y^2 + s_z^2 + s_x^2 + \overline{\theta_y^4}u_y^2$$

$$+ \overline{\theta_y^2\theta_z^2}u_z^2 + \overline{\theta_y^2\theta_x^2}u_x^2 + c/b = kT/bu_y^2;$$

$$s_z[s_x^2 + s_y^2 + s_z^2 + 3u_z^2$$

$$+ u_x^2 + u_y^2 + (c - e^*A)/b] = 0;$$

$$3s_z^2 + s_x^2 + s_y^2 + \overline{\theta_z^4}u_z^2$$

$$+ \overline{\theta_z^2\theta_x^2}u_x^2 + \overline{\theta_z^2\theta_y^2}u_y^2 + c/b = kT/bu_z^2.$$

From these equations it may be seen that spontaneous polarization is possible only if $e^*A > c$. Insofar as the direction in space of the displacement in a spherically symmetric potential well has no physical significance, we shall set $s_x = s_y = s_z$, $u_x = u_y = u_z$; then also $\overline{\theta_x^4} = \overline{\theta_y^4} = \overline{\theta_z^4} = \vartheta_1$ and $\overline{\theta_x^2\theta_y^2} = \overline{\theta_x^2\theta_z^2} = \overline{\theta_y^2\theta_z^2} = \vartheta_2$.. Equations (4.3) then reduce to the following:

$$s_x(3s_x^2 + 5u_x^2 + (c - e^*A)/b) = 0; \tag{4.4}$$

$$5s_x^2 + \vartheta u_x^2 + c/b = kT/bu_x^2, \tag{4.5}$$

where $\vartheta = \vartheta_1 + 2\vartheta_2$. An important difference between Eq. (4.5) and Eq. (2.5) of Ref. 9 is the presence of a term which consains s_x^2. In the region in which spontaneous polarization is absent we obtain

$$u_x^2 = \frac{2kT}{c}\left[\sqrt{1 + \frac{4\vartheta b}{c^2}kT} + 1\right]^{-1}, \tag{4.6}$$

$$\text{if } c > 0,$$

$$u_x^2 = -\frac{2kT}{c}\left[\sqrt{1 + \frac{4\vartheta b}{c^2}kT} - 1\right]^{-1}, \tag{4.7}$$

$$\text{if } c < 0.$$

In the region of spontaneous polarization by eliminating s^2 from (4.4) and (4.5), and taking into account that $Se^*A > 2c$, we obtain

$$u_x^2 = \frac{6kT}{5e^*A - 2c} \tag{4.8}$$

$$\times\left[1 + \sqrt{1 - 12\frac{25 - 3\vartheta}{(5e^*A - 2c)^2}bkT}\right]^{-1}$$

This expression ceases to be real if $T > T'$, where

$$T' = (5e^*A - 2c)^2/12(25 - 3\vartheta)bk. \tag{4.9}$$

If for $T \to T'$ from below the displacement tends to a real value different from zero, then at the transition through the point T' a discontinuous transition into the nonpolar state will occur, while in the opposite case the transition will be continuous. From (4.4), (4.8) and (4.9) we obtain

$$\lim_{T \to T'} s^2 = 3\lim_{T \to T'} s_x^2 \tag{4.10}$$

$$= \frac{1}{2(25 - 3\vartheta)b}[5(5e^*A - 8c) - 6\vartheta(e^*A - c)].$$

Thus, the transition will be of the first kind if

$$5(5e^*A - 8c) > 6\vartheta(e^*A - c), \tag{4.11}$$

and of the second kind if

$$5(5e^*A - 8c) \leqslant 6\vartheta(e^*A - c). \tag{4.12}$$

The equals sign corresponds to the critical case when the phase transition remains continuous, but acquires a number of special properties.

The condition (4.11) is fulfilled only if $c \leq 0$, i.e., in the model of the minima, and in the model of the purely anharmonic vibrator, we have a phase transition of the first kind. As long as ϑ lies within the limits 3-4½, then from (4.11) it follows that the phase transition will be of the first kind also in the model with one minimum if e^*A is much larger than c. In the case of a phase transition of the second kind the Curie point may be found from (4.4) and (4.5) if one take into account that from $T = T_C$ the dispersion satisfies both these equations with $s = 0$:

$$T_C = \frac{\vartheta}{25bk}(e^*A - c)\left(e^*A + \frac{5-\vartheta}{\vartheta}c\right). \quad (4.13)$$

Expression (4.13) agrees with expression (2.11) of Ref. 9, if one sets $\vartheta = 3$.

In the neighborhood of the Curie point s^2 is proportional to $T_C - T$ and, differentiating (4.4) and (4.5), we find

$$s^2 = -\frac{25k}{5(5e^*A - 8c) - 6\vartheta(e^*A - c)}(T_C - T) + \ldots \quad (4.14)$$

As we appraoch the fulfillment of the condition for a phase transition of the first kind the coefficient of $T_C - T$ increases, and in the critical case becomes infinite. On the basis of the data obtained above one may also determine the discontinuity in the specific heat for the transition through the Curie point. The average value of the Hamiltonian function for a single ion is determined by the formula

$$\frac{2}{3}\bar{H}_1 = kT - (e^*A - c)s_x^2 + cu_x^2 + \frac{b}{2}(3s_x^4 + \vartheta u_x^4 + 10s_x^2u_x^2). \quad (4.15)$$

The specific heat for a single ion in the neighborhood of the Curie point is given by

$$\frac{2}{3}C_1 = k - (e^*A - c)\frac{ds_x^2}{dT} + c\frac{du_x^2}{dT} + \vartheta bu_x^2\frac{du_x^2}{dT} + 5bu_x^2\frac{ds_x^2}{dT}. \quad (4.16)$$

Close by and below the Curie point we obtain from the above expression

$$\frac{2}{3}C_1 - k = \frac{15k}{6\vartheta(e^*A - c) - 5(5e^*A - 8c)}\left[c + \frac{1}{5}(e^*A - c)\right]. \quad (4.17)$$

As we approach the region of validity of the inequality (4.11) this quantity grows indefinitely. In the neighborhood of the upper Curie point the specific heat is determined by the formula

$${}^2/_3\, C_1 - k = k[\vartheta(e^*A - c) + 5c]/[2\vartheta(e^*A - c) + 5c]. \quad (4.18)$$

This quantity remains angular as the region of validity of the inequality (4.11) is approached. Thus, the present investigation shows that in the model of the minima the phase transition must be of the first kind; in the model with the single minimum it must be also of the first kind if e^*A is much larger than c, and of the second kind if e^*A is smaller than c. The sharpness of the transition of the second kind may vary within wide limits, depending on the relationships between the force parameters e^*A and c. The one-dimensional case does not qualitatively differ from the case discussed above.

5. MODEL THEORY OF A FERROELECTRIC WITH DIATOMIC MOLECULES

The potential energy of the atoms forming the molecule taking into account their mutual polarization, but not taking into account the polarization of the medium, is given by

$$\frac{c_1'}{2}\xi_1^2 + c_{12}'\xi_1\xi_2 + \frac{c_2'}{2}\xi_2^2 + \frac{b_1}{4}\xi_1^4 + \frac{b^2}{4}\xi_2^4,$$

where ξ_1 and ξ_2 are the displacements of the atoms measured from their equilibrium positions. The potential energy of the molecule in the electric field determined by the polarization of the medium may be written in the form

$$-{}^1/_2\, e_1^*E_{ef_1}\xi_1 - {}^1/_2\, e_2^*E_{ef_2}\xi_2 \quad (5.1)$$

with the following expressions for the effective fields[10]:

$$E_{ef_1} = A_{11}'s_1 + A_{12}'s_2; \quad E_{ef_2} = A_{21}'s_1 + A_{22}'s_2. \quad (5.2)$$

The primes on A_{ik} denote that in the calculation of the corresponding structural sums one must omit the neighboring ion present in the molecule under investigation. The potential energy per molecule is thus equal to

$$U = \frac{c'_1}{2}\xi_1^2 + c'_{12}\xi_1\xi_2 + \frac{c'_2}{2}\xi_2^2 \tag{5.3}$$
$$+ \frac{b_1}{4}\xi_1^4 + \frac{b^2}{4}\xi_2^4 - {}^1/_2\, e_1^*(A'_{11}s_1 + A'_{12}s_2)\,\xi_1 - {}^1/_2\, e_2^*$$
$$\times (A'_{21}s_1 + A'_{22}s_2)\,\xi_2.$$

The average value of the Lagrangian function is found in the usual way

$$\overline{L} = \frac{m_1}{2} u_1^2\overline{\dot{\theta}_1^2} + \frac{m_2}{2} u_2^2\overline{\dot{\theta}_2^2} \tag{5.4}$$
$$- \frac{c'_1}{2}(s_1^2 + u_1^2) - \frac{c'_2}{2}(s_2^2 + u_2^2) - c'_{12}s_1s_2$$
$$- \frac{b_1}{4}(s_1^4 + 6s_1^2u_1^2 + \overline{\theta_1^4}u_1^4)$$
$$- \frac{b_2}{4}(s_2^4 + 6s_2^2u_2^2 + \overline{\theta_2^4}u_2^4) + \frac{1}{2}e_1^*A'_{11}s_1^2$$
$$+ \frac{1}{2}e_2^*A'_{22}s_2^2 + \frac{1}{2}(e_1^*A'_{12} + e_2^*A'_{21})\,s_1s_2.$$

The conditions for $\overline{L}$ to be an extremum after the temperature has been introduced into them have the form

$$s_1^3 + 3s_1u_1^2 + s_1(c'_1 - e_1^*A'_{11})/b_1 \tag{5.5}$$
$$+ s_2[c'_{12} - {}^1/_2(A'_{12} + A'_{21})]/b_1 = 0;$$

$$s_2^3 + 3s_2u_2^2 + s_2(c'_2 - e_2^*A'_{22})/b_2 \tag{5.6}$$
$$+ s_1[c'_{12} - {}^1/_2(A'_{12} + A'_{21})]/b_2 = 0;$$

$$3s_1^2 + \overline{\theta_1^4}u_1^2 + c'_1/b_1 - kT/b_1u_1^2 = 0; \tag{5.7}$$
$$3s_2^2 + \overline{\theta_2^4}u_2^2 + c'_2/b_2 - kT/b_2u_2^2 = 0. \tag{5.8}$$

These equations turn out to be similar in many respects to the corresponding equations for a crystal composed of two rigid lattices, but there are also differences which lead to a large variety of possible cases. This is connected with the fact that the ferroelectric ion (for example, $e_1^*A'_{11} > c'_1$) may exist either in a potential well with two minima ($c'_1 < 0$), or with one minimum ($c'_1 > 0$). Let us examine the possible variants very briefly, since the corresponding discussion is in many respects analogous to the case of rigid lattices.

1. Neither ion is ferroelectric: $e_1^*A'_{11} < c'_1$ and $e_2^*A'_{22} < c_2$. In this case only $c'_1 > 0$ and $c'_2 > 0$ are possible since $e_1^*A'_{11} > 0$ and $e_2^*A'_{22} > 0$ (the polarization forces determined by the displacement of the ion aid its further displacement, but do not hinder it). The substance is a paraelectric if

$$|c'_{12} - {}^1/_2(e_1^*A'_{12} + e_2^*A'_{21})| \tag{5.9}$$
$$< [(c'_1 - e_1^*A'_{11})(c'_2 - e_2^*A'_{22})]^{1/2}.$$

In the opposite case only one phase transition exists.

2. Only one ion is ferroelectric: $e_1^*A'_{11} > c'_1$, $e_2^*A'_{22} < c'_2$ or, conversely, $e_1^*A'_{11} < c'_1$, $e_2^*A'_{22} > c'_2$. The substance is a ferroelectric and there exists one phase transition.

3. Both ions are ferroelectric. In this case there are two phase transitions if condition (5.9) is satisfied, and one phase transition in the opposite case.

In order to draw conclusions in regard to the nature of the phase transitions one must examine the equation which determines the Curie points or the isolated points. In order to simplify calculations this investigation is carried out under the assumption

$$|c'_1| = |c'_2|;\ b_1 = b_2;\ \overline{\theta_1^4} = \overline{\theta_2^4};$$
$$|c'_1 - e_1^*A'_{11}| = |c'_2 - e_2^*A'_{22}|$$

and leads to the following results:

First Case. If condition (5.9) is not fulfilled, then a positive Curie temperature is obtained. Thus, if a phase transition is possible it will be of the second kind.

Second Case. $e_1^*A'_{11} > c'_1$ and $e_2^*A'_{22} < c_2$. Here, two subcases are possible: $c'_1 < 0$ and $c'_1 > 0$. The first subcase is analogous to the second case of rigid lattices, so that the transition will be of the first kind if the interaction forces are small in comparison with the self-forces, or to be more precise, if $|c'_{12} - {}^1\!/_2(e_1^*A'_{12} + e_2^*A'_{21})|$ is small in comparison with $|e_1^*A'_{11} - c'_1|$ or $|e_2^*A'_{22} - c'_2|$. In the opposite case the transition will be of the second kind. If $c'_1 > 0$, then the phase transition will be of the second kind.

Third Case. Both ions are ferroelectric. Here three subcases are possible:

a) $c'_1 < 0$ and $c'_2 < 0$. Analysis shows that if condition (5.9) is fulfilled, then both phase transitions are of the first kind. If this condition is not fulfilled, then only a single phase transition of the second kind is possible.

b) $c_1' > 0$ and $c_2' > 0$. In this subcase if condition (5.9) is satisfied, then both phase transitions are of the second kind. If condition (5.9) is not satisfied, then only a single phase transition of the second kind is possible.

c) $c_1' < 0$ and $c_2' > 0$. In this subcase there is at least one phase transition of the second kind which will also be the only one if condition (5.9) is not fulfilled. The nature of the other phase transition in the case that condition (5.9) is fulfilled is to a large extent determined by the relationships between the force parameters of the vibrators.

From the above it is possible to draw the conclusion that a phase transition of the first kind is favored by the negative sign of the direct coefficients of elasticity, and by a small value of the interaction forces between the two ions.

One may also note that the total polarization determined by the displacements of both ions may turn out to be equal to zero, and then the third case apparently describes a crystal of the type of Rochelle salt. Here a change in sign of one of the displacements after the lower phase transition leads to the disappearance of the macroscopic spontaneous polarization, and it turns out to be possible only within a certain temperature interval.

---

[1] J. Slater, J. Chem. Phys. **9**, 16 (1941).

[2] W. Braunbeck, Z. Physik **38**, 549 (1926).

[3] M. Born and M. Goeppert-Meyer, *Theory of Solids*, ONTI (Moscow-Leningrad), 1938 (Russian translation).

[4] L. Boltzmann, *Lectures on Kinetic Theory of Gases*, GITTL (Moscow), 1953 (Russian translation).

[5] V. Kh. Kozlovskii, Thesis, Institute of Silicate Chemistry, Academy of Sciences, USSR (Leningrad), 1955.

[6] W. Känzig, Helv. Phys. Acta **24**, 175 (1951).

[7] W. Mason and B. Mathias, Phys. Rev. **74**, 1622 (1948).

[8] G. Smolenskii and V. Kozlovskii, J. Exptl. Theoret. Phys. (U.S.S.R.) **26**, 684 (1954).

[9] G. Smolenskii and V. Kozlovskii, J. Tech. Phys. (U.S.S.R.) **23**, 445 (1953).

[10] V. Kozlovskii, J. Tech. Phys. (U.S.S.R.) **21**, 1388 (1951).

Translated by G. M. Volkoff
152

Letters to the Editor

Pulsed Coherent Generation of Millimeter Radiowaves by Nonrelativistic Electron Bunches

G. A. Askar'ian
P. N. Lebedev Physical Institute
Academy of Sciences, USSR

(Submitted to JETP editor August 10, 1955)
J. Exptl. Theoret. Phys. (U.S.S.R.) 30, 584-586
(March, 1956)

THE proposed[1,2] and partly realized[3] methods of coherent generation of millimeter waves by electron bunches possess a number of properties limiting their applicability and efficacy. Thus, for instance, a complicated experimental set-up containing an accelerator and buncher of relativistic electrons is necessary for the wave generation through relativistic transformation of emission frequencies taking place during the passage of the bunch through the field of the undulator[1-3] or the accelerator[1]. The difficulty of formation of compact, strong, relativistic bunches and preservation of their size during sufficiently long flight in fields in the presence of Coulomb divergence and spread of the trajectories of the electrons forming the bunch prevent the actual realization of the method and its application.

The proposed methods of microwave generation by nonrelativistic electron bunches radiating during accelerated or oscillatory motion (under the influence of applied electromagentic fields) or uniform Cerenkov motion in a narrow channel in a dielectric or close to a dielectric surface[1] are in practice inconvenient, since the condition of the proximity to the dielectric (the cross section of the channel or the distance to the dielectric surface should be smaller than the wavelength of the generated radiation) together with the necessity of safeguarding a long path of flight bring about heavy current losses and limitations connected with the necessity of strong collimation and the impossibility of employing strong compact bunches.

The method of generation of microwaves proposed here makes use of the radiation emitted during the bombardment of a metallic or dielectric anticathode with electronic bunches or by rebounding of the bunches from a strong localized field. The possibility of employing compact (during the short timed interaction), strong electronic bunches constitutes the main advantage of the pulsed method, permitting the placing of the interaction region in the focus of the buncher. Although pulsed bunches create radiation having a continuous spectrum, the minimum wavelength of intensively emitted radiation, determined by the compactness of the bunch at the moment of action, can be shifted into the spectral region where the use of methods employing long-acting bunches is not very effective or altogether impossible.

We shall estimate the angular distribution and the total energy of radiation for the case of normal incidence of a nonrelativistic bunch upon a layer of metal. For a bunch consisting of N electrons, moving with the velocity v, the distribution of radiation accompanying the annihilation of a bunch and its image in the frequency region in which the emitted wavelength is greater than the bunch dimensions

$$\mathcal{E}^{\mathrm{ann}}(\theta)\,d\omega\,d\Omega \approx (N^2e^2v^2/\pi^2c^3)\sin^2\theta\,d\omega\,d\Omega$$

(θ is the angle between the direction of reception and the velocity vector of the bunch image) and

$$\mathcal{E}^{\mathrm{ann}}_{\omega}d\omega \approx (4N^2e^2v^2/3\pi c^3)\,d\omega\,.$$

The main advantages of metallic anticathodes are larger value of thermal and electrical conductance and high thermal endurance, enabling the use of strong currents without impairing the stability. With a pulsed current $I \sim 300$ mA, $N \sim 10^9$ and the kinetic energy of electrons in the bunch $T_{\mathrm{kin}} \sim 30$ kev, the pulsed power of radiation in the bandwidth $\Delta\lambda \sim \lambda \sim 0.1$ cm

$$w_{\mathrm{pulsed}} \approx 8INe\beta^2/3\lambda \sim 130\ \mathrm{W}.$$

Among the deficiencies of metallic anticathodes should be noted the small efficiency coefficient of transformation of the bunch energy into radiation and inconvenient angular distribution of the radiation.

A second method of generation consists in pulsed generation of radiation, arising through incidence of the beam on an indentation on the surface of a dielectric, transparent for the millimeter waves, but possessing sufficient conductivity for the direct current.

The energy of the radiation in the dielectric is:

$$\mathcal{E}^{\mathrm{brems}}_{\mathbf{n}\omega}(\theta')\,d\Omega\,d\omega = c'\varepsilon\,|\mathbf{E}_{\omega}|^2R_0^2\,d\Omega\,d\omega$$

($c' = c/\sqrt{\epsilon}$; θ' is the angle between the direction of reception $\mathbf{n}$ and the initial bunch velocity $\mathbf{v}_0$).

Summing the Fourier components of the wave fields of all electrons, and using the formulas for the case of infinite dielectric (neglecting the boundary effect of reflection is obviously permissible in the case of $v_0 \approx c'$, i.e., in the case of prevalence of the radiation in the forward direction) we shall obtain, while the coherence condition

$$\omega\left(\frac{x}{v_0} + \frac{y \sin\theta}{c'}\right) \ll 1,$$

is satisfied (x and y denote the longitudinal and the lateral dimensions of the bunch, respectively),

$$\mathbf{E}_\omega = \sum_{i=1}^{N} \mathbf{E}_{i\omega} = \frac{e}{2\pi\varepsilon c'^2 R_0} \sum_{i=1}^{N} \int \frac{[\mathbf{n}\,[(\mathbf{n} - \mathbf{v}_i / c')\,\dot{\mathbf{v}}_i]]}{(1 - \mathbf{v}_i \mathbf{n} / c')^2}$$

$$\times \exp\left[j\omega \left\{ t_1' + \frac{R_0}{c'} - \frac{\mathbf{r}_i(t_i')\,\mathbf{n}}{c'} \right\} \right] dt_i'$$

$$\approx \frac{(eN) \exp\{i\omega R_0 / c'\}}{2\pi\varepsilon c'^2 R_0} \frac{[\mathbf{n}\,[\mathbf{n}\mathbf{v}_0]]}{(1 - \mathbf{v}_0 \mathbf{n} / c')}.$$

(This is true since for the plane boundary and for $\beta' \approx 1$ in the coherent region $\mathbf{E}_\omega^{\mathrm{brems}} \approx -\mathbf{E}_\omega^{\mathrm{trans}}$ in order to prevent the vanishing of the Fourier component of interest of the resulting wave field it is necessary to attenuate the bremsstrahlung or the transitional radiation at least in the desired bandwidth, or to create the needed phase shift between radiation pulses. This can be done, for instance, making narrow axial channels in the dielectric, about 1 cm deep, which should be sufficient for destroying the longitudinal condition of coherence of the bunch or a part of it at one end of the channel, or for the desired phase shift between the radiation pulses.)

Using the obtained expression for $\mathbf{E}_\omega$, we shall write down the formulas for the spectral-angular and the spectral distributions of the energy of the transitional or the bremsstrahlung radiations:

$$\mathcal{E}_{\mathbf{n}\omega}(\theta')\,d\Omega d\omega = \frac{\sqrt{\varepsilon}\,(eN)^2 v_0^2 \sin^2\theta'}{4\pi^2 c^3 (1 - \beta_0' \cos\theta')^2}\,d\Omega d\omega;$$

$$\mathcal{E}_{\mathbf{n}\omega}(\theta'_{\mathrm{max}}) = \frac{\sqrt{\varepsilon}\,(eN)^2 v_0^2}{4\pi^2 c^3 (1 - \beta_0'^2)};$$

$$\mathcal{E}_\omega d\omega = \frac{\sqrt{\varepsilon}\,(Ne)^2 v_0^2}{\pi c^3 \beta_0'^3} \left\{ \ln \frac{1 + \beta_0'}{1 - \beta_0'} - 2\beta_0' \right\} d\omega,$$

where θ'_{max} is the angle corresponding to the maximum intensity ($\cos\theta'_{\mathrm{max}} = \beta_0'$).

These formulas should coincide with the radiation distribution formulas for the sudden stopping of a point charge in dielectric[4], since in the spectral region of interest the wavelength of the emitted radiation exceeds the dimensions of the braking region and of the bunch.

Obviously, the use of dielectric anticathodes, permitting only moderate currents due to their thermal limitations will be purposeful in the region $\beta_0 \approx c'$ in which the intensity and direction of radiation rise sharply on entering the dielectric.

We shall compare the bremsstrahlung radiation in the dielectric anticathode with the "annihilation" radiation, following the head-on incidence of a nonrelativistic electron bunch upon a metallic anticathode: for $\sqrt{\epsilon} \sim 3$ ($T_{\mathrm{kin}} \sim 30$ kev) and the mean value of $1/(1 - \beta'^2) \approx 10^2$:

$$\frac{\mathcal{E}_{\mathbf{n}\omega}^{\mathrm{brems}}(\theta'_{\mathrm{max}})}{\mathcal{E}_{\mathbf{n}\omega}^{\mathrm{ann}}(\theta_{\mathrm{max}})} = \frac{\sqrt{\varepsilon}}{4(1 - \beta_0'^2)} \approx 75; \qquad \frac{\mathcal{E}_\omega^{\mathrm{brems}}}{\mathcal{E}_\omega^{\mathrm{ann}}} \approx 9.$$

The mean yield of radiation energy $w = 4\,W$ in $\Delta\omega \sim 2 \times 10^{12}$ ($\Delta\lambda \sim \lambda \sim 0.1$ cm) for the total current intensity of the bunches entering the channels of a thermally stabilized dielectric anticathode $I_b \sim 1$mA, and for the number of electrons in the bunch $N \sim 10^9$

It should be noted that the cited values of radiation energy in the region $\Delta\lambda \sim \lambda \sim 0.1$ cm are obtained for the continuous distribution spectrum, which allows the energy to be redistributed in the spectrum, e.g., phase-shifted bremsstrahlung radiation or employing bunches with periodically modulated charge density.

The final choice of the anticathode will depend on the specific conditions and purposes of the tube. The separation of the millimeter waves from the x-ray background can be done using, for instance, bent waveguides bringing out the radiation from behind the protecting screens or using a dielectric transparent for the microwaves as a filter.

The idea of construction of a millimeter wave generator simple in production and use and sufficiently intensive, seems to be promising, since its realization will enable wide application of millimeter waves.

---

[1] V. L. Ginzburg, Izv. Akad. Nauk SSSR, Ser. Fiz. 11, 165 (1947).

[2] H. Motz, J. Appl. Phys. 22, 527 (1951).

[3] H. Motz, J. Appl. Phys. 24, 826 (1953).

[4] V. L. Ginzburg and I. M. Frank, J. Exptl. Theoret. Phys. (U.S.S.R.) 16, 15 (1946).

Translated by H. Kasha
110

Angular Momentum Distribution and the Spatial Distribution of Nucleons in Nuclei

S. I. Larin
Moscow State University

(Submitted to JETP editor May 21, 1955)
J. Exptl. Theoret. Phys. (U.S.S.R.) 30, 587-589
(March, 1956)

WITH the help of the Thomas-Fermi model, a relation is established between the spatial distribution of particles $\rho(r)$ and the distribution of the angular momentum $n(L)$ giving the number of particles with a given angular momentum L[1] From the condition $n(L)=0$, $\rho(r)$ being known, the numbers of particles Z_l can be found for which l-states occur first, and the mean square of the angular momentum[2] can be determined as well. The latter can be written in the form:

$$\overline{L^2} = \frac{6}{25}\left(\frac{9\pi}{4}\right)^{2/3} Z^{2/3}\Xi; \quad \Xi = \frac{5\int\limits_0^\infty \rho^{5/3}(r)\, r^4 dr}{\left[3\int\limits_0^\infty \rho(r)\, r^2 dz\right]^{5/3}} \tag{1}$$

Knowing $\rho(r)$, $\overline{L^2}$ can be found. In the case of a nucleus, however, $\rho(r)$ of nucleons is not well enough known. Then, vice versa, from the empirical data about the first appearance of odd protons* in states with $l = 1, 2, 3, 4, 5, \ldots$ for $Z = 3, 9, 21, 41, 71, \ldots$ we can obtain information about $\rho(r)$[3-5] (strictly speaking, for nuclei with Z close to Z_l). Information about $\rho(r)$ for nuclei with any Z can be obtained, in principle, from the comparison of $\overline{L}^2$ calculated from Eq. (1), with the empirical data for $\overline{L}^2$ found from the scheme of level filling according to the formula

$$\overline{L^2}_{\rm emp} = \frac{1}{Z}\sum_i l_i(l_i+1) \quad (\hbar = 1). \tag{2}$$

The most acceptable scheme of level filling of odd protons and neutrons is the following one[6,7]:

$$1s \underset{2}{\Big|} 2p_{3/2} \underset{(6)?}{\vdots}\ 2p_{1/2} \underset{8}{\Big|} 3d_{5/2} \underset{14}{\vdots}\ 2s3d_{3/2} \underset{20}{\Big|} 4f_{7/2} \underset{28}{\Big|} 3p \underset{34}{\vdots}\ 4f_{5/2} \underset{40}{\vdots}\ 5g_{9/2} \underset{50}{\Big|} 4d_{5/2},\ 5g_{7/2} \underset{64}{\vdots}\ 3s,\ 4d_{3/2} \underset{(70)?}{\vdots}$$

$$6h_{11/2} \underset{82}{\Big|} 5f_{7/2},\ 6h_{9/2} \underset{100}{\vdots}\ 4p_{3/2},\ 5f_{5/2},\ 4p_{1/2} \underset{(112)?}{\vdots}\ 7i_{13/2} \underset{126}{\Big|} 6g_{9/2},\ 7i_{11/2},\ 5d_{5/2},\ 6g_{7/2},\ 4s, \tag{3}$$

$$5d_{3/2},\ 8j_{15/2} \underset{(184)}{\Big|} \ldots$$

The scheme (3) is (in the section 126-184) an extrapolation of the Meyer-Jensen scheme. Comparing $\overline{L}^2$ from Eq. (1) with $\overline{L}^2_{\rm emp}$ from Eq. (3) and assuming a certain $\rho(r)$, we can find a relation between the parameters of $\rho(r)$. Taking as the simplest $\rho(r)$ a constant density distribution within a sphere of radius R, we obtain $\xi = 1$ and $\overline{L}^2 = 0.885Z^{2/3}$ much larger than $\overline{L}^2_{\rm emp}$. On the other hand, lowering L^2 results in the density $\rho_0 e^{-br^2}$ or $\rho_0 e^{-\alpha r}$ ($\xi = 0.472$, $\overline{L}^2 = 0.418Z^{2/3}$). The density giving the correct $\overline{L}^2$ should therefore be in between a constant and $\rho_0 e^{-\alpha r}$.

The density distributions dependent on one parameter result in constant values of ξ and cannot be in agreement with empirical $\overline{L}^2$ for all nuclei (see Ref. 5). Taking the effect of nuclear density saturation into account and neglecting for the time being the influence of Coulomb forces, we shall assume the nuclear density to be constant in the central part of the nucleus and falling off on the periphery. This condition is met by the following density distributions[5,8,9]:

$$\rho^{(\mathrm{I})}(x) = \begin{cases} \rho_0^{(\mathrm{I})} & (x \leqslant x_0) \\ \rho_0^{(\mathrm{I})}\cdot e^{-(x-x_0)} & (x > x_0), \end{cases} \quad (x = \alpha r,\ x_0 = \alpha R_0^{(\mathrm{I})}); \tag{4}$$

$$\rho^{(\mathrm{II})}(y) \begin{cases} \rho_0^{(\mathrm{II})}, & (y \leqslant y_0) \\ \rho_0^{(\mathrm{II})}(y_0/y)^2 e^{-(y-y_0)}, & (y > y_0), \end{cases} \quad (y = \beta r,\ y_0 = \beta R_0^{(\mathrm{II})}). \tag{5}$$

The parameters x_0 and y_0 represent here the ratio of the radii of the region of constant density $R_0^{(\mathrm{I})}$

and $R_0^{(\mathrm{II})}$ to the effective thicknesses of the surface layer $1/\alpha$ and $1/\beta$.

From the requirement of agreement between $\overline{L}^2$ calculated for the densities (4) and (5) and $\overline{L}^2_{\mathrm{emp}}$ we have found the values of x_0 and y_0 for different Z. The resultant dependence of x_0 and y_0 on Z has a saw-tooth character (see the Figure, curve *1*) analogous to the dependence of $\overline{L}^2_{\mathrm{emp}}$ on Z according to (3). In view of the fact that y_0 changes in a relatively smaller range than x_0, $\rho^{(\mathrm{II})}(r)$ should be given first choice. The parameters x_0 and y_0 rise in the regions of completion of the levels $3d_{5/2}$, $4f_{7/2}$, $5g_{9/2}$, etc., attaining maxima for nuclei with magic Z, which corresponds to the relatively thinner surface layer in magic nuclei. Additional maxima of x_0 and y_0 appear as the result of the completion of the levels $5g_{7/2}$, $6h_{9/2}$, $7i_{11/2}$, $\cdot$ ($N=64, 100, \sim150, \ldots$). We note that the above treatment is applicable only in the case of spherically symmetric magic nuclei. The parameters x_0 and y_0 can, however, be correlated with the effective thickness of the surface layer, obtained by averaging $\rho(r)$ over the angles in real (generally) deformed nuclei and therefore, with the qualitative values of the eccentricity of the nuclei, found from the quadrupole moment (see Figure, curve *4*). Thus, the minima of x_0 and y_0 correspond, in the region of heavy nuclei, to the most strongly deformed nuclei.

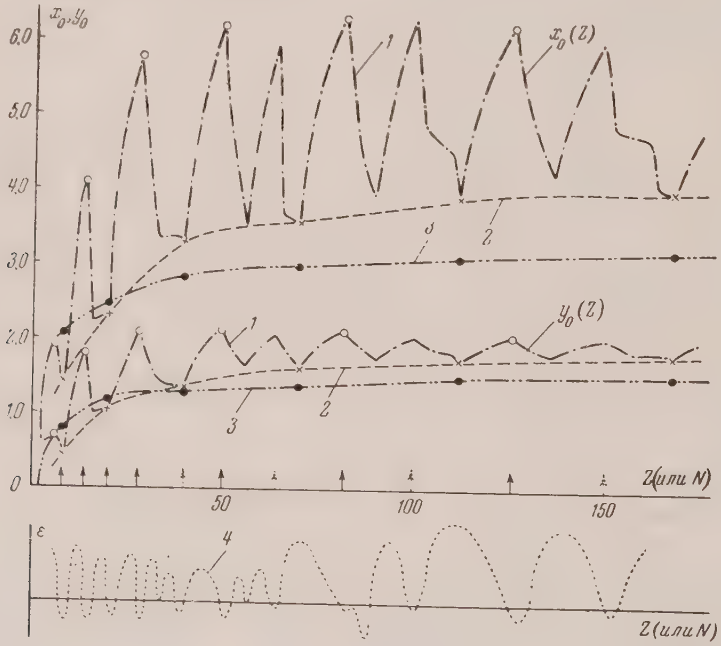

FIG. 1.

It is interesting to note that the values of x_0 and y_0 found from $\overline{L}^2$ and the numbers of first occurrence of Z_l for identical nuclei (see Figure, curves *3* and *4*, respectively) do not coincide. This is connected with the fact that L^2_{emp}, in contrast to Z_l, is determined by all completed states for given Z. Taking into account that the scheme of level filling is not finally established and bearing in mind the statistical character of Eq. (1), the obtained values of x_0 and y_0 should be regarded as qualitative only, expecially for non-magic nuclei.

Disregarding other details, we shall determine the remaining parameters $\rho_Z(r)$ of the protons (4) and (5) using the empirical Coulomb energies of nuclei[10]. Taking the mean values $x_0 \approx 4.8$ and $y_0 \approx 1.8$ (for $Z > 20$) and assuming $\rho_Z(r)/\rho_N(r) = Z/N$, we obtain

$$R^{(\mathrm{I})}_{0Z} = 0.92\times10^{-13}\,A^{1/3}; \tag{6}$$

$$R^{(\mathrm{II})}_{0Z} = 0.73\times10^{-13}\,A^{1/3}.$$

On the basis of nonuniform density of nucleons, of the type (4) and (5), we can analyze the effective empirical nuclear radii, finding the mean values of different powers of r from $\rho(r)$, on which the various effects depend**. Thus, the mean value of r^2 from $\rho_Z^{(II)}(r)$ is

$$\overline{R_Z^{2(II)}} = 3/5\left[(y_0^3 + 5y_0^2 + 10y_0 + 10)/y_0^2(y_0+3)\right] R_{0Z}^{2(II)}. \quad (7)$$

Finding the mean square radius $\{\overline{R_Z^{2(II)}}\}^{1/2}$ for the average $y_0 \approx 1.8$ and introducing the equivalent radius of constant density proton distribution that gives the same $\{\overline{r^2}\}^{1/2}$ $(R_Z = (5/3)^{1/2}\{\overline{R_Z^2}\}^{1/2}$, we find

$$R_Z^{(II)} \cong 1{,}21\times10^{-13}\ A^{1/3} \quad (8)$$

in good agreement with empirical electromagnetic nuclear radii[11].

Since for the densities (4) and (5) the nucleon density differs markedly from zero at distances larger than $R_Z \sim 1.2 \times 10^{-13}A^{1/3}$ one can understand qualitatively, on the basis of the examined $\rho(r)$, the considerably larger values of nuclear radii $(1.5 \times 10^{-13}A^{1/3})$ obtained from the cross section in processes in which nucleons (and evidently π-mesons) take part and data found from α-decay where the effective radii are connected with the region of action of nuclear forces.

If we shall assume the same $\rho(r)$[(4) and (5)] and the same level scheme (3) for neutrons, the corresponding parameters x_{0N} and y_{0N} for $\rho(r)$ will be correlated with N as x_0 and y_0 with Z.

Finally, we note that both $\{\overline{R_Z^{2(II)}}\}^{1/3}$ and the effective radii

$$\tilde{R}_Z^{(II)} = R_{0Z}^{(II)} + 1/\beta = (1 + 1/y_{0Z})\, R_{0Z}^{(II)}$$

will change nonmonotonically because of the sawtooth like change of y_{0Z}. Magic nuclei will have lower $\{\overline{R_Z^2}\}^{1/2}$ and $\tilde{R}_Z$. Therefore, the relative drop in the value of the radius should be more pronounced for the doubly-magic nuclei. The effective empirical nuclear radii show also relative drops for the magic and some sub-magic nuclei[12]. Such nonmonotonic character of the effective nuclear radii can be regarded as caused by deviations from spherical symmetry.

I wish to express my thanks to Prof. D. D. Ivanenko and N. N. Kolesnikov for the discussion of the problem and valuable remarks.

Note added in Proof: For the density of the form $\rho_z(r) = \rho_0[1 + e^{K(r-c)}]^{-1}$ the parameter Kc calculated from $\bar{L}$ for Au ($Z = 79$) is in sufficient agreement with the value $Kc \approx 12.0$, for which best agreement between theory and experiment is observed for the cross section angular dependence for the scattering of high-energy electrons on Au_{79} nuclei[13].

---

* In the following, dealing with protons, we shall keep in mind that unless otherwise mentioned, the results are valid for neutrons as well.

** The parameters x_0 and y_0 were determined from the numbers of first occurrence and the r^2 also in Ref. 7.

[1] P. Gombas, *The Statistical Theory of the Atom*, Moscow, 1951.

[2] J. H. Jensen and J. M. Luttinger, Phys. Rev. **86**, 907 (1952).

[3] D. Ivanenko and A. Sokolov, Dokl. Akad. Nauk SSSR 74, 33 (1950).

[4] M. Born and L. Yang, Nature 166, 399 (1955).

[5] N. Kolesnikov, Dokl. Akad. Nauk SSSR 103, 57 (1955).

[6] P. F. Klinkenberg, Rev. Mod. Phys. 24, 63 (1952).

[7] N. Kolesnikov, Dissertation, Moscow State University, 1955.

[8] B. Kerimov, Dissertation, Moscow State University, 1950.

[9] R. Wilson, Phys. Rev. 88, 350 (1852).

[10] A. Green and N. Engler, Phys. Rev. 91, 40 (1953).

[11] F. Bitter and H. Feshbach, Phys. Rev. 92, 837 (1953).

[12] D. Ivanenko and S. Larin, J. Exptl. Theoret. Phys. (U.S.S.R.) 24, 359 (1953).

[13] R. Hofstadter, Proc. 5th Ann. Rochester Conf., Jan. 1955.

Translated by H. Kasha
111

Some Cases of Generation of Heavy Unstable Particles on Beryllium Nuclei

N. G. BIRGER, V. V. GUSEVA, G. B. ZHDANOV
S. A. SLAVATINSKII AND G. M. STASHKOV
P. N. Lebedev Physical Institute
Academy of Sciences, USSR

(Submitted to JETP editor September 23, 1955)
J. Exptl. Theoret. Phys. (U.S.S.R.) 30, 590-591
(March, 1956)

IN recent years, it has been made evident[1-3] that hyperons and K-mesons can be created by pairs in reactions of the type:

$$\pi^- + p \rightarrow \Lambda + K \quad \text{or} \quad N + N \rightarrow \Lambda + K + N.$$

In the case of interaction of π-mesons with free protons, a correlation of the positions of the planes of emission and of decay of the hyperons is observed. Such a correlation is not observed if the hyperons are produced as a result of irradiation of heavy nuclei (Pb) by cosmic rays[4].

Single cases of formation of hyperons and K-mesons on light nuclei (Be) irradiated by cosmic rays have been observed in our experiments performed at an altitude of 3860 m above sea level. The experimental set-up consisted of a Wilson chamber with a diameter of 30 cm and a depth of illumination of 8 cm. The chamber contained a 5 cm thick beryllium plate, and under it a 1 cm thick lead plate. The chamber was in an 8,500 oersted field of an electromagnet. The chamber was controlled by a system of counters separating electron-nuclear showers.

For 25 observed cases of generation of showers on beryllium, there were observed 3 cases of decay of heavy particles (formed on the beryllium), during their flight. The main characteristics of these cases are reported in Table I.

Figure 1 shows the photograph of case 117.63.

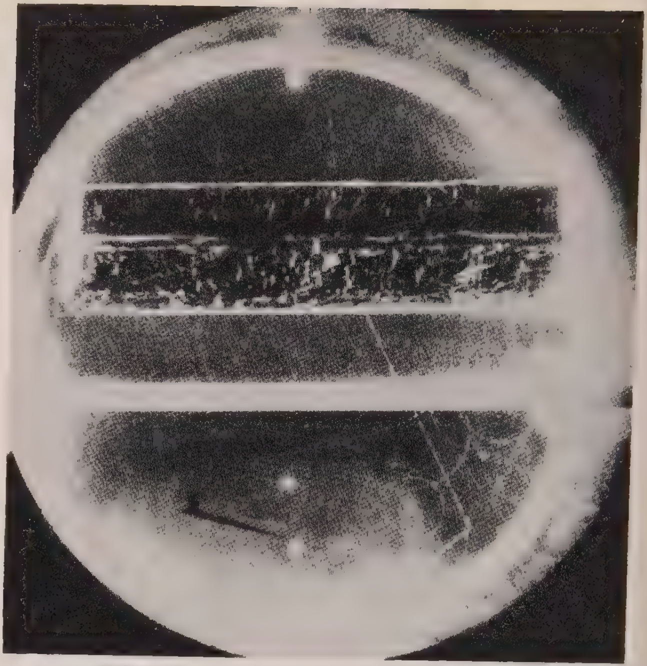

FIG. 1

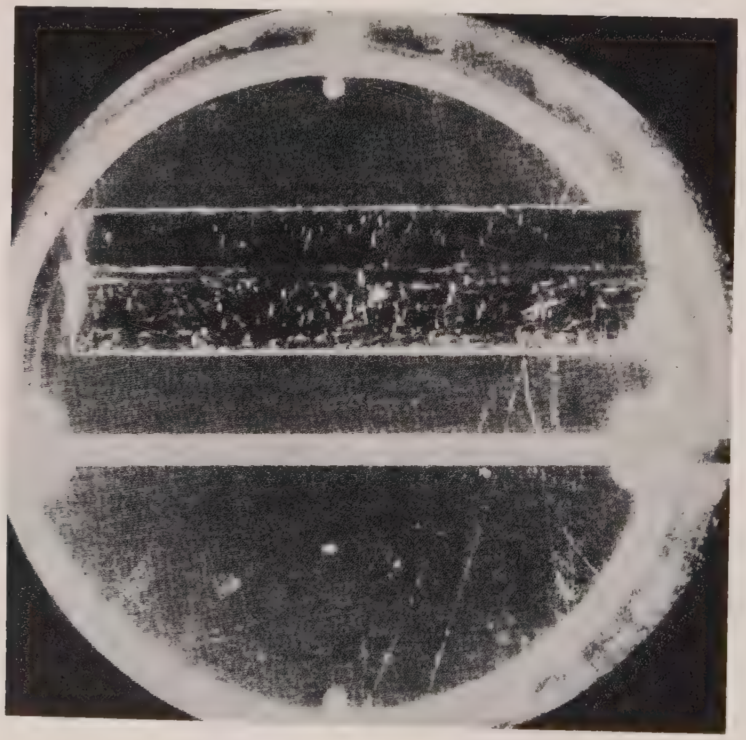

FIG. 2

We analyzed all the known schemes of decay of charged hyperons and heavy mesons with emission of a single charged secondary particle. The

TABLE I

No. of Photograph	Primary Particles						Secondary Particles						
	Momentum $p \times 10^8$ ev/c	Sign of Charge	Angle with the Generating Particle θ_p^0*	Angle[1] of Uncoplanarity δ	Assumed Nature of the Particle	Half Life[2] $T = \frac{L^{**}}{3p/M}$ sec	No. of Particle	$p \times 10^8$ ev/c	Ionization	R grams/cm^2 Pb	Angle with Primary θ	Angle Between Secondary θ_{12}	Assumed Nature of Secondary Particles
117.63	$8.6^{+15}_{-3.5}$	+	20 ± 2	---	Σ^+	7×10^{-10}	1	---	$\frac{I_{\text{prim}}}{I_{\text{sec}}} = 1.4 \pm 0.4$	---	93 ± 2	---	π-meson
120.54	---	Neutr.	9 ± 4	1 ± 2	Λ^0	4×10^{-10}	1	> 12 ---	$I_1 \sim I_{\min}$	---	2 ± 2	---	Proton
							2		$I_2 \gtrsim 2.6\, I_1$	13	47 ± 2	49 ± 2	π-meson
112.66	---	Neutr.	11 ± 2	3 ± 2	θ^0	---	1	$5.3^{+3.5}_{-1.5}$	$I_1 \sim I_{\min}$		14 ± 1		$\pi(\mu)$-meson
							2	---	$I_2 \sim I_{\min}$	---	39 ± 1	53 ± 0.5	---

---

[1] Angle of uncoplanarity between the trace of the V^0-particle with the plane of the secondary particles. All angles in degrees.

[2] L-Path of the decaying particle from the point of generation to the point of decay, in centimeters.

TABLE II

No. of Case	Assumed Nature of the Particle	φ^0
117.63	Σ+	57±10
120.54	Λ^0	74±10
112.66	θ^0	15±5

TABLE III

Nature of the Particle	Angle φ between the planes of formation and of decay, according to data from Refs. 1-3.							
Λ^0 θ^0	5+5 —	30±20 —	27±10 70±5	38±5 —	~20 ~90	~40 ~0	— 22±10	— 58±3
$\Sigma\pm$	7±5	20±20	10±10					

hypothesis of a decay-scheme of the hyperon: $\Sigma^+ \to \pi^+ + n$ fits best the observed values of the momentum, of the angle and of the ionization ratio pertaining to the primary and secondary particles. The observed half-life of the particle is also in good agreement with this hypothesis. For the energy of decay of the hyperon we get

$Q = (125^{+175}_{-20})$ mev.

Figure 2 shows the photograph of case 120.54: generation of V^0-particles in a shower. Two types of neutral V-particles are known: the Λ^0 and θ^0-particles. The analysisof the decay-schemes of these particles [$\Lambda^0 \to p + \pi^-$ and $\theta^0 \to \pi^+ + \pi^-$] has shown that, in the observed case, a Λ^0-particle decayed into a fast proton and a slow π^--meson. In case 112.66 one also observes the decay of a V^0-particle formed on the beryllium plate. The positively charged secondary particle cannot be a proton because of the observed values of the momentum and of the ionization. One must then assume that the decay follows the scheme $\theta^0 \to \pi^+ + \pi^- + 214$ mev. In this case, the momentum of particle l must be equal to 6.3×10^8 ev, which is in good agreement with the experimental value. In all the observed cases the direction of the charged particle (which generated the V-particle on a Be nucleus) is known; hence, one can measure the angle φ between the plane of generation of the V-particle and the plane of its decay (see Table II).

Table III shows the data on angles φ for all cases known in the literature of pair generation of hyperons and K-particles resulting from irradiation of hydrogen by π -mesons.

For all 9 observed cases of formation of hyperons in a π^-_p interaction, the angle $\varphi$is such that $\varphi \leq 40°$; this indicates that hyperons have large spins. At the same time, for hyperons formed on a Be nucleus, we have $\varphi \geq 40°$ (Table II). This is probably due to the Be nucleus (such as scattering of hyperons or their generation by secondary particles of the shower).

The authors thank A.E. Chudakov for discussion of the results, K. A. Kotel'nikov, V. M. Maksimenko, C. V. Riabikov for taking part in the study of the photographs, and also C. Fedorov for helping in the photometering of the tracks.

---

[1] Fowler, Shutt, Thorndike and Whittemore, Phys. Rev. 91, 1287 (1953); 93, 861 (1954); 98, 121 (1955).

[2] W. D. Walker, Phys. Rev. 98, 1407 (1955).

[3] Block, Harth, Fowler, Shutt, Thorndike and Whittemore, Phys. Rev. 99, 261 (1955).

[4] G . D. James and R. A. Salmeron, Phil. Mag. 46, 571 (1955).

Translated by E.S. Troubetzkoy
112

Linearization of the Hartree Equations

P. S. Zyrianov and V. M. Eleonskii
The Ural Polytechnical Institute

(Submitted to JETP editor September 24, 1955)
J. Exptl. Theoret. Phys. (U.S.S.R.) 30, 592
(March, 1956)

In addition to the existing methods of description of collective interactions[1-4] we may consider another one based on the linearization of the Hartree equation near the solutions with constant density.

In the equations

$$i\hbar \frac{\partial\psi_i}{\partial t} + \frac{\hbar^2}{4m}\Delta\psi_i - \left\{\int G(|\mathbf{r}-\mathbf{r}'|) \times \sum_j |\psi_j(\mathbf{r}')|^2 \, d\mathbf{r}'\right\}\psi_i(\mathbf{r}) = 0 \qquad (1)$$

let us make the substitution

$$\psi_i(\mathbf{r}, t) = \sqrt{P_i(\mathbf{r}, t)} \exp\{-iS_i(\mathbf{r}, t)/\hbar\}.$$

This leads to the system of equations

$$\partial P_i/\partial t + m^{-1}\operatorname{div}(P_i \nabla S_i) = 0, \qquad (2)$$

$$\frac{\partial}{\partial t}S_i + \frac{1}{2m}(\nabla S_i)^2 + \int G(|\mathbf{r}-\mathbf{r}'|) \times \sum_j P_j(\mathbf{r}')\,dr' - \frac{\hbar^2}{4m}\left\{\frac{\Delta P_i}{P_i} - \frac{1}{2}\left(\frac{\nabla P_i}{P_i}\right)^2\right\} = 0.$$

The form of these equations is identical to the form of the equations of irrotational motion of an ideal compressible fluid. The states of the system which are close to a constant space density of particles can be described by equations obtained by the linearization of equations (2) near the solutions, with $P_j^0 = \text{const} = P_0$, $S_j^0 = E_j^0 t + \bar{S}_j^0(\mathbf{r})$; $\Delta S_j^0 = m\mathbf{v}_j^0$ [$\mathbf{v}_j^0$ is the velocity of the jth particle in the state of a uniform space density of particles, $E_j^0 = m(v_j^0)^2/2$].

Let us look for the solutions $P_j S_j$ of the linearized equations in the form of a superposition of plane waves [$\sim \exp(i\mathbf{k}\mathbf{r} - i\omega t)$]. The conditions of the solvability of homogeneous algebraic equations for the amplitudes gives the dispersion relation

$$1 = P_0 k^2 (G(k)/m) \sum_j [(\omega - \mathbf{k}\mathbf{v}_j^0)^2 - \hbar^2 k^4/4m^2]^{-1}, \qquad (3)$$

where $G(k)$ is the Fourier component of the interaction potential $G(r)$.

Equation (3), whose solution gives the dependence of ω on k, coincides with the dispersion relation derived in Ref. 3 by another method.

The advantage of the collective description of the interaction by Eqs. (1) is that these equations permit the formulation of the limiting problem of an isolated system of interacting particles confined to a bounded region of space (in analogy to the limiting problem of hydrodynamics of an ideal fluid).

In particular, we can use Eqs. (1) to formulate the problem of free surface oscillations of heavy nuclei (given the potential of interaction between nucleons). So far, we have not considered the effect of the symmetry of the wave function on Eq. (3). In the case of the Fermi statistics, when each fermion state is filled by two particles, i.e., the resulting spin is equal to zero, the Hartree-Fock equations (taking into account the antisymmetry of the wave function) differ from the Hartree Eq. (1) by the additional term

$$-\int G(|\mathbf{r} - \mathbf{r}|) \sum_j \psi_j^*(\mathbf{r})\, \psi_j(\mathbf{r}')\, \psi_i(\mathbf{r}')\, d\mathbf{r}',$$

which takes into account the exchange effect.

---

[1] A. A. Vlasov, *Many Particle Theory*, GITTL, Moscow, 1950.

[2] Iu. L. Klimontovich and V. P. Şilin, J. Exptl. Theoret. Phys. (U.S.S.R.) 23, 151 (1952).

[3] D. Bohm and D. Pines, Phys. Rev. 82, 625 (1951); 85, 338 (1952); 92, 609 (1953); D. Pines, Phys. Rev. 92, 626 (1953).

[4] N. D. Zubarev, J. Exptl. Theoret. Phys. (U.S.S.R.) 25, 548 (1953).

Translated by E.S. Troubetzkoy
113

Some Remarks Concerning the Macroscopic Theory of Superconductivity

V. L. GINZBURG
P. N. Lebedev Physical Institute
Academy of Sciences, USSR

(Submitted to JETP editor November 24, 1955)
J. Exptl. Theoret. Phys. (U.S.S.R.) 30, 593-595
(March, 1956)

IN the macroscopic theory of superconductivity developed in Ref. 1 (see also Ref. 2, in which further pertinent works are cited), the free energy density for a superconductor in the absence of a magnetic field is taken to be

$$F_{s0}(T) = F_{n0}(T) + \alpha(T)\,|\Psi|^2 + {}^1\!/_2\,\beta\,|\Psi|^4, \qquad (1)$$

where F_{n0} is the free energy density in the normal state and $|\Psi|^2$ is the concentration of "superconducting electrons". Further, α and β are coefficients expressible in terms of the critical magnetic field for the bulk metal H_{cm} and the weak field penetration depth δ_0:

$$H_{cm}^2 = 4\pi\alpha^2/\beta; \quad \delta_0^2 = mc^2\beta/4\pi e^2|\alpha|. \qquad (2)$$

Equation (1) represents an expansion in powers of $|\Psi|^2$; in general, however, it is possible to break off the expansion after the $|\Psi|^4$ term only in the immediate vicinity of the second-order phase transition under consideration, i.e., for $T_c - T \ll T_c$, where T_c is the critical temperature. Under these conditions it is also possible to set $\alpha = (d\alpha/dT)_c(T - T_c)$ and $\beta = \beta(T_c)$, as was done in Ref. 1 and subsequently. As we move away from T_c and, in particular, as $T \to 0$ it becomes impossible to write an expression for $F_{s0}(T)$ based upon general considerations; on the other hand, it would be desirable to obtain even semi-empirical formulas which would permit comparison of theory with experiment for all temperatures. For this purpose Bardeen[3] adopted the expression:

$$F_{s0}(T) = F_{n0}(T) + \frac{H_0^2}{4\pi}\left\{\left(\frac{T}{T_c}\right)^2\left(1-\sqrt{1-\left|\frac{\Psi}{\Psi_0}\right|^2}\right) - \frac{1}{2}\left|\frac{\Psi}{\Psi_0}\right|^2\right\}, \qquad (3)$$

(Ψ_0 being the equilibrium value of Ψ at $T = 0$) which is used in connection with the so-called two-fluid model for a superconductor.[4] The two-fluid model, however, meets with serious objections[2,4], and the use of Eq. (3) is actually based only upon the usually adequate relations*

$$H^2_{cm} = H^2_0 [1 - (T/T_c)^2]^2, \qquad (4)$$

$$\delta^2_0 = \delta^2_{00} [1 - (T/T_c)^4]^{-1}.$$

At the same time, one can also, taking Eq. (2) into consideration, arrive at Eq. (4) by using Eq. (1) for all T and setting:

$$\alpha = -\frac{e^2\delta^2_{00}H^2_0}{mc^2}\left[1-\left(\frac{T}{T_c}\right)^2\right]\cdot\left[1+\left(\frac{T}{T_c}\right)^2\right]^{-1}; \qquad (5)$$

$$\beta = \frac{4\pi e^4\delta_{00}H^2_0}{m^2c^4}\left[1+\left(\frac{T}{T_c}\right)^2\right]^{-2}.$$

(this has been pointed out previously[2,3]).

Eq. (3) has no general advantages as compared with Eqs. (1) and (5). At the same time, Eq. (1) is considerably simpler than Eq. (3), and its applicability at all temperatures should cause no particular surprise. This comes from the fact that the ratio of the superconducting electron concentration $n_s = |\Psi|^2$ to the total concentration of conduction electrons n_0 is, even at $T = 0$, on the order of 1/5 (this is for Sn and Al, approximate data on the value of n_0 being used[2]). Therefore, the ratio n_s/n_0, in terms of which the expansion in Eq. (1) is evidently performed, is small for all T, which makes it possible to stop the expansion after the $|\Psi|^4$ term with good accuracy. We note finally that by modifying Eqs. (5) in a corresponding fashion one can readily, starting from Eqs. (1) and (2), arrive at expressions for H_{cm} and δ_0 which agree in the closest way with experiment; Eq. (3), on the other hand, is closely tied up with the relations (4), which are known to be in error for $T \to 0$. If we use Eqs. (1) and (5), all of the basic formulas obtained in Ref. 1 and subsequently (see Ref. 2) can be left unaltered, since the temperature dependence of α and β plays no part in these calculations. Thus, the characteristic parameter κ has the form

$$\varkappa = \frac{\sqrt{2}\,e}{hc}H_{cm}\delta^2_0 = 2.16\times10^7\cdot H_0\delta^2_{00}\left[1+\left(\frac{T}{T_c}\right)^2\right]^{-1} \qquad (6)$$

$$= \varkappa_0\left[1+\left(\frac{T}{T_c}\right)^2\right]^{-1};$$

we shall disregard here the extremely dubious possibility that the charge e in Eq. (6) may be unequal to the charge of the free electron (see Ref. 2). From Eq. (6) it is clear that $\kappa_0 = 2\kappa_c \equiv 2\kappa(T_c)$. Further, following Ref. 1, the surface energy on the boundary between the normal and superconducting phases for $\sqrt{\kappa} \ll 1$ is equal to

$$\sigma_{ns} = \Delta H^2_{cm}\ 8\pi; \quad \Delta = 1.89\times\delta_0/\varkappa; \quad \sqrt{\varkappa} \ll 1. \qquad (7)$$

Even for $\kappa = 0.02$ the limiting expression (7) is accurate to no better than ~ 15%; for larger κ it is necessary to use the results obtained numerically (see Table I)**. The limiting expression for σ_{ns} obtained in Ref. 3 from Eq. (3) is considerably more involved than Eq. (7), into which it transforms for $T \to T_c$. Even for $T = 0$, however, the value obtained for σ_{ns} in Ref. 3 is only 17% greater than that found from Eq. (7). A comparison of the theory with experiment[7] is presented in Table II, in which data from Refs. 4, 8 and 9 are also used.

TABLE I

$\varkappa$	Δ/δ_0 numerical calculation	Δ/δ_0 From Eq. (7)
0.01	168.4	189
0.02	79.8	94.5
0.05	28.5	37.8
0.08	16.2	23.6
0.165	6.25	11.5
0.25	3.39	7.56
0.30	2.39	6.30
0.4	1.30	4.73
0.5	0.676	3.78
0.6	0.286	3.15
0.70	0.020	2.70
0.7071	0.000	2.67
0.80	−0.171	2.36

TABLE II

	Al	Sn
δ_{00} (CM)	4.93×10^{-6}	5.1×10^{-6}
H_0	96	304.5
$\varkappa_0$	0.050	0.171
Δ_0 (CM):		
Theory	$28.5\ \delta_{00} = 14.1\times10^{-5}$	$6.0\ \delta_{00} = 3.06\times10^{-5}$
Experiment	15.3×10^{-5}	1.8×10^{-5}

For Al the agreement between theory and experiment is excellent; this evidently applies as well to the temperature dependence of Δ, which is clear from Eqs. (4), (6) and (7) or Table I.

In the case of Sn, however, it is difficult to judge the degree of agreement between theory and experiment, since tin is anisotropic and the quantity Δ is measured relative to an interphase boundary parallel to the tetrad axis[9], while δ_{00} refers to appolycrystal. Further, due to this anisotropy, one cannot assume that the possible errors in determining Δ by the method of Refs. 7 and 9 will be the same for Al and Sn. In order to verify the theory on the present plan it will be necessary to make measurements of $\Delta(T)$ for a number of cubical metals. As regards the determination of the anisotropy of δ_0 and Δ, this appears to be an independent and, moreover, extremely important problem (see Refs. 2 and 10).

For Al and other cubic crystals it is necessary also to determine the dependence of the penetration depth upon the intensity of the magnetic field. For the case in which $\kappa \ll 1$ and the penetration depth δ_1 for a weak alternating field is measured in the presence of a strong external field H we have[1,11]

$$(\delta_1 - \delta_0) / \delta_0 = (3\varkappa / 4\sqrt{2})\,(H / H_{cm})^2. \qquad (8)$$

As follows from the numerical calculations for $\kappa \leq 0.4$ and $H = H_{cm}$, Eq. (8) is correct to within 15%, the true values for δ_1 exceeding those obtained from Eq. (8). If the penetrating depth δ, and not δ_1, is measured directly for a strong field H, $(\delta - \delta_0)\,\delta_0$ will be smaller by a factor of three than is indicated by Eq. (8). The temperature dependence for δ_1 and δ can be seen from Eqs. (6) and (8). Using a variational method, Bardeen obtained for δ the expression (5.29) of Ref. 3, which for $T \to T_c$ coincides with ours. (In Ref. 3 the quantity δ is confused with the experimentally-measured[12] quantity δ, and in consequence the deviation from experiment by a factor of 2 to 3 noted in Ref. 3 does not exist.) For $T < T_c$ the expression for δ from Ref. 3 differs from that obtained in a more accurate manner from Eq. (3)[1]. Here there is obtained from Eq. (3) an expression which differs fundamentally from Eq. (8); this might, in principle, permit one to choose between Eqs. (1) and (3) on the basis of experimental data [from Eq. (3) it follows that as $T \to 0$ the depth δ_1 ceases to depend upon H; this result is connected with the fact that, according to Eq. (3), in a state of equilibrium $\partial^2 F_{s0}/\partial\Psi^2 \to \infty$ as $T \to 0$].

---

* The limitations of Eq. (3) in this connection are evident from the fact that the expression (4) for H_{cm} leads to the relation $c_e = aT^3$ for the electronic component of the specific heat in the superconducting state. At the same time it follows, from both theoretical considerations[5] and, more important, from experimental data[6], that the dependence of c_e upon T is exponential, although at not too low temperatures Eq. (4) can be used for H_{cm} as a good approximation.

** The author wishes to express his indebtedness to F. I. Strizhevskaia, who performed all of the numerical calculations with the aid of an electronic computer.

[1] V. L. Ginzburg and L. D. Landau, J. Exptl. Theoret. Phys. (U.S.S.R.) 20, 1064 (1950).

[2] V. L. Ginzburg, J. Exptl. Theoret. Phys. (U.S.S.R.) 29, 748 (1955); Soviet Phys. JETP **2**, 589 (1956).

[3] J. Bardeen, Phys. Rev. **94**, 554 (1954).

[4] J. Shoenberg, *Superconductivity*, Cambridge, 1952.

[5] V. L. Ginzburg, J. Exptl. Theoret. Phys. (U.S.S.R.) 14, 134 (1944).

[6] Corak, Goodman, Satterthwaite and Wexler, Phys. Rev. **96**, 1442 (1954); **99**, 1660 (1955).

[7] T. E. Faber, Proc. Roy. Soc. (London) **231A**, 353 (1955).

[8] T. E. Faber and A. B. Pippard, Proc. Roy. Soc. (London) **231A**, 336 (1955).

[9] T. E. Faber, Proc. Roy. Soc. (London) **223A**, 174 (1954).

[10] V. L. Ginzburg, J. Exptl. Theoret. Phys. (U.S.S.R.) 23, 236 (1952).

[11] V. L. Ginzburg, Usp. Fuz. Nauk **48**, 25 (1952).

[12] A. B. Pippard, Proc. Roy. Soc. (London) **203A**, 210 (190).

Many Electron Quantum Theory Dispersion Formulas for Metals in the Infrared Region

V. I. CHEREPANOV

Ural State University

(Submitted to JETP editor April 4, 1955)

J. Exptl. Theoret. Phys. (U.S.S.R.) **30**, 598

(March, 1956)

SOKOLOV et al[1,2] have derived general quantum theory dispersion formulas by the method of the density operator of the many electron theory. However, the authors have limited themselves to the visible and ultraviolet spectral ranges where the major role in light absorption is played by the quantum transitions of the electron system into higher energy states. Meanwhile, it is not difficult to consider the absorption of infrared light by the same method. Vonsovskii[3] has reviewed the effect of oscillating electric field of low frequency on a system of coupled electrons in a crystal by the method of the density operator. However, since he did not take damping into account, he obtained only the expression for the polarization current, while the conduction current turned out to be zero.

We can include the damping of the electron motion by replacing in the calculations the energy of the excited state E by the complex quantity $E - i\hbar\Gamma$, where Γ is the damping factor. Using the wavefunction of a system of N interacting electrons in the form given by Sokolov[1], it is not difficult to generalize the calculations to this case. We obtain the following expression for the dielectric constant ϵ and the conductivity σ:

$$\varepsilon = 1 - 4\pi e^2 S^* / m(\omega^2 + \Gamma^2), \qquad (1)$$

$$\sigma = e^2 \Gamma S^* / m(\omega^2 + \Gamma^2),$$

where e is the electron charge, m is the electron mass, ω the frequency of light and S^* a tensor representing the effective number of conduction electrons whose components are

$$(S^*)_{\alpha\beta} = \frac{1}{\hbar V} \qquad (2)$$

$$\times \sum_{j=1}^{N} \int (k \mid \hat{\rho}(0) \mid k) \frac{\partial}{\partial k_{j\alpha}} \left(k \left| \sum_{i=1}^{N} \hat{\mathrm{P}}_{i\beta} \right| k \right) dk \, (\alpha, \beta = x, y, z).$$

In this expression V is the volume of the unit crystal cell, $\hat{\rho}(0)$ is the density matrix at the initial moment, ΣP_i is an operator of the total momentum, and the index k represents all of the quantum numbers $k_1, \ldots, k_N$ that determine the state of the system.

If we discard in Eq. (1) the damping terms by setting $\Gamma = 0$, we obtain the formula derived by Vonskovii[3] for the dielectric constant. In the case of noninteracting electrons, Eq. (2) becomes a corresponding expression of the one electron band theory.

Thus, the dispersion formulas for the infrared spectral range have the same form in the many electron theory as in the one electron band theory of metals. The concept of an effective number of conduction electrons retains the same meaning in the many electron theory. However, the effective number of conduction electrons is determined by a density matrix of the entire system of the metal, and also by the matrix elements of the total momentum of the system. Therefore, a correct description of the optical properties of metals in the infrared spectral range should include the interactions between electrons.

We note that Eq. (1) cannot be obtained by a simple substitution $\omega \to \omega - i\Gamma$ in the expression for ϵ given by Vonskovii[3], because such a substitution has a meaning only for the natural frequency of the system and not for the light frequencies.

To determine the numerical values of S^* it is necessary to apply the described scheme in any particular many electron model of a metal. That allows us then to solve the problem of the effect of the coupling of electrons among themselves on the value of the effective number of conduction electrons.

---

[1] A. V. Sokolov, J. Exptl. Theoret. Phys. (U.S.S.R.) **25**, 341 (1953).

[2] Sokolov, Chepanov and Shteinberg, J. Exptl. Theoret. Phys. (U.S.S.R.) **28**, 330 (1955).

[3] S. V. Vonsovskii, Izv. Akad. Nauk SSSR, Ser. Fiz. **12**, 337 (1948).

Translated by M. J. Stevenson
117

Elastic Scattering of 18. 7 MEV Protons by Nickel and Copper Nuclei

R. A. VANETSIAN AND E. D. FEDCHENKO

(Submitted to JETP editor, December 21, 1955)
J. Exptl. Theoret. Phys. (U.S.S.R.) 30, 577-578 (March, 1956)

A COMPARISON of experimental data for elastic scattering of nucleons with energies from a few mev to a few tens of mev by nuclei [1-10] with the existing theoretical calculations[11,12] shows that the differential cross section for elastic scattering qualitatively corresponds with the "black body" model, but there is no quantitative agreement. Calculations based on the optical model with sharp boundaries for the potential well[13] give too large a value for the differential cross section for large angles as compared with the experimental data. Only the consideration of the diffuse boundary of the nucleus[14] gave results closer to the experimental data of the calculations for heavy nuclei.

In the present work the elastic scattering of 18.7 mev protons from the neighboring nuclei —

Ni and Cu was studied. Nickel and Cu differ very little in size, but they have different spins, magnetic moments and quadrupole moments. For Ni, $I = 0$, $\mu = 0$, $q = 0$; for Cu, $I = 3/2$, $\mu = 2.22$ and 2.38, $q = -0.1$.

The source of protons was a linear accelerator, which yielded (after magnetic analysis and collimation) an intensity of incident beam on the target of the order of 10^8 protons/sec. The beam current was measured with the help of a Faraday cylinder attached to an electrometer. The half width of the energy spectrum of the proton beam, incident on the target, was about 400 kev. The target was in the form of a foil of thickness 10-15 μ.*

Detectors of scattered protons were scintillation counters with CsI (Tl) crystal. The total energy resolution of the registering scheme was 3%. Such energy resolution permitted the separation of elastic scattering from inelastic, while the Ni nucleus is excited to 1.33 mev energy, and the Cu nucleus to 0.96 mev.

The differential cross section for elastic scattering was measured at 5° intervals in the range of angles from 20 to 170°. The systematic error for each point was not more than 2.5%.

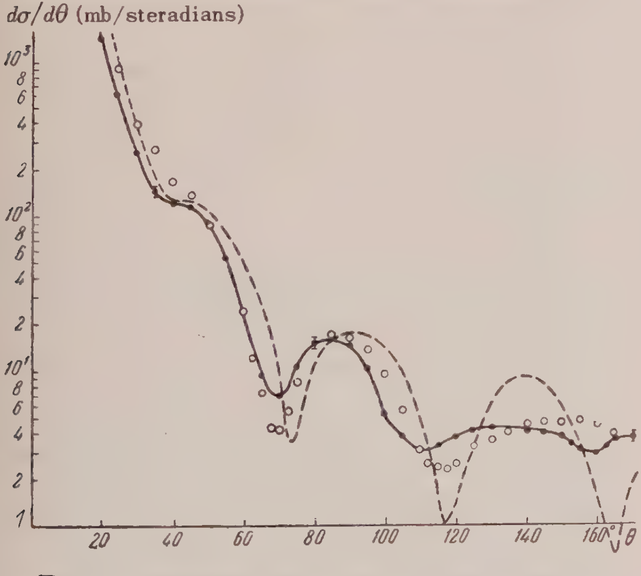

FIG. 1. Differential cross section for the elastic scattering of protons from Ni. Solid curve-cross section obtained in the present work for $E_p = 18.7$ mev. Circles-data obtained by Dayton for $E_p = 18.1$ mev. Dotted line-theoretical curve due to Wood and Saxon, whose calculation was based on the following parameters: $V = 40$ mev, $W = 10$ mev, $R = 5.3 \times 10^{13}$ cm, $a = 0.35 \times 10^{-13}$ cm and $E_p = 18.1$ mev

Figure 1 shows the differential cross section of elastic scattering obtained for Ni, and Fig. 2 that for Cu. For comparison, experimental data are shown on the same figures obtained by Dayton.[10] In Fig. 1 the dotted line represents the theoretical curve by Saxon[14]; this curve is calculated for

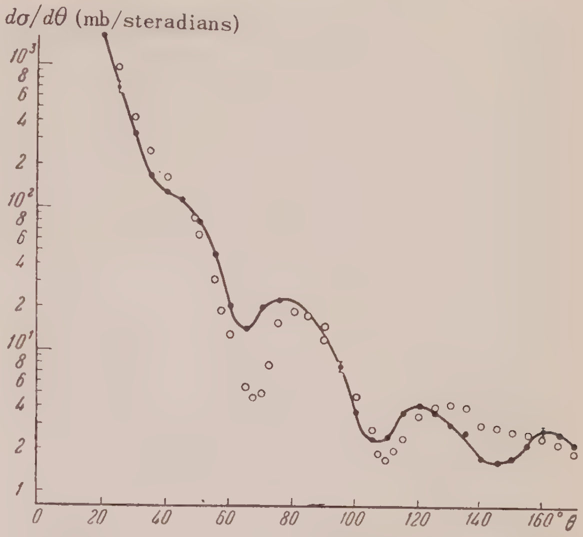

FIG. 2. Differential cross section for the elastic scattering of protons from Cu. Solid curve-cross section obtained in the present work for $E = 18.7$ mev. Circles-data obtained by Dayton for $E_p = 18.7$ mev.

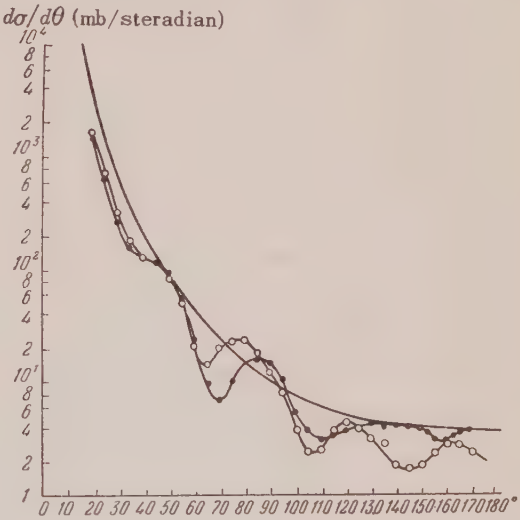

FIG. 3. Differential cross sections for the elastic scattering from Ni (closed circles) and Cu (open circles) for $E_p = 18.7$ mev obtained in the present work. Upper solid curve-cross section for Coulomb scattering for $Z = 29$ and $E_p = 18.7$ mev.

protons with energy 18.1 mev and is based on the optical model with a diffuse boundary of the nucleus.

It is seen from the comparison, that we observed a fourth minimum at large angles, which qualitatively corresponds to the theoretical calculations[14] (the fourth minimum is in the region of 160° for Nickel). Deeper first minima, obtained in Ref. 10, can probably be explained by better energy resolution of the apparatus due to the use of the many-channel analyzer.

Figure 3 shows data for nickel and copper. It is seen from these curves that, in the range of angles up to 110°, the cross section for elastic scattering qualitatively corresponds to the "black body" model; for larger angles, the cross section for these two neighboring elements differs considerably. Since the size of the nickel and copper nuclei are very nearly the same, the observed difference in the cross section could characterize the influence of such factors as spin, magnetic or quadrupole moment, and also the shape of the diffuse boundary. For a final check of this supposition it is proposed that a study of the elastic scattering from various isotopes be undertaken.

---

[1] E. Amaldi, Nuovo Cimente, 3, 203 (1946).

[2] L. M. Goldman, Phys. Rev. 89, 349 (1953).

[3] C. Baker and J. Dodd, Phys. Rev. 85, 1051 (1952).

[4] W. E. Burcham and W. M. Gibson, Phys. Rev. 91, 1266 (1953).

[5] J. W. Burkig and B. T. Whiyht, Phys. Rev. 82, 451 (1951).

[6] P. C. Gugelot, Phys. Rev. 87, 525 (1952).

[7] B. L. Cohen and R. V. Neidigh, Phys. Rev. 93, 282 (1954).

[8] B. Cork, Phys. Rev. 87, 78 (1953).

[9] R. Britton, Phys. Rev., 88, 283 (1953).

[10] J. E. Dayton, Phys. Rev., 95, 756 (1954).

[11] A. I. Akhiezer and I. J. Pomeranchuk, Usp. Fiz. Nauk, 39, 153 (1949).

[12] R. E. LeLeviere and D. S. Saxon, Phys. Rev. 87, 40 (1952).

[13] D. M. Chose and F. Rohrlich, Phys. Rev. 94, 81 (1954).

[14] R. D. Wood and D. S. Saxon, Phys. Rev. 95, 777 (1954).

Translated by M. Polonsky
106

Concerning the Electric Charge of the Neutron

I. S. SHAPIRO AND I. V. ESTULIN
Moscow State University

(Submitted to JETP editor December 2, 1955)
J. Exptl. Theoret. Phys. (U.S.S.R.) 30, 579-580
(March, 1956)

ACCORDING to the present point of view, the neutron does not have an electric charge. This conviction was originally based on experimental data concerning the ionization caused by neutrons during their passage through gases[1]. An estimate of the upper bound for the neutron charge , based on these data, gives a value less than 1/700 of the electron charge e.[2] However, a considerably more precise estimate of the upper bound for the neutron charge can be obtained if it is based on the neutrality of atoms and molecules. Recently, Rabi (see Ref. 3), experimenting with a molecular beam of CsI, came to the conclusion that the charge of this molecule, if not equal to zero, is less than $10^{-10}\ e$. Considering this, and assuming that the proton charge is equal to the charge of an electron, or differs from it by a small quantity equal in magnitude and opposite in sign to the charge of the neutron, it can be obtained that the charge of the neutron is less than $2 \times 10^{-12}\ e$. An analysis of this type assumes that the law of conservation of charge is absolutely accurate. At the present time one cannot exclude the possibility of constructing theories (many dimensional type) with more general conservation laws, in which strict conservation of electric charge, taken separately, does not necessarily hold. It should be also noted that, for instance in a 5-dimensional theory by Rainer[4] , any particle of a finite mass, including a neutron, is given an electric charge. In view of the above considerations, it is interesting to consider the question of the possibility of the direct determination of an upper boundary for the charge of a free neutron.

From the experiments on the observation of the neutron-electron interaction[5] it is difficult to make any conclusions about the magnitude of an upper boundary for the neutron charge in view of the uncertainty of the data concerning the meson cloud of the nucleon.[1] A direct estimate of the magnitude of the upper bound of the neutron charge can be obtained from the fact that the interaction cross section of a thermal neutron with the nucleus does not depend on the charge of the nucleus. This gives evidence for the smallness of the Born parameter:

$$2\pi Zqc / 137v \ll 1, \qquad (1)$$

where q is the ratio of the electric charge of the neutron to the charge of the electron, v – speed of neutron, and c – speed of light. For a thermal neutron ($v \sim 2 \times 10^5$ cm/sec) and for a heavy nucleus $Z \cong 90$ we obtain, based on Eq. (1), the estimate $q \ll 10^{-6}$. In the present work a direct experiment leading to a considerably smaller value of the upper bound of the neutron charge is reported. This experiment consisted of an attempt to observe the deflection of a neutron beam in an electric field.

Let us assume that a narrow beam of thermal neutrons, having kinetic energy W, passes through a plane electric condenser of length l, and perpendicular to the direction of the electric field intensity E. With the charge of a neutron equal to qe, the deflection of the beam Δx directly at the exit from the condenser will be

$$\Delta x = qeEl^2 / 4W. \qquad (2)$$

By measuring the deflection Δx one can, using Eq. (2), determine q.

In the experiment conducted in the present work the intensity of the neutron beam, which was filtered by graphite in front of the collimator, was approximately 10^6 neutrons / cm^2 – sec. The width of the beam was determined by a collimator consisting of two sheets of cadmium with slit openings 2 mm wide and 50 cm from each other (figure 1). Perpendicular to the plane of the slits aluminum plates of the electric condenser b were placed. The distance between the condenser plates was 7.5 mm. In front of the receiver of the thermal neutrons c was placed an exit slit of Cadmium which could be moved by means of a micrometer screw in the direction perpendicular to the neutron beam and parallel to the direction of E (axis X on figure 1). A special vernier allowed the slit to be placed at any point of axis X with a precision of 0.01 mm. The width of the slit in the main experiments was 1 mm. All parts of the equipment after careful centering were fastened on the rigid metal frame. As will be seen from the following, direct measurements with neutrons proved the exactness of the centering of the apparatus.

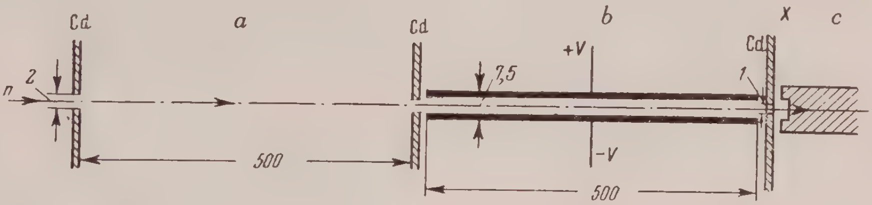

FIG. 1. Apparatus: a– neutron collimator; b– electric condenser; c–neutron receiver. Dimensions are given in mm.

The average neutron energy used in the experiment, measured by absorption of neutrons in boron, was W = 0.026 ev. The background in the neutron receiver for the conditions of this experiment was 2% of the number of counts caused by the neutrons of the direct beam. The contribution of the neutrons above cadmium (absorption) did not exceed this value.

The spatial distribution of neutrons in the beam was studied by moving the slit along the axis X every 0.5 mm. As is seen from Fig. 2, on which are shown the results of these measurements, the dimension of the region with maximum neutron intensity corresponds to the width of the collimator slits (2 mm). The half width of the curve is approximately 4.5 mm. Dotted lines show the position of the condenser plates. The distribution found is fully explained by the geometry of the apparatus, corresponding exact centering of all parts of the apparatus, and absence of scattering on the edges of the cadmium diaphragms. It is also seen from figure 2 that the neutron beam does not touch the condenser plates.

In measurements with the electric field, the voltage on the condenser plates was 10 kv, and the exit slit was put at the points on the axis X shown by crosses in figure 2. During the placement of the slit at points on the axis X corresponding to the descending parts of the neutron distribution curve, a 0.03 mm deflection of the neutron beam should have caused 1% change in the number of registered neutrons. The measurements were conducted in such a way that the readings with the electric field were alternated with the readings without the field. In the table are given the values obtained for the quantity $\Delta N/N$, where ΔN – is the reading difference with and without the field, and N – is the total number of registered neutrons. The numbering of points corresponds to the labeling in Fig. 2. In the table are also given the probable statistical errors. In the last column of the table is given the smallest displacement of the neutron beam which could be detected in this experiment.

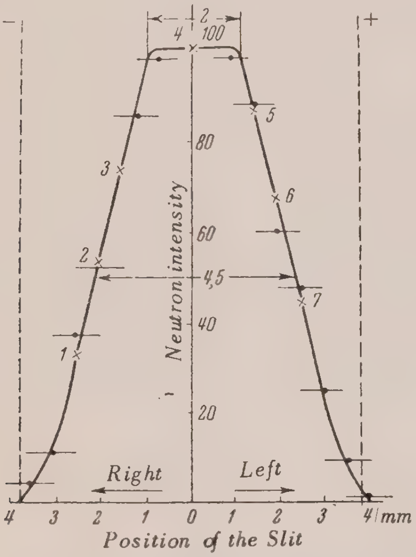

FIG. 2. Dependence of the intensity of neutrons on the position of the exit slit on the axis perpendicular to the neutron beam and parallel to the electric field intensity.

As is seen from the table, the effect does not exceed the experimental errors. In other words, the displacement of the beam under the influence of the electric field was not detected. This means that the displacment of the neutron beam was less than 0,02 mm. Considering this fact and Eq. (2), we obtain the following value for the upper bound of the neutron charge.

Number of the point	Relative effect $\Delta N/N$ in %	The smallest detectable displacement of the beam in mm
1	+0,3±1,0	0,03
2	—0,2±0,5	0,02
3	—0,8±0,8	0,05
4	—0,8±0,7	1,00
5	—0,6±0,5	0,05
6	—0,8±0,7	0,05
7	—0,55±0,4	0,02

$$q < 6\times 10^{-12}.$$

In conclusion we express our thanks to I. M. Frank for the discussion of the present work and to V. P. Kudriashov who helped us during the conduction of the experiment.

---

*Based on the angular anisotropy of the scattering of thermal neutrons from venom atoms, Feld[3] gives, without deduction, the estimate $q < 10^{-18}$ e. It is not completely clear, however, how this number was obtained.

[1] P. I. Die, Proc. Roy. Soc. London 136 A, 727 (1932).

[2] S. Fluegge, *Introduction to Nuclear Physics* (with J. Mattauch, *Nuclear Physics Tables*) Interscience Publisher, N.Y., 1946.

[3] Experimental Nuclear Physics, edit. E. Segre, vol. 2, Ch. 7 IIL, Moscow, 1955 (Russian translation).

[4] Iu. B. Ramer, J. Exptl. Theoret. Phys. (U.S.S.R.) 20, 199 (1950).

[5] L. Foldy, Phys. Rev., 87, 693 (1952).; *Interactions of neutrons with electrons*, Usp. Fiz. Nauk 49, 301 (1953).; D. Y. Hughes, J. A. Harwey, M. D. Goldberg and M. I. Strafne, Phys. Rev., 90, 497 (1953).

Translated by M.Polonsky
107

Transformation of the λ-Transition in Helium to a Special Transition of the First Kind in the Presence of a Heat Flow

V. P. PESHKOV
Institute for Physical Problems
Academy of Sciences, USSR

(Submitted to JETP editor December 15, 1955)
J. Exptl. Theoret. Phys. (U.S.S.R.) 30, 581-582
(March, 1956)

IT is known that the λ-transition in liquid helium, as well as the transition to a superconducting state in the absence of a field, are typical examples of transitions of the second kind, that is, occurrences without release of heat and without change in volume. However, the superconducting transition in the presence of a magnetic field, and, consequently, of superconducting surface currents, changes from a transition of the second kind to a transition of the first kind, that is, it takes place with absorption or release of heat. Although the temperature of the transition from a superfluid to a normal state in liquid helium is lowered at increased pressure, the λ-transition remains a transition of the second kind, and it was assumed in the past that it is impossible by any changes in parameters to convert it to a transition of the first kind. We succeeded in observing a transformation, by means of a heat flow, of the λ-transition in helium to a transition of the first kind. The observation was made on an apparatus (which will be later described in more detail), consisting of a chamber of bow-shaped glass 3 mm thick and two plane parallel glasses, closed by platinum foil. A heater was located in the base of the bow, which produced a heat flow in the direction of the foil. Helium was introduced inside the chamber through a capillary, sealed to the base of the bow. Interference bands of equal width were observed in light from a low pressure Hg. lamp. The space in the chamber was shaped as a small wedge: 13 bands could be put within 12 mm. The chamber was placed in a Dewar flask with liquid helium, held at a temperature below the λ-point: inside it, however, there was no liquid helium at atmospheric pressure. When some noticeable power was released in the heater, the temperature inside the chamber increased, because some temperature jumps were produced at the boundary line between the foil and the liquid He II. When the temperature corresponding to the λ-transition was reached inside the chamber, a visible boundary line appeared in it, which moved from the heater to the cold end with increasing power or with an increase in the temperature of the outer bath. Fig. 1 shows a series of photographs, in the first of which the boundary line has not yet appeared, and in the following, the boundary, marked by a small line, is found in places progressively closer to the platinum foil. A visible boundary line signifies that in the presence of a heat flow between He I and He II in a λ-transition there is a jump in density, that is the transition under those circumstances is found to be a transition of the first kind. With a decrease in the magnitude of the heat flow the jump in density decreases, the boundary line becomes less and less discernable and finally it becomes invisible. One can determine from the gradual displacement of interference bands the dependence of the magnitude of the density jump on the value of heat flow.

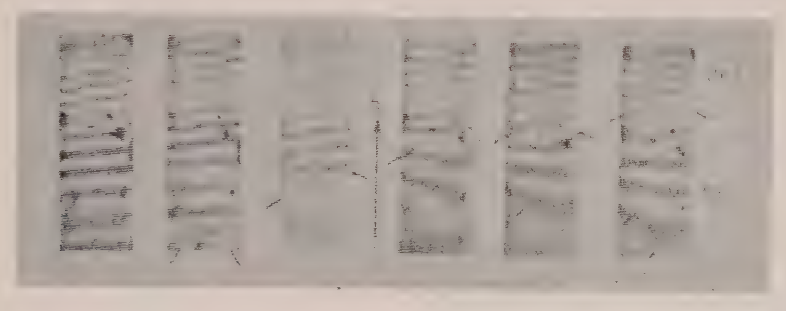

FIG. 1. The displacement of the boundary line between He I and He II with the increase of heat flow density

Raising the temperature of the outer bath and simultaneously decreasing the heat flow, so as to make the boundary remain in the same place, no displacement (within an error of a 1/4 band) is observed in the He II region in the interval of heat flow density change from 0.16 W/cm^2 to 0. This indicates that the density of He II is changed by less than 0.1 %; consequently the displacement of the λ-transition in presence of a heat flow of 0.16 W/cm^2 is smaller than 0.03°. But in the He I region, as the heat flow was decreased, there was a gradual shift of interference bands in the direction of the boundary and a decrease in their separation, which corresponded to an increase in density and a decrease in the temperature gradient. With a change in the density of flow of 0.16 to 0.04 W/cm^2, the picture at the boundary line was displaced by 2.5 bands. The dependence of the magnitude of the density jump on the value of heat flow can be determined from the displacement of interference bands.

The results of the experiment are shown in Fig. 2. It can be seen that the jump in density is proportional to the square of the heat flow, and that for 0.16 W/cm^2 the density of He I is smaller at the boundary than the density of He II by 1.3×10^{-3} gr/cm^3 or approximately by 1%, which corresponds to a rise in temperature of 0.3°. The lower curve in Fig. 2 corresponds to the jump in temperature calculated from the density. Therefore, in presence of a heat flow through the boundary line, the equilibrium between He I and He II is established

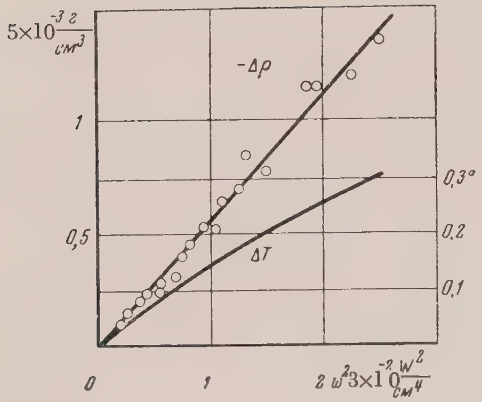

FIG. 2. The dependence of the density jump (upper curve, left scale) at the boundary between He I and He II, and the temperature (lower curve, right scale) on the square of the heat flow density.

with a jump in density and temperature. To estimate the jump in temperature more precisely, the dependence of the density change of He^4 on temperature was taken at a pressure of 1 atm. (fig. 3). The density was determined from the passage of interference bands in the same apparatus. On the X-axis is shown, instead of temperature, the helium vapor movement in the bath, because in this presentation the density of He I changes linearly in a large interval. Inasmuch as, for transitions of the second kind, the equality at the boundary line of temperatures and pressures, and also entropies and densities is characteristic, whereas in a transition of the first kind, the temperatures and pressures are equal and jumps occur in the entropy and the density, the transition of He I to HeII and back, in presence of a heat flow, should be called either a special transition of the first kind, or a transition of zero order, since here at the boundary line not only the values of entropies and volumes, but also those of temperatures and probably pressures suffer a break. The presence of a temperature jump between two phases of liquid helium does not have direct analogy and it can be explained by a change in the mechanism of heat transfer at the boundary. If in He I one can speak of a thermal movement of strongly bonded but still separate helium atoms, the heat flow in He II is effected by a quantum movement of thermal excitations of photons and rotons. It is obvious that the interaction between these types of heat transfer is accomplished with difficulty, which causes the jump in temperature.

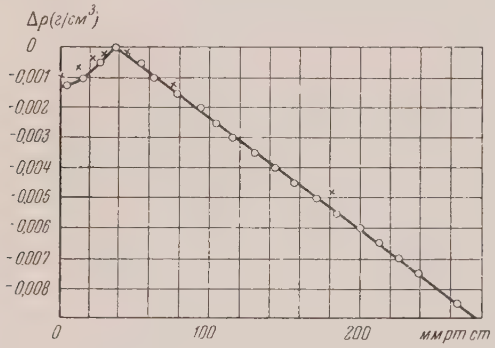

FIG. 3. The change in the density of liquid helium under 1 atm. pressure as a function of temperature, expressed in helium vapor pressures in the bath. o — present measurement data, ×— data by Keesom [Physica 1 128 (1933)]

The experiments to study the described phenomena are continuing.

In conclusion I express my gratitude to N. I. Kondrat'ev, who built the apparatus, and also to A. I. Filimonov and I. A. Uriutov, who helped with the measurements.

Translated by S. Pakswer
108

Relativistically Invariant Formulation of Electrodynamics without Longitudinal and Scalar Fields

E. M. LIPMANOV
Novozybkov State Pedagogical Institute

(Submitted to JETP editor, February 17, 1955)
J. Exptl. Theoret. Phys. (U.S.S.R.) 30, 583-584 (March, 1956)

IT was shown [1] that the generalized Coulomb field of charges can already be excluded in a relativistically invariant way in classical electrodynamics, a fact which facilitates the transition to the quantum theory. However, the problem of formulation of quantum electrodynamics in the Heisenberg representation and the transition to the interaction representation has only been superficially raised and needs a more exact treatment. In the present note, it will be shown that the formulation of quantum electrodynamics in the Heisenberg representation can be obtained from the variational principle

$$\delta \int L d\omega = 0, \qquad (1)$$

where $d\omega = dxdydzcdt$, and the Langrangian function is of the following form;*

$$L = -\frac{1}{2}\left(\frac{\partial a_\mu(x)}{\partial x_\nu}\right)^2 \tag{2}$$

$$-\frac{\hbar c}{2}\bar{\psi}(x)\left[\gamma_\mu\left(\frac{\partial}{\partial x_\mu} - \frac{ie}{\hbar c}a_\mu(x)\right) + \varkappa_0\right]\psi(x)$$

$$-\frac{\hbar c}{2}\bar{\psi}'(x)\left[\gamma_\mu\left(\frac{\partial}{\partial x_\mu} + \frac{ie}{\hbar c}a_\mu(x)\right) + \varkappa_0\right]\psi'(x)$$

$$+\frac{1}{2c}n_\mu j_\mu(x)\varphi(x) - \left(\frac{\partial a_\mu(x)}{\partial x_\nu} - \frac{\partial a_\nu(x)}{\partial x_\mu}\right)n_\mu\frac{\partial\varphi(x)}{\partial x_\nu}.$$

Here $\psi(x)$ and $\psi'(x)$ are the spinor and the charge-conjugate spinor of the Dirac quantized field, $a_\mu(x)$ is the operator of the photon field, and the operator $\varphi(x)$ is assumed to be expressed in terms of the 4-current density in the following way:

$$\varphi(x) = \frac{1}{c}\int_\sigma n_\nu\frac{\partial\mathscr{D}(x-x')}{\partial x_\nu}j_\lambda(x')\,d\sigma'_\lambda. \tag{3}$$

where the space-like surface σ is passing through the point x and is chosen to be plane. The photon field is subjected to two additional conditions;

$$n_\mu a_\mu'(x) = 0; \quad \partial a_\mu(x)/\partial x_\mu = 0. \tag{4}$$

The commutation relations between the field operators on the space-like surface σ are identical with the well-known covariant commutation relations for the "free" photon and electron-positron fields, satisfying the linear equations of motion.[2] From (1) and (2) we obtain the following equations of motion for the field operators:

$$\Box^2 a_\mu(x) = -\frac{1}{c}j_\mu'(x) \tag{5}$$

$$+\frac{\partial}{\partial x_\mu}n_\nu\frac{\partial\varphi(x)}{\partial x_\nu} - n_\mu\Box^2\varphi(x),$$

$$\left[\gamma_\mu\left(\frac{\partial}{\partial x_\mu} - \frac{ie}{\hbar c}a_\mu(x)\right) + \varkappa_0\right]\psi(x) \tag{6}$$

$$-\frac{ie}{2\hbar c}\gamma_\mu n_\mu\{\psi(x), \varphi(x)\} = 0,$$

$$\left[\gamma_\mu\left(\frac{\partial}{\partial x_\mu} + \frac{ie}{\hbar c}a_\mu(x)\right) + \varkappa_0)\right]\psi'(x) \tag{7}$$

$$+\frac{ie}{2\hbar c}\gamma_\mu n_\mu\{\psi'(x), \varphi(x)\} = 0,$$

where { } denotes an anti-commutator. The nonlinear terms in the equations for the operators of the electron-positron field arise from the Coulomb charge interaction. The Coulomb field itself does not enter the theory. In connection with this, the theory is no longer gauge-invariant.[1]

The transition to interaction representation is effected by the canonical transformation

$$\Psi[\sigma] = U[\sigma]\Phi, \tag{8}$$

where Φ is the constant vector of the state of the system in the Heisenberg representation, and $\psi[\sigma]$ is the vector of state in the interaction representation. The unitary operator $U[\sigma]$ satisfies the equation **

$$U[\sigma] = U[\sigma_0] - \frac{i}{\hbar c}\int_{\sigma_0}^{\sigma}\widetilde{H}(x')U[\sigma']\,d\omega', \tag{9}$$

where $\widetilde{H}(x)$ is the energy density of the interaction of the fields***

$$\widetilde{H}(x) = -\frac{1}{c}\widetilde{j}_\nu(x)\widetilde{a}_\nu(x) - \frac{1}{2c}n_\nu\widetilde{j}_\nu(x)\widetilde{\varphi}(x). \tag{10}$$

The field operators are transformed in the following way:

$$\widetilde{F}(x) = U[\sigma]F(x)U^{-1}[\sigma]. \tag{11}$$

In order to find the equations of motion in the interaction representation, ir is necessary to write down the transformation formulas of the derivatives of the operators. The Schwinger transformation formulas[2] cannot be applied in this case, since it is assumed in their deduction that the transformation operator $F(x)$ commutes with the interaction Hamiltonian in various points of the space-like surface σ, and in the present case when, for instance, $F(x) = \psi(x)$, the said assumption is not fulfilled.

Making use of the relation

$$\frac{\partial}{\partial x_\nu}\int_{\sigma_0}^{\sigma}F(x')\,d\omega' = \int_\sigma F(x')\,d\sigma'_\nu, \tag{12}$$

we obtain, on the basis of (11) and (9), the transformation formulas for the derivatives

$$\frac{\partial\widetilde{F}(x)}{\partial x_\nu} = \frac{\partial}{\partial x_\nu}(U[\sigma]F(x)U^{-1}[\sigma]) \tag{13}$$

$$= U[\sigma]\frac{\partial F(x)}{\partial x_\nu}U^{-1}[\sigma] - \frac{i}{\hbar c}\int_\sigma[\widetilde{H}(x'), \widetilde{F}(x)]\,d\sigma'_\nu,$$

which are applicable also in the case when the operators $F(x)$ and $H(x)$ do not commute in various points on σ.

By means of the formulas (13), we find the desired equations of motion in the interaction representation

$$(\gamma_\nu \partial/\partial x_\nu + \varkappa_0)\tilde{\psi}(x) = 0, \qquad \Box^2 \tilde{a}_\mu(x) = 0 \qquad (14)$$

in accordance with Ref. 1.

---

*Notation of Refs. 1 and 2 is used throughout.

**The integral equations for $U[\sigma]$ and the vector of state $\Psi[\sigma]$. are, in contrast to the differential equations, applicable without reservation in the case of plane σ.

***Operators in interaction representation are labelled by ~.

[1] E. M. Lipmanov, J. Exptl. Theoret. Phys. (U.S.S.R.) 27, 135 (1954).

[2] J. Schwinger, Phys. Rev. 74, 1439 (1948).

Translated by H. Kasha
109

On the Theory of Asymmetric Fission of Heavy Nuclei

S. G. Ryzhanov
Kishinev State University

(Submitted to JETP editor December 2, 1955)
J. Exptl. Theoret. Phys. (U.S.S.R.) 30, 599-601
(March, 1956)

In the present communication we shall show that the dependence of the yield of fragments on their charges and mass numbers, in the case of spontaneous fission as well as in the case of fission by thermal and fast neutrons, can be obtained by a single method, if one adopts the hypothesis suggested by Frenkel[1]. This hypothesis consists in regarding both spontaneous and induced fussion as a tunnel effect originating, respectively, from the ground or excited state of the fissioning nucleus. The potential barrier for fission is assumed to be due, on one hand, to the specific nuclear potential "well", and on the other, by the electric (Coulomb) repulsion of the fragments. From this point of view, α-decay is regarded as the most sharply asymmetric fission. The well-known quantum-mechanical formula for α-decay[2] can be easily extended to the asymmetric fission of a nucleus with charge Z_0 into fragments of charge Z_1 and Z_2.

Let E be the sum of the kinetic energies of the fragments; $v = \sqrt{2E/M}$ their relative velocity (M is the reduced mass of the fragments); ρ the radius of the specific nuclear potential well; $\sigma = Z_1 Z_2 e^2/\rho E$. It is easy to obtain the following formula for the probability of fission w:

$$w = w_0 \times \exp\left\{-\frac{4Z_1Z_2e^2}{\hbar v}\left(\arccos \sigma^{-1/2} - \sigma^{-1}(\sigma-1)^{1/2}\right)\right\}, \qquad (1)$$

where the coefficient w_0 in front of the exponential is of the order of magnitude of the fundamental frequency of nuclear vibrations ($w_0 \approx 3\times 10^{21}$ sec^{-1}). The sum of the kinetic energies of the fragments if found from the relation

$$E = E_1 + E_2 - E_0 - Q, \qquad (2)$$

where E_0, E_1 and E_2 are the binding energies of the fissioning nucleus and of the two fragments, and Q the energy of their internal excitation[3]. The binding energies are calculated from the semi-empirical formula[4]. Formula (1) has been applied to the fission of uranium nuclei. The correct order of magnitude for the period of spontaneous fission, 10^{21} sec, is obtained with $E = 150$ mev and the radius $\rho = (A_1^{1/3} + A_2^{1/3})\ \ 1.5\times 10^{-13}$ cm. (Here a preliminary approximate integration of Eq. (1) has been carried out over all fragments A_1 and A_2 satisfying the condition $A_1 + A_2 = A_0$). The hypothesis underlying the calculation of τ_{sp} assumes that the fission takes place through the intermediate stage of spheres in contact, which in no way contradicts the thermo-hydrodynamical mechanism of fission. An analogous calculation for Th^{232}_{90} gives the period of spontaneous fission as $\tau_{sp} > 10^{18}$ years. The asymmetry of the fission can be easily obtained from (1). Let us denote by $\overline{w}$ the probability of symmetric fission and let us expand $\ln(w/\overline{w})$ into a series according to powers of the variables

$$\xi = \left(\frac{Z_0 - 2Z_1}{Z_0}\right); \qquad \eta = \frac{\overline{E} - E}{\overline{E}}$$

($\overline{E}$ is E for symmetric fission). We then obtain, with sufficient accuracy, the formula

$$\ln\frac{w}{\overline{w}} = \frac{Z_0^2 e^2}{\hbar v}\left\{\xi \arccos(\overline{\sigma})^{-1/2} - \left(\arccos(\overline{\sigma})^{-1/2} + \frac{\sqrt{\overline{\sigma}-1}}{\overline{\sigma}}\right)\frac{\eta}{2}\right\}. \qquad (3)$$

The results of calculations with this formula are given in Fig. 1; conversion of fragment charges into their mass numbers was carried out with the aid of the semi-empirical tables of Ref. 5; the same reference was used for comparison with experimental data. In these calculations account was taken of the dependence of E on the mass numbers A_1 or A_2, given in Fig. 2, which was constructed using Eq. (2). In view of the symmetry of the plot of the fission yield with respect to the light and the heavy fragment groups, in Fig. 1 only the mass numbers of the fragments of the heavy group are marked on the axis of abscissas; Fig. 2 is similarly constructed. Calculations according to (3) show that the influence of the asymmetry of the charges of the fragments on the asymmetry of probability of fission is considerably more important than asymmetry in the masses, in the sense of the original explanation given in Ref. 6.

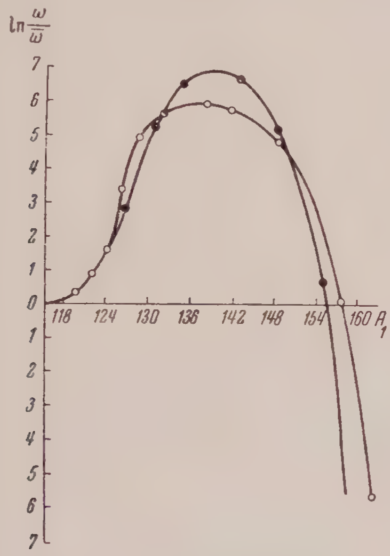

FIG. 1. ● – calculated using formula (1), o – experimental values from Ref. 5.

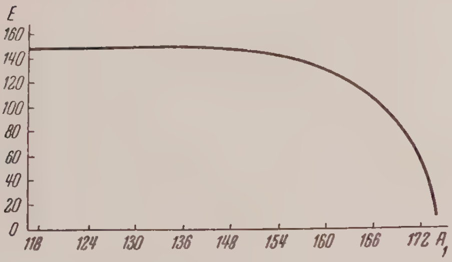

FIG. 2.

Formula (1) makes it possible to interpret the dependence of τ_{sp} on the stability parameter $x = Z^2A^{-1}/(Z^2A^{-1})_{st}$. This parameter is proportional to the ratio of the electric (Coulomb) energy of the nucleus to its surface energy (the term $\gamma A^{2/3}$ in the binding energy). The subscript "st" indicates "stability limit" with respect to fission.

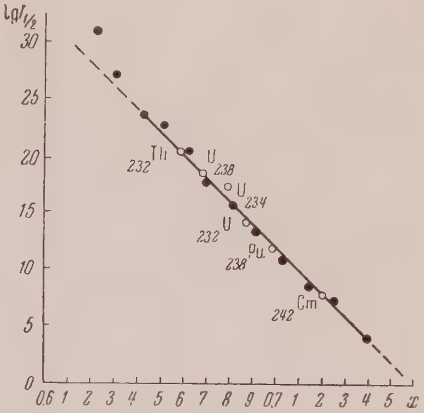

FIG. 3. ● – calculated using formula (4), o – experimental values from Ref. 7; dotted line is Seaborg's.

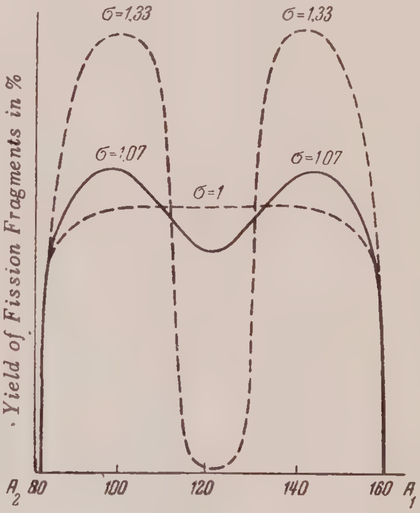

FIG. 4.

The dependence of the period of spontaneous fission of the stability parameter for the sequence of nuclei Th^{232}_{90}, $U^{238}_{92}-U^{232}_{92}$, Pu^{238}_{94}, Cm^{242}_{96} was experimentally determined in Ref. 7. As a result of an approximate integration of (1) the following formula has been obtained for the half-period of spontaneous fission $T_{1/2}$ (years)

$$\lg T_{1/2} \approx -28 + 1.027\,(M_p\gamma r_0^2/\hbar^2)^{1/2} A^{7/6} x\Delta\,(3x-1)^{-1/2}. \tag{4}$$

Here M_p is the mass of the nucleon, r is the rigid radius of the nucleon, γ is the coefficient in front of $A^{2/3}$ in the binding energy of the fissioning nucleus, A is its mass number and

$$\Delta = \arccos \bar{\sigma}^{-1/2} - (\bar{\sigma} - 1)^{1/2} \bar{\sigma}^{-1}$$

for symmetric fission. Figure 3 illustrates the agreement between calculation and experimental data. The period of fission of U^{236}_{92} nuclei by capture of thermal neutrons, according to Ref. 8 $\sim 10^{-12}$sec., which is, in fact, obtained from Eq. (1), if one assumes that the radius of the potential well for the excited level is 1.2 times greater than for the ground level (the energy difference of these levels $\sim$ 6 mev). This assumption is entirely acceptable, since the bottom of the well has parabolic shape. This assumption is equivalent to taking into account of the influence of the deformation of the nuclear surface on the probability of tunnel fission; this has been done in the case of α-decay in Ref. 9, where it was also shown that deformation of the nucleus very considerably increases the probability of the tunnel transition. Extension of these calculations to asymmetric fission shows that it is sufficient to take the relative deformation of the nucleus due to polarization by the captured neutron as equal to 0.5 in order to explain the difference in the periods of spontaneous and induced fissions. Deformations of this order of magnitude are entirely reasonable.[10] It is interesting to note that the influence of deformation on ln $(\omega/\bar{\omega})$ is so slight that on a logarithmic scale asymmetric fission (spontaneous as well as induced by thermal neutron capture) is represented by almost the same graph. Application of (1) to fission by fast particles, with energy of the order of 15 – 25 mev, is illustrated in Fig. 4 and shows good agreement with experiment.[11] In the calculations it was assumed that the kinetic energy of the (fast) particle causing fission is completely transferred into the energy of the fission fragments. Thus the hypothesis, put forward in Ref. 1, does in fact give a unified explanation of the basic regularities of asymmetric fission. An explanation of the fission threshold by slow neutrons in the nuclei Th^{232}_{90}, Pa^{231}_{91}, U^{238}_{92} can also be given from the point of view here set forth and does not require the assumption of a supra-tunnel mechanism of fission.[12]

[1] Ia. I. Frenkel, *Principles of the Theory of Atomic Nuclei*, Academy of Sciences Press, 1950, p. 159.

[2] H. Bethe, *Nuclear Physics*, Part II, GITTL, 1948, p. 184 (Russian translation).

[3] K. Way and E. Wigner, Phys. Rev. 73, 1318 (1948).

[4] E. Fermi, *Nuclear Physics*, IIL, 1950, p. 14. (Russian translation).

[5] Zh. Sigel, Usp. Fiz. Nauk 33, 1, 77 (1947).

[6] Ia. I. Frenkel, Izv. Akad. Nauk SSSR Fiz. Ser. 10, 415 (1946).

[7] G. T. Seaborg, Phys. Rev., 85, 157 (1952).

[8] R. R. Wilson, Phys. Rev. 72, 98 (1947).

[9] L. A. Sliv and L. K. Peker, Dokl. Akad. Nauk SSSR 99, 727 (1954).

[10] A. Bohr and B. R. Mottelson, Problems of Contemporary Physics, 9, p. 34, 1955. (Russian translation).

[11] A. Newton, Phys. Rev. 75, 17 (1949); R. W. Spence, BNL – C – 9, 1949.

[12] N. Bohr and J. A. Wheeler, Phys. Rev. 56, 426 (1939).

Translated by A. V. Bushkovitch
118

Pion-proton Interactions at 1.4 BEV

A. I. NIKISHOV

(Submitted to JETP editor July 12, 1955)
J. Exptl. Theoret. Phys. (U.S.S.R.) 30, 601-603
(March, 1956)

Eisberg et al.[1] have made a detailed study of the interaction of negative pions with protons at 1.37 bev. The analysis by Belen'kii and Nikishov[2] of $n-p$ collisions at 1.7 bev shows that a direct comparison of experimental results for multiple particle production with Fermi's[3] statistical theory in its original form leads to considerable divergence of theory and experiment. When, however, the statistical theory also allows for the formation of isobar states the discrepancy disappears, leaving a quite satisfactory agreement with experiment.

It is also of interest to compare with the statistical theory including isobar states the experimental data on the interaction of negative pions with protons. We shall use the notation N for nucleon, N' for isobar state and π for pion. The important cases here are those which give the following states as a result of pion-nucleon collisions: $N\pi$ – elastic scattering; $N'\pi$, $N\pi\pi$ – the production of one secondary meson; $N'\pi\pi$, $N\pi\pi\pi$ – the production of two secondary mesons. The statistical weights of these states are calculated as in Refs. 2 and 4. For brevity we shall write $N'\pi\pi \equiv 2N'$ etc.

After correcting for identity, spin and isotopic spin conservation, the relative statistical weights of processes $1N$, $2N$, $1N'$, $2N'$, $3N$ and $3N'$ (in %) are, respectively, 21, 30, 29, 13, 6 and 1. The last process can thus be neglected. Furthermore,

Table 1

Charged reaction products	Milburn's results with $R=1.3\times10^{-13}$ cm	Including isobars		Experiment
		$R=1.3\cdot10^{-13}$ cm	$R=1,4\cdot10^{-13}$ cm	
$(\pi^-+p)_{el}$	0,32	0.16	0,15	0,11
$(\pi^-+p)_{inel}$	0.29	0.29	0,29	0.35
$\pi^++\pi^-$	0.36	0.50	0,50	0,50
$\pi^++2\pi^-+p$	0.03	0 05	0.06	0,04

TABLE 2

Number of secondary pions	Experiment	By Fermi's theory with $R=1.4\times10^{-13}$cm	Including isobars with $R=1.4\times10^{-13}$cm
0	12	22	16
1	71	65	67
2	24	20	24

these weights are subdivided according to charge states.

It follows from the calculation that the observed interactions comprise approximately 78% of the total number of interactions. The remaining interactions give only neutral particles. These are reactions leading to the states (n 0), (n 00) and (n 000).

Let us compare these results with experiment and with the calculations which neglect isobars. We shall first compare our calculation with the calculation in Ref. 1 which neglects isobar states and with the experimental data of Table VIII of Ref. 4. This table gives the distribution of the observed charged products of $\pi^- - p$ collisions. $(\pi^- - p)_{el}$ denotes instances in which the observed secondary particles satisfy energy and momentum conservation laws; $(\pi^- - p)_{inel}$ denotes instances when these laws are not satisfied so that neutral undetected particles are also involved. We reproduce a part of this table supplemented by two columns containing our results (Table 1).

We note that the calculation is not compared with all elastic collisions but only with the incoherent portion of them, since Fermi's theory involves only the latter.[1,4]

It is also possible to compare the number of instances with different pion multiplicities. Here, however, the experimental results are much less definite. Eisberg observed 147 interactions. Of these 95 were inelastic; the 52 elastic collisions are subdivided into 40 coherent and 12 incoherent cases. Thus there were noted 107 collisions resulting in charged products, which are those of interest to us. Furthermore, the 95 observed inelastic collisions are subdivided (with considerable indeterminacy) into 71 with the creation of one secondary meson and 24 with the creation of two secondary mesons. This subdivision is compared with the calculations by Fermi's theory neglecting isobars and by formulas which raise the multiplicity considerably (the mesons are considered extreme relativistic particles). The results are given in Table IV of Ref. 1. We again copy a portion of this table and add a column containing the results of our calculations, which are more precise and also allow for isobars (Table 2).

The agreement is seen to be satisfactory.

Finally, we shall compare the meson and nucleon momentum distributions in the center of mass system for the reactions (p −0) and (n +−). In calculating the momentum distribution for the $N\pi$ process we assume that an isobaric state decays isotropically in its own reference system. In addition, we assume that the width of an isobar level is zero. We thus obtain the graphs of Figs. 1 and 2.

It is evident that allowance for the width of an isobar level would result in still better agreement of the calculation with experimental data. Thus the results for $\pi^- - p$ interactions are in satisfactory agreement with the statistical theory when

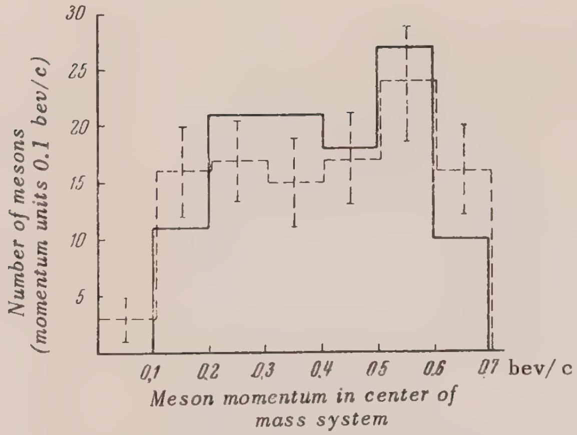

FIG. 1. Meson momentum distribution in the center of mass system for the reactions (p – 0) and (n + –). Dashed line – Eisberg et al, experimental distribution; solid line– distribution according to the statistical theory including isobars.

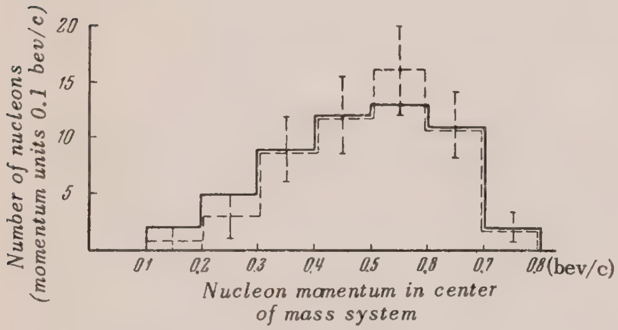

FIG. 2. Nucleon momentum distribution in the center of mass system for the reactions (p –0) and (n + –). Dashed line– Eisberg et al., experimental distribution; solid line– distribution according to the statistical theory including isobar states.

it includes isobar states.

We also note that according to the above calculation the meson momentum distribution is in contradiction with the statistical theory when isobar states are neglected, but is not in contradiction with the assumption that particle creation can only take place through isobaric states. However, the marked spread of Q (isobar decay energy) can be interpreted as being due to the fact that a considerable part is played by creation without immediate isobaric states.

In conclusion I wihh to express my gratitude to Professor S. Z. Belen'kii for interesting discussions and for his continued interest.

---

[1] L. M. Eisberg et al., Phys. Rev. 97, 797 (1955).

[2] S. Z. Belen'kii and A. I. Nikishov, J. Exptl. Theoret. Phys. (U.S.S.R.) 28, 744 (1955); Soviet Phys. JETP 1, 593 (1955).

[3] E. Fermi, Phys. Rev. 92, 452 (1953).

[4] R. H. Milburn, Rev. Mod. Phys. 27, 1 (1955).

[5] W. B. Fowler et al., Phys. Rev. 95, 1026 (1954).

Translated by I. Emin
119

On the Interaction between Nucleon and Antinucleon

Iu. A. TARASOV
Moscow State University

(Submitted to JETP editor October 13, 1955)
J. Exptl. Theoret. Phys. (U.S.S.R.) 30, 603-605 (March, 1956)

WE investigate by means of the "old" Tamm method the interaction between nucleon and antinucleon. The Schrödinger equation for the wave functional of the system has the form:

$$(H_0 + H')\Psi = W\Psi, \qquad (1)$$

where W is an eigenvalue of the total energy of the system. Let us expand Ψ in a series of eigenfunctions of H_0:

$$\Psi = \sum_{\lambda, m, n} a_\lambda^{mn}\psi_\lambda^{mn}. \qquad (1a)$$

Here m is the number of mesons in a free state, n is the number of nucleon pairs, λ denotes momenta, spins and isotopic spins of the particles, a_λ^{mn} is the probability amplitude of finding the system in the state(λ, m,n). From Eq. (1), we obtain an integral equation for the amplitude a_λ^{mn}

$$[W - E_\lambda^{mn}]\, a_\lambda^{mn} = \sum_{q=n-1}^{n+1} \sum_{p=m\pm1} \sum_\mu \langle \lambda mn \,|\, H' \,|\, \mu pq \rangle\, a_\mu^{pq}. \qquad (1b)$$

From this equation it is possible to obtain an equation for the amplitude a_λ^{01} corresponding to the state in which only a nucleon and an antinucleon are present. We have

$$[W - E_\lambda^{01}]\, a_\lambda^{01} = \sum_\mu [\langle \lambda 01 \,|\, H' \,|\, \mu 11 \rangle\, a_\mu^{11} + \langle \lambda 01 \,|\, H' \,|\, \mu 10 \rangle\, a_\mu^{10} + \langle \lambda 01 \,|\, H' \,|\, \mu 12 \rangle\, a_\mu^{12}]. \qquad (2)$$

The second term corresponds to the transformation of the nucleon and antinucleon into a meson. Let us confine ourselves to the case that only one virtual meson is present and there are no virtual pairs. Then it is only necessary to form the amplitudes a^{11}_{μ} and a^{10}_{μ} corresponding to the presence of a meson and a pair, and one meson. The equations, cut off according to the number of particles, have the form

$$[W-E^{11}_{\mu}]\, a^{11}_{\mu} = \sum_{\rho} \langle \mu\, 11 \,|\, H' \,|\, \rho\, 01\rangle\, a^{01}_{\rho}, \qquad (3)$$

$$[W-E^{10}_{\mu}]\, a^{10}_{\mu} = \sum_{\nu} \langle \mu\, 10 \,|\, H' \,|\, \nu\, 01\rangle\, a^{01}_{\nu}.$$

Substituting (3) into (2), we obtain an equation for a^{01}_{λ}

$$[W-E^{01}_{\lambda}]\, a^{01}_{\lambda} \qquad (4)$$

$$= \sum_{\mu,\nu} \Bigg[\frac{\langle \lambda\, 01 \,|\, H' \,|\, \mu\, 11\rangle \langle \mu\, 11 \,|\, H' \,|\, \nu\, 01\rangle}{W-E^{11}_{\mu}} + \frac{\langle \lambda\, 01 \,|\, H' \,|\, \mu\, 10\rangle \langle \mu\, 10 \,|\, H' \,|\, \nu\, 01\rangle}{W-E^{10}_{\mu}} \Bigg] a^{01}_{\nu}.$$

Let $p'_n i'$, α' denote momentum, spin and isotopic spin of the nucleon, $p'_{\bar{n}}$, j', β' momentum, spin and isotopic spin of the antinucleon before meson exchange and $\mathbf{p}_n$, i, α, $\mathbf{p}_{\bar{n}}$, j, β the corresponding quantities after meson exchange. Then Eq. (4) takes the form:

$$[W-E^{01}(\mathbf{p}_n, \mathbf{p}_{\bar{n}})]\, a^{01}(\mathbf{p}_n \mathbf{p}_{\bar{n}})$$

$$= \int \Delta_2 (\mathbf{p}_n, \mathbf{p}_{\bar{n}}, \mathbf{p}_{n'}, \mathbf{p}_{\bar{n}'}, \mathbf{k}, W)\, a^{01}(\mathbf{p}'_n, \mathbf{p}'_{\bar{n}})\, d\mathbf{p}'_n d\mathbf{p}'_{\bar{n}}\, d\mathbf{k}, \qquad (5)$$

$$\Delta_2 = \frac{\langle \mathbf{p}^{ia}_n \,|\, H' \,|\, \mathbf{p}^{i'\alpha'}_{n'}\rangle \langle \mathbf{p}^{j\beta}_{\bar{n}} \,|\, H' \,|\, \mathbf{p}^{j'\beta'}_{\bar{n}'}\rangle}{W - E_{\mathbf{p}_{n'}} - E_{\mathbf{p}_{\bar{n}}} - \omega_{\mathbf{p}_{\bar{n}} - \mathbf{p}_{\bar{n}'}}} + \frac{\langle \mathbf{p}^{i\alpha}_n\, \mathbf{p}^{j\beta}_{\bar{n}} \,|\, H' \,|\, \mathbf{k}\rangle \langle \mathbf{k} \,|\, H' \,|\, \mathbf{p}^{i'\alpha'}_{n'}\, \mathbf{p}^{j'\beta'}_{\bar{n}'}}{W-\omega_{\mathbf{k}}}.$$

We take the interaction Hamiltonian in the charge-symmetric form: $H' = ig \bar{\Psi} \gamma_0 - (\tau\varphi)\, \Psi$. Calculating the matrix elements and integrating with respect to $d' \mathbf{p}_n$ and $d\, \mathbf{p}'_{\bar{n}}$, Eq. (5) reduces to the form

$$[W-E^{01}(\mathbf{p}_n, \mathbf{p}_{\bar{n}})]\, a^{01}(\mathbf{p}_n, \mathbf{p}_{\bar{n}}) = \int \Delta^{11}_2 a^{01}\, d\mathbf{k} \qquad (6)$$

$$+ \int \Delta^{10}_2 (\mathbf{p}_n, \mathbf{p}_{\bar{n}}, \mathbf{p}'_n, \mathbf{p}_n + \mathbf{p}_{\bar{n}} - \mathbf{p}'_n)\, a^{01} d\mathbf{p}_n,$$

where

$$\Delta^{11}_2 = \frac{g^2}{8\pi^3} \frac{[\bar{U}^{i\alpha}(\mathbf{p}_n)\gamma_5 \tau^{\sigma}_{\alpha\alpha'} U^{i'\alpha'}(\mathbf{p}_n - \mathbf{k})]\, [\bar{V}^{j'\beta'}(-\mathbf{p}_{\bar{n}} - \mathbf{k})\gamma_5 \tau^{\sigma}_{\beta'\beta} V^{j\beta}(-\mathbf{p}_{\bar{n}})]}{\omega_{\mathbf{k}}(W - E_{\mathbf{p}_n - \mathbf{k}} - E_{\mathbf{p}_{\bar{n}}} - \omega_{\mathbf{k}})} \qquad (6a)$$

$$\Delta^{10}_2 = \frac{g^2}{8\pi^3} \frac{[\bar{U}^{i\alpha}(\mathbf{p}_n)\gamma_5 \tau^{\alpha\beta} V^{j\beta}(-\mathbf{p}_{\bar{n}})]\, [V^{j'\beta'}(\mathbf{p}'_n - \mathbf{p}_n - \mathbf{p}_{\bar{n}})\gamma_5 \tau^{\sigma}_{\beta'\alpha'} \bar{U}^{i'\alpha'}(\mathbf{p}'_n)]}{\omega_{\mathbf{k}}(\omega_{\mathbf{k}} - W)}$$

Passing to the center-of-mass system ($\mathbf{p}_n - \mathbf{k} = \mathbf{p}'$, $\mathbf{p}_n = \mathbf{p}$, $\mathbf{p}_{\bar{n}} + \mathbf{k} = -\mathbf{p}'$, $\mathbf{p}_{\bar{n}} = -\mathbf{p}$) and carrying out the calculations, Eq. (6) reduces to the form

$$[W-2E(\mathbf{p})]\, a^{01}(\mathbf{p}) = \int \Delta_2 (\mathbf{p}\mathbf{p}'W)\, a^{01}(\mathbf{p}')\, d\mathbf{p}', \qquad (7)$$

where

$$\Delta_2 = \frac{g^2}{8\pi^3} \frac{(E_{\mathbf{p}} + M)(E_{\mathbf{p}'} + M)}{4E_{\mathbf{p}'}E_{\mathbf{p}}} \qquad (8)$$

$$\frac{\tau_1 \tau^T_2 (\sigma_1 \mathbf{R})(\sigma^T_2 \mathbf{R})}{\omega_{\mathbf{p}-\mathbf{p}'}(\omega_{\mathbf{p}-\mathbf{p}'} + E_{\mathbf{p}'} + E_{\mathbf{p}} - W)}$$

$$+ \frac{g^2}{8\pi^3} \frac{\tau^{\beta'\alpha'}\tau^{\alpha\beta}\delta_{ij}\delta_{j'i'}}{\mu(W-\mu)};$$

$$\mathbf{R} = \mathbf{p}'/(E_{\mathbf{p}'} + M) - \mathbf{p}/(E_{\mathbf{p}} + M).$$

In order to pass from the transposed matrices σ^T and τ^T to the unual ones, let us pass to different wave functions. Let us make on the indices j and β the transformation

$$\varepsilon_{\lambda j} a_j = a'_{\lambda}; \quad \varepsilon_{\nu\beta} a_{\beta} = a'_{\nu}; \quad \varepsilon = \begin{pmatrix} 0 & 1 \\ -1 & 0 \end{pmatrix}. \qquad (9)$$

Then σ^T_2 will become $\epsilon \sigma^T_2 \epsilon^{-1} = -\sigma_2$ and τ^T_2 will become $(-\tau_2)$. In the exchange term the matrices transform as follows:

$$\delta_{ij}\delta_{j'i'} \to \varepsilon_{jk}\delta_{ik}\delta_{i'm}\varepsilon^{-1}_{mj'} = {}^1\!/_2(\sigma_1\sigma_2 - 1);$$

$$\tau_{\alpha\beta}\tau_{\beta'\alpha'} \to \varepsilon_{\beta n}\tau_{\alpha n}\tau_{m\alpha'}\varepsilon^{-1}_{m\beta'} = {}^1\!/_2(\tau_1\tau_2 + 3). \qquad (10)$$

We then obtain

$$\Delta_2 = \frac{g^2}{8\pi^3} \left\{ \frac{(E_{\mathbf{p}} + M)(E_{\mathbf{p}'} + M)}{4E_{\mathbf{p}}E_{\mathbf{p}'}} \frac{\tau_1\tau_2 (\sigma_1 R)(\sigma_2 R)}{\omega_{\mathbf{p}-\mathbf{p}'}(\omega_{\mathbf{p}-\mathbf{p}'} + E_{\mathbf{p}} + E_{\mathbf{p}'} - W} \right\} + \frac{g^2 (\sigma_1\sigma_2 - 1)(\tau_1\tau_2 + 3)}{8\pi^3\, 4\mu (W-\mu)}. \qquad (11)$$

Then, multiplying both sides of Eq. (7) by $(W+2E_p)/(W+2M)$, introducing the binding energy $\mathcal{E}=W-2M$ and passing to the coordinate representation, we obtain the equation

$$\left(\frac{\nabla^2}{M\rho}+\mathcal{E}\right)\Phi^{01}(\mathbf{r})=\int U_2(\mathbf{r}\mathbf{r}'W)\,\Phi^{01}(\mathbf{r}')\,d\mathbf{r}', \qquad (12)$$

where $\rho=1+\mathcal{E}/4M$ and

$$U_2(\mathbf{r}\mathbf{r}'W)=\int\frac{[(2E_{\mathbf{p}}+W)(2E_{\mathbf{p}'}+W)]^{1/2}}{4M\rho}\,\Delta_2(\mathbf{p}\mathbf{p}'W)\,e^{i(\mathbf{p}\mathbf{r}-\mathbf{p}'\mathbf{r}')}d\mathbf{p}\,d\mathbf{p}'. \qquad (13)$$

The quantity M_ρ plays the role of reduced mass. Passing to the nonrelativistic limit $E_\rho \sim M$, $W\sim 2M$, we obtain the equation

$$(\nabla^2/M\rho+\mathcal{E})\,\Phi^{01}(\mathbf{r})=V_2(\mathbf{r})\,\Phi^{01}(\mathbf{r}), \qquad (14)$$

where

$$V_2(\mathbf{r})=-\frac{1}{3}(\tau_1\tau_2)\frac{g^2}{4\pi}\left(\frac{\mu}{2M}\right)^2 \qquad (15)$$

$$\times\left\{\sigma_1\sigma_2+S_{12}\left[1+\frac{3}{\mu r}+\frac{3}{(\mu r)^2}\right]\right\}\frac{e^{-\mu r}}{r}$$

$$-\frac{1}{3}(\sigma_1\sigma_2)(\tau_1\tau_2)(2M)^{-2}\,\delta(r)$$

$$+\frac{(\tau_1\tau_2+3)(\sigma_1\sigma_2-1)}{4\mu(2M-\mu)}\,\delta(r).$$

From this it is seen that the interaction potential between nucleon and antinucleon has a sign opposite to that of the interaction potential between two nucleons. The exchange term does not give a contribution in the nonrelativistic limit. Investigation in the relativistic region shows that the first term of equality (8) gives attraction at small distances, in contradistinction to the case of the two-nucleon system. The exchange term becomes large if $W\sim\mu$. This indicates that the possibility is not excluded of the formation of the bound nucleon-antinucleon system with large binding energy. This problem, which involves the relativistic region, requires a supplementary investigation. It would be interesting to investigate it also using the "new" Tamm method proposed by Dyson.

In conclusion, the author expresses his gratitude to Iu. M. Shirokov for advice and discussion of this problem.

---

[1] M. Levy, Phys. Rev. 88, 72, 725 (1952).

Translated by A. V. Bushkovitch
120

Angular Distribution of Fission Fragments

V. M. Strutinskii

(Submitted to JETP editor
October 13, 1955)
J. Exptl. Theoret. Phys. (U.S.S.R.) 30, 606-608
(March, 1956)

THE anisotropic angular distribution of fission fragments from fission induced by fast neutrons[1,2], protons[3] and gamma rays[4,5] has been observed experimentally. A number of general features of the angular distribution of the fragments follow from the conservation of angular momentum. Thus the principal qualitative difference of the angular distribution of fragments from nucleon-induced fission from that of photofission, which is the maximum at $\vartheta=0$, as contrasted with the maximum at $\vartheta=\pi/2$ for photofission, results from the different spin orientation of the compound nucleus. When a fast nucleon is captured, the spin of the compound nucleus is oriented predominantly in a direction perpendicular to the beam. The component of the radiation moment along the direction of the beam is ± 1; thus for a dipole radiation the spin of the compound nucleus is oriented predominantly along the beam. This difference in the orientation of the compound nucleus spin results generally in the experimentally observed shape of the angular distribution.*

With the increase of nucleon energy the anisotropy of the angular distribution must increase because of the increased angular momentum transferred to the nucleus. When the target nucleus spin I_0 differs from zero the angular distribution will be more isotropic because of the greater isotropy of spin distribution of the compound nuclei. The angular distribution of photofission fragments is especially dependent on the initial spin when the angular momentum transferred to the nucleus is relatively small. Thus for $I_0 \leq 1$ the angular distribution of fission fragments due to dipole radiation has maxima at $\vartheta = 0, \pi$; when the spin of the compound nucleus I is $I_0 \pm 1$ (compound nucleus spin oriented parallel to the photon moment), and for $\vartheta = \pi/2$ when $I = I_0$.

The angular distribution of the fragments is generally more isotropic the larger the spin of the fragments; however, the angular distribution of the fragments depends on the fission mechanism, especially when the spin of the fragments is comparable with the spin of the compound nucleus. The general theory of the angular distribution of particles with spin has been discussed frequently (see, for example, Ref. 6). For analysis of the experimental data on the angular distribution of fission fragments it is convenient to have simpler expressions giving the distribution of the components of fragment spins along the line joining the centers of mass of the fragments.

The general form of the wave function of two fragments in states τ_1 and τ_2 with orbital momentum l, and resulting from decay of a compound nucleus with spin (I, M), is

$$\psi_{IM} = \sum\nolimits_{lS\tau} f_{lS\tau}(r) \sum_{m\mu} C^{IM}_{lm\,S\mu}\, \chi_{S\mu\tau}\, Y_{lm}(\mathbf{n}), \tag{1}$$

where $\bar{n}$ is the unit separation vector of the fragments; $C^{c\gamma}_{a\alpha b\beta}$ are Clebsch-Gordon coefficients; $\chi_{S\mu\tau}$ is the internal wave function of the fragments for spin S; $|j_1 - j_2| \leqslant S \leqslant j_1 + j_2$, $\tau \equiv (\tau_1, \tau_2)$. In (1) $f_{lS\tau}$ is the radial wave function at infinity

$$f_{lS\tau} \sim \alpha_{lS\tau} \frac{1}{r} \exp\{ik_{S\tau} r\}.$$

In (1) we transform $\chi_{S\mu\tau}$ to a system of coordinates whose axis z' is parallel to $\bar{n}$

$$\chi_{S\mu\tau} = \sum\nolimits_{\varkappa} D^{S}_{\mu\varkappa}(\mathbf{n})\, \chi_{S\varkappa\tau},$$

where $D^{S}_{\mu\varkappa}$ is the transformation matrix [7], and $\varkappa$ is the component of S along z'. Then ψ_{IM} can be written as

$$\psi_{IM} = \sum g_{S\tau\varkappa}\, D^{I}_{\mu\varkappa}(\mathbf{n})\, \chi_{S\varkappa\tau}, \tag{2}$$

$$g_{S\varkappa\tau} = \sum\nolimits_{l} \sqrt{\frac{2l+1}{4\pi}}\, f_{lS\tau}\, C^{I\varkappa}_{l0S\varkappa}$$

At infinity

$$g_{S\varkappa\tau} \sim \beta_{S\varkappa\tau} \frac{1}{r} \exp\{ik_{S\tau} r\}.$$

The relative probability $b_{S\varkappa\tau}$ of fragment production in the state $(S\varkappa\tau)$ is:

$$b_{S\varkappa\tau} = |\beta_{S\varkappa\tau}|^2 = \Big|\sum\nolimits_{l} \alpha_{lS\tau} \sqrt{\frac{2l+1}{4\pi}}\, C^{I\varkappa}_{l0S\varkappa}\Big|^2. \tag{3}$$

In accordance with (2) the angular distribution of fission fragments from the compound nucleus with spin (I,M) is*

$$f_{IM}(\vartheta) = \sum_{\substack{S \\ |\varkappa| \leqslant \min(I,S)}} b_{S|\varkappa|} \sum_{\varkappa = \pm|\varkappa|} |D^{I}_{M\varkappa}(\mathbf{n})|^2, \tag{4}$$

where $b_{S|\varkappa|}$ denotes the probability for production of fragments in state $(S, \varkappa)$:

$$b_{S|\varkappa|} = \overline{b_{S\varkappa\tau}} = \frac{1}{4\pi} \sum\nolimits_{l} (2l+1)\, \overline{|\alpha_{lS\tau}|^2}\, (C^{I\varkappa}_{l0S\varkappa})^2. \tag{5}$$

The bar denotes summation over all observed states. In (5) interference terms (with $1 \neq 1'$) are neglected since these drop out through averaging over a large number of states of the system. The angular distribution of fragments for this reaction is

$$F_{I_0}(\vartheta) = \sum_{M_0 IM} \rho_{IM;\, I_0 M_0}\, f_{IM}(\vartheta), \tag{6}$$

where $\rho_{IM;\, I_0 M_0}$ is the probability for the formation of a compound nucleus in a state with spin (I, M), when the initial nucleus was in a state with spin (I_0, M_0). In Eq. (6), $M = M_\sigma + 1/2$ for nucleon-induced fission and $M = M_0 \pm 1$ for photofission.

Neglecting the rotation of the system as a whole**; it is reasonable to assume that the axial symmetry of the system is not disturbed at any stage of the fission process. In this case $\varkappa$ is the integral of motion and $\varkappa$ can denote the state of the deformed nucleus.*** The value of $\varkappa$ in the fissioning nucleus determines the orientation of the nuclear axis of symmetry with respect to the spin direction of the compound nucleus (the compound nucleus spin I component along the nuclear axis is $\varkappa$) and, consequently, the distribution of $\varkappa$ determines the angular distribution of the fragments. A comparison with experiment enables us to determine the probability of fission for a given value of $\varkappa$. Thus, a comparison with the experimentally observed angular distribution of fragments from the photofission of Th^{232} (4, $E_\gamma \approx 8$ mev) gives the value 0.29 for b ($\varkappa = \pm 1$) with b ($\varkappa = 0$) taken as unity. As the excitation energy increases the level separation of the fissioning nucleus for different $\varkappa$ decreases, the distribution of $\varkappa$ becomes more uniform and the angular distribution becomes more isotropic. For neutron-induced fission this decrease of anisotropy associated with higher excitation energy may be compensated by an increase of angular momentum transferred to the nucleus. For sufficiently high excitation energies the different values of $\varkappa$ (with fixed S) are of practically equal probability: all spin orientations of the fragments become equally probable. Then fission with $S \geq I$ contributes isotropically to the angular distribution since with $S \geq I$ in (4) the summation is performed over all values of $|\varkappa| \leq I$. Fission with $S < I$ gives an anisotropic contribution to the angular distribution with the maximum of the angular distribution, just as for spinless fragments, perpendicular to the compound nucleus spin, although it decreases as S increases. For high excitation energies the fragment angular distribution from photofission of an even-even nucleus induced by dipole radiation may be written as $1/2\ \sin^2$theta$+ \delta$ where δ is the relative probability for the formation of fragments with spin $S \geq 1$. We note that equal probabilities for different $\varkappa$, which follows from (5), also means equal probability of different orbital moments l which are allowed by a given S.

The experimentally observed dependence of the anisotropy of angular distribution on the mass ratio of the fragments is clearly due to the different excitations of the fissioning nuclei in symmetric and asymmetric fission.

Symmetry properties impose certain restrictions on fission and angular distribution. Thus it follows from (3) that with $\varkappa = 0$ fission into two equal fragments is forbidden if the spin of the compound nucleus is odd (particularly in the fission of an even-even nucleus by dipole radiation). The parity of the spatial wave function of these nuclei agrees with the parity of S^7 but the coefficients C^{I0}_{l0S0} vanish if the sum $I + S + l$ is odd. It is clear, however that this and other similar cases of forbidding of individual instances of fission are not of great importance.

I am profoundly grateful to A. B. Migdal, B. T. Geilikman and V. M. Galitskii for their interest and for valuable discussions.

---

* This is obvious for spinless fragments; in this case the direction of fragment flight perpendicular to the fragment orbital momentum is also perpendicular to the compound nucleus spin.

**

$$D^I_{M0} = \sqrt{\frac{4\pi}{2I+1}}\, Y_{IM},$$

$$\sum_{\varkappa=\pm|\varkappa|>0} |D^I_{M\varkappa}|^2$$

$$= 2(-1)^{|\varkappa|-M} \sum_{\substack{\lambda=0 \\ (\text{even})}}^{2I} C^{\lambda 0}_{IMI-M} C^{\lambda 0}_{I|\varkappa|I-|\varkappa|} P_\lambda(\cos\vartheta).$$

*** Rotation of the system can be neglected if the level spacing of the fissioning nucleus is large compared with the characteristic rotational energy $E_{\text{rot}} \sim l(l+1)/2\mu R^2$ where μ is of the order of the reduced mass of the fragments.

**** The distribution of $\varkappa$ existing at the instant of fission is preserved at infinity since the centrifugal energy of the fragments can always be neglected compared with their kinetic energy.

[1] Brolley, Dickinson and Henkel, Phys. Rev. 99, 159 (1955).

[2] J. E. Brolley and W. C. Dickinson, Phys. Rev. 94, 640 (1954).

[3] B. L. Cohen et al., Phys. Rev. 94, 625 (1954).

[4] E. J. Winhold, Phys. Rev. 87, 1139 (1952).

[5] A. W. Fairhall et al., Phys. Rev. 94, 733 (1954).

[6] J. Blackett, L. C. Biedenharn and others in Prob. Contemp. Phys. USSR 6 (1955) (Russian translation).

[7] L. D. Landau and E. M. Lifshitz, *Quantum Mechanics*, Moscow-Leningrad, 1949.

Translated by I. Emin
121

Density of Linear Boiling of a Superheated Liquid Along the Track of an Ionizing Particle

G. A. ASKAR'IAN

(Submitted to JETP editor November 26,1955)
J. Exptl. Theoret. Phys. (U.S.S.R.) 30, 610-611
(March, 1956)

THE prospects for the utilization of bubble chambers[1-3] in experimental nuclear physics depend on the possibility of determining the ionizing power of particles from the bubble density distribution along a track. A number of theoretical papers[4-6] devoted to the design and study of the operation of bubble chambers throw no light on this very important feature of the new particle recorder, although the literature contains indications of the comparitively strong dependence of initial boiling density on the superheating of the liquid, which reflects the difficulty of calibrating the instrument.

The elementary theory of induced boiling which is developed in the present article is based on the electrodynamical model of stimulated disturbance of superheated liquids. Here it is assumed that the disturbance of the liquid results from the formation and mutual repulsion of closely situated, similarly charged, multimolecular groups (forming the walls of newly created microcavities) which are collected by ions appearing at the passage of an ionizing particle. (The theory developed below also contains the elements necessary for the construction of a theory of other possible forms of the electrodynamical model.)

In the calculation we shall assume that for the induced production of a bubble in the superheated liquid under normal operating conditions, it is sufficient that at a distance not exceeding the "'localization interval'' λ two positive ions should be formed whose electrons would receive during ionization the energy $\epsilon > \epsilon_d$. In fact, the condition for the localization of the ions and the condition for sufficient withdrawal of the electron component may be regarded as the definitions of the parameters λ and ϵ_d. It is evident that these parameters are independent of the ionizing power of the particles but are determined by the properties of the medium and the degree of superheating; the parameter ϵ_d takes into consideration the average condition under which the approach of oppositely charged centers is unimportant, at least during the time of formation of the bubble nucleus.

For the purpose of calculating the probability of establishing conditions sufficient for the creation of a bubble we divide the track of a δ-electron with energy ϵ into sections equal to λ. The average number of all positive ions produced by the δ-electron in the i the section is:

$$\bar{\nu}_i \approx (1/\varepsilon^*_{\text{ion}})\,(d\varepsilon/dx)_{x=x_i}\lambda;$$

(ϵ^*_{ion} is the portion of the entire energy expended required per ion). The average number of ions whose electrons received in ionization the energy $\epsilon > \epsilon_d$ is

$$\bar{\nu}_{i\,\text{d}} \approx (1/\varepsilon^*_d)\,(d\varepsilon/dx)_{x=x_i}\lambda.$$

(Here ϵ^*_d is tne portion of the total expended energy required per ion with sufficiently distant electron. We separate these ions out, and formally raise the effective ionization energy to ϵ_d. It is clear that ϵ^*_d exceeds ϵ_d but both are of the same order of magnitude, in analogy to the relation between ϵ_{ion} and the ionization energy.)

According to Poisson's equation, the probability of producing two ions in the distance λ_i with electrons sufficiently distant is

$$w(2\text{ in }\lambda_i) \approx \frac{\bar{\nu}^2_{i\,\text{d}}}{2!}\exp(-\bar{\nu}_{i\,\text{d}}) \approx \frac{\bar{\nu}^2_{i\,\text{d}}}{2},$$

since $\bar{\nu}_{i\,d} \ll 1$ (the coefficient 2 can be dropped since allowance for the fluctuations of ions at both ends of the interval gives a coefficient close to unity. Such a procedure amounts to the addition of the probability of production of two ions (with distant electrons) in the i th interval of the net of path subdivisions shifted by $\lambda/2$.

The probability of creating sufficient conditions for the formation of a cavity somewhere along the path of the δ-electron under consideration with initial energy ϵ is

$$\sum_i w(2\text{in}\lambda_i) \approx \varepsilon^{*-2}_{\text{d}} \sum (d\varepsilon/dx)^2_i\lambda^2_i$$

$$\approx \lambda\varepsilon^{*-2}_{\text{d}}\int\left(\frac{d\varepsilon}{dx}\right)^2 dx \approx \lambda\varepsilon^{*-2}_{\text{d}}\int_{\varepsilon^*_{\text{d}}}^{\varepsilon}\frac{d\varepsilon}{dx}\,d\varepsilon.$$

Using the well-known equation for energy loss $d\epsilon/dx \approx a/\epsilon$, which holds true in a wide range of δ-electron energies, we obtain

$$w(\varepsilon) \approx \lambda a\varepsilon^{*-2}_{\text{d}}\ln(\varepsilon/\varepsilon^*_{\text{d}}) + w(1\text{in}\lambda_1).$$

The number of δ-electrons with energy from ϵ to $\epsilon + d\epsilon$ produced by the ionizing particle per unit track length is

$$dN(\varepsilon) = KZ^2\beta^{-2}d\varepsilon/\varepsilon^2$$

(Ze and βc are the charge and velocity of the ionizing particle). Consequently,the mean number of bubbles per unit track length is

$$\bar{n} \approx \int_{\varepsilon^*_{\text{d}}}^{\varepsilon_{\max}} w(\varepsilon)\,dN(\varepsilon) \approx \frac{\lambda KZ^2a}{\beta^2\varepsilon^{*3}_{\text{d}}},$$

since the maximum possible transfer of energy to the electron is $\epsilon_{\max} \gg \epsilon_d{}^*$

The principal qualitative results of the theory are (1) the separation of the variables which characterize the ionizing particles and the variables which characterize the state of the medium, and (2) the linear dependence of the boiling density on the ionizing power of the particles: $\bar{n} \approx Z^2\beta^2\Phi$, where Φ is the state function of the medium.

We shall now estimate the order of magnitude of $\bar{n}$ for a relativistic, singly charged particle passing through diethyl ether at a temperature of 140 ° (the ether density under the given operating conditions is $\rho \approx 0.5$ g/cm^3). We have

$$K \approx \pi N_0 r_0^2\rho mc^2 \approx 0{,}075\ mc^2$$

(N_0 is Avogrado's number; r_0 and m are the classical radius and mass of the electron). We also assume that $a \approx (mc^2/2)^2$. (For an estimate of the order of magnitude of a we have converted to density from the empirical equation for the energy losses of electrons in aluminum $d\beta_e/dx = 2.2\beta_e^{-3}$ cm^{-1} [7]).

Substituting the calculated values of the constants, we obtain

$$\bar{n} \approx 0{,}02\lambda(mc^2/\varepsilon^*_{\text{d}})^3 \approx 30\ \text{bubbles/cm}.$$

for admissible parameter values $\lambda \sim 3 \times 10^{-7}$ cm and $\epsilon_d \sim 0.3$ kev. (Experiment gives $n \sim$ from 10 to 100 depending on the degree of superheating.) A certain arbitrariness in the choice of specific values of the parameters λ and $\epsilon_d{}^*$ which we have assumed for illustrative purposes in our estimate of the order of magnitude of $\bar{n}$, was due to the absence of data regarding the dependence of the parameters on the degree of superheating. This dependence is unimportant, however, for a comparison of the ionizing powers of two particles passing through the liquid when the extent of superheating is either unknown or not accurately determined. The comparative estimate is particularly useful when the bubble chamber is used with an accelerator, when, simultaneously with the tracks of particles participating in the investigated nuclear reactions, there are also recorded the tracks of particles of known energy emitted by the accelerator.

It is evident that all that has been said above may apply not only to a superheated liquid but also to a supersaturated solution of a gas in a liquid.[8] A gassy liquid behaves very much like a superheated one[9] when pressure is released, the decreased resistance of the liquid to disturbance (because of excess dissolved gas) lowers the required operating pressures and justifies an experimental attempt to realize a gas bubble chamber.

It can be expected that the above considerations concerning the role of the formation of molecular groups and the introduction of the concepts of the localization interval, withdrawal energy and sufficient conditions for the creation of microcavities will facilitate the study of the peculiar and complicated phenomena which take place in bubble chambers.

---

[1] D. Glaser, Suppl. del Nuovo Cimento 11, No. 2,361 (1954).

[2] D. Glaser, Scient. Amer. 2, 46 (1955).

[3] D. Glaser and D. C. Rahm, Phys. Rev. 97, 474 (1955).

[4] G. Martelli, Nuovo Cimento 12, 250 (1954).

[5] L. Bertranza and G. Martelli, Nuovo Cimento 1,324 (1955).

[6] L. Bertranza, G. Martelli and A. Zacutti, Nuovo Cimento 2, 487 (1955).

[7] F. Rasetti, *Elements of Nuclear Physics*, GITTL, 1940, p. 56. (Russian Translation)

[8] G. Askar'ian, J. Exptl. Theoret. Phys. (U.S.S.R.) 28, 636 (1955).

[9] E. I. Nesis and Ia. I. Frenkel', J. Tech. Phys. (U.S.S.R.) 22, 1500 (1952).

Translated by I. Emin
123

The Elastic Scattering of Protons by Tritium

L. A. MAKSIMOV

(Submitted to JETP editor December 2, 1955)
J. Exptl. Theoret. Phys. (U.S.S.R.) 30, 615 (March, 1956)

THE experimental data on the angular distribution of $p - H^3$ scattering[1] fit very well on a curve of the form $a + b \cos\theta + c \cos^2\theta$ (see the Figure). In the angles measured (up to 54.7°) there is little Coulomb scattering. It is possible to carry through a phase analysis of the experimental data taking into consideration moments of relative motion $l = 0$ and 1. The vector scheme of the decomposition in this instance is:

$$s_{1/2} + 1/2 = 0^+ + 1^+, \; p_{1/2} + 1/2$$
$$= 0^- + 1^-, \; p_{3/2} + 1/2 = 1^- + 2^-.$$

In agreement Ref. 2 we assume that the principal role is played by the phases

$$\delta_0 = \delta(s_{1/2}, 0^+), \qquad \delta_1 = \delta(p_{3/2}, 1^-)$$
$$\delta_2 = \delta(p_{3/2}, 2^-).$$

The analysis shows that the experimental data cannot be accounted for if only three phases are used. It is necessary to take into account the phase which can materially increase the terms in $\cos\theta$ and $\cos^2\theta$, i.e., the phase $\delta_3 = \delta(p_{1/2}, 1)$.

For three values of proton energy we have obtained the phases which describe satisfactorily the angular distribution of the scattering (see the figure):

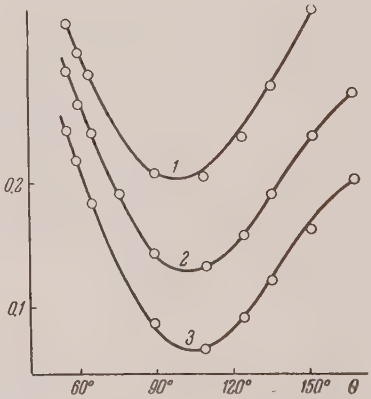

Curves of the shape $a + b \cos + c \cos^2\theta$ obtained from the phases mentioned in the text (θ is the angle in the center of mass system). o – experimental points. The curves are displaced relative to each other by 0.05; *1* – 2.54; *2* – 3.03; *3* – 3.50 mev

For E = 2.54 mev:

$$\delta_0 = 90°;\ \delta_1 = 33°;\ \delta_2 = 27°;\ \delta_3 = 5.7°.$$

For E = 3.03 mev:

$$\delta_0 = 90°;\ \delta_1 = 48°;\ \delta_2 = 18.5°;\ \delta_3 = 14°$$

or

$$\delta_0 = 80;\ \delta_1 = 43°;\ \delta_2 = 25°;\ \delta_3 = 10°.$$

For E = 3.50 mev:

$$\delta_0 = 90°;\ \delta_1 = 52°;\ \delta_2 = 16°;\ \delta_3 = 21°.$$

Experiment gives three parameters, so that the choice of phases is not unique. But the unusually small constant term in the angular distribution strongly reduces the arbitrariness in the selection of phases. Thus the phase δ_0, which accounts for potential scattering, cannot be chosen to be smaller than 70°.

Thus the scheme for the interaction of a proton with H^3 which was proposed by Baz' and Smorodinskii[2] is not in contradiction with the experimental results for the elastic scattering of protons by tritium.

In conclusion I wish to thank Professor Ia. A. Smorodinskii for suggesting the subject and for his guidance.

Note in the proof: Frank and Gammel[3] have carried through a phase analysis of $p - H^3$ scattering assuming LS coupling.

[1] Claassen, Brown, Freier and Stratton, Phys. Rev. 82, 589 (1951).

[2] A. I. Baz' and Ia. A. Smorodinskii, J. Exptl. Theoret. Phys. (U.S.S.R.) 27, 382 (1954).

[3] R. M. Frank and J. L. Gammel, Phys. Rev. 99, 1406 (1955).

Translated by I. Emin
126

Absorption Curve Moments for Solid Solutions

G. Ia. Glebashev
Kazan State University

(Submitted to JETP editor November 28, 1955)
J. Exptl. Theoret. Phys. (U.S.S.R.) 30, 612 (March, 1956)

MEASUREMENTS of resonance absorption in solid solutions enable us to make conclusions about the character of the interaction forces between the particles. The first calculation of the moments of these absorption curves was carried out by Kittel.[1] However, he took into account only the dipole interactions. Below are presented the results of a calculation of the moments of absorption curves when not only dipole, but also exchange, interaction forces of paramagnetic ions are present.

A crystal of solid solution of two salts grows in a bath of their liquid solution. The filling of any particular lattice point of the growing crystal by one or the other ion appears to be a random process. The probability of occupation of a lattice point by a paramagnetic ion will be considered to be independent of the manner in which the remaining crystal lattice points are filled. This is the case when there is a small difference between the binding energies of the ions of both metals in the crystal, between their masses, etc. We shall calculate the moments of the paramagnetic resonance absorption curve in solid solutions at high frequencies.

1. The zero order moment is

$$\nu_0 = \mathrm{Sp}\sum_j S_{x_j}^2 = \overline{N}\frac{\lambda}{2}(2S+1)^{\overline{N}}$$

$$= N_0 f\frac{\lambda}{3}(2S+1)^{N_0 f},$$

where N is the average number of paramagnetic ions, equal to $N_0 f$ (N_0 is the number of lattice points in the crystal), $\lambda = S(S+1)$ (S is the spin quantum number).

2. The second order moment is

$$\Delta\overline{\nu_2} = h^{-2}\frac{\lambda}{3}\frac{\Sigma B_{jk}^2\overline{\delta_j\delta_k}}{\overline{N}} = h^{-2}\frac{\lambda}{3}\sum_k B_{jk}^2 f,$$

where $\delta_j(\delta_k)$ are equal to unity if the lattice point $j(k)$ is occupied by a magnetic ion and to zero in the opposite case, and $\delta_j\delta_k = f$.[2]

3. The fourth order moment is

$$\Delta\overline{\nu_4} = h^{-4}\Big\{f\Big[\sum_k A_{jk}^2B_{jk}^2\Big(\frac{2}{5}\lambda^2 - \frac{3}{10}\lambda\Big)$$

$$+ A_{jk}B_{jk}^3\Big(\frac{4}{15}\lambda^2 - \frac{2}{10}\lambda\Big) + B_{jk}^4\Big(\frac{\lambda^2}{5} - \frac{\lambda}{15}\Big)\Big]$$

$$+ f^2\Big[\sum_{k,l} 3B_{jk}^2B_{jl}^2 + 2A_{jk}^2(B_{jl} - B_{kl})^2$$

$$+ A_{jk}A_{kl}(B_{jk} - B_{jl})(B_{kl} - B_{jl})$$

$$+ 2A_{jk}B_{jk}(B_{jl} - B_{kl})^2\Big]\frac{\lambda^2}{9}\Big\}$$

where the remaining symbols are taken from an article of Van Vleck.[2]

The numerical values of the moments are not given in the present work, but they could be easily evaluated. It is not difficult to see that the quantity

$$X = \Delta\overline{\nu_4}/(\Delta\overline{\nu_2})^2$$

increases with a decreasing concentration of paramagnetic ions, and the moments decrease. It is possible to expect the half width of the curve to decrease as well. However, the measurements of Kashaev[3] show that the halfwidth increases at first with dilution, reaches a maximum at some value of f and then decreases with further dilution. The increase of the halfwidth at small dilutions may not even contradict an increase in the quantity X at the same time.

Indeed, such case was observed by Kumagi et al[4] who studied the change of the halfwidth of the curve with the change in separation d between two neighborhood paramagnetic ions. In particular, with a decrease in d (as long as the volume forces are small) the halfwidth increases with an increase in the quantity X though the latter is very small. The halfwidth reaches a maximum and then, as the volume forces begin to increase rapidly, it begins to decrease.

A direct comparison of the theoretical moments with the experimental data cannot be carried out not only because the available curves are not measured on sides (only halfwidths were measured) but also because the insufficient sensitivity of the present experimental techniques makes a careful investigation of the absorption curve (particularly its sides) of solid solutions almost impossible since the absorption decreases rapidly with dilution.

In conclusion the author expresses a deep gratitude for the valuable advice and discussions to C. A. Al'tshuler and B. M. Kozyrev.

---

[1] C. Kittel and E. Abrahams, Phys. Rev. 90, 238 (1953).

[2] J. H. Van Vleck, Phys. Rev. 74, 1168 (1948).

[3] Kh. Kashaev, Dissertation, KFAN, 1954.

[4] Kumagai, Ono, Havaski, Shimada, Shono and Ibamoto, Phys. Rev. 83, 1077 (1951).

Translated by M. J. Stevenson
124

Nonlinear Equations in Quantum Field Theory

V. IA. FAINBERG

P. N. Lebedev Physical Institute
Academy of Sciences, USSR

(Submitted to JETP editor, October 25, 1955)
J. Exptl. Theoret. Phys. (U.S.S.R.) 30, 608-609 (March, 1956)

THE purpose of the present note is to show that the equations gotten by Low[1] follow from general relations for the Green's function which were found by Lehman, Symanzik and Zimmerman[2], starting from general requirements of relativistic invariance, causality and boundary conditions. For simplicity, the proof is carried through for the example of the equation for the Green's function of the meson-nucleon system, which is simply related to the matrix element of the S-matrix for the scattering of mesons by nucleons.

The Green's function of the meson-nucleon system is defined in the following manner:

$$\tau(xx';yy') \tag{1}$$
$$= (\Psi_0, T\{\varphi(x)\varphi(y)\psi(x')\overline{\psi}(y')\}\Psi_0),$$

where Ψ_0 is the state vector of the physical vacuum in the Heisenberg representation and $\psi(x)$ and $\varphi(x)$ are the Heisenberg operators corresponding to the nucleon and meson fields. For simplicity the meson is taken to be neutral. Instead of $\tau(xx';yy')$ it is convenient to consider the quantity

$$\langle p'|x,y|p\rangle \tag{2}$$
$$= \int\limits_{x_0\to+\infty,\, y_0\to-\infty} dx'\,dy\,\overline{u}_{p'}(x')\,\gamma_4\,\tau(xx',yy')\,\gamma_4\,u_p(y').$$
$$= (\Psi_p, T\{\varphi(x)\varphi(y)\}\Psi_p).$$

where $u_p(x)$ is a solution of the free Dirac equation for particles with momentum p and energy $p_0 = \sqrt{p^2 \mp M^2}$, and Ψ_p is the state vector of one nucleon in the Heisenberg representation.

If causality and the boundary conditions are employed then, analogously to what is done in Ref. 2, it is possible to obtain relations of the following form for the Green's function:

$$\langle p'|x,y|p\rangle = \sum_{n=0}^{\infty}\sum_{\lambda}(-i)^n\Big\{\eta(x-y) \tag{3}$$
$$\times\int K_{\xi_1}\ldots K_{\xi_n}\langle p'|x,\xi_1\ldots\xi_n|\lambda\rangle$$
$$\times\Delta^{(+)}(\xi_1-\eta_1)\ldots\Delta^{(+)}(\xi_n-\eta_n)\,K_{\eta_1}\ldots K_{\eta_n}$$
$$\langle p|y,\eta_1\ldots\eta_\eta|\lambda\rangle^*\,d\xi_1\ldots d\xi_n d\eta_1\ldots d\eta_n$$
$$+\eta(y-x)\int K_{\xi_1}\ldots K_{\xi_n}\langle p'|y,\xi_1\ldots\xi_n|\lambda$$
$$\rangle\,\Delta^{(+)}(\xi_1-\eta_1)\ldots\Delta^{(+)}(\xi_n-\eta_n)$$
$$\times K_{\eta_1}\ldots K_{\eta_n}\langle p|x,\eta_1\ldots\eta_n|\lambda\rangle^*\,d\xi_1\ldots d\xi_n d\eta_1\ldots d\eta_n\Big\}.$$

Here $K_x = \Box_x - \mu^2$ where μ is the renormalized meson mass; * designates the Hermitian conjugate;

$$\Delta^+(x) = -i(2\pi)^{-3}\int dq\,\delta(q^2+\mu^2)\,e^{iqx}\,\eta(q)$$

is a commutator function;

$$\eta(x) = \begin{cases} 1, & x_0 > 0 \\ 0, & x_0 < 0 \end{cases};$$

and the summation in (3) is over the number of mesons n and the number of nucleons and antinucleons λ.

The matrix element of the S-matrix for a transition of a meson from a state of momentum q to a state of momentum q' is related to the Green's function in the following way:

$$\langle p', q' \mid S \mid p, q\rangle \tag{4}$$
$$= -\int f^*_{q'}(x)\, f_q(y)\, K_x K_y \langle p' \mid x, y \mid p\rangle\, dx\, dy,$$

where $f_q(x) = (2q_0)^{-1/2} \exp[iqx]$ is a solution of the Klein-Gordon equation;

$$qx = \mathbf{q}\mathbf{x} - q_0 x_0, \quad q_0 = \sqrt{\mathbf{q}^2 + \mu^2}.$$

Using this relation, and also the relations

$$\sum_{\mathbf{q}} f_q(\xi)\, f^*_q(\eta) = i\Delta^{(+)}(\xi - \eta);$$

$$\eta(x) = \frac{1}{2\pi i} \int_{-\infty}^{+\infty} \frac{e^{i\alpha x}}{\alpha - i\varepsilon}\, d\alpha.$$

we immediately obtain from (3)

$$\langle p', q' \mid S \mid p, q\rangle \tag{5}$$
$$= \frac{1}{2\pi i} \sum_{\mathbf{q}_1 \ldots \mathbf{q}_n, n, \lambda} \Big\{ \int \frac{d\alpha}{\alpha - i\varepsilon} \langle p', q' + \alpha \mid S \mid \lambda, q_1 \ldots q_n\rangle$$
$$\langle \lambda, q_1 \ldots q_n \mid S \mid p, q + \alpha\rangle \cdot$$
$$+ \int \frac{d\alpha}{\alpha - i\varepsilon} \langle p', -q + \alpha \mid S \mid \lambda, q_1 \ldots q_n\rangle$$
$$\langle \lambda, q_1 \ldots q_n \mid S \mid p_1, -q' + \alpha\rangle \Big\}$$
$$+ \int dx\, dy\, \delta(x_0 - y_0)\, f^*_{q'}(x)\, f_q(y) \langle p' \mid [K_x \varphi(x), \dot{\varphi}(y)]_- \mid p\rangle.$$

Here $<\lambda q_1 \ldots q_n \mid S \mid p, q + \alpha>$ is the matrix element of the S-matrix for a transition of a meson with momentum $\mathbf{q}$, energy $q + \alpha$ and a nucleon with energy-momentum p to a state with n mesons and λ nucleons and antinucleons. The last term on the right-hand side of (5) is zero if the interaction is linear in the meson field. If the sum in (5) is restricted to the states ($n = 0$, $\lambda = 0$) and ($n = 1$, $\lambda = 1$) and we go over to matrix elements on the energy surface then we get Low's equation.

We emphasize that the relation (5) with the restriction given above becomes an equality only if there is provided the inhomogeneous term ($n = 0$, $\lambda = 1$), which depends on the concrete form of the interaction. The inhomogeneous term can be found exactly only in the limit $q, q' \to 0$, therefore the applicability of the equation is essentially limited to the nonrelativistic domains of nucleon energy and meson energy. For arbitrary q, q' the inhomogeneous term can be expressed in terms of the exact renormalized one-particle Green's function and vertex part. Therefore, attempts to treat the equations found by Low relativistically run into kinds of problems; first, the exact forms of the renormalized one-particle Green's function and vertex part are unknown, and secondly, as shown in the works cited,[3] the renormalized Green's function possesses nonphysical poles, reflecting the fact that the renormalized coupling constant becomes zero.[4]

Note added in proof. Analogous questions are considered in recently appearing work.[5]

[1] F. E. Low, Phys. Rev. 97, 1392 (1955).

[2] Lehman, Symanzik and Zimmerman, Nuovo Cimento 1, 205 (1955).

[3] Landau, Abrikosov and Khalatnikov, Dokl. Akad. Nauk SSSR 95, 497, 773, 1177 (1954); 96, 261 (1954). Abrikosov, Galanin, and Khalatnikov, Dokl. Akad. Nauk SSSR 97, 793 (1954).

[4] E. S. Fradkin, Soviet Phys. JETP 1, 604 (1955). L. D. Landau and I. Ia. Pomeranchuk, Dokl. Akad. Nauk SSSR 102, 489 (1955). L. D. Landau and I. Ia. Pomeranchuk, Dokl. Akad. Nauk SSSR 102, 489 (1955).

[5] Duimio, Gulmanelli and Scotti, Nuov. Cim. 2, 1132 (1955).

Translated by D. Finkelstein
122

Isomeric States of Deformed Nuclei

L. K. PEKER
Academy of Sciences, USSR

(Submitted to JETP editor December 2, 1955)
J. Exptl. Theoret. Phys. (U.S.S.R.) 30, 616-617
(March, 1956)

AS is well known, the term "isomer" denotes an excited state of a nucleus characterized by a long lifetime. The small probability of decay of such states may be due to a large difference between their spins and that of the ground state ($\Delta I \geq 3$).[1] Besides this, the decay probability of the excited state depends substantially on the nature of the levels between which γ-transitions are taking place, and in some cases (the nuclei of Lu^{177}, Ta^{181}, Re^{187}, Np^{237}, Pu^{239} and others) the decay probability turns out to be small (and the lifetime large), although the spins of the isomeric states in the nuclei mentioned differ from the spins of lower levels by one or two units.[2]

In the present note, by "isomeric states" we shall mean only those states, whose large lifetime is due to a large difference of their spin and the spin of the ground state; we shall further restrict our considerations to nuclei of odd mass number A.

The explanation of the properties of such isomeric states has been one of the most substantial successes of the one-particle nuclear shell model.[2-6] Within the framework of this model it turned out to be possible to describe correctly, in the overwhelming majority of cases, the multipolarity of isomeric transitions of type M4 and E3, and also to explain the concentration of isomers in the so-called "islands of isomerism" $39 \leq Z, N \leq 49$: $63 \leq Z, N \leq 81$; $93 \leq Z, N \leq 125$[3,4]. Out of the 86 known cases of isomerism in nuclei with odd A only two ($_{42}\mathrm{Mo}^{93}_{51}$ and $_{31}\mathrm{Ga}^{65}_{34}$) lie outside of the boundaries of the islands, while in four or five cases multipole order of isomeric transitions of type M3, E4 is observed which is not describable by the single-particle model.

However, a more detailed analysis of isomeric states with the single-particle model meets with a number of difficulties. According to the model isomers with an odd number of protons and an odd number of neutrons should occur equally often, and the boundaries of the islands for them should coincide. In reality it turns out that, in general, they do not coincide. Thus, in odd neutron nuclei, isomeric states are observed with $63 \leq N \leq 81$, while in odd proton nuclei, only with $77 \leq Z \leq 81$. In the next island, $93 \leq N \leq 125$, isomeric transitions described by the single-particle model (type M4) are observed only with $N > 113$ (10 cases), while in nuclei with $93 \leq N \leq 115$, only 5 isomeric transitions of an anomalous type (E3, M3, E4) are observed. Finally, the single-particle shell model does not account for isomeric transitions of type E3 which occur with $Z, N = 41$, 43, 45, 47.[6]

Recently, attempts have been made to overcome some of these difficulties[5,7,8]. However, they cannot be regarded as satisfactory, since they do not explain all of the facts. It will be shown below that taking into account of the deformation of the nucleus makes it possible to remove all of the mentioned difficulties without any additional assumptions. From an analysis of various experimental data (quadrupole moments, isotope shifts, etc.) it follows that the deformation of nuclei in which at least one of the shells (proton or neutron) is close to being filled, is small. For such nuclei, in calculating the single-particle levels in the first approximation, one can use a spherically-symmetrical potential of the same type as in the single-particle model.[5] For this reason, the states of weakly deformed nuclei may be characterized by an exact quantum number j (j is the angular momentum of the odd particle), and hence they may be described in the terminology of the single-particle model as $p_{1/2}$; $g_{9/2}$; $d_{5/2}$; $d_{3/2}$; $h_{11/2}$ etc. For such nuclei all the basic results of the single-particle model hold, and in the overwhelming majority of cases one finds in these nuclei the usual isomeric transitions of types M4 or E3. However, as soon as we pass to nuclei in which both shells are far from being filled, the situation changes essentially, since here it becomes necessary to take into account the nonsphericity of the nuclei. In such nuclei the potential will not be spherically symmetrical. In the case of axial symmetry in deformed nuclei, not the total angular momentum j, but its projection Ω on the axis of symmetry, is an exact quantum number.

In order for the phenomenon of isomerism to occur, it is necessary that either the ground or the excited state of the nucleus possess a large spin $I = \Omega = 9/2$, $11/2$ or $13/2$. In slightly deformed nuclei, large values of the spin $I = j$ will occur in all nuclei with an odd number of nucleons in the level j. It is easy to show that in filling the levels $j = 9/2$; $11/2$; $13/2$ the number of such nuclei is 5,6,7 $[(2j + l)/2]$. At the same time in nuclei with a marked deformation, the maximum value of the spin $I = \Omega = j$ occurs only once, since in a level with a given Ω (in particular, the largest one) only two nucleons may be present. Thus it may be expected that levels with large spins in deformed nuclei will occur considerably more rarely than predicted by the single-particle model. Since the deformation removes the degeneracy of the energy levels in the quantum number Ω, their number is considerably increased. As a result, the probability of occurrence of levels with strongly varying spins ($\Delta I \geq 3$) next to each other, is substantially reduced.

The two above-mentioned factors have as a consequence that in strongly deformed nuclei ($63 \leq Z \leq 75$; $93 \leq N \leq 115$) favorable conditions for the existence of isomeric states are not realized. If one uses the single-particle level scheme obtained by Nillsen which takes deformation into account[10], it is possible to indicate in which nulcei of this region isomeric states should occur, and also to determine the possible multipolarities of the transitions into these levels. An analysis based on this scheme shows that such nuclei must be: $_{66}\mathrm{Dy}_{95}^{165}$ with isomeric transition of type E3[2]; $_{72}\mathrm{Hf}_{107}^{179}$ (E3, M3)[2]; $_{74}\mathrm{W}_{109}^{183}$ (E3, M3)[2]; $_{74}\mathrm{W}_{111}^{185}$ (E3, M3)[2]; $_{76}\mathrm{Os}_{115}^{191}$ (M3 + E4)[11]; as well as $_{68}\mathrm{Er}_{99}^{167}$; $_{72}\mathrm{Hf}_{105}^{177}$; $_{70}\mathrm{Yb}_{101}^{171}$. In the first five nuclei isomeric states have already been observed, and their expected multipolarity (which agrees with experimental data) is given in parentheses. In an analogous manner it is possible to explain the absence of an isomeric state in the heaviest isotope $_{43}\mathrm{Tc}_{58}^{101}$ [12], since this nucleus is more strongly deformed than the lighter isotopes Tc^{93-99} in which isomeric states are observed. Taking account of deformation makes it also possible to explain the appearance in the island $41 \leq Z, N \leq 47$ of isomeric transitions of type E3[9].

Thus, taking into account of deformation makes it possible to explain the absence of isomeric states in nuclei with $63 \leq Z \leq 75$. the small number of isomeric transitions and their anomalous multipolarity with $93 \leq N \leq 115$, as well as the absence of an isomeric state in Tc^{101} and the appearance of transitions of type E3 in the region $39 < Z, N < 49$.

In conclusion, it is a pleasant duty to express my deep gratitude to L. A. Sliv for detailed discussion of this paper.

---

[1] C. E. Weizsäcker, Naturwiss 24, 813 (1936).

[2] M. Goldhaber and R. D. Hill, Rev. Mod. Phys. 24, 179 (1952).

[3] L. W. Nordheim, Phys. Rev. 75, 1894 (1949).

[4] E. Feenberg and K. C. Hammack, Phys. Rev. 75, 1877 (1949).

[5] M. G. Mayer, Phys. Rev. 78, 16 (1950).

[6] M. Goldhaber and A. W. Sunyar, Phys. Rev. 83, 906 (1951).

[7] R. Katz, Phys. Rev. 91, 1487 (1953).

[8] G. Scharff-Goldhaber, Phys. Rev. 90, 587 (1953).

[9] A. Bohr and B. Mottelson, Kgl. Danske Videnskab. Selskab. Mat. — fys. Medd., 27, 16 (1953).

[10] S. Nillsen, Kgl. Danske Videnskab, Selskab., Mat. — fys. Medd. 29, 14 (1955).

[11] W. Michelich, Bull. Amer. Phys. Soc. 30, 46 (1955).

[12] D. R. Wiles, Phys. Rev. 93, 181 (1954).

Translated by A. V. Bushkovitch

Energy Spectrum of High Energy Ionizing Particles Passed Through a Thick Layer of Matter

Iu. F. Orlov

(Submitted to JETP editor December 2, 1955)
J. Exptl. Theoret. Phys.(U.S.S.R.) 30 613-614 (March, 1956)

THE energy spectrum of a fast ionizing particle after passage through a thin layer of matter for which the average energy loss $\overline{\Delta E} \ll E$ is determined by the relation

$$s \equiv \overline{\Delta E}/\varepsilon_{\max} L_i,$$

where L_i is the well-known ionization logarithm and $\epsilon_{\max}$ (E) is the maximum energy loss per ionizing collision where m is the electron rest mass,

$$L_i = 2\left(\ln \frac{2m\beta^2}{I_{\text{cp}}(1-\beta^2)} - \beta^2\right), \tag{1}$$

$$\varepsilon_{\max} = \frac{2m(E^2 - \mu^2)}{\mu^2}, \quad \beta = v/c,$$

where m is the rest mass of an electron, μ the rest mass of the ionizing particle and I_{ave} is the ionization potential. If $W(\epsilon, E)$ is the probability per unit path length of a collision with an energy loss ϵ, then the distribution function for energy loss Δ after passage through a layer δx has the form[1,2]:

$$f(\delta x, \Delta) = (2\pi)^{-1} \tag{2}$$

$$\times \int_{-\infty}^{\infty} dz \exp\left\{iz\Delta - \delta x \int_0^{\infty} W(\varepsilon, E)(1 - e^{-iz\varepsilon})\, d\varepsilon\right\}.$$

For $S \ll 1$ Eq. (2) gives the curve due to Landau,[1] and for $S \gg 1$ it yields a Gaussian distribution.[2]

For the case of a thick layer ($S \gg 1$) we shall obtain a more accurate distribution function than the Gaussian. If we allow first $s \gg 1$, but with $\overline{\Delta E} \ll E$, then the distribution function can be expanded in Hermite polynomials:

$$\varphi(\delta x, y) = (2\pi)^{-1/2} e^{-y^2/2}\left(1 + \sum_{n \geqslant 3} a_n H_n(y)\right); \tag{3}$$

$$H_n(y) = (-1)^n e^{y^2/2} \frac{d^n}{dy^n} e^{-y^2/2}, \quad a_n(\delta x) \tag{4}$$

$$= (n!)^{-1} \int_{-\infty}^{\infty} \varphi(\delta x, y) H_n(y)\, dy,$$

$$y=(\Delta-\overline{\Delta})(\overline{\Delta^2}-\overline{\Delta}^2)^{-1/2},\ \varphi(\delta x,y)$$
$$=(\overline{\Delta^2}-\overline{\Delta}^2)^{1/2}f(\delta x,\ \overline{\Delta}+y(\overline{\Delta^2}-\overline{\Delta}^2)^{1/2}),\qquad(5)$$

Using the formula for a derivative of a δ-function

$$\partial^n\delta(\alpha)/\partial\alpha^n=(2\pi)^{-1}(i)^n\int_{-\infty}^{\infty}y^n\exp(i\alpha y)\,dy,$$

we obtain

$$\varphi(\delta x,\ y)=(2\pi)^{-1/2}e^{-y^2/2}\left[1+\frac{\beta_3}{6\beta_2^{3/2}}H_3(y)+\frac{\beta_4}{24\beta_2^2}H_4(y)+\frac{\beta_3^2}{72\beta_2^3}H_6(y)+\ldots\right],\qquad(6)$$

$$\beta_n=\delta x\overline{\varepsilon^n}=\delta x\int_0^{\varepsilon_{\max}}\varepsilon^nW(\varepsilon,\ E)\,d\varepsilon,\ n>1.\qquad(7)$$

Since $W(\epsilon,E)=$ const. $(\beta\epsilon)^{-2}$ and const. $\beta^{-2}\delta x=\overline{\Delta E}/L_i$, we have:

$$\varphi(\overline{\Delta E},\ y)=(2\pi)^{-1/2}e^{-y^2/2}\Big[1+\frac{1}{12}s^{-1/2}(y^3-3y)+\frac{1}{72s}(y^4-6y^2+3)+\frac{1}{288s}(y^6-15y^4+45y^2-15)+\ldots\Big].\qquad(8)$$

The series of Eq. (8) is asymptotic. For $l/s\sim1$, $y\sim2$ the first two terms give an accuracy of abuut 10%; for $y\lesssim1$ one may use four terms of Eq. (8).

Assume now that $\overline{\Delta E}\sim E_0$. We shall denote the distribution function of energy after passage through a thick layer x by $\phi(x,\epsilon)$. It will evidently be given by the relation

$$\Phi(x,\ E)=\int_0^{\infty}\Phi(x-\delta x,\ E+\Delta)f(\delta x,\ \Delta)\,d\Delta.\qquad(9)$$

Expanding ϕ as a series in powers of Δ and δx and letting δx go to zero, we obtain the differential equation

$$\frac{\partial\Phi}{\partial x}=\overline{\varepsilon}\frac{\partial\Phi}{\partial E}+\frac{1}{2!}\overline{\varepsilon^2}\frac{\partial^2T}{\partial E^2}+\frac{1}{3!}\overline{\varepsilon^3}\frac{\partial^3\Phi}{\partial E^3}+\cdots\qquad(10)$$

If we discard in Eq. (10) the terms with high order of $\overline{\epsilon^n}$, $n\geq3$ and in the coefficients of $\overline{\epsilon}$ and $\overline{\epsilon^2}$ we replace E by $\overline{E}(x)$, we obtain a Gaussian distribution. This case corresponds to the following two assumptions.* First, $\phi(x,\epsilon)$ should be sufficiently narrow so that it is possible to neglect the dependence of the diffusion coefficient $\overline{\epsilon^2}$ on E and replace E by $\overline{E}(x)$, second, the energy of the particle should not be so large that great energy losses ϵ would take place. For highly relativistic particles these conditions are not fulfilled.

The approximation will be more accurate if instead of $\overline{\epsilon^n}$ in Eq. (10) we take the quantity

$$\int_0^{\infty}\Phi(x,\ E)\,dE\int_0^{\varepsilon_{\max}}\varepsilon^nW(\varepsilon,\ E)\,d\varepsilon.$$

For a faster computation of corrections we notice that the quantity β_n has the same additive properties according to Eq. (7) as the quantity $\beta_2=\overline{\Delta^2}-\overline{\Delta}^2$ which enters into Eq. (5) for y. Precisely this property of β_2 was used by Pomeranchuk, who obtained the Gaussian distribution for a thick layer. Therefore we shall first obtain a distribution function for a thick layer by replacing all β_n in Eq. (6) by

$$B_n(\overline{E})=\int_{\overline{E}}^{E_0}\left|\frac{dx}{dE_1}\right|dE_1\int_0^{\infty}\Phi(x(E_1),\ E)\,dE\times\int_0^{\varepsilon_{\max}}\varepsilon^nW(\varepsilon,\ E)\,d\varepsilon.\qquad(11)$$

In order to obtain $\beta_2=\overline{(E-\overline{E})^2}$ to the first order of l/s, it is sufficient to take for ϕ in Eq. (11) the Gaussian curve of Pomeranchuk; to compute β_3 it is possible to let $\phi(E,E_1)$ equal to $\delta(E-E_1)$. In this approximation

$$B_2=\overline{(E-\overline{E})^2}={}^2/_3(mL_i^{-1}\mu^{-2})\times(E_0^3-\overline{E}^3+3\overline{E}\mu^2-3E_0\mu^2)+{}^4/_3(m^2L_i^{-2}\mu^{-4})$$
$$\times[3E_0^4/4-E_0^3\overline{E}-\mu^2E_0^3/\overline{E}+3\mu^2E_0\overline{E}+\overline{E}^4/4-2\mu^2\overline{E}^2-3\mu^4-3\mu^4\ln(E_0/\overline{E})];\qquad(12)$$

$$B_3/6B_2^{3/2}={}^1/_6(mL_i/2\mu^2)^{1/2}[(E_0^5-\overline{E}^5)/5-2\mu^2(E_0^3-\overline{E}^3)/3+\mu^4(E_0-\overline{E})]+3\mu^4E_0/\overline{E}]$$
$$\times[(E_0^3-\overline{E}^3)/3-\mu^2(E_0-\overline{E})]^{-3/2};\qquad(13)$$

$$\Phi(y)=(2\pi)^{-1/2}e^{-y^2/2}[1+(B_3/6B_2^{3/2})\times(y^3-3y)+\ldots],\qquad(14)$$

$$y=-B_2^{-1/2}(E-\overline{E}).\qquad(15)$$

The Eq. (14) has a simple and descriptive form for $\overline{E}\ll E_0$. For example, at the end of the passage for $E_0\gg\mu$:

$$\Phi(y)=(2\pi)^{-1/2}e^{-y^2/2}\left[1+\frac{1}{10}\left(\frac{3mL_iE_0}{2\mu^2}\right)^{1/2}(y^3-3y)\right.$$
$$\left.+\frac{1}{28}\frac{mL_iE_0}{\mu^2}(y^4-6y^2+3)+\frac{3}{400}\frac{mL_iE_0}{\mu^2}(y^6-15y^4+45y^2-15)+\ldots\right]; \tag{16}$$

$$y^2\approx(E-\overline{E})^2(3L_i\mu^2/2mE_0^3)(1+3mE_0/2L_i\mu^2)^{-1}; \tag{17}$$

$$B_n\approx(2m/\mu^2)^{n-1}E^{2n-1}/(n-1)(2n-1)L_i(E_0),\ \overline{E}\ll E_0. \tag{18}$$

From Eq. (16) it is evident that for sufficiently large ratio $L_i mE_0/\mu^2$, the distribution function differs substantially from a Gaussian one even at the end of the passage. The curve has a characteristic "tail" at the low energy and a sharp cutoff on the high energy side. Its maximum is displaced in the direction of greater energies relative to its center of gravity ($y=0$).

---

[1] L. D. Landau, J. Phys. USSR 8, 201 (1944).

[2] I. Ia. Pomeranchuk, J. Exptl. Theoret. Phys. (U.S.S.R.) 18, 759 (1948).

Translated by M. J. Stevenson
125

The Propagation of Sound in Moving Helium II and the Effect of a Thermal Current upon the Propagation of Second Sound

I. M. KHALATNIKOV
Institute for Physical Problems, Academy of Sciences, USSR

(Submitted to JETP editor December 15, 1955)
J. Exptl. Theoret. Phys. (U.S.S.R.) 30, 617-619 (March, 1956)

FROM ordinary hydrodynamics it is well known that an "entrainment" of sound occurs in a moving fluid. A similar phenomenon must take place in the hydrodynamics of a superfluid. Inasmuch as in the case of a superfluid two types of motion (normal, with a velocity $\mathbf{v}_n$, and superfluid, with a velocity $\mathbf{v}_s$) as well as two types of sound vibrations, propagated with different velocities, are possible, it is natural that the picture of sound propagation in a moving superfluid liquid should differ from the corresponding phenomenon in classical hydrodynamics.

Let sound oscillations of frequency ω be propagated in a direction characterized by the unit vector $\mathbf{n}$ (along the x-axis) through helium II in which normal and superfluid motions are taking place with the constant velocities $\mathbf{v}_n$ and $\mathbf{v}_s$. The wave vector $\mathbf{k}$ is equal to $\mathbf{n}\omega/u$, where u is the velocity of sound. We shall determine here the velocities of first and second sound in the moving Helium II under the assumption that the motion proceeds at velocities which are small by comparison with the velocity of sound. Let us write the complete set of hydrodynamic equations for Helium II:

$$\frac{\partial\rho}{\partial t}+\operatorname{div}\mathbf{j}=0,$$

$$\frac{\partial j_i}{\partial t}+\frac{\partial}{\partial x_k}(p\delta_{ik}+\rho_n v_{ni}v_{nk}+\rho_s v_{si}v_{sk})=0,$$

$$\frac{\partial\rho s}{\partial t}+\operatorname{div}\rho s v_n=0,\quad \frac{\partial\mathbf{v}_s}{\partial t}+\nabla\left(\Phi+\frac{v_s^2}{2}\right)=0.$$

Here ρ is the density, s is the entropy per unit mass, p is the pressure, $\mathbf{j}=\rho_n\mathbf{v}_n+\rho_s\mathbf{v}_s$ is the mass current density, ρ_n and ρ_s are the densities of the normal and superfluid components, and $\Phi=\Phi_0(p,T)-\rho_n(\mathbf{v}_n-\mathbf{v}_s)^2/2\rho$ is the thermodynamic potential, depending upon the relative velocity $\mathbf{v}_n-\mathbf{v}_s$. If we take the pressure and temperature as independent variables, then from the thermodynamic identity for the potential

$$\rho\,d\Phi=-\rho s\,dT+dp+(\mathbf{j}-\rho\mathbf{v}_s)\,d(\mathbf{v}_n-\mathbf{v}_s)$$

it follows that the density ρ and the entropy s are functions of the relative velocity $\mathbf{v}_n-\mathbf{v}_s$:

$$s=s_0+\frac{\partial}{\partial T}\left(\frac{\rho_n}{2\rho}\right)(\mathbf{v}_n-\mathbf{v}_s)^2,\quad s_0=-\left(\frac{\partial\Phi_0}{\partial T}\right),$$

$$\frac{1}{\rho}=\frac{1}{\rho_0}-\frac{\partial}{\partial p}\left(\frac{\rho_n}{2\rho}\right)(\mathbf{v}_n-\mathbf{v}_s)^2,$$

$$\frac{1}{\rho_0}=\left(\frac{\partial\Phi_0}{\partial T}\right)_p$$

We shall look for increments linear in $\mathbf{v}_n$ and $\mathbf{v}_s$ to the velocity of sound for the stationary fluid. For this purpose it is necessary to rewrite the hydrodynamic equations to include terms quadratic in the velocity. We shall introduce the notation $\mathbf{v}=\mathbf{j}/\rho$ and $w=\mathbf{v}_n-\mathbf{v}_s$. The components of these vectors in the direction of the wave vector $\mathbf{k}$ we shall identify by the index k, and those in a plane perpendicular to $\mathbf{k}$ by the index $\perp$. In a traveling sound wave, all quantities depend upon the argument $(x - ut)$, derivatives with respect to which we shall indicate by a prime. To the accuracy we require, the hydrodynamic equations assume the form (with $U = u - v_k$)

$$-U\frac{\partial\rho}{\partial T}T' - U\frac{\partial\rho}{\partial p}p' - U\rho^2\frac{\partial}{\partial\rho}\left(\frac{\rho_n}{2\rho}\right)(w_k w_k' + w_\perp w_\perp') + \rho v_k' = 0, \tag{1}$$

$$p' + (2\rho_s\rho_n/\rho)\,w_k w_k' - \rho U v_k' = 0, \tag{2}$$

$$(\rho_s\rho_n/\rho)(w_k w_\perp' + w_k' w_\perp) - \rho U v_\perp' = 0, \tag{3}$$

$$\left[-\rho U\frac{\partial s}{\partial T} + w_k\frac{\partial}{\partial T}\;(\rho_s s)\right]T' + \left[-\rho U\frac{\partial s}{\partial p} + w_k\frac{\partial}{\partial p}(\rho_s s)\right]p' + \rho_s s w_k' = 0, \tag{4}$$

$$\left[-s - Uw_k\frac{\partial}{\partial T}\left(\frac{\rho_n}{\rho}\right)\right]T' - U\frac{\partial}{\partial p}\left(\frac{\rho_n}{p}\right)w_k p' + \left(\frac{\rho_n}{\rho}U - \frac{3\rho_n\rho_s}{\rho^2}w_k\right)w_k'$$
$$-\left(\frac{\rho_n}{\rho}v_\perp + \frac{\rho_s\rho_n}{\rho^2}w_\perp\right)w_\perp' - \frac{\rho_n}{\rho}w_k v_k' - \frac{\rho_n}{\rho}w_\perp v_\perp' = 0, \tag{5}$$

$$[v_\perp' - (w_\perp\rho_n/\rho)'] = 0. \tag{6}$$

Simultaneous solution of this system of equations will yield equations determining the values of the velocity of sound u. In this process the components of the equations of motion perpendicular to the wave vector k [Eqs. (3) and (6)] can be separated from the remaining equations. This is due to the fact that the components $v_\perp$ and $w_\perp$ enter into Eqs. (1) and (5) only in terms of the second order. In this way we find:

$$\left(U^2\frac{\partial\rho}{\partial p} - 1\right)\left\{\left(\rho_n\rho U^2\frac{\partial s}{\partial T} - s^2\rho\rho_s\right)\right.$$
$$\left.-Uw_k\left(4\rho_s\rho_n\frac{\partial s}{\partial T} - 2\rho s\frac{\partial\rho_n}{\partial T}\right)\right\} = 0; \tag{7}$$

$$U - w_k\rho_s/\rho = 0. \tag{8}$$

The roots of Eq. (7) determine the velocities of first and second sound in moving Helium II. For first sound we find a solution which is identical with that known from ordinary hydrodynamics: $u_1 = c_1 + v_k$, $c_1^2 = \partial p/\partial\rho$. For the velocity of second sound we have:

$$u_2 = c_2 + v_k + w_k\left(\frac{2\rho_s}{\rho} - \frac{s}{\rho_n}\frac{\partial\rho_n}{\partial T}\frac{\partial T}{\partial s}\right), \tag{9}$$

$$c_2^2 = \frac{\rho_s}{\rho_n}s^2\frac{\partial T}{\partial s}.$$

From (8) we find that the oscillations of the transverse components of velocity $v_\perp$ and $w_\perp$ in a plane perpendicular to the direction of the wave vector are propagated with the velocity

$$u = v_k + w_k\rho_s/\rho = \mathrm{v}_n\mathrm{k}/k. \tag{10}$$

According to (6) no superfluid motion takes place in a direction perpendicular to the wave vector k. The direct implication of the solution (10) is that the transverse oscillations of the normal velocity are propagated with a velocity equal to v_n. These oscillations of the normal velocity are analogous to the viscous waves of an ordinary fluid.

The velocities c_1 and c_2 are the velocities of sound for stationary helium. If the magnitudes of the velocities in the sound wave are small by comparison with the constant velocity components, it will be possible to neglect the nonlinear effect arising from the variation of c_1 and c_2 along the profile of the sound wave (see Ref. 1 for further details).

From Eqs. (9) it follows that if a constant thermal current is present in Helium II it will carry the second sound along. In the thermal current j = 0 and, consequently, v= 0 as well. Further, we have $\mathrm{w} = \mathrm{v_n} - \mathrm{v_s} = \mathrm{v_n}\rho/\rho_\mathrm{s}$. In this case Eq. (9) assumes the form:

$$u_2 = c_2 + \frac{(\mathrm{v}_n\mathrm{k})}{k}\frac{\rho}{\rho_s}\left(\frac{2\rho_s}{\rho} - \frac{s}{\rho_n}\frac{\partial\rho_n}{dT}\frac{\partial T}{\partial s}\right) \tag{11}$$
$$= c_2 + \gamma v_{nk}.$$

The quantity $\mathrm{v_n}$ is related to the thermal current density q by means of the equation $\mathrm{q} = \rho s T \mathrm{v}_n$. The coefficient γ preceding v_{nk} in (11) is a function of temperature of order unity. The dependence of γ on temperature is shown in the figure. In the temperature region above 1 ° K, where only the roton components of thermodynamic quantities are of importance, we have, approximately, $\rho_n \sim s$ and $\gamma = (\rho_s - \rho_n)/\rho_s$. From the fact that γ changes sign at several temperatures it follows that the "entrainment" of the second sound can take place either in the direction of the thermal current or opposite to it.

Finally, we comment on the effect of a thermal current upon the velocity of second sound in standing waves. From the symmetry of the standing waves, it follows that this effect will be quadratic with respect to the ratio of the "entrainment" velocity to the velocity of second sound. Even for velocities $\mathrm{v}_k \sim 1$ m/sec, the

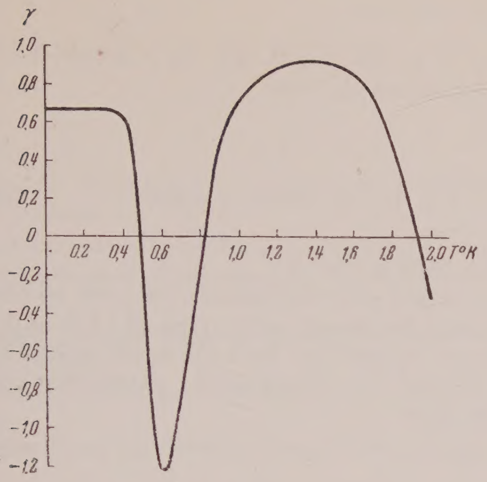

effect upon the velocity of second sound in a standing wave is of the order of a fraction of a percent:

In conclusion, I thank L. D. Landau for his consideration of these results.

---

[1] I. M. Khalatnikov, Dokl. Akad. Nauk SSSR 79, 237 (1951).

Translated by S. D. Elliott
128

Remarks on One Variant of the Equations of a Nonlocal Field

A. R. Asanov
Leningrad Physico-Technical Institute
Academy of Sciences, USSR

(Submitted to JETP editor January 19, 1955)
J. Exptl. Theoret. Phys. (U.S.S.R.) 30, 619-620
(March, 1956)

In a nonlocal field theory, where the wave-function of a particle $U(x_\mu, \xi_\mu)$ depends on "internal" variables ξ_μ as well as the ordinary space-time variables x_μ $(\mu = 1, 2, 3, 4)$ it is natural to interpret the orbital angular momentum of "internal" motion as the intrinsic angular momentum (spin) of the particle. We will assume the function U to be scalar; then the equation of Markov[1] for a free particle in the momentum representation has the form:

$$\Big\{\omega^2 k_\mu^2 - \frac{\partial^2}{\partial r_\mu^2} + r_\mu^2 + \frac{2}{k_\mu^2}\Big[\Big(k_\mu \frac{\partial}{\partial r_\mu}\Big)^2 - (k_\mu r_\mu)^2\Big]\Big\}\chi(k_\mu, r_\mu) = 0, \qquad (1)$$

where

$$\chi(k_\mu, r_\mu) = \int \exp\{-ik_\mu x_\mu\}\, U(x_\mu, r_\mu)\, d^4x,$$

and λ and ω are constants with the dimensions of lengths. We introduce the notation $f = -\omega^2 k^2_\mu$; this is the square of the mass measured in units of $\hbar/\omega$. In a rest system Eq. (1) assumes the form

$$\Big(-\frac{\partial^2}{\partial r_i^2} + r_i^2 - \frac{\partial^2}{\partial r_0^2} + r_0^2\Big)\chi = f\chi, \qquad (2)$$

where $i = 1, 2, 3$ and r_0 is the real variable $r_0 = -ir_4$. The solutions of (2) will be sought in the form $X(r_\mu) = g(r_i)\,\Phi(r_0)$, separating the dependence on space and time variables. On the function X we impose the requirement of boundedness in all of the 4-space of internal coordinates.

For the functions $g(r_i)$ and $\Phi(r_0)$ we get the equations

$$(-(\partial^2/\partial r_i^2) + r_i^2)\, g = kg, \qquad (3)$$

$$(-(\partial^2/\partial r_0^2) + r_0^2)\,\Phi = (f - k)\,\Phi, \qquad (4)$$

where k is a constant of separation of variables. The solution of Eq. (3) in spherical coordinates $r = |\mathbf{r}|, \theta, \varphi$, as is well known, has the form

$$g_{klm}(r, \theta, \varphi) = Y_{lm}(\theta, \varphi)\, r^l e^{-r^2/2} L^{l+1/2}_{(k-2l-3)/4}(r^2),$$

where Y_{lm} is the spherical function and L is the associated Laguerre polynomial. Here the quantity k assumes the values

$$k = 4n + 2l + 3, \qquad (5)$$

where $l = 0, 1, 2, \ldots$; $n = 0, 1, 2 \ldots$

Thus for given k the internal angular momentum l can assume the values $0, 2, \ldots, (k-3)/2$ or $k, 3, \ldots, (k-3)/2$ depending on whether k is odd or even. The projection of the internal angular momentum m assumes the values $|m| \lesssim l$.

Equation (4) has bounded solutions only for

$$f - k = 2n_0 + 1, \quad n_0 = 0, 1, 2, \ldots \qquad (6)$$

Its solution then has the form

$$\Phi_{n_0}(r_0) = H_{n_0}(r_0)\, e^{-r_0^2/2},$$

where H_n is the Hermite polynomial. From condition[0] (6) we obtain that for given f the quantity k can assume the values $3, 5, \ldots, f-1$. However, from conditions (5) and (6) it is evident that f can assume the values $2\beta + 4$

where $\beta = 0, 1, 2, \ldots$.

For given f the desired solution of (2) has the form

$$\chi_{fklm}(r, \theta, \varphi, r_0) = g_{klm}(r, \theta, \varphi)\, \Phi_{(f-k-1)/2}(r_0)$$

and is degenerate with multiplicity $(\beta+1)(\beta+2)(\beta+3)/6$. The obtained solutions make it possible to classify all states according to their mass, internal angular momentum and "internal time number" k. Thus, for $f = 4$ we have the lowest nondegenerate state, in which $k = 3$ (corresponding to $n_0 = 0$) and the angular momentum $l = 0$. For $f = 6$, we have two states with different spins; in the first $k = 3$, $l = 0$ and in the second $k = 5$, $l = 1$. For $f = 8$, for example, we have in addition to states $k = 3$, $l = 0$ and $k = 5$, $l = 1$ also the states for $k = 7$ with angular momenta $l = 0$ and $l = 2$.

The considerations presented have, finally, an illustrative character and lie in the direction of attempts[2,3] to introduce spin in a natural way in a theory with a mass spectrum.

In conclusion we express our gratitude for his guidance to Prof. M. A. Markov.

---

[1] M. A. Markov, Dokl. Akad. Nauk SSSR 101, 449 (1955).

[2] V. L. Ginzburg and I. E. Tamm, J. Exptl. Theoret. Phys. (U.S.S.R.) 17, 227 (1947).

[3] Hara, Marumori, Ohnuki and Shimodaira, Prog. Theor. Phys. 12, 177 (1954).

Translated by D. Finkelstein
129

Further Discussion on the Quantum Theory of the Radiating Electron

A. A. SOKOLOV
Moscow State University

(Submitted to JETP editor December 25, 1954)
J. Exptl. Theoret. Phys. (U.S.S.R.) 30, 623 (March, 1956)

NELIP[1] has made a series of critical remarks in his reply to our work on the quantum theory of the radiating electron. However, these critical remarks are based on a modification of our Eq. 18[2] which is given by Nelip[1] in the form

$$\varepsilon = (1 - \beta^2 \sin^2\vartheta)\left(1 + \frac{\nu}{2n}\right) + O\left(\frac{\nu^2}{n^2}, \frac{\nu^3}{n^3}\cdots\right), \qquad \text{(A)}$$

(cf. Eq. A, p. 423 of Ref. 1). As a matter of fact, this formula has the form

$$\varepsilon = (1 - \beta^2 \sin^2\vartheta)(1 + \nu/2n). \qquad \text{(B)}$$

(cf. Eq. (18) of Ref. 2).

In connection with this formula we made an observation that the higher order terms of $(\frac{\nu}{n})^2$ of the expansion should also have the small multiplier $(1 - \beta^2 \sin^2\vartheta)$. Therefore the expression (A) has the form

$$\varepsilon = (1 - \beta^2 \sin^2\vartheta)\left(1 + \frac{\nu}{2n}\right) + \left(1 - \beta^2 \sin^2\vartheta\right) O\left(\frac{\nu^2}{n^2}, \frac{\nu^3}{n^3}\cdots\right), \qquad \text{(C)}$$

which was indeed used by us in our previous work[2] and also in our following articles on the quantum theory of the radiating electron (cf., for example, Eq. (43) of Ref. 3).

Furthermore, Nelip[1] ascribes to us still a second inaccurate formula (B) (p. 423) which does not follow in any way out of our Eqs. (16) and (18) of Ref. 2. Therefore the critical remarks that our method developed in Ref. 2 has a small region of applicability by its limitation to the magnitudes $\nu^3/n^2 \ll 1$ appear to be a misunderstanding as they are based on the modification pointed out above. From our original Eq. (18)[2] it follows that the terms discarded by us are of the order $(\nu/n)^2$.

Therefore we cannot accept the criticism made by Nelip and our previous observations should remain valid.[4,5]

---

[1] N. F. Nelip, J. Exptl. Theoret. Phys. (U.S.S.R.) 27, 421 (1954).

[2] Sokolov, Klepikov and Ternov, J. Exptl. Theoret. Phys. (U.S.S.R.) 24, 249 (1953).

[3] A. A. Sokolov and I. M. Ternov, J. Exptl. Theoret. Phys. (U.S.S.R.) 25, 698 (1953).

[4] A. A. Sokolov, J. Exptl. Theoret. Phys. (U.S.S.R.) 24, 488 (1953).

[5] Sokolov, Matveev and Ternov, Dokl. Akad. Nauk SSSR 102, 65 (1955).

Translated by M. J. Stevenson
131

CONTENTS - *Continued*

		Russian Reference
N. G. Birger, V. V. Guseva, G. B. Zhdanov, S. A. Slavatinskii and G. M. Staskov	617	30, 590
Linearization of the Hartree Equations . P. S. Zyrianov and V. M. Eleonskii	620	30, 592
Some Remarks Concerning the Macroscopic Theory of Superconductivity . . . V. L. Ginzburg	621	39, 593
Many Electron Quantum Theory Dispersion Formulas for Metals in the Infrared Region . . . V. I. Cherepanov	623	30, 598
Elastic Stattering of 18.7 mev Protons by Nickel and Copper Nuclei . . . R. A. Vanetsian and E. D. Fedchenko	624	30, 577
Concerning the Electric Charge of the Neutron . . . I. S. Shapiro and I. V. Estulin	626	30, 579
Transformation of the λ-Transition in Helium to a Special Transition of the First Kind in the Presence of a Heat Flow . . . V. P. Peshkov	628	30, 581
Relativistically Invariant Formulation of Electrodynamics without Longitudinal and Scalar Fields . . . E. M. Lipmanov	630	30, 583
On the Theory of Asymmetric Fission of Heavy Nuclei . . . S. G. Ryzhanov	632	30, 599
Pion-proton Interactions at 1.4 bev . . . A. I. Nikishov	634	30, 601
On the Interaction between Nucleon and Antinucleon . . . Iu. A. Tarasov	636	30, 603
Angular Distribution of Fission Fragments . . . V. M. Strutinskii	638	30, 603
Density of Linear Boiling of a Superheated Liquid along the Track of an Ionizing Particle . . . G. A. Askar'ian	640	30, 610
The Elastic Scattering of Protons by Tritium . . . L. A. Maksimov	642	30, 615
Absorption Curve Moments for Solid Solutions . . . G. Ia. Glebashev	643	30, 612
Nonlinear Equations in Quantum Field Theory . . . V. Ia. Fainberg	644	30, 608
Isomeric States of Deformed Nuclei . . . L. K. Pekar	645	30, 616
Energy Spectrum of High Energy Ionizing Particles Passed through a Thick Layer of Matter . . . Iu. F. Orlov	647	30, 613
The Propagation of Sound in Moving Helium II and the Effect of a Thermal Current upon the Propagation of Second Sound . . . I. M. Khalatnikov	649	30, 617
Remarks on One Variant of the Equations of a Nonlocal Field . . . A. R. Asanov	651	30, 619
Further Discussion on the Quantum Theory of the Radiating Electron . . . A. A. Sokolov	652	30, 623

SOVIET PHYSICS JETP VOLUME 3, NUMBER 4 NOVEMBER, 195

CONTENTS

Russian Reference
Nikolai Nikolaevich Semenov . . . 471 30, 625
The Compton Effect at High Energies . . . A. A. Abrikosov 474 30, 386
Concerning the Interaction Cross Sections of Neutrons with Nuclei . . . P. E. Nemirovskii 484 30, 551
Dynamical Birefringence of Polymethylmethacrylate Solutions with Various Solvents and the Form of the Macromolecules . . . V. N. Tsvetkov, E. V. Frisman and L. S. Mukhina 492 30, 649
Contribution to the Theory of Production and Annihilation of Antiprotons . . . L. M. Afrikian 503 30, 734
The Conductivity of Silver Bromide in the Presence of Bromine . . . L. M. Shamovskii, A. A. Dunina and Mi I. Gosteva 511 30, 640
The Dielectric Properties of Castor Oil at High Pressures . . . L. F. Vereschagin, L. F. Kuznetsov and T. I. Alaeva 519 30, 661
Magnetic Analysis of the (d, p) Reaction Products in the Investigation of Spin and Parity of Levels of the Daughter Nucleus . . . Iu. A. Nemilov and V. F. Litvin 523 30, 686
The Interaction of the States of Two Zones in the Single-electron Scheme . . . Iu. M. Seidov and V. S. Galishev 526 30, 695
Magnetic Analysis Study of Energy Levels of S^{33} . . . L. M. Khromchenko 531 30, 681
Reflection of Slow Electrons from the Surface of Pure Tungsten and from Tungsten Covered by Thin Films . . . N. D. Morgulis and D. A. Gorodetskii 535 30, 667
Investigation of the Dependence of the Dielectric Constant and the Tangent of the Dielectric Loss Angle of Barium Titanate on the Strength of a High Frequency Electric Field . . . E. V. Sinakov and V. V. Galpern 541 30, 675
Scattering of 250 mev Photons by Free Electrons . . . L. V. Kurnosova, L. A. Razorionov and P. A. Cherenkov 546 30, 690
Application of Singular Integral Equation Theory to Problems of the Scattering of Particles in an External Field . . . N. P. Klepikov 550 30, 701
On the Singularity of the Electromagnetic Potential in the Higher Approximations of Perturbation Theory . . . Iu. M. Lomsadze 554 30, 707
Explanation of the Transition Effect for the "Stars" in the Stratosphere . . . Zh. S. Takibaev 559 30, 713
The Free Path Length of a Nonlocalized Exciton in a Polar Crystal . . . A. I. Ansel'm and Iu. A. Firsov 564 30, 719
Phase Diagram for the Liquid-Vapor System of Helium Isotopes (He^3-He^4). I. . . . B. N. Esel'son and N. G. Berezniak 568 30, 628
Point Charge Interaction Energy in Ionic Crystals . . . T. I. Liberberg-Kucher 580 30, 724
Relativistic Spherical Functions . . . A. Z. Dolginov 589 30, 746
Cerenkov Radiation in Anisotropic Ferrites . . . V. E. Pafomov 597 30, 761
The Dynamics of Ionic Lattices of Ferroelectric Crystals in Limiting Cases . . . V. Kh. Kozlovskii 601 30, 766

Letters to the Editor:

Pulsed Coherent Generation of Millimeter Radiowaves by Nonrelativistic Electron Bunches . . . G. A. Askar'ian 613 30, 584
Angular Momentum Distribution and the Spatial Distribution of Nucleons in Nuclei . . . S. I. Larin 615 30, 587
Some Cases of Generation of Heavy Unstable Particles on Beryllium Nuclei

(*Contents continued on inside back cover*)